AWARD NUMBER:	W81XWH-11-1-0211
Title:	"The Role of Novel Substituted Diindolyl Methane Analogues in the Treatment of Triple-Negative and ErbB2-Positive Breast Cancer"
PRINCIPAL INVESTIGATOR	Mandip S. Sachdeva
CONTRACTING ORGANIZATION:	Florida A&M University Tallahassee, FL 32307-3200
REPORT DATE;	July 2017
TYPE OF REPORT:	FINAL
PREPARED FOR :	U.S. Army Medical Research and Materiel Command Fort Detrick, Maryland 21702-5012

REPORT DOCUMENTATION PAGE		*Form Approved* *OMB No. 0704-0188*
Public reporting burden for this collection of information is estimated to average 1 hour per response, including the time for reviewing instructions, searching existing data sources, gathering and maintaining the data needed, and completing and reviewing this collection of information. Send comments regarding this burden estimate or any other aspect of this collection of information, including suggestions for reducing this burden to Department of Defense, Washington Headquarters Services, Directorate for Information Operations and Reports (0704-0188), 1215 Jefferson Davis Highway, Suite 1204, Arlington, VA 22202-4302. Respondents should be aware that notwithstanding any other provision of law, no person shall be subject to any penalty for failing to comply with a collection of information if it does not display a currently valid OMB control number. **PLEASE DO NOT RETURN YOUR FORM TO THE ABOVE ADDRESS.**		
1. REPORT DATE July 2017	**2. REPORT TYPE** **Final**	**3. DATES COVERED** 1May2011 - 30Apr2017
4. TITLE AND SUBTITLE "The Role of Novel Substituted Diindolyl Methane Analogues in the Treatment of Triple-Negative and ErbB2-Positive Breast Cancer"		**5a. CONTRACT NUMBER** **5b. GRANT NUMBER** **W81XWH-11-1-0211** **5c. PROGRAM ELEMENT NUMBER**
6. AUTHOR(S) **Dr. Mandip S. Sachdeva** Email: mandip.sachdeva@famu.edu		**5d. PROJECT NUMBER** **5e. TASK NUMBER** **5f. WORK UNIT NUMBER**
7. PERFORMING ORGANIZATION NAME(S) AND ADDRESS(ES) **Florida A&M University** Tallahassee, FL 32307-3200		**8. PERFORMING ORGANIZATION REPORT**
9. SPONSORING / MONITORING AGENCY NAME(S) AND ADDRESS(ES) U.S. Army Medical Research and Materiel Command Fort Detrick, Maryland 21702-5012		**10. SPONSOR/MONITOR'S ACRONYM(S)** **11. SPONSOR/MONITOR'S NUMBER(S)**
12. DISTRIBUTION / AVAILABILITY STATEMENT Approved for Public Release; Distribution Unlimited		
13. SUPPLEMENTARY NOTES		
14. ABSTRACT The mission of the proposed HBCU/MI Breast Cancer Partnership Training Award at Florida A & M University (FAMU) is to develop a rich intellectual environment that will promote and strengthen the research capabilities of FAMU investigators in the area of breast cancer research. The objectives this proposal are (1) to provide mentorship and training to FAMU researchers in breast cancer research area to enhance the research expertise and competitive ability; (2) to train FAMU investigators through a well defined research project investigating the anticancer potential of C-DIM analogs in treatment of breast cancer; (3) to develop FAMU investigators grantsmanship skills by submitting extramural grants for independent funding; and (4) to create awareness among FAMU researchers and African American Community about breast cancer biology and therapy. The outcome of this proposal will lead to novel oral therapeutic strategies for treatment of triple negative breast cancer (TNBC) and ErbB2-positive breast cancer) EPBC and also result in publications in highly ranked journals. This approach will result in establishment of a successful and independently funded breast cancer research program at FAMU. Our ultimate goal is to become an independent research and training program of excellence for minority investigators		

15. SUBJECT TERMS **Triple negative breast cancers**					
16. SECURITY CLASSIFICATION OF:			**17. LIMITATION**	**18. NUMBER**	**19a. NAME OF RESPONSIBLE PERSON** USAMRMC
a. REPORT U	**b. ABSTRACT** U	**c. THIS PAGE** U	UU	120	**19b. TELEPHONE NUMBER** *(include area code)*

Table of Contents

Page

2. **Section I: A brief introduction covering the purpose and scope of the research effort**

Breast cancer is the second leading cause of cancer-related deaths and approximately 15%-20% of patients are diagnosed with TNBC, which do not express estrogen receptor (ER), progesterone receptor (PR) and human epidermal growth factor receptor 2 (HER2). It is a particularly lethal subtype of breast cancer with a 5-year survival rate as low as 40%. The life expectancy after detection of visceral metastasis in TNBC patients is estimated as 3 to 22 months. The over-expression of ErbB2 (HER2) occurs in approximately 20–25% of all breast tumors and the outcome of current therapies for ErbB2-positive breast cancers (EPBC) remains unsatisfactory due to short intervals to recurrence, short overall survival, resistance and toxic side effects. African American women are 34% more likely to die from breast cancer than white women. The TNBC and EPBC are high risk breast cancers and the choice of orally available chemotherapeutic agents is limited. Hormonal therapy (ER modulators) and HER antibody based therapy are far safer than cytotoxic drug based regimens. But triple negative breast cancers are not responsive to hormonal or HER targeting therapy. Given the challenge in treating TNBC and EPBC and its inherent poor prognosis, the use of novel orally active C-DIM analogues will have major clinical implications for the treatment of breast cancer. Orally administered Diindolyl methane (DIM) analogue DIM-C-pPhC6H5 alone showed potent anticancer activity and also exhibited additive to synergistic anticancer activity in combination with docetaxel (doc). Based on this success, our ultimate objective is to design, synthesize and evaluate the novel orally effective DIM analogues to treat TNBC and EPBC by establishing the breast cancer research program with the support of proposed HBCU/MI Partnership Training Award. The proposed studies will synthesize C-DIM analogs (DIM10 and DIM 12, 14) and investigate the structure-dependent anticancer activities in TNBC and EPBCusing both cell and laboratory animal models. Our hypothesis is that the novel C-DIM analogues will show potent anticancer activity against TNBC and EPBC and the use of C-DIM analogues could be a novel approach for the treatment of breast cancer. Moreover, evaluation of anticancer efficacy of DIM loaded tumor targeted nanoparticles in TNBC patient derived tumorgrafts(PDX) could be helpful in understanding its clinical outcome.

3. **Section II: Research Accomplishments**
Comprehensive Summary of the Project:

A. Initially we synthesized two C-DIM analogues C-DIM-5 and C-DIM-8, these compounds were synthesized based on the previous methods from Dr. Safe's lab. The invitro anticancer effects were significant as shown in **Fig 1-3 and Table 1**. Further, based on observations from Dr. Safe's laboratory that C-DIM-10 & C-DIM-14 inactivated pro-oncogenic TR3 in pancreatic cancer, we synthesized C-DIM-10 and C-DIM-14 analogues. These compounds were evaluated for in vitro anticancer activity in TNBC (MDA-MB-468, MDA-MB-231 and MDA-MB-453) and EPBC (BT474 and SKBR3) cells. We found that these compounds inhibited growth of both breast cancer types and their IC_{50} values for these compounds were ranged from 8-18 µM(Fig 4-6 and Table 2-3). The clonogenic assay with C-DIM-10 and 14 showed significant inhibition of colony formation in all the cells types used in the study at 3, 10 and 20 µM concentrations. Cell cycle analysis showed C-DIM induced cell cycle arrest at G1 phase and Annexin-V staining confirmed that C-DIM10 and C-DIM-14 induced apoptosis these cells(**Publication 1**)

In the cell migration assay both DIM-10 and 14 inhibited breast cancer cell migration effects and both compounds were more effective against EPBC compared to TNBC type. DIM-10 was more potential that to DIM-14 in most of these responses.

B. The solubility of the novel C-DIMs was found to be very poor (<1 µg/ml). It is expected that due to poor water solubility the oral bioavailability of these compounds would be low. Caco-2 and PAMPA permeability studies also indicated very low oral bioavailability of DIM-10 and 14.

C. Pharmacokinetic studies with DIM-10 and DIM-14 suggested that due to poor oral aqueous solubility, these compounds have limited oral bioavailability. To improve oral bioavailability novel oral nanoparticle based formulations were prepared and their Pharmacokinetic and Pharmacodynamic effects were studied. The nanostructured lipid carrier (NLC) containing DIM-10 resulted in the significant increase in the oral bioavailability and anticancer effects in MDA-231 orthotopic TNBC model. The micellar form of DIM-14 also exhibited improved pharmacokinetic profile and significant increase in the anticancer effects(publications(**Publication 2-3**).

D. The combination treatment of DIM-10 with standard anticancer drug Doxorubicin produced additive anticancer effects while reducing the Doxorubicin induced cardiotoxicity. The combination treatment of DIM-10 with Telmisartan resulted in significant increase in the anticancer effects in TNBC animal models compared to individual treatment with either DIM-10 or Telmisartan(Fig 6-9, Publications 4-5).

E. Our abstract presented during the AAPS annual meeting at Chicago October 14-18th, 2012 was selected for the media highlight and public outreach. Only 10 abstracts were chosen for this meeting from various areas of research and our was one of those. The importance of this work has been published in several news channels worldwide, few of those channels are Eureka Alert, Yahoo news, Science Daily news etc.

The media highlight was on various web sites and some examples are:
http://www.aaps.org/news.aspx
http://www.eurekalert.org/emb_releases/2012-10/aaop-sfv101112.php
http://www.naturalnews.com/032410_parsley_tumors.html
http://www.naturalnews.com/029204_broccoli_cancer_cells.html

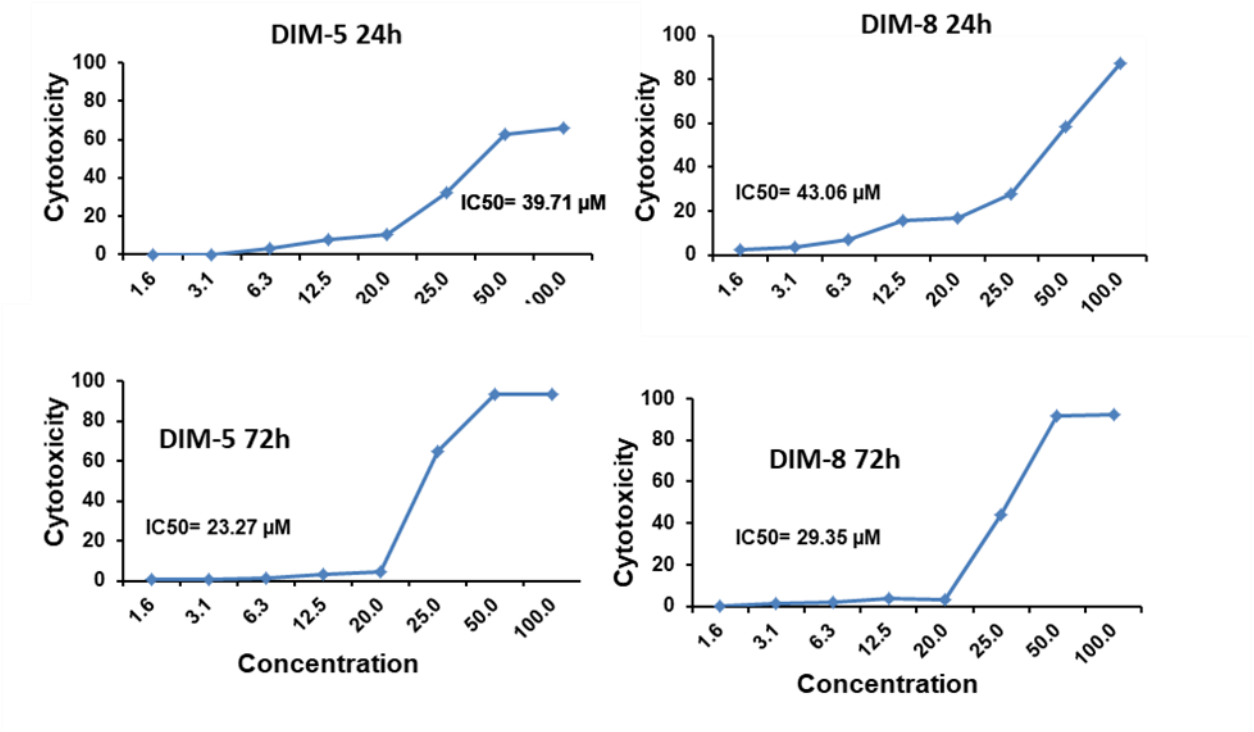

Figure 1: Cytotoxicity data of DIM-5 and 8 on SKBR3 cancer cells.

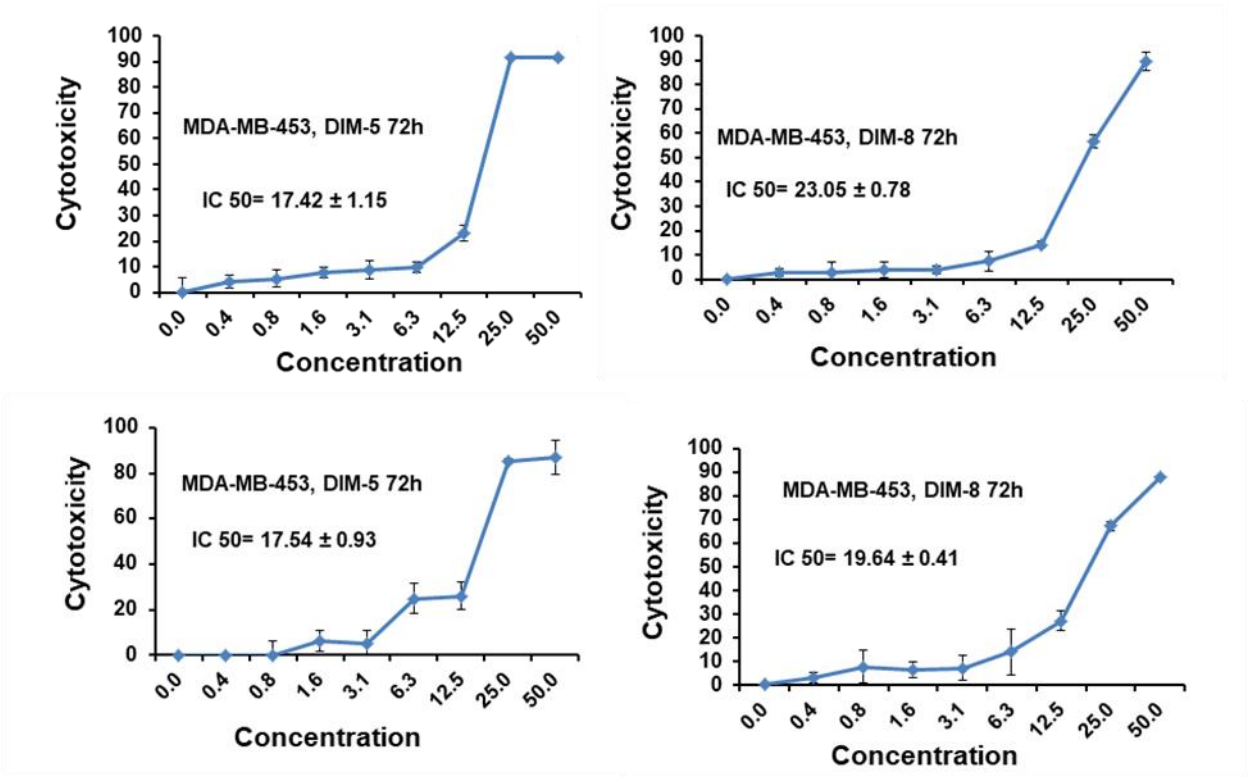

Figure 2: Cytotoxicity data of DIM-5 and 8 on TNBCs (MDA-MB-231 and MDA-MB-453)

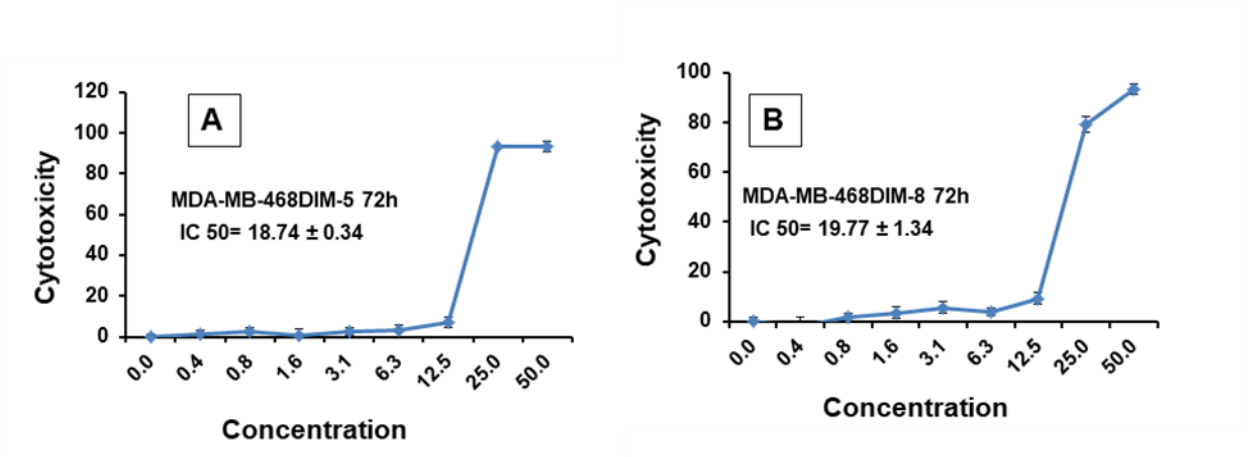

Comparative IC_{50} values at 72h C

	IC_{50} Values (µM) at 72h			
Cell Type	SKBR3	MDA-MB-468	MDA-MB-453	MDA-MB-231
DIM-5	23.27	18.74	17.54	17.42
DIM-8	29.35	19.77	19.64	23.05

Figure 3 and Table 1: Cytotoxicity data of DIM-5 and 8 on TNBCs (MDA-MB-468 and comparative IC_{50} values of DIM-5 and 8 on breast cancer cells at 72 h post treatment.

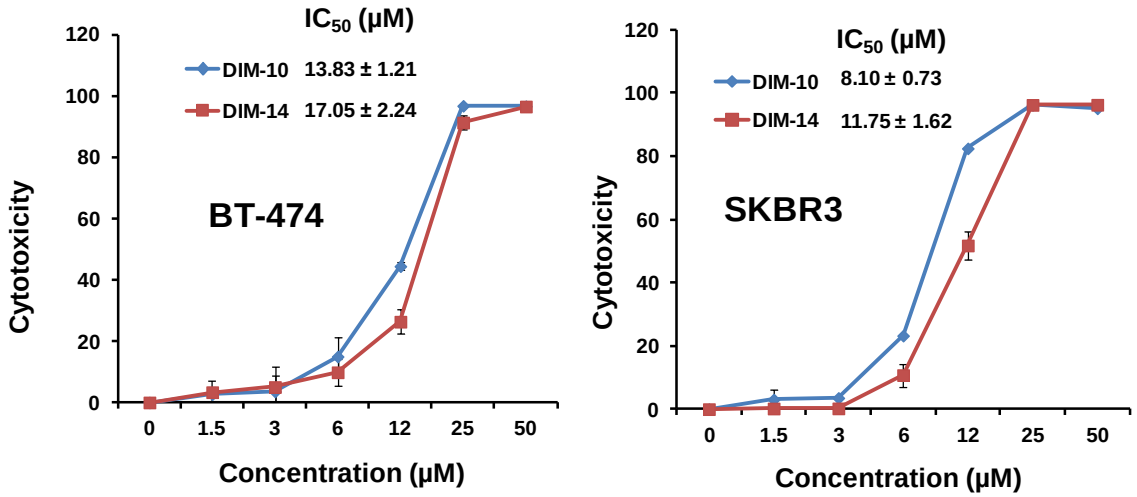

Figure 4: Cytotoxicity data of DIM-10 and 14 on EPBC breast (BT 474 and SKBR3) cancer cells.

HER positive cells	IC50 (μM)	
Cell Type	**DIM-10**	**DIM-14**
BT-474	13.83 ± 1.21	17.05 ± 2.24
SKBR3	8.10 ± 0.73	11.75 ± 1.62

Table 2: comparative IC_{50} values of DIM-10 and 14 on EPBC breast cancer cells (BT474 and SKBR3) at 72 h post treatment. Each data point is represented as mean ± SEM (n=6). Each experiment repeated 3 times.

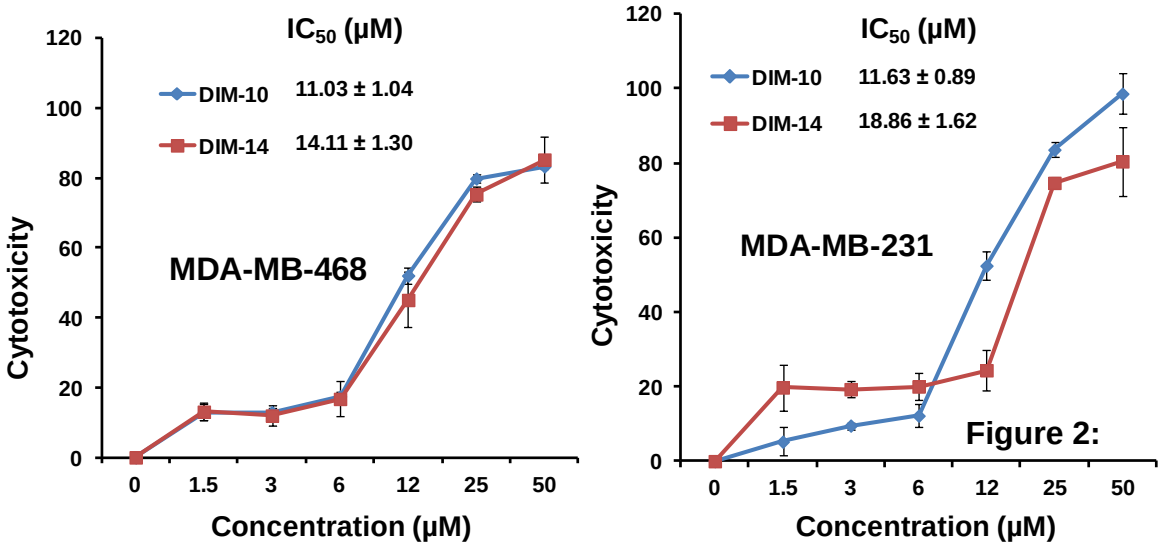

Fig. 5. Cytotoxicity data of DIM-10 and 14 on TNBCs (MDA-MB-468 and MDA-MB-231) cancer cells. Each data point is represented as mean ± SEM (n=6). Each experiment repeated 3 times.

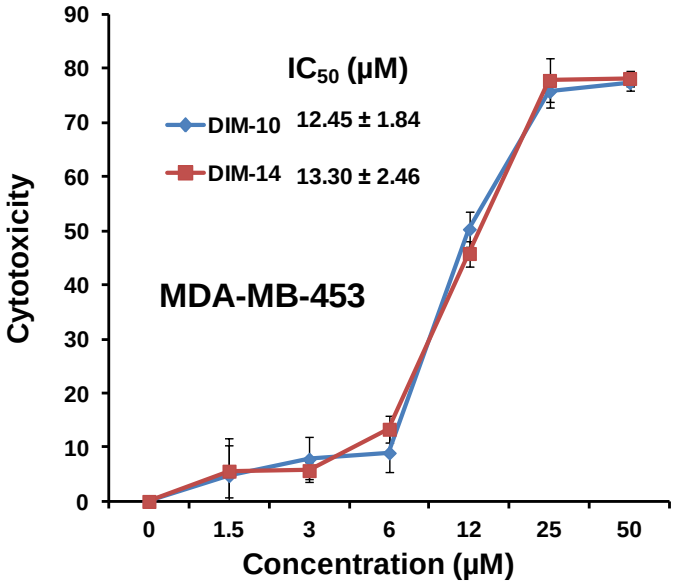

TNBC cells	IC50 (μM)	
Cell Type	DIM-10	DIM-14
MDA-MB-468	11.03 ± 1.04	14.11 ± 1.30
MDA-MB-231	11.63 ± 0.89	18.86 ± 1.62
MDA-MB-453	12.45 ± 1.84	13.30 ± 2.46

Figure 6 and Table 3: Cytotoxicity data of DIM-10 and 14 on TNBCs (MDA-MB-453 and comparative IC_{50} values of DIM-10 and 14 on TNBC breast cancer cells at 72 h post treatment. Each data point is represented as mean ± SEM (n=6). Each experiment repeated 3 times.

Anticancer evaluation in breast cancer models:

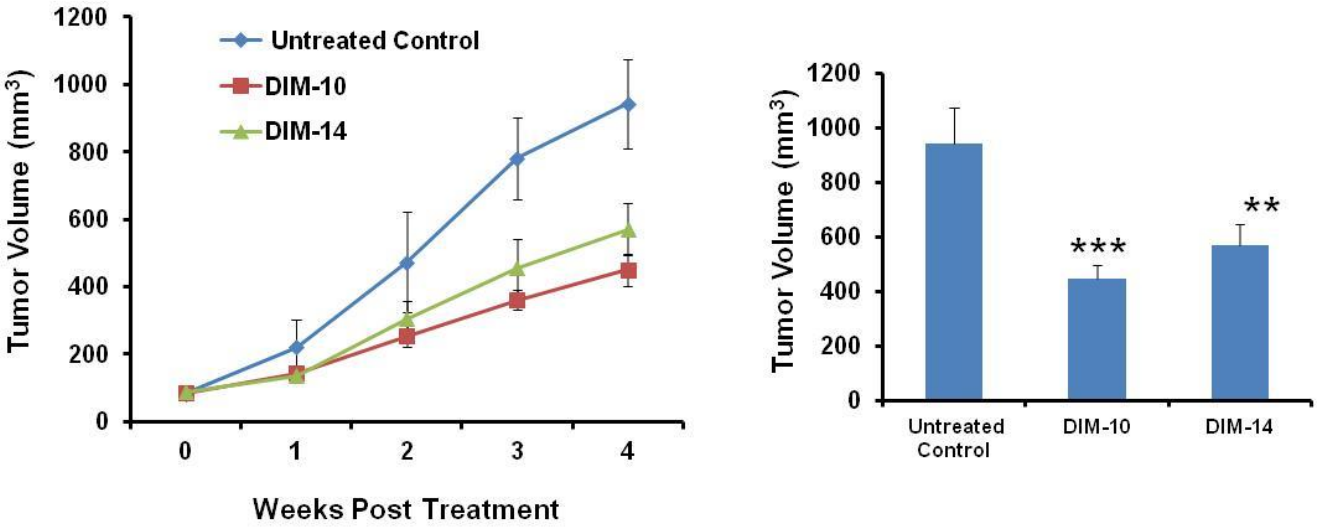

Figure 7: Effect of DIM-10 and DIM-14 (30 mg/kg/ daily) on tumor progression in MDA-MB-231 TNBC model. Each data point is represented as mean±sem (n=6-7). ***P<0.001, ** P<0.01 Vs control

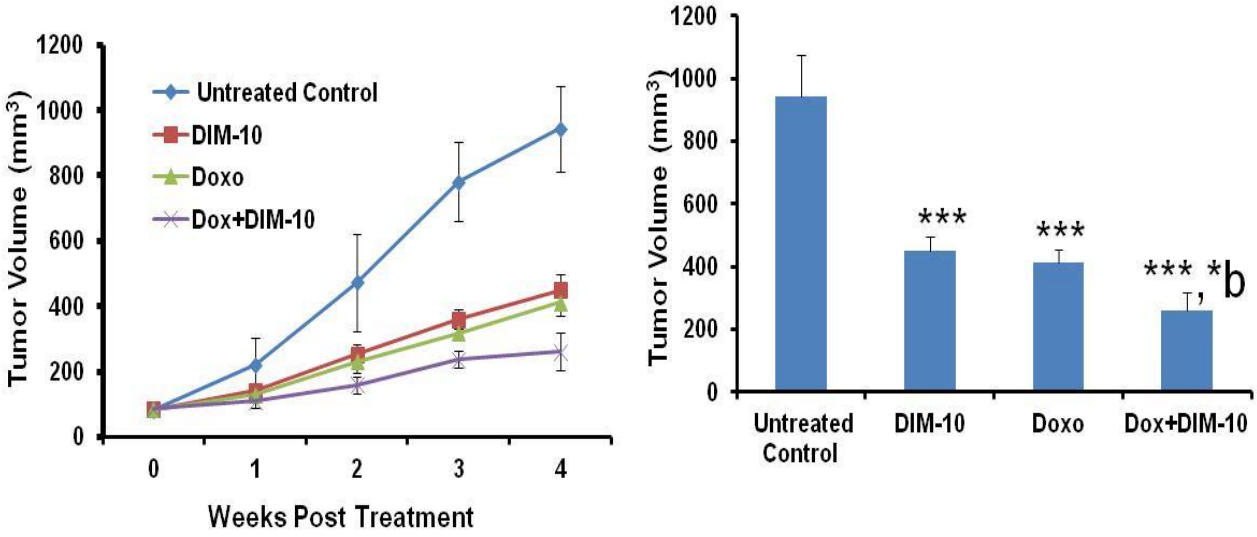

Figure 8: Effect of DIM-10 (30/mg/kg/ day, oral), Doxorubicin (5 mg/kg/week, iv), and DIM-10+Doxo (30 mg/kg/ day and 5 mg/kg iv) on tumor progression in MDA-MB-231 TNBC model. Each data point is represented as mean ± sem (n=6-7). ***P<0.001 Vs control and B Vs TEL and DIM-10.

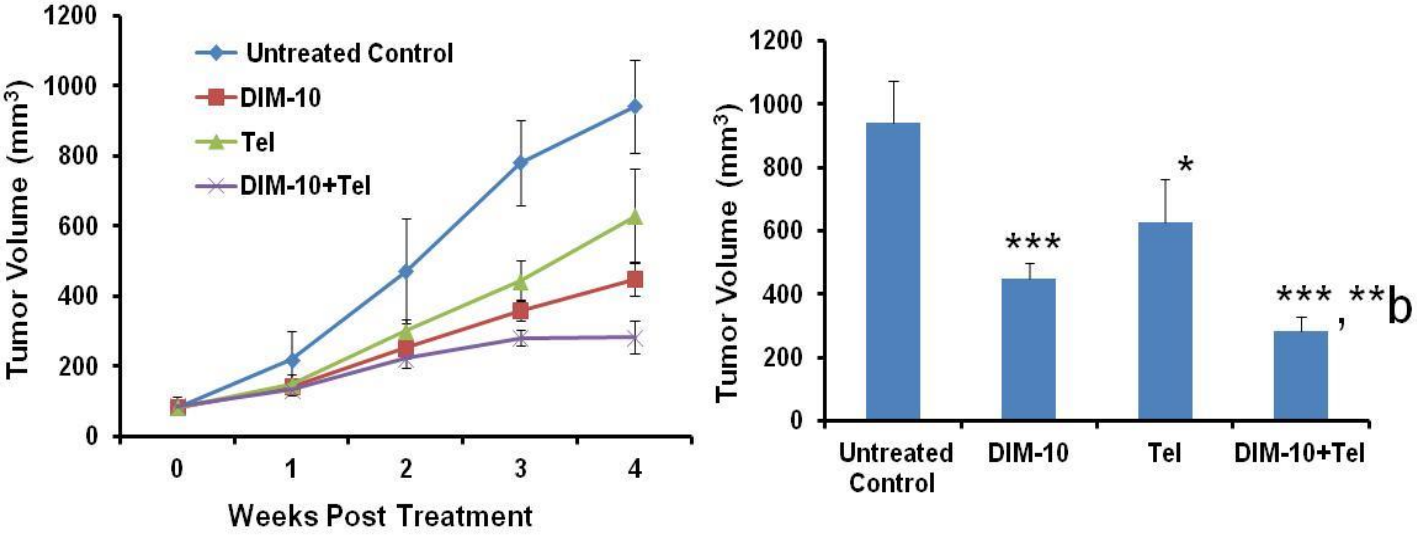

Figure 9: Effect of DIM-10 (30/mg/kg/ day, oral), Telmisartan (10 mg/kg/day, oral) on tumor progression in MDA-MB-231 TNBC model. Each data point is represented as mean ± sem (n=6-7). ***P<0.001,**P<0.01 Vs control and B Vs TEL

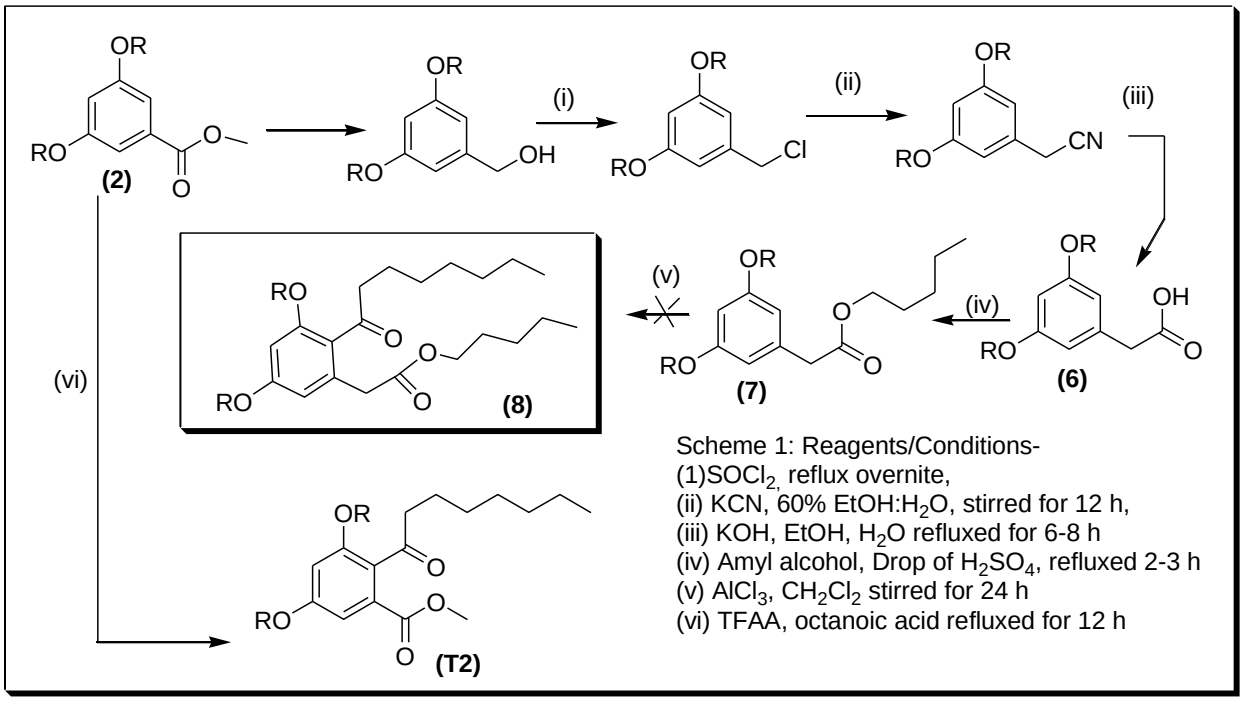

F. The novel role of DIM as an orphan nuclear receptor 4A1 (NR4A1) antagonist was explored in TNBC. NR4A1 is overexpressed in mammary tumors and transfection of MDA-MB-231 breast cancer cells with siNR4A1 decreased cell proliferation and induced apoptosis. NR4A1 binds and inactivates p53 and knockdown of NR4A1 or treatment of p53 wild-type lung cancer cells with an NR4A1 antagonist or transfection with siNR4A1 results in activation of p53 and induction of sestrin 2 which activates AMPKα and inhibits the mTOR pathway (Figure 1).

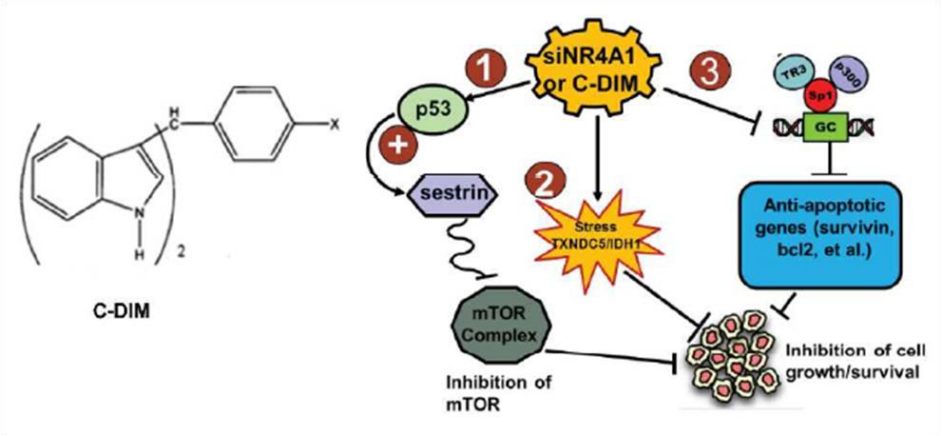

Figure 10. NR4A1-regulated pathways and effects of NR4A1 knockdown on breast cancer cell proliferation. NR4A1-regulated pathways/genes that can be targeted by C-DIM/NR4A1 antagonists.

Both the DIM derivatives showed significant reduction in tumor weight and volume in MDA-MB-231 orthotopic tumor bearing mice (Figure 11). Effects of C-DIM/NR4A1 antagonists were comparable to that observed after NR4A1 knockdown. The C-DIM compounds with a p-carboxymethylpenyl group (DIM-C-pPhCO2Me) and cyano substitutent (DIM-C-pPhCN) have been identified as NR4A1 antagonists. After knockdown of NR4A1 in these cells, treatment with DIM-C-pPhCO2Me resulted in only minimal growth inhibition confirming a role for NR4A1 in mediating the growth inhibitory effects of DIM-C-pPhCO2Me (Figure 12A). Treatment of MDA-MB-231 cells with DIM-C-pPhCO2Me also increased ROS after 12 and 24 hr (Figure 12B) and this was also accompanied by decreased expression of TXNDC5 and IDH1 and induction of markers of ER stress (p-PERK, ATF4, CHOP and XBP-1s). Treatment of the cells with DIM-C-pPhCO2Me for 24 hr induced cleavage (activation) of caspases 7 and 8 and PARP (Figure 4A) and enhanced annexin V staining in MCF-7 (Figure 12C) and similar results were observed for the p-cyanophenyl compound (DIM-C-pPhCN). The NR4A1 antagonist DIM-C-pPhCN also inhibited the mTOR pathway. siNR4A1 or treatment with DIM-C-pPhCO_2Me decreased expression of survivin, bcl2 and EGFR in MDA-MB-231. Reduction in the expression of same markers was observed in *in vivo* anticancer studies in MDA-MB-231 xenograft solid tumor bearing athymic nude mice (Figure 13B and 13C). DIM-C-pPhCO_2Me and siNR4A1 also

induced sestrin 2 and inhibited mTOR in p53 mutant SKBR3 and MDA-MB-231 cells and the mechanisms of this response was also investigated (Publication **6**).

.

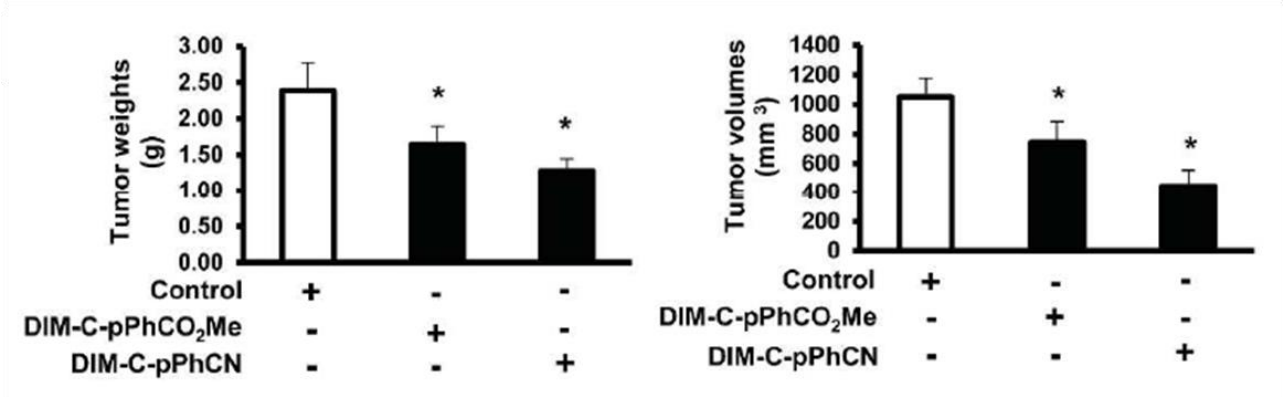

Figure 11. Athymic nude mice bearing MDA-MB-231 cells (orthotopic) were administered corn oil (control), DIM-C-pPhCO$_2$Me or DIM-C-pPhCN (50 mg/kg d) by oral gavage for 28 days, and effects on tumor growth and weight were determined (* significantly decreased; $p<0.01$).

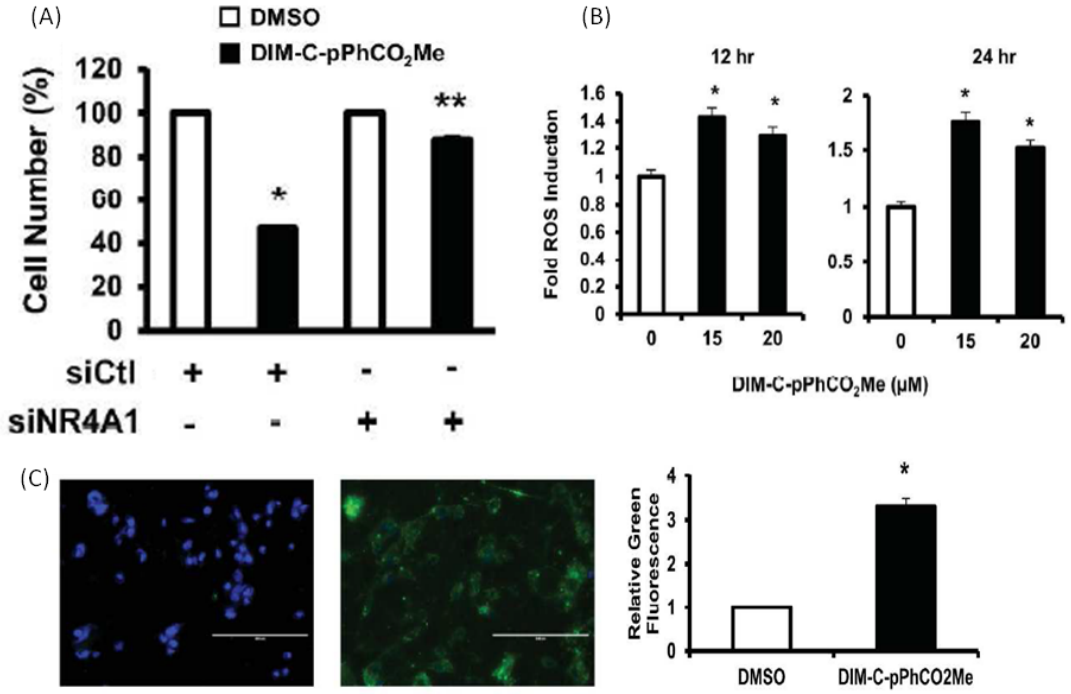

Figure 12. (A) NR4A1-regulated pathways and effects of NR4A1 knockdown on breast cancer cell proliferation. Cells were transfected with siCtl (non-specific oligonucleotide) or siNR4A1 and then treated with 20 μM DIM-C-pPhCO$_2$Me for 24 hr and the number of cells were then counted. (B) DIM-C-pPhCO$_2$Me induces ROS and stress. Cells were treated with DIM-C-pPhCO$_2$Me and

ROS was determined after 12 or 24 hr. (C) DIM-C-pPhCO$_2$Me induces apoptosis in cells were treated with DIM-C-pPhCO$_2$Me for 24 hr. Annexin V staining

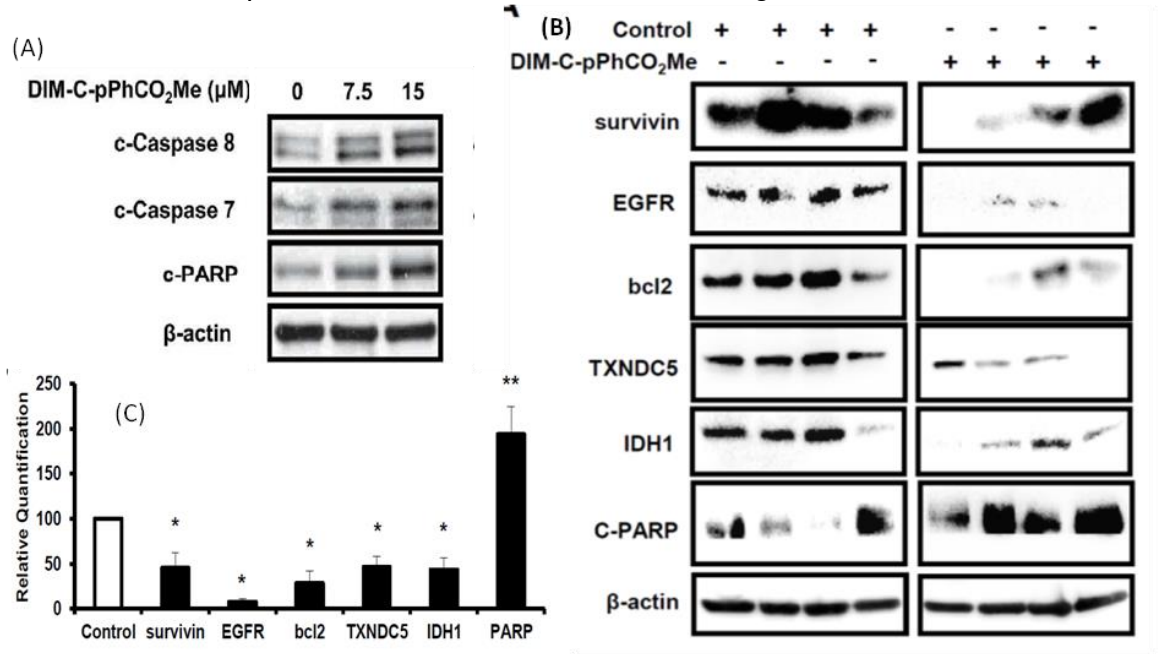

Figure 13. (A) DIM-C-pPhCO$_2$Me induces apoptosis in cells were treated with DIM-C-pPhCO$_2$Me for 24 hr. Whole cell lysates were analyzed by western blots (B) Effects of NR4A1 antagonists on selected gene product expression in tumors. Orthotopic tumors in athymic nude mice bearing MDA-MB-231 cells were treated with DIM-C-pPhCO2Me (50 mg/kg/d) or vehicle (control) for 28 days. Lysates from tumors from control and DIM-C-pPhCO2Me-treated mice were analyzed by western blots and (C) bands were quantitated and normalized relative to β-actin.

G. We prepared the liposomes containing DIM and also conjugated them to CREKA peptide. We also evaluated them in vitro models and cell lines already in our laboratory. We also developed a doxorubicin(DOX) resistant MDA-MB231 cell lines in the laboratory since the PDX model did not work very well. The DOX resistant cell line was then used for animal model studies. We also showed in vitro that our formulation induces apoptosis in this cell line.

Acridine orange apoptosis assay MDA-MB-231/DOX resistant cells were plated in 96-well tissue culture plate, at a density of 1x10^4 cells/well and allowed to incubate overnight and were treated with 10 µg/ml of DIM-10 in DMEM media from stock solution in DMSO. After 24 h of DIM-10 exposure, cells were washed with PBS and incubated with acridine orange/ethidium bromide for 30 mins. Fluorescent microscopic images were captured for evaluating apoptosis. A dose response effect was seen.

Anticancer efficacy studies:

Balb/c nu/nu mice were injected with 2 million Doxorubicin resistant tumor cells in mammary fat pad. After 14 days, animals were randomly divided into four groups (Saline solution, DIM-10 solution, DPL and CDPL) of 10 animals each. Treatment were started on 15th day of cell inoculation. DIM-10 solution and formulations equivalent to 10 mg/kg DIM-10 were administered by tail vein. Treatment was given every other day for 2 weeks. Animals were sacrificed, 3 days after the last dose of DIM-10. Tumor volume was measured and tumors were used for immunohistochemistry (IHC) and western blot analysis. Our results in Fig 2 show that targeted liposomes containing DIM were the most potent($p<0.01$) in tumor regression as compared to all other formulations(**Publication 7 and 8**).

Fig 14. Orthotopic xenograft DOX resistant triple negative breast tumor bearing animals treated with intravenous DIM10 formulation(10mg/kg) showed significant reduction in average breast tumor volume compared to control group. DPL= DIM Liposomes, CDPL: CREKA peptide conjugated DIM liposomes.

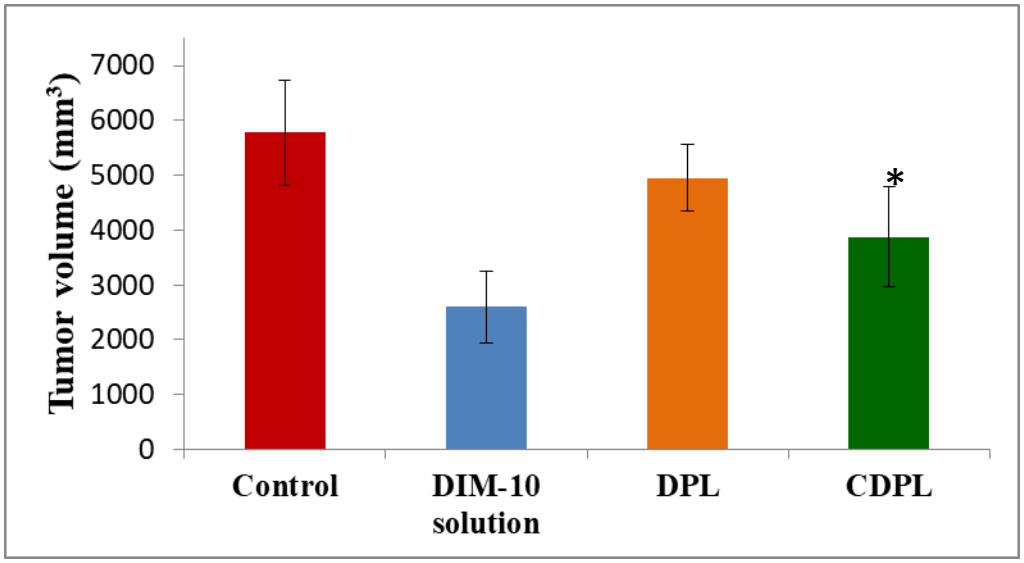

Collaboration and training:

a) Several post-doctoral fellows and students have been trained through this proposal. For example Chandu Godugu, Ketan Patel, Imran Vohra, Arindam Mondal, Ravi Doddapeneni are some of the post-doctoral fellows who have been trained on this project. Also graduate students Ebony Nottingham, Cedar Boakye, Arvind Bagde were all trained through this project. Cedar Boakye has graduated with a Ph.D and is currently a reviewer at FDA. Chandu Godugu is an Assistant Professor in NIPER Hyderabad and Ketan Patel is an Assistant Professor in St. John, College of Pharmacy. Ravi Doddapeneni is a Senior Scientist at the University of Miami.

b) PI has also been able to find new collaborations with Dr. Arun Rishi from Wayne State University. Collaboration with Dr. Stephen Safe also led to new projects and publications.

Section III: Problem Areas
Currently there are no problem areas
Section IV: A description of work to be performed during the next reporting period.
This is the final report. At this point we are trying to finish all the manuscripts

Section V: Administrative Comments (Optional) - Description of proposed site visits

and participation in technical meetings, journal manuscripts in preparation,

coordination with other organizations conducting related work, etc.

Presentations:

1. Novel diindolylmethane derivatives inhibit Triple negative breast cancer (TNBC) and ErbB2-positive breast cancer (EPBC). Presented at AAPS meeting, 2012.
   This Research work was selected for the media coverage in AAPS annual meeting, Chicago October 14-18th, 2012. Our work was covered in various news sites like Eureka Alert, Yahoo news, Science Daily news etc.

2. April Prather, Chandraiah Godugu, Apurva R. Patel, Stephen Safe, Mandip Sachdeva, Anticancer Effects of Novel Diindolylmethane Derivatives in Triple Negative Breast Cancer (TNBC) and ErbB2-Positive Breast Cancer (EPBC) Types, MBRS feeder conference, FAMU, 2012 (Won first prize $300).

3. Chandraiah Godugu, Apurva R Patel, Ravi Doddapaneni, Srujan Marepallly, Mandip Singh Sachdeva and Mahavir Chougule. Effect of telmisartan on triple negative breast cancer (TNBC) and lung cancer tumor progression and intratumoral distribution of nanoparticles. Presented at the AACR meeting in washington DC, 2013

4. Jaganmohan Somagoni, Chandraiah Godugu, Ravi Doddapaneni, Stephen H Safe and **Mandip Singh**. Treatment of pulmonary arterial hypertension by the use of a novel PPAR gamma agonist, diindolylmethane in a nanoparticle formulation. American Association of Pharmaceutical Science (AAPS) Annual Meeting & Exposition 2014, San Diego, CA.

5. Ketan Patel, Stephen Safe and Mandip Singh. 'Fibrin binding peptide anchored, Diindolylmethane derivative loaded liposomes for overcoming doxorubicin resistance in triple negative breast cancer. Presented at the AAPS meeting in Denver, Colorado, 2016.

Publications:

1. Hedrick, S.O. Lee, R. Doddapaneni, **M. Singh**, S. Safe, Nuclear receptor 4A1 as a drug target for breast cancer chemotherapy, Endocrine-related cancer, 22 (2015) 831-840. **Both Mandip Singh and Stephen Safe are corresponding authors in this paper.**
2. T. Andey, G. Sudhakar, S. Marepally, A. Patel, R. Banerjee, **M. Singh**, Lipid nanocarriers of a lipid-conjugated estrogenic derivative inhibit tumor growth and enhance cisplatin activity against triple-negative breast cancer: pharmacokinetic and efficacy evaluation, Molecular pharmaceutics, 12 (2015) 1105-1120.
3. A.R. Patel, R. Doddapaneni, T. Andey, H. Wilson, S. Safe, **M. Singh**, Evaluation of self-emulsified DIM-14 in dogs for oral bioavailability and in Nu/nu mice bearing stem cell lung tumor models for anticancer activity, Journal of controlled release : official journal of the Controlled Release Society, 213 (2015) 18-26.
4. R. Doddapaneni, K. Patel, I.H. Owaid, **M. Singh**, Tumor neovasculature-targeted cationic PEGylated liposomes of gambogic acid for the treatment of triple-negative breast cancer, Drug delivery, 23 (2016) 1232-1241.
5. K. Patel, R. Doddapaneni, N. Chowdhury, C.H. Boakye, G. Behl, **M. Singh**, Tumor stromal disrupting agent enhances the anticancer efficacy of docetaxel loaded PEGylated liposomes in lung cancer, Nanomedicine, 11 (2016) 1377-1392.
6. E. Hedrick, S.O. Lee, R. Doddapaneni, **M. Singh**, S. Safe, NR4A1 Antagonists Inhibit beta1-Integrin-Dependent Breast Cancer Cell Migration, Molecular and cellular biology, 36 (2016) 1383-1394.
7. C. Godugu, R. Doddapaneni, S.H. Safe, **M. Singh**, Novel diindolylmethane derivatives based NLC formulations to improve the oral bioavailability and anticancer effects in triple negative breast cancer, European journal of pharmaceutics and biopharmaceutics : official journal of Arbeitsgemeinschaft fur Pharmazeutische Verfahrenstechnik e.V, 108 (2016) 168-179.
8. N. Chowdhury, I. Vhora, K. Patel, R. Doddapaneni, A. Mondal, **M. Singh**, Liposomes co-Loaded with 6-Phosphofructo-2-Kinase/Fructose-2, 6-Biphosphatase 3 (PFKFB3) shRNA Plasmid and Docetaxel for the Treatment of non-small Cell Lung Cancer, Pharmaceutical research, 34 (2017) 2371-2384.

1. **References**
2. **Appendices**

Copies of publications are attached with the document.

Nuclear receptor 4A1 as a drug target for breast cancer chemotherapy

Erik Hedrick, Syng-Ook Lee[1], Ravi Doddapaneni[2], Mandip Singh[2] and Stephen Safe

Department of Veterinary Physiology and Pharmacology, Texas A&M University, 4466 TAMU, College Station, Texas 77843-4466, USA
[1]Department of Food Science and Technology, Keimyung University, Daegu 704701, Republic of Korea
[2]Department of Pharmaceutics, College of Pharmacy and Pharmaceutical Sciences, Florida A&M University, Tallahassee, Florida 32307, USA

Correspondence should be addressed to S Safe or M Singh
Emails
ssafe@cvm.tamu.edu or mandip.sacheva@gmail.com

Abstract

The orphan nuclear receptor 4A1 (NR4A1) is overexpressed in mammary tumors and breast cancer cell lines. The functional activity of this receptor was investigated by RNA interference with oligonucleotides targeted to NR4A1 (siNR4A1) and by treatment with NR4A1 antagonists. Breast cancer cells were treated with NR4A1 antagonists or transfected with siNR4A. Effects on cell proliferation and apoptosis as well as specific genes associated with these responses were investigated in MCF-7, SKBR3, and MDA-MB-231 cells, and in athymic nude mice bearing MDA-MB-231 cells as xenografts. Transfection of MCF-7, MDA-MB-231, and SKBR3 breast cancer cells with siNR4A1 decreased cell proliferation and induced apoptosis in these cell lines. Transfection of breast cancer cells with siNR4A1 also decreased expression of Sp-regulated genes including *survivin*, *bcl-2*, and epidermal growth factor receptor, inhibited mTOR signaling in MCF-7 cells that express WT p53, and activated oxidative and endoplasmic reticulum stress through downregulation of thioredoxin domain-containing 5 and isocitrate dehydrogenase 1. 1,1-*Bis*(3′-indolyl)-1-(*p*-substituted phenyl)methanes (C-DIMs) are NR4A1 ligands that act as NR4A1 antagonists. Treatment with selected analogs also inhibited breast cancer cell and tumor growth and induced apoptosis. The effects of C-DIM/NR4A1 antagonists were comparable to those observed after NR4A1 knockdown. Results with siNR4A1 or C-DIMs/NR4A1 antagonists in breast cancer cells and tumors were similar to those previously reported in pancreatic, lung, and colon cancer cells. They demonstrate the potential clinical applications of NR4A1 antagonists in patients with tumors that overexpress this receptor.

Key Words
- NR4A1
- indole derivative
- antagonists

Endocrine-Related Cancer (2015) **22**, 831–840

Introduction

Nuclear receptor 4A1 (NR4A1, Nur77, TR3) is a member of the NR4A orphan receptor sub-family of nuclear receptors. NR4A receptors (NR4A1, NR4A2, and NR4A3) play essential roles in metabolic processes, inflammation, vascular function, steroidogenesis, and the CNS (Maxwell & Muscat 2006, Pearen & Muscat 2010, Lee *et al.* 2011). NR4A1 is overexpressed in multiple tumors and cancer cell lines. Results of receptor knockdown by RNA interference (RNAi) demonstrate that in solid tumors the receptor is pro-oncogenic and regulates cell growth and survival (Uemura & Chang 1998,

http://erc.endocrinology-journals.org
DOI: 10.1530/ERC-15-0063

Published by Bioscientifica Ltd.

Bras *et al*. 2000, Kolluri *et al*. 2003, Zeng *et al*. 2006, Lee *et al*. 2010, 2011, 2012, 2014*a*, Wu *et al*. 2011). Several pro-apoptotic agents including phorbol esters and adamantyl-derived retinoids induce expression and nuclear export of NR4A1 which subsequently binds mitochondrial bcl-2 to form a pro-apoptotic complex that decreases mitochondrial membrane potential (Li *et al*. 2000, Lin *et al*. 2004, Zhang 2007). This has led to the development of peptide mimics that convert bcl-2 into an apoptotic complex; similar results have been reported for the taxane-derived anticancer agent paclitaxel (Kolluri *et al*. 2008, Ferlini *et al*. 2009). Cytosporone B and related analogs have been identified as ligands for NR4A1 (Zhan *et al*. 2008, Liu *et al*. 2010), and two additional compounds, (ethyl 2-(2,3,4-trimethoxy-6-(1-oct-anoyl)phenyl)acetate and 1-(3,4,5-trihydroxyphenyl) no-nan-1-one), also bind NR4A1 (Zhan *et al*. 2012, Wang *et al*. 2014). Ethyl 2-(2,3,4-trimethoxy-6-(1-oct-anoyl) phenyl)acetate inactivates nuclear NR4A1, whereas 1-(3,4,5-trihydroxyphenyl)no-nan-1-one and cytosporone B induce nuclear export of NR4A1.

Studies in this laboratory have been investigating a series of 1,1-*bis*(3′-indolyl)-1-(*p*-substituted phenyl) methane (C-DIM) analogs and their effects on NR4A1 and NR4A1-dependent transactivation (Chintharlapalli *et al*. 2005, Lee *et al*. 2009, 2010, 2012, 2014*a*,*b*, Cho *et al*. 2010). Since NR4A1 exhibits pro-oncogenic activity, we have been focused on the identification of C-DIMs that inactivate NR4A1. The *p*-hydroxyphenyl analog (DIM-C-pPhOH) was characterized as a compound that inactivated nuclear NR4A1 in cancer cell lines but this was not accompanied by nuclear export of NR4A1 (Lee *et al*. 2010, 2012, 2014*a*). Subsequent studies comparing the effects of DIM-C-pPhOH and knockdown of NR4A1 (siNR4A1) by RNAi identified three major pro-oncogenic pathways and associated genes regulated by NR4A1 that were inhibited by DIM-C-pPhOH: i) NR4A1 regulates expression of genes such as survivin through interactions with specificity protein 1 (Sp1) bound to their proximal GC-rich promoters (Lee *et al*. 2010); ii) NR4A1 inactivates p53 to enhance mTOR signaling in lung and colon cancer cells expressing WT p53 (Lee *et al*. 2012, 2014*b*); and iii) NR4A1 regulates expression of thioredoxin domain-containing 5 (TXNDC5) and isocitrate dehydrogenase 1 (IDH1) to maintain low levels of oxidative stress (Lee *et al*. 2014*a*; Fig. 1A).

Recent studies show that NR4A1 is overexpressed in ER-positive and ER-negative breast tumors (Muscat *et al*. 2013). NR4A1 expression in breast tumors is correlated with decreased relapse-free survival (Zhou *et al*. 2014). Results of NR4A1 overexpression in breast cancer cells suggest that NR4A1 may be anti-migratory (Alexopoulou

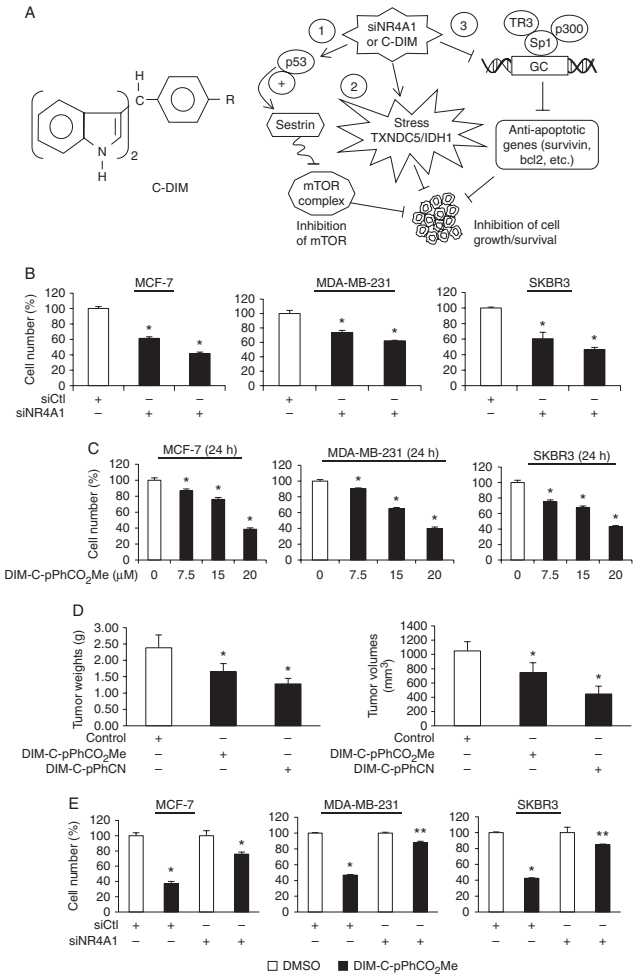

Figure 1
NR4A1-regulated pathways and effects of NR4A1 knockdown on breast cancer cell proliferation. (A) NR4A1-regulated pathways/genes that can be targeted by C-DIM/NR4A1 antagonists. (B) Cells were transfected with two siNR4A1 oligonucleotides (1 and 2) and cell numbers were determined after 72 h. (C) Cells were treated with different concentrations of DIM-C-pPhCO$_2$Me for 24 h and the number of cells were then determined. (D) Athymic nude mice bearing MDA-MB-231 cells (orthotopic) were administered corn oil (control), DIM-C-pPhCO$_2$Me or DIM-C-pPhCN (50 mg/kg per day) by oral gavage for 28 days, and effects on tumor growth and weight were determined (significantly decreased; *$P<0.01$). (E) Cells were transfected with siCtl (non-specific oligonucleotide) or siNR4A1 and then treated with 20 μM DIM-C-pPhCO$_2$Me for 24 h and the number of cells were then counted. The control (untreated) groups (set at 100%) in studies on the growth inhibitory effects of C-DIMs after knockdown are cells transfected with siNR4A1 and treated with DMSO. Results (B, C and D) are means ± S.E.M. for at least three separate determinations for each treatment group. Significant ($P<0.05$) growth inhibition is indicated (*) and a significant decrease in the growth inhibitory effects of DIM-C-pPhCO$_2$Me after NR4A1 knockdown is also indicated (**).

et al. 2010). However, a recent study reported pro-migratory activity for this receptor (Zhou *et al*. 2014). Research in this laboratory has demonstrated pro-oncogenic functions of NR4A1 in pancreatic, colon, and lung cancer cells. This

http://erc.endocrinology-journals.org
DOI: 10.1530/ERC-15-0063

Published by Bioscientifica Ltd.

study investigates the functions of this receptor in breast cancer cells and the effects of C-DIM/NR4A1 antagonists. The results clearly demonstrate the pro-oncogenic functions of NR4A1 in breast cancer and also demonstrate that C-DIM/NR4A1 antagonists represent a potential novel approach for treating breast cancer patients that over-express this orphan receptor.

Materials and methods

Cell lines and antibodies

MCF-7, MDA-MB-231, and SKBR3 human breast cancer cell lines were purchased from American Type Culture Collection (Manassas, VA, USA) and were kept frozen until initiation of these studies. The cells were received at low passage (<15) and new frozen stocks were used every 6–8 weeks. The three cell lines were authenticated by Biosynthesis (Lewisville, TX, USA) on 3rd February 2015. Cells were maintained at 37 °C in the presence of 5% CO_2 in DMEM/Ham's F-12 medium with 10% fetal bovine serum with antibiotic. β-actin antibody and DMEM were purchased from Sigma–Aldrich. Sp1 antibody was purchased from Millipore (Temecula, CA, USA). Caspases 7 and 8, sestrin 2 (SESN2), bcl2, CHOP, ATF4, IDH1, IRE, ATF6, GRP78, and epidermal growth factor receptor (EGFR) antibodies were purchased from Santa Cruz Biotechnologies. Caspase 3, cleaved poly ADP ribose polymerase (c-PARP; 9541), phospho mTOR, mTOR, phospho AMPKα, AMPKα, phospho p70S6K, p70S6K, phospho S6RP, S6RP, phospho 4EBP1, 4EBP1, and survivin antibodies were purchased from Cell Signaling Technologies (Danvers, MA, USA). TXNDC5 antibody was purchased from Genetex (Irvine, CA, USA). XBP-1s and phospho PERK were obtained from Biolegend (San Diego, CA, USA). The Apoptotic, Necrotic, and Healthy Cells Quantification Kit was purchased from Biotium (Hayward, CA, USA). Cells were visualized under an EVOS fl, Fluorescence microscope, from Advanced Microscopy Group using a multiband filter set for FITC, rhodamine, and DAPI. The C-DIM compounds were prepared and immunostaining for NR4A1 was carried out as previously described (Lee *et al*. 2010, 2012, 2014*a*).

Cell proliferation assay

MCF-7, MDA-MB-231, and SKBR3 breast cancer cells (1.0×10^5/well) were plated in 12-well plates and allowed to attach for 24 h. Cells were treated with 1,1-*bis*(3′-indolyl)-1-(*p*-carboxymethylphenyl)methane (DIM-C-pPhCO_2Me) in DMSO for 24 or 48 h or transfected with siNR4A1 or iGL2 (control siRNA) in lipofectamine for 72 h. Cells were then trypsinized and counted using a Coulter Z1 cell counter and growth inhibition was determined. Each experiment was carried out in triplicate and results were expressed as the mean ± S.E.M. for each set of experiments. Cells were also treated with C-DIMs after NR4A1 knockdown.

Annexin V staining

MCF-7, MDA-MB-231, and SKBR3 cells (1.0×10^5/well) were seeded in two-well Nunc Lab-Tek chambered B#1.0 Borosilicate coverglass slides from Thermo Scientific (Waltham, MA, USA) and were allowed to attach for 24 h. The medium was then changed to DMEM/Ham F-12 medium containing 2.5% charcoal-stripped fetal bovine serum, and either DMSO or DIM-C-pPhCO_2Me (15 μM) was added for 24 h. For siRNA treatment, cells were transfected with iGL2 or 100 nm siNR4A1 (1 or 2) for 72 h. Apoptosis was analyzed by Apoptotic and Necrotic Assay Kit (Biotium), which contained FITC–Annexin V, ethidium homodimer III, and Hoechst 3342. Apoptosis, Necrotic, and Healthy Cell Detection Kit was used according to the manufacturer's protocol and cells were visualized under an EVOS fl, fluorescence microscope, from Advanced Microscopy. The proportion of apoptotic cells was determined by the amount of green fluorescence observed in the treatment groups relative and normalized to the control group.

Western blot analysis

Breast cancer cells (3.0×10^5/well) were seeded in DMEM/Ham's F-12 medium in six-well plates. Cells were allowed to attach for 24 h and treated with varying concentrations of DIM-C-pPhCO_2Me for 24 h or with 100 nm of siNR4A1 for 72 h. Cells were lysed with high salt lysis buffer (with protease inhibitor cocktail) and quantitated with a Bradford reagent. Lysates were then analyzed by SDS–PAGE and transferred onto a PVDF membrane by wet electroblotting. Membranes were then incubated with a primary antibody, followed by a secondary antibody. Western blot analysis was determined as described and Immobilon western chemiluminescence substrates (Millipore) were used to develop images captured on a Kodak 4000 MM Pro image station (Molecular Bioimaging, Bend, OR, USA).

siRNAi assay

Breast cancer cells were seeded (1.2×10^5/well) in six-well plates in DMEM/Ham's F-12 medium supplemented with 2.5% charcoal-stripped fetal bovine serum and left to

http://erc.endocrinology-journals.org
DOI: 10.1530/ERC-15-0063

Published by Bioscientifica Ltd.

attach for 24 h. Knockdown of NR4A1 was carried out using Lipofectamine 2000 reagent according to the manufacturer's protocol. Small inhibitory RNAs and GL2 (non-specific oligonucleotide) were prepared and purchased from Sigma–Aldrich. The siRNA complexes used in the study are as follows: siGL2-5′-CGU ACG CGG AAU ACU UCG A-3′; siNR4A1 (1)-SASI_Hs02_00333289; siNR4A1 (2)-SASI_Hs01_00182072.

Generation and measurement of reactive oxygen species (ROS)

Cellular ROS levels were ascertained using the cell permeable probe CM-H_2DCFDA (5-(and-6)-chloromethyl-2′7′-dichlorodihydrofluorescein diacetate acetyl ester) from Invitrogen. Following treatment of the cells for 12 or 24 h with DIM-C-pPHCO_2Me or siNR4A1 for 72 h, cells that were plated on a six-well culture plate were trypsinized, neutralized, then loaded with 10 μM of probe for 20 min, and washed once with serum free medium. ROS was then measured by flow cytometry using Accuri's C6 Flow Cytometer (Accuri, Ann Arbor, MI, USA).

Triple negative breast cancer (TBNC) orthotopic xenograft model

Female BALB/c nude mice (6–8 weeks old) were obtained (Charles River Laboratory, Wilmington, MA, USA) and maintained under specific pathogen-free conditions, housed in isolated vented cages and allowed to acclimate for 1 week with a standard chow diet. The animals were housed at Florida A&M University in accordance with the standards of the Guide for the Care and Use of Laboratory Animals and the Association for Assessment and Accreditation of Laboratory Animal Care (AAALAC). The protocol of the animal study was approved by the Institutional Animal Care and Use Committee (IACUC), Florida A&M University, FL, USA. MDA-MB-231 cells (1×10^6 cells) were detached, resuspended in 100 μl of PBS with matrigel (BD Bioscience, Bedford, MA, USA), and implanted subcutaneously in the mammary fat pad of mice. When tumors reached about 40–50 mm^3 in size, the animals were randomized into control and treatment groups (six animals per group) and mice were treated with placebo or DIM-C-pPhCO_2Me or 1,1-*bis*(3′-indolyl)-1-(*p*-cyanophenyl)methane (DIM-C-pPhCN) (50 mg/kg per day) in nano liquid carrier (administered in sodium carboxymethyl cellulose) by oral gavage every 2nd day for 4 weeks. Tumor volumes and weights, and body weight were determined. The tumor size was measured using Vernier calipers, and the tumor volume was estimated by the formula: tumor volume (mm^3) = ($L\times W^2$)$\times$½, where L is the length and W is the width of the tumor. Tumor lysates were obtained and analyzed for protein expression by western blots.

Statistical analysis

Statistical significance of differences between the treatment groups was determined by Student's *t*-test. The results are expressed as means with error bars representing 95% CIs for three experiments for each group unless otherwise indicated. A P value <0.05 was considered statistically significant. All statistical tests were two-sided.

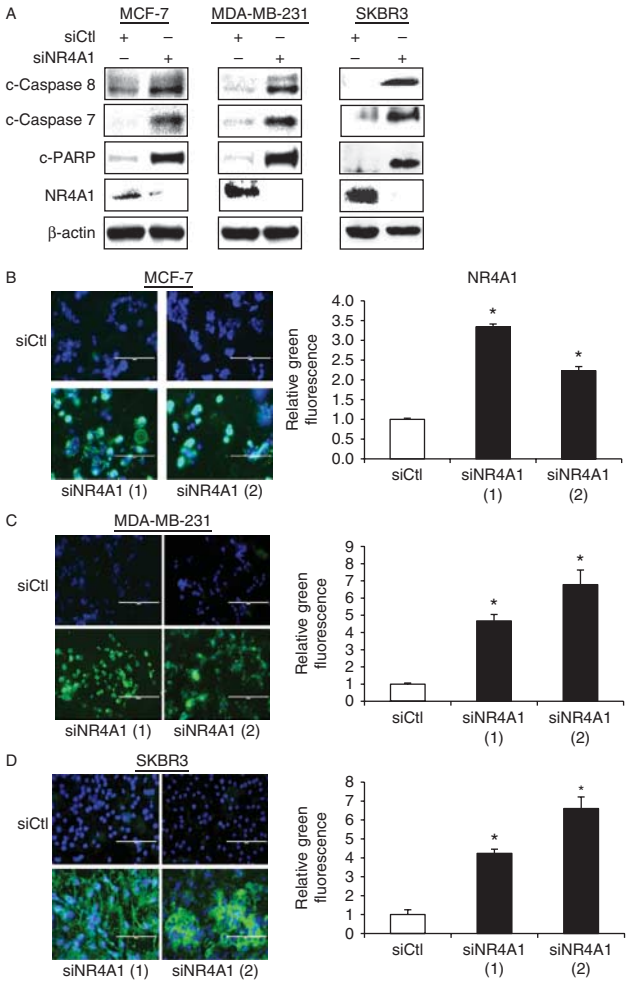

Figure 2
siNR4A1 induces apoptosis in breast cancer cells. (A) Cells were transfected with siNR4A1 and whole cell lysates were analyzed by western blots. Cells were transfected with siNR4A1 (two oligonucleotides) and effects on Annexin V staining in MCF-7 (B), MDA-MB-231 (C), and SKBR3 (D) cells were determined and quantitated. Results (B, C and D) are means±S.E.M. for at least three separate determinations and significant ($P<0.05$) induction of Annexin V staining is indicated (*).

http://erc.endocrinology-journals.org
DOI: 10.1530/ERC-15-0063

Published by Bioscientifica Ltd.

Results

Inhibition of cell proliferation by siNR4A1 and DIM-C-pPhCO$_2$Me

The orphan nuclear receptor NR4A1 is overexpressed in ER-positive and ER-negative breast cancer cells (Muscat *et al*. 2013). The role of this receptor in regulating breast cancer cell growth and survival was investigated by RNAi in ER-positive (MCF-7), ER-negative (MDA-MB-231), and erbB2 (SKBR3) overexpressing breast cancer cell lines. Cells were transfected with two different oligonucleotides against NR4A1 (siNR4A1-1/siNR4A1-2). This resulted in $\geq$50% growth inhibition in MCF-7 and SKBR3 cells, and 35% inhibition of MDA-MB-231 cell proliferation (Fig. 1B). The C-DIM compounds with a *p*-carboxymethylpenyl group (DIM-C-pPhCO$_2$Me) and cyano substitutent (DIM-C-pPhCN) have been identified as an NR4A1 antagonists (Lee *et al*. 2014*b*). Figure 1C and Supplemental Figure S1A, see section on supplementary data given at the end of this article demonstrate that the former compound significantly inhibits growth of MCF-7, MDA-MB-231 cells after treatment for 24 and 48 h. IC$_{50}$ values were 20, 19, and 19 μM after treatment of MCF-7, MDA-MB-231, and SKBR3 cells, respectively, for 24 h and 13, 19, and 12 μM after treatment for 48 h. In contrast, treatment of non-transformed MCF-10A mammary cells with the high affinity NR4A1 ligand DIM-C-pPhOH (30 μM) for 24 or 48 h did not affect cell proliferation (Supplemental Figure S1B). Moreover, in an orthotopic model for breast cancer in athymic nude mice using MDA-MB-231 cells treatment with 50 mg/kg per day and weight compared to the corn oil controls (Fig. 1D). In contrast, after knockdown of NR4A1 in these cells, treatment with DIM-C-pPhCO$_2$Me resulted in only minimal growth inhibition, which confirms a role for NR4A1 in mediating the growth inhibitory effects of DIM-C-pPhCO$_2$Me (Fig. 1E).

siNR4A1 and DIM-C-pPhCO$_2$Me induce apoptosis and activate growth inhibitory genes/pathways in breast cancer cells

NR4A1 also regulates pro-survival genes and pathways in pancreatic and lung cancer cells. Figure 2A results show transfection of breast cancer cells with siNR4A1 induced cleavage of caspases 8 and 7 as well as PARP cleavage. Moreover, siNR4A1 also induced Annexin V staining MCF-7 (Fig. 2B), MDA-MB-231 (Fig. 2C), and SKBR3 (Fig. 2D) cells confirming that NR4A1 regulated anti-apoptotic pathways in these cell lines. Treatment of the cells with DIM-C-pPhCO$_2$Me for 24 h also induced cleavage (activation) of caspases 7 and 8 and PARP (Fig. 3A). Similar results were observed for the *p*-cyanophenyl compound (DIM-C-pPhCN) which is an NR4A1 ligand and antagonist in colon cancer cells (Lee *et al*. 2014*b*; Supplemental Figure S1C). DIM-C-pPhCO$_2$Me also enhanced Annexin V staining in MCF-7, MDA-MB-231, and SKBR3 cell lines (Fig. 3B). Moreover, DIM-C-pPhCO$_2$Me-induced apoptosis (PARP cleavage) was reversed after co-administration with the pancaspase inhibitor ZVAD–FMK (Fig. 3C). Thus, both NR4A1 knockdown and NR4A1 antagonists decreased

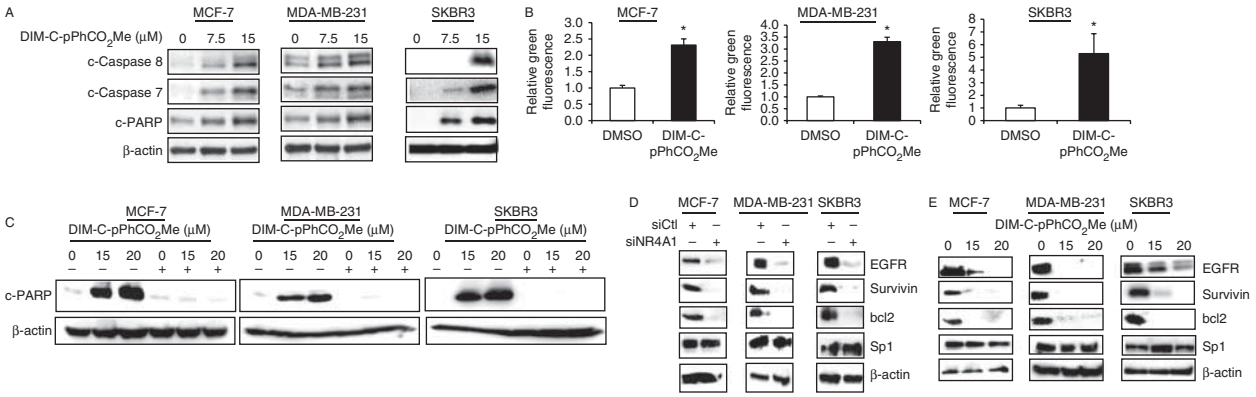

Figure 3

DIM-C-pPhCO$_2$Me induces apoptosis and siNR4A1 and DIM-C-pPhCO$_2$Me decrease expression of selected genes with GC-rich promoters in breast cancer cells. (A) Cells were treated with DIM-C-pPhCO$_2$Me for 24 h and whole cell lysates were analyzed by western blots. (B) MCF-7, MDA-MB-231, and SKBR3 cells were treated with DIM-C-pPhCO$_2$Me for 24 h and Annexin V staining was determined and quantitated. Quantitative results are means$\pm$S.E.M. for three separate determinations and significant ($P<0.05$) induction of Annexin V is indicated (*). (C) Cells were treated with DMSO or DIM-C-pPhCO$_2$Me alone or in combination with the pan-caspase inhibitor ZVAD-FMK, and PARP cleavage was analyzed by western blots. Cells were transfected with siNR4A1 (D) or treated with DIM-C-pPhCO$_2$Me (E), and whole cell lysates were analyzed by western blots.

http://erc.endocrinology-journals.org
DOI: 10.1530/ERC-15-0063

Published by Bioscientifica Ltd.

breast cancer cell growth and induced apoptosis as well as decreased NR4A1/Sp1-regulated genes as previously described (Lee *et al.* 2014*b*). Figure 3D shows that after knockdown of NR4A1 (siNR4A1) in MCF-7, MDA-MB-231, and SKBR3 cells, there was a significant decrease in expression of several Sp1-regulated genes including EGFR, survivin, and bcl-2. However, Sp1 protein levels were unchanged. Similar results were observed in the same cell lines after treatment with the NR4A1 antagonists DIM-C-pPhCO$_2$Me (Fig. 3D) and DIM-C-pPhCN (Supplemental Figure S1D).

siNR4A1 and DIM-C-pPhCO$_2$Me induce ROS and endoplasmic reticulum stress

It was recently reported that NR4A1 regulates expression of genes such as IDH1 and TXNDC5 that maintain high levels of reducing equivalents and minimize ROS-mediated cellular stress (Lee *et al.* 2014*a*,*b*). Knockdown of NR4A1 by RNAi induced ROS by two- to fourfold in MCF-7, MDA-MB-231, and SKBR3 cells (Fig. 4A). This was accompanied by decreased expression of both TXNDC5 and IDH1 in these cell lines (Fig. 4B). Moreover, after transfection with siNR4A1, we also observed enhanced markers of endoplasmic reticulum (ER) stress including increased phosphorylation of PERK and increased expression of ATF-4, CHOP, GRP78, IRE1, ATF6, and spliced XBP-1 (XBP-1s) in the breast cancer cell lines (Fig. 4C). Treatment of MCF-7, MDA-MB-231, and SKBR3 cells with the NR4A1 antagonist DIM-C-pPhCO$_2$Me also increased ROS after 12 and 24 h (Fig. 5A, B and C). This was also accompanied by decreased expression of TXNDC5 and IDH1 (Fig. 5D) as well as induction of markers of ER stress (p-PERK, ATF4, CHOP, ATF6, IRE1, GRP78, and XBP-1s; Fig. 5E), as previously observed in pancreatic cancer cells (Lee *et al.* 2014*a*). The role of ROS in mediating the effects of DIM-C-pPhCO$_2$Me on activation of stress gene products was investigated in MCF-7, SKBR3, and MDA-MB-231 cells by cotreatment with the antioxidant GSH which reversed induction of the stress genes by the C-DIM/NR4A1 antagonist (Fig. 5F). We also observed that the NR4A1 antagonist DIM-C-pPhCN decreased expression of IDH1 and TXNDC5 in breast cancer cells (Supplemental Figure S1E). In addition, western blot analysis of tumor lysate from control and DIM-C-pPhCO$_2$-Me-treated mice confirmed that DIM-C-pPhCO$_2$Me significantly induced PARP cleavage, decreased expression of Sp-regulated survivin, EGFR and bcl2 gene products and also decreased levels of TXNDC5 and IDH1 (Supplemental Figure S2A and B, see section on supplementary data given at the end of this article).

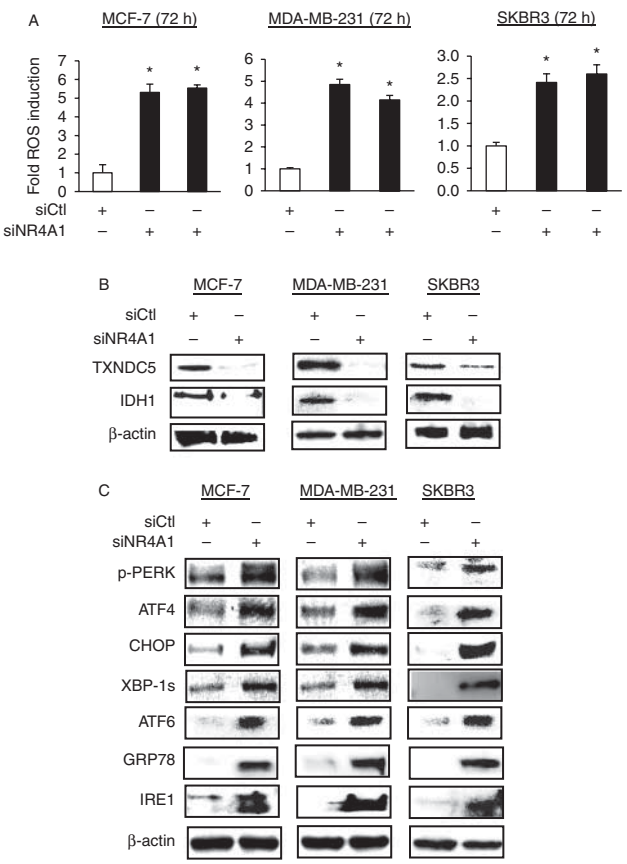

Figure 4
NR4A1 knockdown induces ROS and cellular stress. (A) Cells were transfected with siNR4A1 or siCtl and ROS was determined. Cells were transfected with siNR4A1 and whole cell lysates were analyzed by western blots for IDH1 or TXNDC5 (B) and ER stress gene products (C). Results in (A) are means±S.E.M. for three separate determinations and significant ($P<0.05$) induction of ROS is indicated (*).

siNR4A1 and DIM-C-pPhCO$_2$Me inhibit mTOR signaling

Transfection of p53-positive MCF-7 cells with siNR4A1 (Fig. 6A) or treatment with DIM-C-pPhCO$_2$Me (Fig. 6B) induced SESN2, activated AMPKα (phosphorylation), and decreased phosphorylation of mTOR and mTOR downstream genes. Similar results were observed for DIM-C-pPhCN (Supplemental Figure S1F). These results are consistent with previous studies in lung cancer cell lines where inactivation of NR4A1 activated p53-dependent activation of SESN2 which in turn activated AMPKα (Lee *et al.* 2012). Surprisingly, we also observed that transfection of p53-mutant MDA-MB-231 and SKBR3 cells with siNR4A1 induced SESN2, activated AMPKα, and inhibited mTOR signaling (Fig. 6C). Similar results were observed

http://erc.endocrinology-journals.org
DOI: 10.1530/ERC-15-0063

Published by Bioscientifica Ltd.

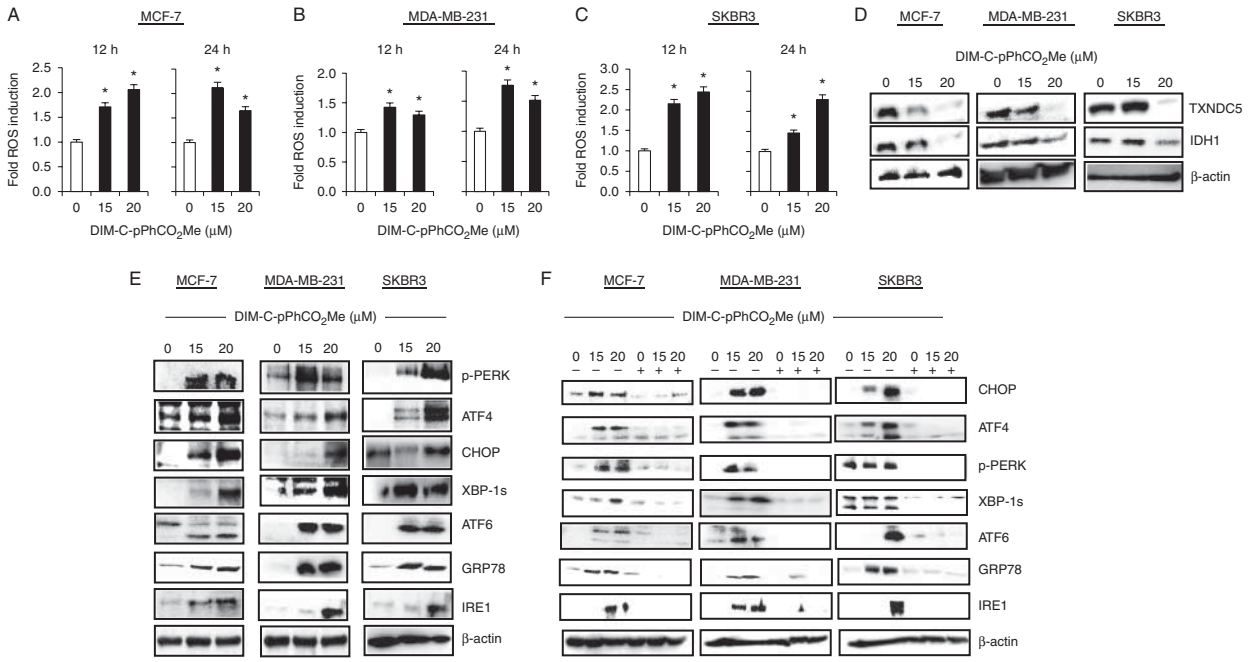

Figure 5

DIM-C-pPhCO$_2$Me induces ROS and stress. MCF-7 (A), MDA-MB-231 (B), and SKBR3 (C) cells were treated with DIM-C-pPhCO$_2$Me and ROS was determined after 12 or 24 h. Cells were treated with DIM-C-pPhCO$_2$Me and whole cell lysates were analyzed by western blots for expression of TXNDC5 (D), IDH1 (D), and stress gene products (E). (F) Cells were treated with DMSO, DIM-C-pPhCO$_2$Me alone or in combination with GSH, and whole cell lysates were analyzed for stress gene products by western blots. Results (A) are expressed as means ± S.E.M. for three separate determinations and significant ($P<0.05$) induction of ROS is indicated (*).

after treatment with DIM-C-pPhCO$_2$Me. We also recently observed similar results in a p53-mutant renal adenocarcinoma cell line (Hedrick *et al.* 2015) which showed that induction of SESN2 was ROS-dependent. This was consistent with previous reports showing that SESN2 was an oxygen-sensing gene (Budanov *et al.* 2002). Figure 6D shows that induction of SESN2 and activation of AMPKα in MDA-MB-231 and SKBR3 cells after treatment with DIM-C-pPhCO$_2$Me was inhibited after cotreatment with GSH. These data are consistent with the induction of ROS in these cell lines after transfection with siNR4A1 (Fig. 4A) or treatment with DIM-C-pPhCO$_2$Me (Fig. 5A, B and C). Thus, results of this study demonstrate that NR4A1 regulates multiple pro-oncogenic pathways in breast cancer cells. Immunostaining for NR4A1 demonstrates that the receptor is nuclear and remains in the nucleus after treatment with an antagonist (Supplemental Figure S3, see section on supplementary data given at the end of this article). Thus, C-DIM/NR4A1 antagonists inhibit multiple nuclear NR4A1-mediated genes/pathways (Fig. 1A) and represent a new class of mechanism-based drugs for breast cancer chemotherapy.

Discussion

NR4A1 exhibits pro-oncogenic activity in cancer cell lines derived from solid tumors and is overexpressed in tumors from lung, pancreatic, and colon cancer patients (Chintharlapalli *et al.* 2005, Cho *et al.* 2010, Lee *et al.* 2010, 2012, 2014*a*, Wu *et al.* 2011). Moreover, in lung cancer patients, high expression of NR4A1 is a prognostic indicator for decreased survival (Lee *et al.* 2012). Similar results were recently reported for the expression and prognostic activity of NR4A1 in breast cancer patients. It was also observed that NR4A1 was one of only a few nuclear receptors overexpressed in patients with both ER-positive and ER-negative breast tumors (Muscat *et al.* 2013, Zhou *et al.* 2014). Since an early report indicated that NR4A1 is more highly expressed in early- vs late-stage aggressive breast tumors and exhibited some tumor suppressor-like activity (Alexopoulou *et al.* 2010), we investigated the function of NR4A1 in three different breast cancer cell lines by RNAi and treatment with NR4A1 antagonists. We have recently demonstrated that several C-DIMs including the *p*-hydroxy, carbomethoxy, cyano,

http://erc.endocrinology-journals.org
DOI: 10.1530/ERC-15-0063

Published by Bioscientifica Ltd.

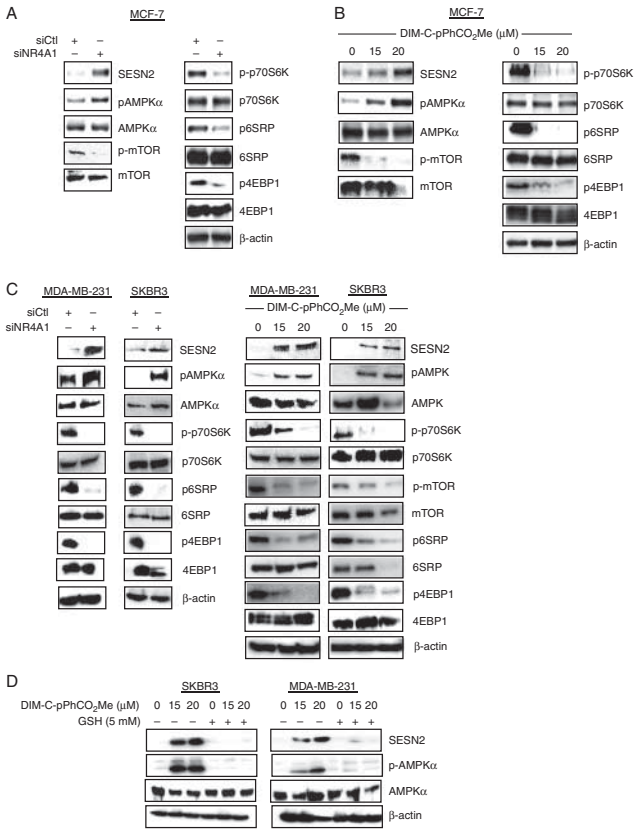

Figure 6

NR4A1 knockdown and DIMC-C-pPhCO$_2$Me inhibit mTOR. MCF-7 cells were transfected with siNR4A1 (A) or treated with DIM-C-pPhCO$_2$Me (B) and whole cell lysates were analyzed by western blots for mTOR pathway gene products. (C) MDA-MB-231 and SKBR3 cells were transfected with siNR4A1 or treated with DIM-C-pPhCO$_2$Me, and whole cell lysates were analyzed for mTOR pathway genes by western blots. (D) MDA-MB-231 and SKBR3 cells were treated with DMSO, DIM-C-pPhCO$_2$Me alone or in combination with GSH and, after 24 h whole cell lysates were analyzed by western blots for sestrin 2 and AMPKα.

and bromophenyl analogs directly bind the ligand binding domain of NR4A1 and exhibit NR4A1 antagonist activity in colon cancer cells (Lee *et al.* 2014*b*). The *p*-carbomethyoxyphenyl analog (DIM-C-pPhCO$_2$Me) and to a lesser extent DIM-C-pPhCN were used as prototypical C-DIMs/NR4A1 antagonists for investigating the anticancer activities of NR4A1 antagonists in breast cancer cells with a focus on inhibition of three previously identified pro-oncogenic NR4A1-regulated pathways (Fig. 1A).

Initial studies investigated the role of NR4A1 in the growth of three prototypical breast cancer cell lines (ER-positive MCF-7, erbB2 overexpressing SKBR3, and triple negative MDA-MB-231 cells). Knockdown of NR4A1 using two different oligonucleotides significantly decreased proliferation of all three breast cancer cell lines and similar growth inhibitory effects were observed for DIM-C-pPhCO$_2$Me (Fig. 1B and C). Moreover, after knockdown of NR4A1 in MCF-7, MDA-MB-231, and SKBR3 cells, treatment with DIM-C-pPhCO$_2$Me had minimal effects (Fig. 1D), suggesting that the growth inhibitory effects of DIM-C-pPhCO$_2$Me were primarily NR4A1-dependent. The effects of NR4A1 knockdown or treatment with DIM-C-pPhCO$_2$Me on several markers of apoptosis, including cleavage of caspases 7 and 8 and PARP as well as induction of Annexin V staining, were also determined in the breast cancer cell lines (Figs 2 and 3). These results demonstrate that NR4A1 regulates pathways that contribute to the growth and survival of breast cancer cell. This parallels the functions previously observed for this receptor in pancreatic, lung, and colon cancer cells (Lee *et al.* 2010, 2012, 2014*a*,*b*).

NR4A1 binds and inactivates p53 (Zhao *et al.* 2006), whereas knockdown of NR4A1 or treatment of p53 WT lung cancer cells with an NR4A1 antagonist or transfection with siNR4A1 results in activation of p53 and induction of SESN2 which activates AMPKα and inhibits the mTOR pathway (Lee *et al.* 2012). mTOR pathway inhibitors have been extensively developed for cancer chemotherapy (Baselga *et al.* 2012, Ciruelos Gil 2014). C-DIM/NR4A1 antagonists represent a new class of mTOR inhibitors which block NR4A1-regulated mTOR activation in cancer cells expressing WT p53 (Lee *et al.* 2012). Results illustrated in Fig. 6A and B show that both siNR4A1 and DIM-C-pPhCO$_2$Me inhibited mTOR pathway in MCF-7 breast cancer cells that express WT p53. In p53 WT lung cancer cells, siNR4A1 and NR4A1 antagonists also induced SESN2 which activates AMPKα and inhibits mTOR, whereas this is not observed in lung cancer cells expressing mutant p53 (Lee *et al.* 2012). Interestingly, DIM-C-pPhCO$_2$Me and siNR4A1 also induced SESN2 and inhibited mTOR in p53 mutant SKBR3 and MDA-MB-231 cells (Fig. 6C). The DIM-C-pPhCO$_2$Me-mediated induction of SESN2 and activation of AMPKα were reversed after cotreatment with GSH (Fig. 6D). These results are consistent with induction of ROS by DIM-C-pPhCO$_2$Me (Fig. 5A, B and C) and the fact that SESN2 is an oxygen-sensing gene that is induced by ROS (Budanov *et al.* 2002).

Like other nuclear receptors, NR4A1 interacts with the Sp1 transcription factor bound to GC-rich sites to activate survivin and other anti-apoptotic/growth promoting genes. siNR4A1 or treatment with a NR4A1 antagonist decreases expression of these genes (Liu & Simpson 1999, Pipaon *et al.* 1999, Suzuki *et al.* 1999, Lu *et al.* 2000, Shimada *et al.* 2001, Sugawara *et al.* 2002). Figure 3C and D

http://erc.endocrinology-journals.org
DOI: 10.1530/ERC-15-0063

Published by Bioscientifica Ltd.

show that siNR4A1 or treatment with DIM-C-pPhCO$_2$Me decreased expression of survivin, bcl2 and EGFR in MDA-MB-231, MCF-7, and SKBR3 cells. However, Sp protein levels were unchanged. Molecular analysis of NR4A1-dependent regulation of survivin showed that in pancreatic cancer cells, NR4A1 and p300 cooperatively activated survivin expression by interacting with Sp1 bound to the proximal GC-rich region of the survivin promoter (Lee *et al*. 2010). Regulation of growth-promoting and survival genes which contain GC-rich promoters by NR4A1 is consistent with the growth inhibitory and apoptotic effects of siNR4A1 and C-DIM/NR4A1 antagonists on breast cancer cells and tumors. It is comparable to that observed in lung, colon and pancreatic cancer cell lines (Lee *et al*. 2010, 2012, 2014*a*,*b*).

A recent study showed that NR4A1 maintains low levels of oxidative and ER stress in pancreatic cancer cells by regulating expression of TXNDC5 and IDH1 which maintain cellular levels of reducing equivalents (Lee *et al*. 2014*a*). DIM-C-pPhCO$_2$Me or siNR4A1 decreased expression of TXNDC5 and IDH1 in breast tumors (*in vivo*; Supplemental Figure S2) and in MCF-7, MDA-MB-231, and SKBR3 cells. This was accompanied by increased levels of ROS and induction of markers of ER stress (Figs 4 and 5). These results are consistent with previous studies in pancreatic cancer cells. There is also emerging evidence that both TXNDC5 and IDH1 are overexpressed in breast cancer cells and tumors (Xu *et al*. 2010, Chang *et al*. 2013). Their expression and functions in breast cancer cells are currently being investigated.

In summary, results of this study are consistent with a pro-oncogenic role for NR4A1 in breast cancer as an important regulator of cell growth and survival. NR4A1-regulated pro-oncogenic pathways and genes are similar to those observed in pancreatic, lung, and colon cancer cells and tumors (Lee *et al*. 2010, 2012, 2014*a*,*b*). This study also demonstrated the effectiveness of the NR4A1 antagonists DIM-C-pPhCO$_2$Me and DIM-C-pPhCN as inhibitors of breast cancer cell and tumor growth as well as survival. Current structure-activity studies are focused on identifying the most effective C-DIM/NR4A1 antagonists for future clinical applications in breast cancer chemotherapy, including the inhibition of breast invasion (Zhou *et al*. 2014) through inhibition of nuclear NR4A1 by receptor antagonists.

Supplementary data

This is linked to the online version of the paper at http://dx.doi.org/10.1530/ERC-15-0063.

Declaration of interest

The authors declare that there is no conflict of interest that could be perceived as prejudicing the impartiality of the research reported.

Funding

Funding was provided by DOD-CDRMP (BC103116; M Singh), NIEHS (P30-ES023512; S Safe), Texas AgriLife Research, and the Sid Kyle Endowment (S Safe).

References

Alexopoulou AN, Leao M, Caballero OL, Da Silva L, Reid L, Lakhani SR, Simpson AJ, Marshall JF, Neville AM & Jat PS 2010 Dissecting the transcriptional networks underlying breast cancer: NR4A1 reduces the migration of normal and breast cancer cell lines. *Breast Cancer Research* **12** R51. (doi:10.1186/bcr2610)

Baselga J, Campone M, Piccart M, Burris HA III, Rugo HS, Sahmoud T, Noguchi S, Gnant M, Pritchard KI, Lebrun F *et al*. 2012 Everolimus in postmenopausal hormone-receptor-positive advanced breast cancer. *New England Journal of Medicine* **366** 520–529. (doi:10.1056/NEJMoa1109653)

Bras A, Albar JP, Leonardo E, de Buitrago GG & Martinez AC 2000 Ceramide-induced cell death is independent of the Fas/Fas ligand pathway and is prevented by Nur77 overexpression in A20 B cells. *Cell Death and Differentiation* **7** 262–271. (doi:10.1038/sj.cdd.4400653)

Budanov AV, Shoshani T, Faerman A, Zelin E, Kamer I, Kalinski H, Gorodin S, Fishman A, Chajut A, Einat P *et al*. 2002 Identification of a novel stress-responsive gene Hi95 involved in regulation of cell viability. *Oncogene* **21** 6017–6031. (doi:10.1038/sj.onc.1205877)

Chang X, Xu B, Wang L, Wang Y, Wang Y & Yan S 2013 Investigating a pathogenic role for TXNDC5 in tumors. *International Journal of Oncology* **43** 1871–1884. (doi:10.3892/ijo.2013.2123)

Chintharlapalli S, Burghardt R, Papineni S, Ramaiah S, Yoon K & Safe S 2005 Activation of Nur77 by selected 1,1-*bis*(3′-indolyl)-1-(*p*-substituted phenyl)methanes induces apoptosis through nuclear pathways. *Journal of Biological Chemistry* **280** 24903–24914. (doi:10.1074/jbc.M500107200)

Cho SD, Lee SO, Chintharlapalli S, Abdelrahim M, Khan S, Yoon K, Kamat AM & Safe S 2010 Activation of nerve growth factor-induced Bα by methylene-substituted diindolylmethanes in bladder cancer cells induces apoptosis and inhibits tumor growth. *Molecular Pharmacology* **77** 396–404. (doi:10.1124/mol.109.061143)

Ciruelos Gil EM 2014 Targeting the PI3K/AKT/mTOR pathway in estrogen receptor-positive breast cancer. *Cancer Treatment Reviews* **40** 862–871. (doi:10.1016/j.ctrv.2014.03.004)

Ferlini C, Cicchillitti L, Raspaglio G, Bartollino S, Cimitan S, Bertucci C, Mozzetti S, Gallo D, Persico M, Fattorusso C *et al*. 2009 Paclitaxel directly binds to Bcl-2 and functionally mimics activity of Nur77. *Cancer Research* **69** 6906–6914. (doi:10.1158/0008-5472.CAN-09-0540)

Hedrick E, Lee SO, Kim G, Abdelrahim M, Jin UH, Safe S & Abudayyeh A 2015 Nuclear receptor 4A1 (NR4A1) as a drug target for renal cell adenocarcinoma. *PLoS ONE* **10** e0128308. (doi:10.1371/journal.pone.0128308)

Kolluri SK, Bruey-Sedano N, Cao X, Lin B, Lin F, Han YH, Dawson MI & Zhang XK 2003 Mitogenic effect of orphan receptor TR3 and its regulation by MEKK1 in lung cancer cells. *Molecular and Cellular Biology* **23** 8651–8667. (doi:10.1128/MCB.23.23.8651-8667.2003)

Kolluri SK, Zhu X, Zhou X, Lin B, Chen Y, Sun K, Tian X, Town J, Cao X, Lin F *et al*. 2008 A short Nur77-derived peptide converts Bcl-2 from a protector to a killer. *Cancer Cell* **14** 285–298. (doi:10.1016/j.ccr.2008.09.002)

Published by Bioscientifica Ltd.

Lee SO, Chintharlapalli S, Liu S, Papineni S, Cho SD, Yoon K & Safe S 2009 p21 expression is induced by activation of nuclear nerve growth factor-induced Bα (Nur77) in pancreatic cancer cells. *Molecular Cancer Research* **7** 1169–1178. (doi:10.1158/1541-7786.MCR-08-0473)

Lee SO, Abdelrahim M, Yoon K, Chintharlapalli S, Papineni S, Kim K, Wang H & Safe S 2010 Inactivation of the orphan nuclear receptor TR3/Nur77 inhibits pancreatic cancer cell and tumor growth. *Cancer Research* **70** 6824–6836. (doi:10.1158/0008-5472.CAN-10-1992)

Lee SO, Li X, Khan S & Safe S 2011 Targeting NR4A1 (TR3) in cancer cells and tumors. *Expert Opinion on Therapeutic Targets* **15** 195–206. (doi:10.1517/14728222.2011.547481)

Lee SO, Andey T, Jin UH, Kim K, Singh M & Safe S 2012 The nuclear receptor TR3 regulates mTORC1 signaling in lung cancer cells expressing wild-type p53. *Oncogene* **31** 3265–3276. (doi:10.1038/onc.2011.504)

Lee SO, Jin UH, Kang JH, Kim SB, Guthrie AS, Sreevalsan S, Lee JS & Safe S 2014*a* The orphan nuclear receptor NR4A1 (Nur77) regulates oxidative and endoplasmic reticulum stress in pancreatic cancer cells. *Molecular Cancer Research* **12** 527–538. (doi:10.1158/1541-7786.MCR-13-0567)

Lee SO, Li X, Hedrick E, Jin UH, Tjalkens RB, Backos DS, Li L, Zhang Y, Wu Q & Safe S 2014*b* Diindolylmethane analogs bind NR4A1 and are NR4A1 antagonists in colon cancer cells. *Molecular Endocrinology* **28** 1729–1739. (doi:10.1210/me.2014-1102)

Li H, Kolluri SK, Gu J, Dawson MI, Cao X, Hobbs PD, Lin B, Chen G, Lu J, Lin F *et al.* 2000 Cytochrome *c* release and apoptosis induced by mitochondrial targeting of nuclear orphan receptor TR3. *Science* **289** 1159–1164. (doi:10.1126/science.289.5482.1159)

Lin B, Kolluri SK, Lin F, Liu W, Han YH, Cao X, Dawson MI, Reed JC & Zhang XK 2004 Conversion of Bcl-2 from protector to killer by interaction with nuclear orphan receptor Nur77/TR3. *Cell* **116** 527–540. (doi:10.1016/S0092-8674(04)00162-X)

Liu Z & Simpson ER 1999 Molecular mechanism for cooperation between Sp1 and steroidogenic factor-1 (SF-1) to regulate bovine CYP11A gene expression. *Molecular and Cellular Endocrinology* **153** 183–196. (doi:10.1016/S0303-7207(99)00036-2)

Liu JJ, Zeng HN, Zhang LR, Zhan YY, Chen Y, Wang Y, Wang J, Xiang SH, Liu WJ, Wang WJ *et al.* 2010 A unique pharmacophore for activation of the nuclear orphan receptor Nur77 *in vivo* and *in vitro*. *Cancer Research* **70** 3628–3637. (doi:10.1158/0008-5472.CAN-09-3160)

Lu S, Jenster G & Epner DE 2000 Androgen induction of cyclin-dependent kinase inhibitor p21 gene: role of androgen receptor and transcription factor Sp1 complex. *Molecular Endocrinology* **14** 753–760. (doi:10.1210/mend.14.5.0461)

Maxwell MA & Muscat GE 2006 The NR4A subgroup: immediate early response genes with pleiotropic physiological roles. *Nuclear Receptor Signaling* **4** e002. (doi:10.1621/nrs.04002)

Muscat GE, Eriksson NA, Byth K, Loi S, Graham D, Jindal S, Davis MJ, Clyne C, Funder JW, Simpson ER *et al.* 2013 Research resource: Nuclear receptors as transcriptome: discriminant and prognostic value in breast cancer. *Molecular Endocrinology* **27** 350–365. (doi:10.1210/me.2012-1265)

Pearen MA & Muscat GE 2010 Minireview: Nuclear hormone receptor 4A signaling: implications for metabolic disease. *Molecular Endocrinology* **24** 1891–1903. (doi:10.1210/me.2010-0015)

Pipaon C, Tsai SY & Tsai MJ 1999 COUP-TF upregulates NGFI-A gene expression through an Sp1 binding site. *Molecular and Cellular Biology* **19** 2734–2745.

Shimada J, Suzuki Y, Kim SJ, Wang PC, Matsumura M & Kojima S 2001 Transactivation via RAR/RXR-Sp1 interaction: characterization of binding between Sp1 and GC box motif. *Molecular Endocrinology* **15** 1677–1692. (doi:10.1210/mend.15.10.0707)

Sugawara A, Uruno A, Kudo M, Ikeda Y, Sato K, Taniyama Y, Ito S & Takeuchi K 2002 Transcription suppression of thromboxane receptor gene by peroxisome proliferator-activated receptor-γ via an interaction with Sp1 in vascular smooth muscle cells. *Journal of Biological Chemistry* **277** 9676–9683. (doi:10.1074/jbc.M104560200)

Suzuki Y, Shimada J, Shudo K, Matsumura M, Crippa MP & Kojima S 1999 Physical interaction between retinoic acid receptor and Sp1: mechanism for induction of urokinase by retinoic acid. *Blood* **93** 4264–4276.

Uemura H & Chang C 1998 Antisense TR3 orphan receptor can increase prostate cancer cell viability with etoposide treatment. *Endocrinology* **139** 2329–2334. (doi:10.1210/endo.139.5.5969)

Wang WJ, Wang Y, Chen HZ, Xing YZ, Li FW, Zhang Q, Zhou B, Zhang HK, Zhang J, Bian XL *et al.* 2014 Orphan nuclear receptor TR3 acts in autophagic cell death via mitochondrial signaling pathway. *Nature Chemical Biology* **10** 133–140. (doi:10.1038/nchembio.1406)

Wu H, Lin Y, Li W, Sun Z, Gao W, Zhang H, Xie L, Jiang F, Qin B, Yan T *et al.* 2011 Regulation of Nur77 expression by β-catenin and its mitogenic effect in colon cancer cells. *FASEB Journal* **25** 192–205. (doi:10.1096/fj.10-166462)

Xu SG, Yan PJ & Shao ZM 2010 Differential proteomic analysis of a highly metastatic variant of human breast cancer cells using two-dimensional differential gel electrophoresis. *Journal of Cancer Research and Clinical Oncology* **136** 1545–1556. (doi:10.1007/s00432-010-0812-0)

Zeng JZ, Sun DF, Wang L, Cao X, Qi JB, Yang T, Hu CQ, Liu W & Zhang XK 2006 *Hypericum sampsonii* induces apoptosis and nuclear export of retinoid X receptor-α. *Carcinogenesis* **27** 1991–2000. (doi:10.1093/carcin/bgl046)

Zhan Y, Du X, Chen H, Liu J, Zhao B, Huang D, Li G, Xu Q, Zhang M, Weimer BC *et al.* 2008 Cytosporone B is an agonist for nuclear orphan receptor Nur77. *Nature Chemical Biology* **4** 548–556. (doi:10.1038/nchembio.106)

Zhan YY, Chen Y, Zhang Q, Zhuang JJ, Tian M, Chen HZ, Zhang LR, Zhang HK, He JP, Wang WJ *et al.* 2012 The orphan nuclear receptor Nur77 regulates LKB1 localization and activates AMPK. *Nature Chemical Biology* **8** 897–904. (doi:10.1038/nchembio.1069)

Zhang XK 2007 Targeting Nur77 translocation. *Expert Opinion on Therapeutic Targets* **11** 69–79. (doi:10.1517/14728222.11.1.69)

Zhao BX, Chen HZ, Lei NZ, Li GD, Zhao WX, Zhan YY, Liu B, Lin SC & Wu Q 2006 p53 mediates the negative regulation of MDM2 by orphan receptor TR3. *EMBO Journal* **25** 5703–5715. (doi:10.1038/sj.emboj.7601435)

Zhou F, Drabsch Y, Dekker TJ, de Vinuesa AG, Li Y, Hawinkels LJ, Sheppard KA, Goumans MJ, Luwor RB, de Vries CJ *et al.* 2014 Nuclear receptor NR4A1 promotes breast cancer invasion and metastasis by activating TGF-β signalling. *Nature Communications* **5** 3388. (doi:10.1038/ncomms4388)

Received in final form 28 July 2015
Accepted 30 July 2015
Made available online as an Accepted Preprint
30 July 2015

Published by Bioscientifica Ltd.

molecular pharmaceutics

Article

pubs.acs.org/molecularpharmaceutics

Lipid Nanocarriers of a Lipid-Conjugated Estrogenic Derivative Inhibit Tumor Growth and Enhance Cisplatin Activity against Triple-Negative Breast Cancer: Pharmacokinetic and Efficacy Evaluation

Terrick Andey,[†,⊥] Godeshala Sudhakar,[‡,⊥] Srujan Marepally,[§] Apurva Patel,[∥] Rajkumar Banerjee,[‡] and Mandip Singh*[,∥]

[†]Department of Pharmaceutical Sciences, School of Pharmacy, Massachusetts College of Pharmacy and Health Sciences, 19 Foster Street, Worcester, Massachusetts 01608, United States

[‡]Biomaterials Group, CSIR-Indian Institute of Chemical Technology, Uppal Road, Hyderabad, Andhra Pradesh 500007, India

[§]Institute for Stem Cell Biology and Regenerative Medicine (inStem), NCBS-TIFR, UAS-GKVK, Bengaluru, Karnataka 560067, India

[∥]Department of Pharmaceutics, College of Pharmacy and Pharmaceutical Sciences, Florida A&M University, 1520 South Martin Luther King Jr. Boulevard, Tallahassee, Florida 32307, United States

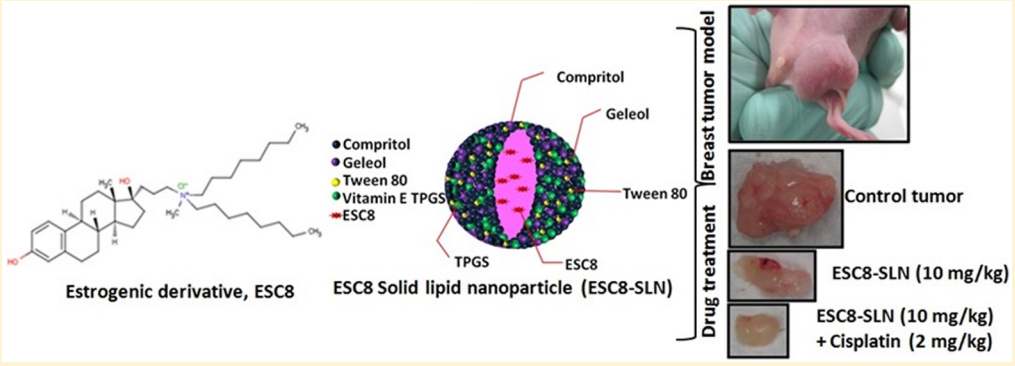

ABSTRACT: Breast cancer is the leading cause of malignancies among women globally. The triple negative breast cancer (TNBC) subtype is the most difficult to treat and accounts for 15% of all cases. Targeted therapies have been developed for TNBC but come short of clinical translation due to acquired tumor resistance. An effective therapy against TNBC must combine properties of target specificity, efficient tumor killing, and translational relevance. The objective of this study was to formulate a nontoxic, cationic, lipid-conjugated estrogenic derivative (ESC8), with demonstrated anticancer activity, for oral delivery in mice bearing triple negative breast cancer (TNBC) as xenograft tumors. The in vitro cell viability, Caco-2 permeability, and cell cycle dynamics of ESC8-treated TNBC cells were investigated. ESC8 was formulated as liposomes, solid lipid nanoparticles (SLNs), and nanostructured lipid carriers (NLCs) and characterized for size, zeta potential, entrapment efficiency, size stability, and tumor biodistribution. Pharmacokinetic modeling of plasma concentration−time course data was carried out following intravenous and oral administration in Sprague−Dawley rats. *In vivo* efficacy investigation of ESC8-SLNC was carried out in Nu/Nu mice bearing MDA-MB-231 TNBC as xenograft tumors, and the molecular dynamics modulating tumor growth inhibition was analyzed by Western blot. *In vitro* ESC8 inhibited TNBC and non-TNBC cell viability with IC_{50} ranging from 1.81 to 3.33 μM. ESC8 was superior to tamoxifen and Cisplatin in inhibiting MDA-MB-231 cell viability; and at 2.0 μM ESC8 enhanced Cisplatin cytotoxicity 16-fold. Intravenous ESC8 (2.0 mg/kg) was eliminated at a rate of 0.048 ± 0.01 h^{-1} with a half-life of 14.63 ± 2.95 h in rats. ESC8 was orally bioavailable (47.03%) as solid lipid nanoparticles (ESC8-SLN). ESC8-SLN (10 mg/kg/day, ×14 days, p.o.) inhibited breast tumor growth by 74% ($P < 0.0001$ vs control) in mice bearing MDA-MB-231 cells as xenografts; and when given in combination with Cisplatin (2.0 mg/kg/biweekly, ×2 weeks, IV), tumor growth was inhibited by 87% ($P = 0.0002$, vs ESC8-SLN; 10 mg/kg/day, ×14 days, p.o). ESC8-SLN tumor growth inhibition was associated with increased expression of p21 and Caspase-9; as well as by inhibition of EGFR, Slug, p-Akt1, Vimentin, NFkβ, and IKKγ. These results show the promise of ESC8 as an oral adjuvant or neoadjuvant against triple negative breast cancer.

KEYWORDS: *estradiol, lipid nanocarriers, triple-negative breast cancer, pharmacokinetics, oral bioavailability*

1. INTRODUCTION

Breast cancer accounts for the highest malignancy among women worldwide and has an annual incidence and mortality of 1,300,000 and 450,000, respectively.[1,2] In the United States, it is

Received: September 4, 2014
Revised: January 30, 2015
Accepted: February 8, 2015
Published: February 8, 2015

DOI: 10.1021/mp5008629
Mol. Pharmaceutics 2015, 12, 1105−1120

estimated that 235,030 new breast cancer cases will be recorded with 40,430 deaths by the end of 2014.[3] Current approved treatments for breast cancer include surgery, radiation, hormone, cytotoxic, and targeted therapies.[4] However, despite advances in diagnosis and treatment protocols the relative survival for distant/metastasized breast cancer is about 24%.

Expression of the estrogen receptor (ER), progesterone receptor (PR), or human epidermal growth factor receptor 2 (HER2) in breast cancers presents as useful targets for many anticancer therapy. To this end, various cytotoxics or combinations thereof have been approved by the Food and Drugs Administration (FDA).[5−7] However, serious adverse effects and acquired tumor resistance to these cytotoxics mitigate their clinical usefulness.[8] Additionally, the negative ER, PR, and HER2 status of triple negative breast cancer (TNBC) preclude the therapeutic effectiveness of many hormone therapies such as aromatase inhibitors (e.g.anastrozole), selective ER modulators (e.g., Tamoxifen), and inhibitors of HER2 (e.g., Trastuzumab).[9,10] This is further complicated by our appreciation of tumor hierarchies as promulgated by the cancer stem cell paradigm. This theory recognizes the heterogeneity of a tumor population as consisting of distinct individual tumor cells or tumor clusters[2,11] and ascribes the tumor resistance to a subpopulation of tumor cells or cancer stem cells (CSCs).[5] These CSCs exhibit features of self-renewal and the ability to differentiate into other cancer cells, and are implicated in promoting the phenotypes of tumor resistance.[8,12,13] Consequently, many therapies fail to eradicate these subpopulations resulting in the high rate of recurrence in breast cancer.[8,13]

Studies have shown the merit of combination therapy for treatment of triple-negative breast cancer (TNBC).[9,14,15] However, CSCs constrain the effectiveness of chemotherapy via acquisition of developmental resistance phenotypes.[8,12,16] Thus, for effective therapeutic outcome adjuvant and/or neoadjuvant chemotherapies (NACTs) must possess expansive therapeutic potency against the different niches within a tumor population. We synthesized a cationic, lipid-conjugated estradiol derivative (ESC8) with tumor cell-killing properties in breast cancer regardless of ER, PR, and HER2 status.[17] ESC8 inhibited TNBC cell viability by induction of apoptosis and autophagy.[17] Apoptosis was induced via the intrinsic pathway by inhibition of Bcl2 resulting in mitochondrial release of cytochrome C and activation of the caspase cascade. Autophagy was mediated by Atg5-dependent activation of LC3B-II as well as by inhibition of PI3K-Akt-mTOR signaling.[17] Translational relevance of ESC8-mediated apoptosis and autophagy in TNBC was demonstrated in a mouse xenograft tumor model by intraperitoneal administration of ESC8 (10 mg/kg) with significant tumor growth inhibition and regression.[17]

The demand for oral anticancer drugs is high especially among patients, chiefly as a means of convenience.[18] For many anticancer agents that are taken daily, the benefit of convenience must be balanced with safety and efficacy of the therapy. ESC8 was well tolerated in noncancer cells and, inferring from its core steroidal structure, which is akin to cholesterol, demonstrated a disposition toward self-assembly into nanoparticles in aqueous media.[17] The primary aim of this study, therefore, was to prepare ESC8 formulation for oral delivery to treat TNBC in a mice xenograft model. We hypothesized that ESC8 lipid nanocarrier formulations would be orally bioavailable, inhibit tumor growth, and enhance platinum-based chemotherapy in a mouse tumor model of TNBC. The aims of this study were to (i) investigate ESC8 anticancer activity in TNBC and non-TNBC cells as a single or combination treatment, (ii) prepare, characterize, and optimize ESC8 lipid nanocarriers (liposomes, solid lipid nanoparticles, and nanostructured lipid carriers) for oral delivery, (iii) investigate the pharmacokinetic properties of ESC8 nanoparticles in rats, (iv) investigate the antitumor activity of ESC8 lipid nanocarriers in a mouse-model of TNBC, and (v) determine the molecular mechanisms mediating the antitumor activities of ESC8 lipid nanocarriers.

2. MATERIALS AND METHODS

2.1. Reagents. 1,2-Dioleoyl-*sn*-glycero-3-phosphocholine (DOPC), 1,2-dioleoyl-*sn*-glycero-3-phosphoethanolamine (DOPE), and 1,2-distearoyl-*sn*-glycero-3-phosphoethanolamine-*N*-[maleimide(polyethylene glycol)-2000] (ammonium salt) (DSPE-PEG(2000) Maleimide) were purchased from Avanti Polar Lipids (Alabaster, AL). Geleolmono, diglycerides, and compritol 888 were obtained from Gattefosse (Paramus, NJ), and d-alpha tocopheryl polyethylene glycol 1000 succinate (vitamin E-TPGS) was procured from Antares Health Products (Simpsonville, SC). EGFR, Slug, p21, phospho-Akt1, Vimentin, NFkβ, and IKKγ primary antibodies were purchased from Cell Signaling Technology (Danvers, MA); β-actin primary antibody, antimouse, and antirabbit secondary antibodies were obtained from Santa Cruz Biotechnology (Dallas, TX). ESC8 was synthesized in large quantities according to the previously published protocol.[17] All other chemicals and reagents used were of cell culture or reagent grade.

2.2. Cell Lines. MDA-MB-231 (HTB-26), MDA-MB-468 (HTB-132), BT-474 (HTB-20), and SK-BR-3 (HTB-30) were procured from the American Type Cell Culture (Manassas, VA). MDA-MB-231 and MDA-MB-468 cells were maintained in DMEM:F12 (1:1), BT-474 in RPMI 1640 media, and SK-BR-3 in McCoy's 5a media. All media were fortified with 10% v/v fetal bovine serum (FBS) and 2% v/v penicillin−streptomycin−neomycin cocktail (PSN). All cell lines were maintained at 37 °C under an atmosphere of air (95%) and carbon dioxide (5%).

2.3. Synthesis and Characterization of ESC8. Estrone and all the chemicals and organic solvents required for synthesis were purchased from either Aldrich (Milwaukee, WI) or SD Fine Chem (Mumbai, India). They were used without further purification. ESC8 was synthesized from estrone in large quantities according to the previously published protocol.[17] All the ^{1}H NMR spectra were recorded in $CDCl_3$ and mixture of $CDCl_3$ and CD_3OD on a Bruker FT 300 MHz instrument with residual undeuterated solvent as an internal reference. Chemical shifts, δ (ppm); coupling constants J (Hz); multiplicity, (s) singlet, (d) doublet, (t) triplet, (q) quartet, (m) multiplet; and integration were reported. HPLC chromatogram for ESC8 was obtained on a Varian Prostar Instrument with 100% methanol as mobile phase and UV wavelength of 210 nm.

2.4. Breast Cancer Cell Viability Assay. Two TNBC cells (MDA-MB-231 and MDA-MB-468) and two non-TNBC cells (BT-474 and SK-BR-3) were used for cell viability studies. Cells were cultured to about 80% confluency in T-75 culture flasks and detached with trypsin (0.25%)-EDTA (0.53 mM). Cells were resuspended (1×10^5 cells/mL) in regular growth media and seeded in a 96-well plate format (0.1 mL/well). Following 16−18 h recovery at 37 °C, treatment was done with DMSO or different concentrations of ESC8 in a 0.2 mL volume experimental media per well. Plates were incubated for 72 h

DOI: 10.1021/mp5008629
Mol. Pharmaceutics 2015, 12, 1105−1120

and cell viability assayed by the crystal violet method.[19] Absorbance was taken at 540 nm and data presented as cell viability (% of DMSO) against concentration (μM). The IC_{50} of ESC8 was estimated by linear regression analysis, and results are presented as mean $IC_{50} \pm$ SD. Experiments were done in triplicates and repeated three times. The procedure was repeated for investigating the anticancer efficacy of ESC8 (25 μM) formulated as lipid nanocarriers against MDA-MB-231 cells and compared with ESC8 in DMSO.

2.5. In Vitro Combination Study in Triple-Negative Breast Cancer Cells. Cells were treated with different concentrations of ESC8 alone or in combination with Tamoxifen or Cisplatin in a 0.2 mL volume per well. Plates were incubated for 72 h and cell viability determined by the crystal violet dye method.[19] Absorbance was taken at 540 nm and data presented as cell viability (% of DMSO) against logarithm (base 10) of concentration. The IC_{50} of ESC8 alone and in combination was estimated by linear regression analysis and the interaction of ESC8 in combination with Cisplatin or Tamoxifen analyzed by combination index (CI) method.[19] Results are presented as mean $IC_{50} \pm$ SD. Combination index was determined using the following formula:

$$CI = (D_a/Dx_a) + (D_b/Dx_b) + [\alpha(D_aD_b)/(Dx_aDx_b)]$$

where Dx_a = dose of drug A to produce 50% cell kill alone; D_a = dose of drug A to produce 50% cell kill in combination with drug B; Dx_b = dose of drug B to produce 50% cell kill alone; D_b = dose of drug B to produce 50% cell kill in combination with drug A; α = 0 for mutually exclusive or 1 for mutually nonexclusive modes of drug action. CI > 1 denotes antagonism; CI = 1, additive effect; and CI < 1 connotes synergism.

2.6. Fluorescence Activated Cell Sorting (FACS) Analysis of Cell Cycle Dynamics. Cell were seeded in T-75 flasks (3×10^3 cell) in base DMEM:F12 media supplement with FBS (10% v/v) and PSN (2% v/v) and incubated for 16–18 h. Cells were treated with DMSO, ESC8 (1 or 2 μM), Cisplatin (5 μM), and ESC8 (1 or 2 μM) + Cisplatin (5 μM) for 24 h. Cells were detached with trypsin/EDTA, washed 2× with PBS, fixed in ethanol (200 proof), and stored at −20 °C until use. The fixed cells were pelleted and ethanol discarded followed by washing with PBS 2×. Cells were passed through a 27 gauge needle 3× and reconstituted in staining solution comprising propidium iodide (40 μg/mL), RNase A (10 μg/mL), and sodium citrate (0.3 μM) in PBS at a density of 1×10^6 cells/mL; stained cells were incubated at 37 °C for 1 h. The relative abundance of cells in the G_1-, G_2-, and S-phase of the cell cycle were investigated using a FACSCalibur (BD Biosciences; San Jose, CA). Results were presented as mean (of average events) ± SD against phase of cell cycle. Experiments were repeated 3× for triplicates per group.

2.7. Caco-2 Permeability Studies of ESC8. Caco2 cells were cultured in DMEM:F12 media supplemented with FBS (10% v/v), PSN (2% v/v), nonessential amino acid solution (1.2%v/v), and HEPES (10 mM). At 80% confluency, cells were detached with trypsin/EDTA and washed 2× with PBS. Single cell suspensions in a 0.5 mL volume (10^5 cells per ml) were seeded in the apical compartment of a Costar Transwell Permeable Support with a polycarbonate membrane (0.4 μm pore size) in a 12-well plate format. The cells were maintained under standard culture conditions for 21 days with media changes done on alternate days for 14 days and daily subsequently. The integrity of the monolayer formed was monitored by measuring the transepithelial electrical resistance (TEER) using a Millicell ERS-2 V-Ohm Meter (Millipore, Billerica, MA). The Caco-2 monolayers in the apical compartment were washed 2× with PBS followed by HBSS–HEPES buffer (pH 5.8). The inserts were then transferred to a new 12-well plate filled with HBSS–HEPES buffer (pH 7.4) in the basolateral compartment. The buffer in the apical compartment was replaced with fresh buffer at pH 5.8. The plates were allowed to equilibrate for 5 min at 37 °C and the apical and basolateral compartment buffers replaced with ESC8 solution (10 μg/mL in pH 5.8 buffer) and blank buffer (pH 7.4) respectively for absorptive studies. For secretory studies, the ESC8 solution dissolved in HBSS–HEPES buffer (pH 7.4) were added to the basolateral compartment and blank buffer (pH 5.8) added to the apical compartment. The contribution of P-glycoprotein (P-gp) in active transport of ESC8 was investigated by pretreatment of Caco-2 monolayers to the P-gp inhibitor, verapamil (1 mM), for 16 h before permeability studies. The plates were incubated at 37 °C and perfused with air (95%) and CO_2 (5%) under constant shaking (50 rpm) for 2 h. Samples (0.2 mL) were collected from the basolateral compartment (absorptive study) or apical compartment (secretory study) and replaced with fresh buffer. Sampling was done at 0.5, 1.0, 1.5, and 2 h. The samples were then injected into an HPLC separated over a C18 column under isocratic conditions with mobile phase comprising ethanol/water (70:30) at a flow rate of 0.5 mL/min. The amount of ESC8 was estimated by interpolating the peak area obtained from a standard plot of area versus amount of ESC8. The apparent permeability (P_{app}) of ESC8 solution was computed according to

$$P_{app}(\text{cm/s}) = (dQ/dt)[(1/Q_o)(1/A)]V_r$$

where dQ/dt = amount of drug in receiver chamber vs time (μg/s); Q_o = initial amount of drug in donor chamber (μg); T = time (s); A = area of membrane insert (cm^2); V_r = volume of solution receiver chamber (cm^3).

Permeability data were presented as P_{app} of ESC8 solution against time with or without verapamil for absorptive and secretory studies. Experiments were repeated 2×, and determinations of permeability were done in duplicates for each group. The above procedure was repeated for assessing the permeability profiles of various ESC8 lipid nanocarriers and compared with ESC8 in DMSO.

2.8. Preparation and Characterization of ESC8 Lipid Nanocarriers. *2.8.1. Preparation of ESC8 Liposomes (ESC8-Lip).* The procedure for preparation of cationic liposomes is as previously described with modifications.[20] Cationic liposomal formulation containing ESC8 comprising DOPC/DOPE/DSPE-PEG(2000) maleimide in the ratio 3:2:2 at a total lipid content of 10 mM was prepared by the thin-film hydration method. A final volume of 2.5 mL of ESC8 liposome was prepared using 19.65 mg of DOPC, 18.60 mg of DOPE, 80.15 mg of DSPE-PEG, and 50 mg of ESC8 to obtain a 5 mg/mL liposome. ESC8 was dissolved in 0.2 mL of ethanol and added to the phospholipid mixture. The total lipid was dispersed in an equi-volume methanol/chloroform mixture (4 mL) in a round-bottom flask, and the solvent evaporated on a warm water-bath under a nitrogen stream to obtain a thin lipid film. Hydration of the film was done for 4 h by adding double-distilled water (ddH_2O) to make 10 mL of liposome. The resulting liposome was bath-sonicated for 30 min and passed through a 0.2 μm syringe-filter 5 times. The liposome was dialyzed against PBS (pH 7.8) for 4 h in a 2000 molecular weight dialyzing

DOI: 10.1021/mp5008629
Mol. Pharmaceutics 2015, 12, 1105–1120

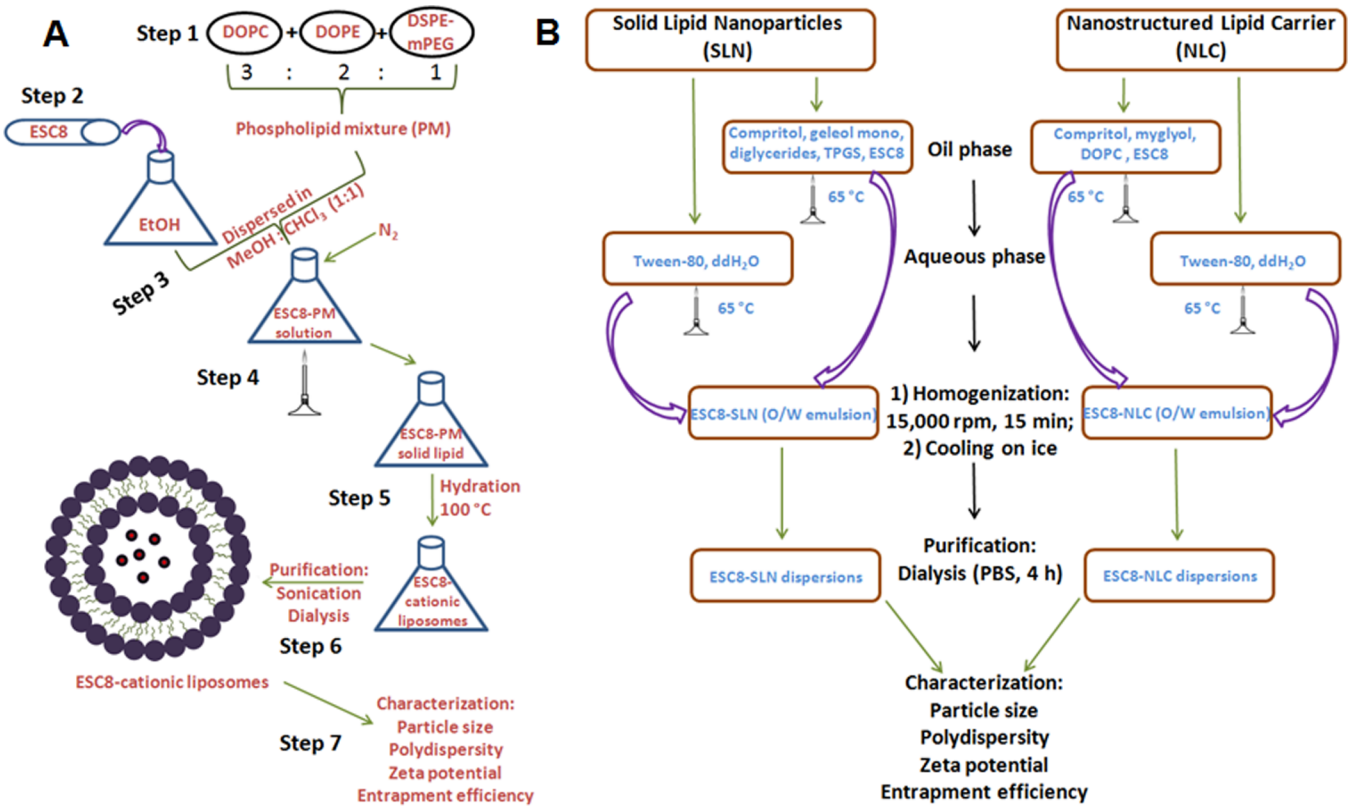

Figure 1. Schematic representation of the synthesis of nanolipid carriers entrapping ESC8. (A) Cationic liposomes entrapping ESC8 (ESC8-Lip) were prepared from DOPC, DOPE, and DSPE-mPEG by solvent evaporation as described in the Materials and Methods. (B) ESC8 was entrapped as solid lipid nanoparticles (ESC8-SLN) or nanostructured lipid carriers (ESC8-NLC) using different combinations of solid and liquid lipid mixtures by emulsification under high speed homogenization as described under Materials and Methods. The nanocarriers formed were characterized for size, polydispersity, zeta potential, and entrapment efficiency.

membrane to remove excess organic solvent. The liposome formulation was characterized for particle size, polydispersity index (PDI), zeta potential, and entrapment efficiency.

2.8.2. Preparation of ESC8 Nanostructured Lipid Carriers (ESC8-NLC). A 5 mL volume sample of ESC8-NLC was made by combining an oil phase composed of compritol (0.5% w/w), migloyl (4% w/w), and DOPC (0.1% w/w) with an aqueous phase comprising Tween-80 (1% w/w) and ddH_2O (94.40% w/w). Briefly, the oil phase with ESC8 (12.5 mg dissolved in 0.2 mL of ethanol) was warmed in a beaker to 65 °C. The aqueous phase was also warmed to 65 °C and added to the oil phase under high speed homogenizing (30,000 rpm for 15 min). The resulting ESC8-NLC was purified by dialysis against PBS (pH 7.8) for 4 h and characterized for particle size, PDI, zeta potential, and entrapment efficiency.

2.8.3. Preparation of ESC8 Solid Lipid Nanoparticles (ESC8-SLN). Solid lipid nanoparticles of ESC8 comprised an oil phase of compritol (0.5% w/w), geleol mono and diglyerides (4% w/w), vitamin E-TPGS (1% w/w), and an aqueous solution consisting of Tween-80 (1% w/w) and ddH_2O(93.5 w/w) giving a final amount of 5 g of SLN. The procedure for preparation of ESC8-SLN is that same as that for ESC8-NLC. The SLN was purified by dialysis and characterized for size, PDI, zeta potential, and entrapment efficiency (Figure 1).

2.8.4. Characterization of ESC8 Lipid Nanocarriers. Particle size and zeta potential of nanoparticles was determined using a Nicomp380 ZLS (Particle Sizing Systems, Port Richey, FL). Nanoparticle formulation (10 μL) was diluted up to 4 mL with ddH_2O, and particle size, PDI, and zeta potential readings were recorded. For entrapment efficiency, ESC8 lipid nanocarriers were filtered by centrifugation using a vivaspin column with molecular weight cutoff (MWCO) of 10 kDa. Entrapment efficiency (EE) was estimated according to

$$EE(\%) = [(W_n - W_r)/W_n] \times 100$$

where W_n = weight of ESC8 in nanoparticle and W_r = weight of ESC8 in centrifugant.

Determinations for particle size, PDI, zeta potential, and entrapment efficiency were done at least three times for each formulation.

ESC8 lipid nanocarriers were also characterized for drug release *in vitro* and for size stability. Release characteristics of ESC8 from lipid carriers (corn oil, liposome, solid lipid nanoparticles, and nanostructured lipid carriers) were investigated using the VanKel 7000 Dissolution System (Varian, Cary, NC) according to the USP Dissolution Apparatus 1 basket method at intestinal conditions (pH 6.8) using an appropriate buffer (comprising 0.75 L of 0.1 N HCl and 0.25 L of 0.2 M Na_3PO_4). ESC8 nanocarriers (10 mg of ESC8 base) were placed in the mesh basket and set to rotate at 50 rpm for 24 h. Sampling (1.0 mL) was done from the external medium at 5, 10, 15, 20, 30, 45, 90, and 120 min; and from 3, 4, 5, 6, 8, 16, and 24 h. Volume correction was maintained by replacing the volume removed with an equal volume of blank buffer. Concentration of drug released was estimated by HPLC. The cumulative concentration of the released drug was normalized

DOI: 10.1021/mp5008629
Mol. Pharmaceutics 2015, 12, 1105−1120

against the initial concentration and plotted as percentage drug release vs time (h).

Size stability was investigated by assessing change in hydrodynamic diameter of nanocarriers with time (7, 14, 28, and 56 days) using the Nicomp380 ZLS. The procedure is as earlier demonstrated under this section; the results were plotted on a graph of hydrodynamic diameter (nm) vs time (days).

2.9. Preparing Plasma Standards of ESC8 for Pharmacokinetic Studies. ESC8 stock solution was prepared by dissolving ESC8 in ethanol (1 mg/mL) and storing at 4 °C. Working solutions of ESC8 were prepared by diluting the primary stock solution to obtain 1.0, 2.5, 5.0, 10.0, 25.0, and 50.0 μg/mL. Plasma calibration standards (0.4, 0.5, 1.0, 2.0, 10.0, and 20.0 μg/mL) were prepared in drug-naive rat plasma obtained from Sprague–Dawley (SD) rats. Rat plasma (160 μL) was spiked with ESC8 working solution (40 μL) and vortexed for 1 min. Quality control (QC) samples were prepared similarly to obtain plasma–drug concentration of 0.4, 1.0, and 10.0 μg/mL corresponding to low, intermediate, and high QC, respectively. Samples were centrifuged at 12,000 × *g* for 10 min and the supernatant collected. Mobile phase consisting of ethanol/water (70:30) was prepared and filtered using a 0.45 μm filter. Samples were injected (0.1 μL) into a Symmetry C18 column connected to a Waters HPLC under isocratic flow of 0.5 mL/min and detection done at 240–320 nm. HPLC runs were done three times for each sample and the same method was maintained for every run.

2.10. Pharmacokinetic Studies of ESC8 in Sprague–Dawley Rats. Sprague–Dawley rats with mean weight of 250 g were divided into 4 groups (n = 3) and given either a single dose of ESC8 as (i) an intravenous bolus (2.0 mg/kg) or (ii) oral liposome or SLN (20.0 mg/kg). The intravenous (i.v.) dose was prepared by dissolving ESC8 in ethanol and dispersing in water to a final volume of 1 mL (5% v/v ethanol). The intravenous dose was administered by tail vein injection while the nanoparticles were administered by oral gavage. Blood samples were collected into heparinized tubes from an initial time at 10 min and the last collection done at 25 h due to a decrease in sensitivity of the detection method. The samples were centrifuged at 12,000 × *g* for 10 min and the plasma collected. To absolute ethanol (20 μL) was added plasma sample (80 μL) and vortexed for 1 min. The mixture was centrifuged at 12,000 × *g* for 15 min to precipitate out plasma proteins. The supernatant was collected and 50 μL run through a C18 symmetry column of an HPLC at a flow rate of 0.5 mL/min under isocratic conditions with mobile phase of ethanol/water (70:30). HPLC runs were done in triplicates for each sample. The peak area of each run was interpolated from the plasma calibration standard plot to obtain the amount of drug. A concentration–time plot of ESC8 was obtained and the data analyzed by WinNonlin (Pharsight, Cary, NC) to obtain the pharmacokinetic parameters for each formulation. The bioavailability (F) of ESC8 nanoparticle was estimated according to

$$F(\%) = (\mathrm{AUC_n} \times \mathrm{dose_{iv}})/(\mathrm{AUC_{iv}} \times \mathrm{dose_n})$$

where $\mathrm{AUC_n}$ = area under the curve of nanocarrier formulation; $\mathrm{dose_{iv}}$ = intravenous dose; $\mathrm{AUC_{iv}}$ = area under the curve of intravenous formulation; and $\mathrm{dose_{iv}}$ = dose of nanocarrier formulation.

2.11. Modeling of TNBC Xenograft Tumors in Mice. Subconfluent MDA-MB-231 cells were harvested using trypsin/EDTA, washed 2× with PBS, and resuspended in serum-free DMEM:F12 media. Cell suspension was diluted in BD Matrigel matrix (BD Biosciences, San Jose, CA) on ice at a 1:6 volume ratio of media to matrigel to a final concentration of 1×10^7 cells/mL. Cell suspensions (1×10^6 cells) were injected into the left mammary fat pad of athymic nude mice in a 100 μL volume.[21]

2.12. Biodistribution of ESC8-SLN and ESC8-NLC in Xenograft Tumors. Mice bearing MDA-MB-231 as tumor xenografts were divided into four groups and administered ESC8-corn oil (10 mg/kg, p.o., n = 2), ESC8-liposome (10 mg/kg, p.o., n = 2), ESC8-SLN (10 mg/kg, p.o., n = 2), or ESC8-NLC (10 mg/kg, p.o., n = 2) by oral gavage. Animals were sacrificed 8 h post-treatment and the tumors excised. Representative tumors (0.5 g from each group) were washed 2× in PBS, sliced into little chunks and homogenized in 5 mL of PBS. The tissue samples centrifuged and the supernatants discarded. The homogenates were washed twice in PBS and ESC8 extracted with absolute ethanol and passed through a 0.45 μm polycarbonate filter. The samples were diluted in mobile phase (ethanol/water; 70:30) and separated by HPLC. ESC8 concentrations were interpolated from standard plot calibrations; the results were presented as tumor concentration of ESC8 (ng/μL).

2.13. Antitumor Efficacy Assessment of ESC8-SLN in a Xenograft Mouse Model. Animals were randomized into 6 groups (n = 4) of (i) untreated group, (ii) blank SLN group, (iii) ESC8-SLN (10 mg/kg) group, (iv) ESC8-SLN (20 mg/kg) group, (v) Cisplatin (2 mg/kg, 2×/week, intraperitoneal) group, and (vi) ESC8-SLN (20 mg/kg) + Cisplatin (2 mg/kg, 2×/week, intraperitoneal) group. Treatment was started when xenograft tumors reached a volume of approximately 65 $\mathrm{mm^3}$. Treatment was done for 14 days and consisted of daily oral (gavage) administration of ESC8-SLN, intraperitoneal injection of Cisplatin solution 2× per week, or the combination thereof for 2 weeks. Cisplatin solution was made by dispersing Cisplatin in normal saline and adjusting pH to 7.4 to obtain a 1 mg/mL suspension. The mixture was bath-sonicated to dissolved Cisplatin. Tumor volume measurements were estimated 2× a week according to

$$\text{tumor volume}(\mathrm{mm^3}) = (W)^2 0.5(L)$$

where W = width of tumor (mm) and L = length of tumor (mm).

2.14. Western Blot Analysis of Xenograft Tumors. Mice were sacrificed under CO_2-induced hypoxia and xenograft tumor resected. Tumor tissue were homogenized in PBS followed by two washed with PBS. The homogenized suspension was centrifuged at 14,000 × *g* for 10 min and the supernatant discarded. Tissue homogenate was suspended in lysis buffer comprising RIPA (G-Biosciences, St. Louis, MO) and protease inhibitor (EMD Millipore, Billerica, MA) and frozen at −80 °C for 2 h. The frozen tissue was probe-sonicated for 1 min and kept on ice for 1 h. The mixture was centrifuged at 12,000 × *g* for 15 min and the supernatant collected. Total protein estimation of tumor tissue lysate was done according manufacturer's instruction using the BCA assay (Thermo Fisher Scientific, Rockford, IL). Protein lysate (50 μg) was separated on a Mini-Protean TGX gel (Bio-Rad Laboratories Inc., Hercules, CA) by SDS-PAGE. Proteins were blotted onto a nitrocellulose membrane and probed for p53, p21, EGFR, Slug, phospho-Akt1, Vimentin, NFkβ, IKKγ, and β-actin. Protein blots were quantified by surface area using the ImageJ

DOI: 10.1021/mp5008629
Mol. Pharmaceutics 2015, 12, 1105–1120

software (National Institutes of Health, Bethesda, MD) and results expressed as β-actin-normalized protein expression with treatment.[22]

2.15. Statistical Analysis. Results were analyzed using GraphPad Prism 5.0 (GraphPad Software, Inc.). Statistical significance in differences in cell cycle was determined by one-way analysis of variance (ANOVA) (**P = 0.0051) followed by Turkey's multiple comparison test (P < 0.05). Caco-2 permeability assay for verapamil (+) vs verapamil (−) was analyzed by paired t test (absorptive, P = 0.1164; secretory, P = 0.6625) and one-way ANOVA for comparing all groups (absorptive vs secretory, P = 0.3102) followed by Bonferonni's multiple comparison test (P < 0.05). Tumor volume was analyzed by one-way ANOVA (***P < 0.0001) followed by Turkey's multiple comparison test (P < 0.05). Differences in protein expression were analyzed using one-way ANOVA (***P < 0.0001) followed by Turkey's post-test (P < 0.05).

3. RESULTS

3.1. ESC8 Inhibits Cell Viabilities of Breast Cancer Cells. ESC8 inhibited cell viabilities of triple-negative (MDA-MB-231 and MDA-MB-468) and nontriple-negative (SK-BR-3 and BT-474) breast cancer cells *in vitro*. The 72 h IC_{50} of ESC8 was 2.70 ± 0.27, 1.38 ± 0.11, 1.94 ± 0.12, and 2.14 ± 0.18 μM in MDA-MB-231, MDA-MB-468, SK-BR-3, and BT-474 cells, respectively. Results (Figure 2) also show concentration-dependent cell killing by ESC8 in all cell lines.

3.2. ESC8 Enhances Cisplatin Cytotoxicity in Triple-Negative Breast Cancer Cells. Cell viability studies of ESC8-treated MDA-MB-231 cells with Cisplatin or tamoxifen were investigated (Figure 3). The 72 h IC_{50} of tamoxifen was 13.64 ± 0.66 and 14.61 ± 2.00 μM when treated alone or in combination with ESC8 (2.00 μM) (Figure 3A). The IC_{50} of Cisplatin decreased from 64.54 ± 4.31 when treated alone to 47.83 ± 1.35 and 4.12 ± 0.27 μM when used in combination with 1.0 and 2.00 μMESC8, respectively (Figure 3B). The combination index of the interaction between Cisplatin and ESC8 is 1.042 (1.00 μM) and 0.665 (2.00 μM) indicating additivity and synergism, respectively.

3.3. Cell Cycle Analysis Triple-Negative Breast Cancer Cells. FACS analysis of cell cycle dynamics of MDA-MB-231 cells was carried out after a 24 h treatment with DMSO, ESC8 (1.00 and 2.00 μM), Cisplatin (5 μM), and ESC8 (1.00 and 2.00 μM) + Cisplatin (5 μM) (Figure 4). Entry of cells into the G_2-phase of the cell cycle was inhibited Cisplatin (5 μM) and was the only significant change observed. The average events in G_2 after treatment with Cisplatin is significantly decreased to 5.13 ± 0.078 compared to DMSO (5.87 ± 0.38) and 1.00 and 2.00 μM ESC8 (6.37 ± 0.16 and 6.57 ± 0.21, respectively). Cisplatin-mediated inhibition of G_2 was reversed by combination treatment with 1.00 and 2.00 μM ESC8 (5.89 ± 0.07 and 6.68 ± 0.36, respectively).

3.4. Caco-2 Permeability Studies of ESC8 Solution. Bidirectional permeability profile of ESC8 across the Caco-2 monolayer with and without verapamil, a P-glycoprotein inhibitor is presented in Table 1. Absorptive flux of total ESC8 was determined by sampling from the basolateral compartment at fixed time points up to 2 h, and the apparent permeability (P_{app}) was estimated. The absorptive apparent permeability of ESC8 alone and with verapamil (1 mM) across the Caco-2 monolayer was 3.98 ± 0.14 × 10^{-6} and 3.65 ± 0.13 × 10^{-6} cm/sec, respectively. Secretory transport of ESC8 was characterized by an apparent permeability of 3.30 ± 0.13 × 10^{-6} and 3.18 ± 0.12 × 10^{-6} cm/sec without and with verapamil, respectively. The efflux ratio of ESC8 alone and with verapamil (1 mM) was estimated to be 0.83 ± 0.03 and 0.87 ± 0.04, respectively.

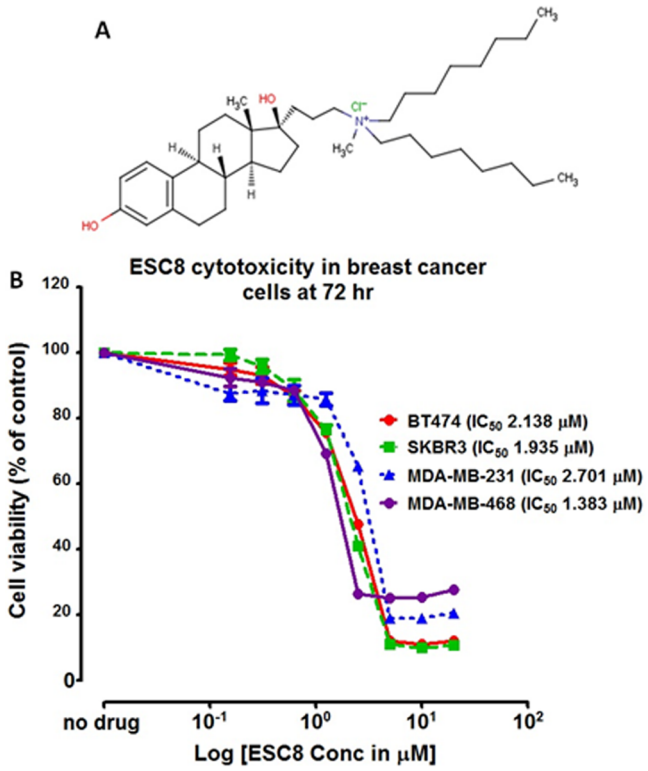

Figure 2. Estradiol derivative ESC8 is cytotoxic to triple negative and nontriple negative breast cancer cells. (A) Structure of the lipid-modified estradiol derivative, ESC8. ESC8 is synthesized by the addition of a long alkyl chain quaternary ammonium moeity at carbon 17 of the estradiol structure. (B) ESC8 exhibits anticancer activities against triple negative (MDA-MB-231 and MDA-MB-468) and nontriple negative (BT-474 and SK-BR-3) breast cancer cells *in vitro*. Breast cancer cells were treated with different concentrations of ESC8 in DMSO and cell viability determined after 72 h as described under Materials and Methods. Data is presented as percentage cell viability with concentration (μM). The IC_{50} (μM) of ESC8 against each cell line was determined by linear regression analysis. Data are presented as the mean ± SD of at least 3 determinations.

3.5. Characterization of Nanoparticles. Results from characterization of ESC8 nanoparticles are presented in Table 2. Particle sizes for ESC8-Lipsome (ESC8-Lip), ESC8-NLC, and ESC8-SLN are 219.0 ± 2.83, 233.5 ± 4.95, and 203.0 ± 11.31 nm, respectively. The differences in particle size are significant for ESC8-Lip vs ESC8-SLN (*P < 0.05), and ESC8-NLC vs ESC8-SLN (***P < 0.05). The differences in mean PDI of 0.34 ± 0.06, 0.33 ± 0.08, and 0.35 ± 0.04 for ESC8-Lip, ESC8-NLC, and ESC8-NLC (P < 0.05), respectively, were not significant. ESC8-Lip is negatively charged (−12.64 ± 0.76 mV), while ESC8-NLC and ESC8-SLN had positive charges of 23.74 ± 1.09 and 14.53 ± 0.36 mV, respectively. The differences in mean zeta potential were significant for ESC8-Lip vs ESC8-NLC (***P < 0.0001), ESC8-Lip vs ESC8-SLN (*P < 0.05), and ESC8-NLC vs ESC8-SLN (***P < 0.0001). Entrapment efficiencies of ESC8-Lip, ESC8-NLC, and ESC8-SLN were 84.62 ± 5.12, 93.75 ± 4.22, and 96.31 ± 6.49%, and the difference in the mean entrapment efficiencies of ESC8-Lip vs ESC8-SLN was significant (*P < 0.05).

DOI: 10.1021/mp5008629
Mol. Pharmaceutics 2015, 12, 1105−1120

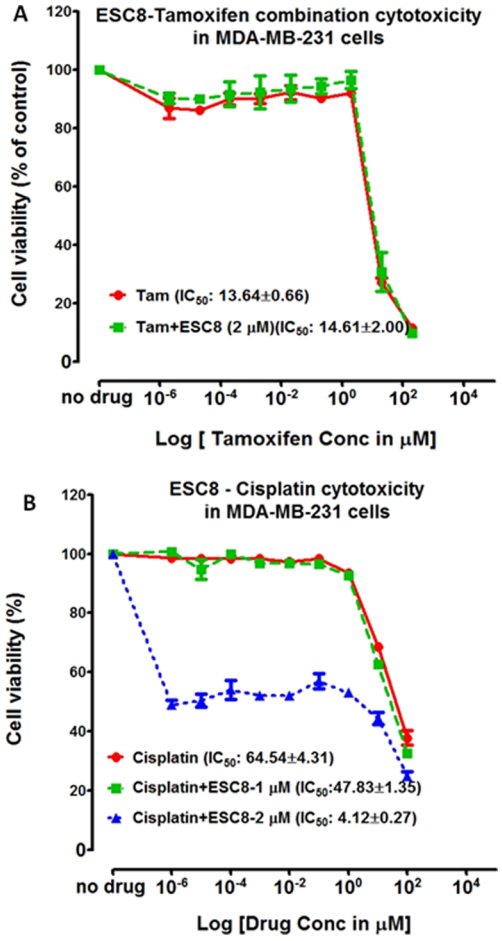

Figure 3. ESC8 inhibits triple negative breast cancer (TNBC) cell viability. Viability of MDA-MB-231 TNBC cells was determined after treatment with (A) Tamoxifen (Tam) and (B) Cisplatin alone or in combination with ESC8 after 72 h. Data is presented as percentage cell viability against concentration (μM). The IC_{50} (μM) of Tam or Cisplatin as a single or combination treatment with ESC8 was determined by linear regression analysis. The interaction between combination treatments was estimated by the isobologram method and presented combination index (CI). Data are presented as the mean ± SD of at least 3 determinations.

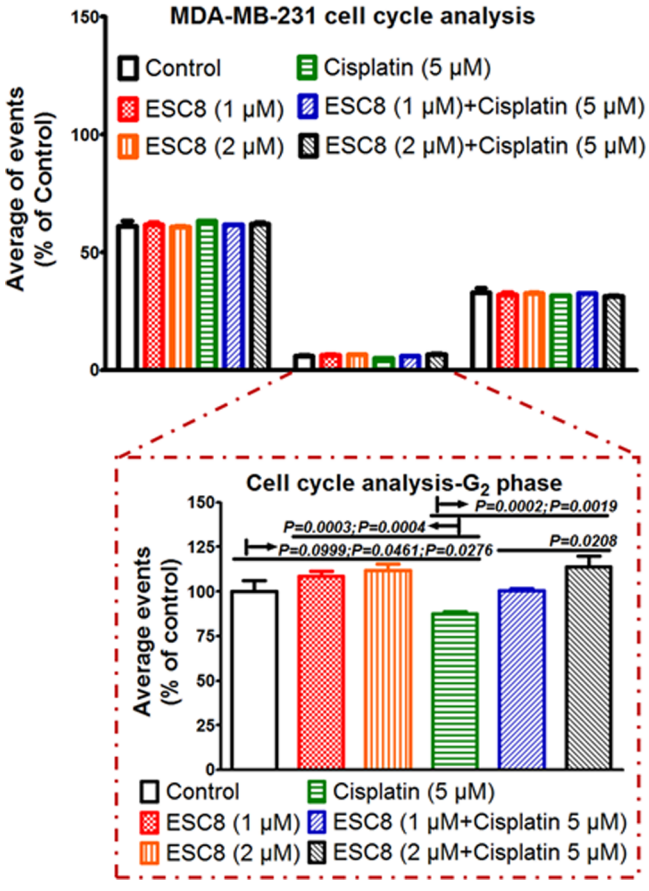

Figure 4. FACS analysis of cell cycle dynamics of triple-negative breast cancer cells. MDA-MB-231 cells were treated with ESC8 (1 and 2 μM), Cisplatin (5 μM), and their combinations for 24 h. Cells were stained with ethidium bromide and analyzed by FACS as described in Materials and Methods. Data are presented as the mean ± SD of 3 determinations of percentage average events against treatment. Statistical analysis was done using GraphPad and the differences observed between means analyzed by unpaired t test. $P < 0.0003$ (Cisplatin, 5 μM vs ESC8, 1 μM); $P = 0.0004$ (Cisplatin, 5 μM vs ESC8, 2 μM); $P = 0.0002$ (ESC8 1 μM + Cisplatin 5 μM); and $P = 0.0019$ (ESC8 2 μM + Cisplatin 5 μM).

A plot of percent drug release versus time and the change in particle size with time is presented in Figure 5. *In vitro* kinetics study compared the release characteristics of ESC8 from formulations with corn oil, liposome, solid lipid nanoparticles (SLN), and nanostructured lipid carriers (NLC). The release of ESC8 from SLN closely followed that of NLC with an initial burst release of 42.81 ± 0.83% and 37.37 ± 3.29%, respectively, at 1 h. Drug release followed first-order kinetics with almost a complete release of 98.78 ± 4.95% and 96.14 ± 3.74% for ESC8-SLN and ESC8-NLC by 24 h. ESC8 release from liposomes was relatively greater than corn oil at all time points but was lower with respect to SLN and NLC. At 1 and 24 h, 17.89 ± 0.29% and 85.03 ± 3.88% of ESC8 was released from liposomes compared to 7.31 ± 0.82% and 78.82 ± 3.19%, respectively, from corn oil. While the differences in the drug release from SLN and NLC were not considered at all points ($P > 0.05$), the differences in drug release from SLN and NLC compared to liposome and corn oil were significant ($P < 0.0001$).

Table 1. Permeability Studies of ESC8 Solution Across the Caco-2 Monolayer[a]

	$P_{app} \times 10^{-6}$ (cm/s)		efflux ratio (ER)
	A → B	B → A	(B → A)/(A → B)
ESC8 [25 μM]	3.98 ± 0.14	3.30 ± 0.13	0.83 ± 0.03
(+)verapamil [1 mM]	3.65 ± 0.13	3.18 ± 0.12	0.87 ± 0.04

[a]Permeability of ESC8 from apical to basolateral (A → B) compartment (absorptive transport) and from basolateral to apical (B → A) compartment (secretory transport) of Caco-2 monolayer was investigated at different time points. Apparent permeability determinations (cm/s) were made with or without a P-glycoprotein inhibitor (verapamil) to verify the contribution of P-glycoprotein in active transport of ESC8. Efflux ratio was determined by dividing the absorptive flux by secretory efflux. Results were presented as means with standard deviation. Statistical analysis of the differences observed was performed using t test. The differences were not significant ($P < 0.05$).

The change in particle size with time is present in Figure 5B. Particle size for all formulations showed linear increases with time; with maximum increases observed at the end of 8 weeks.

DOI: 10.1021/mp5008629
Mol. Pharmaceutics 2015, 12, 1105−1120

Table 2. Characterization of ESC8 Nanoparticles for Oral Delivery[a]

formulation	particle size (nm)	PDI	zeta potential (mV)	EE (%)
ESC8-Lip	219 ± 2.83*	0.34 ± 0.06	−12.64 ± 0.76***	84.62 ± 5.12
ESC8-NLC	232.5 ± 4.95***	0.33 ± 0.08	23.74 ± 1.09	93.75 ± 4.22
ESC8-SLN	203 ± 11.31	0.35 ± 0.04	14.53 ± 0.36***	96.31 ± 6.49*

[a]ESC8-Lip, ESC8-liposome formulation; ESC8-NLC, ESC8-nanostructured lipid carrier; ESC8-SLN, ESC8-solid lipid nanoparticles; PDI = polydispersity index; EE = entrapment efficiency. Statistics: One-way ANOVA ($P < 0.05$) followed by Bonferonni's multiple comparison test. Particle size: ESC8-Lip vs ESC8-SLN (*$P < 0.05$); ESC8-NLC vs ESC8-SLN (***$P < 0.0001$). Zeta potential: ESC8-Lip vs ESC8-SLN (***$P < 0.0001$); ESC8-SLN vs ESC8-NLC (***$P < 0.0001$). EE: ESC8-Lip vs ESC8-SLN (*$P = 0.0307$).

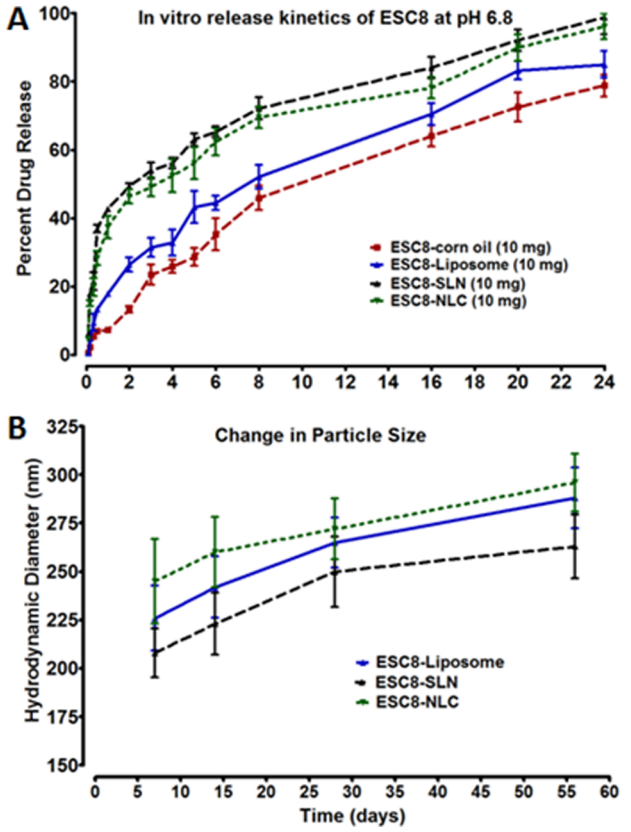

Figure 5. *In vitro* release kinetics and stability of particle size of ESC8 lipid nanocarriers. (A) ESC8 release from lipid nanocarriers (corn oil, liposomes, solid lipid nanoparticles, and nanostructured lipid carriers) were determined using the USP Dissolution Apparatus 1 Basket method under intestinal conditions of pH as described in Materials and Methods. The results were computed as cumulative drug release from nanocarriers vs time (h) and plotted as means with standard deviation. (B) The hydrodynamic particle diameters of ESC8-liposomes, ESC8-SLN, and ESC8-NLC were determined as described at 7, 14, 27, and 56 days intervals. The results were presented as hydrodynamic diameter (nm) vs time (days). All data were obtained from triplicates for each experiment.

These maximum increases represented 27.4%, 26.4%, and 20.8% for ESC8-liposome, ESC8-SLN, and ESC8-NLC, respectively, as a percentage of size at 56 days versus 7 days.

3.6. Anticancer Efficacy and Caco-2 Permeability of ESC8 Lipid Nanocarriers. The anticancer efficacy of ESC8 against MDA-MB-231 cells was investigated across ESC8 in DMSO and three lipid formulations comprising ESC8-liposome, ESC8-SLN, and ESC8-NLC. As presented in Table 3, the differences in efficacy of ESC8 was not considered significant ($P > 0.05$). However, permeability characteristics of ESC8 lipid nanocarriers were significantly altered compared

Table 3. Anticancer Efficacy and Caco-2 Permeability of ESC8 Formulations[a]

ESC8 formulation	MDA-MB-231 IC_{50} [μM]	Caco-2 permeabilty P_{app} × 10^{-6} [cm/s]	
		A → B	B → A
ESC8 solution	2.72 ± 0.18	3.79 ± 0.24	3.36 ± 0.47
ESCS-liposome	2.78 ± 0.26	3.76 ± 0.42	1.58 ± 0.20
ESC8-SLN	2.69 ± 0.21	3.95 ± 0.28	1.22 ± 0.13
ESC8-NLC	2.76 ± 0.33	3.83 ± 0.16	1.26 ± 0.11

[a]ESC8 solution and ESC8 lipid nanocarriers were investigated in MDA-MB-231 cells and Caco-2 monolayer for anticancer efficacy permeability properties, respectively. Efficacy results were calculated from cell viability studies following treatment with formulations containing different concentration of ESC8 base. The respective IC_{50} values were computed as the mean with standard deviation. Permeability of ESC8 from apical to basolateral (A → B) compartment (absorptive transport) and from basolateral to apical (B → A) compartment (secretory transport) of Caco-2 monolayer was investigated at different time points. Apparent permeability was estimated and presented as means with standard deviation. Statistical analysis of the differences observed was performed using *t* test. The differences observed for IC_{50} and absorptive flux (P_{app}, A → B) were not considered significant ($P < 0.05$); differences observed for secretory efflux (P_{app}, B → A) were considered significant ($P < 0.05$).

to ESC8 solution. Although, the absorptive flux of ESC8 across formulations did not vary significantly, the efflux ratio was shifted to favor increased drug retention in the basolateral compartment (percent efflux ratio, i.e., % ER) of ESC8 was reduced 2−3 times in ESC8-liposomes (% ER, 42%), ESC8-SLN (% ER, 31%), and ESC8-NLC (% ER, 33%) compared to ESC8 solution (% ER, 89%).

3.7. Rat Plasma Pharmacokinetics of ESC8 Intravenous Bolus Injection. The concentration−time plot of ESC8 in rat plasma following a single IV bolus injection of ESC8 (2 mg/kg) was estimated from peak area of HPLC chromatograms of injected plasma samples (Figure 6). Curve fitting into a one-compartment model was done using the WinNonlin software, and the pharmacokinetic parameters are presented in Table 4. Following intravenous bolus injection (2 mg/kg) in Sprague−Dawley rats ($n = 3$), curve fitting of plasma concentration−time data into a one-compartment distribution, and first order elimination pharmacokinetic model, the elimination rate for ESC8 was 0.048 ± 0.01 h^{-1} with an elimination half-life of 14.63 ± 2.95 h, and a systemic clearance rate of 0.91 ± 0.24 (L/h/kg). At steady state concentration, volume of distribution of ESC8 was 1.93 ± 0.35 L/kg. The AUC and AUMC were 5469.60 ± 783.62 μg·h/mL and 115484.14 ± 16292.31 μg·h^2/mL, respectively, and the mean residence time was 21.11 ± 3.86 h.

3.8. Rat Plasma Pharmacokinetics of ESC8 Formulations. The concentration−time plot of different ESC8 oral

DOI: 10.1021/mp5008629
Mol. Pharmaceutics 2015, 12, 1105−1120

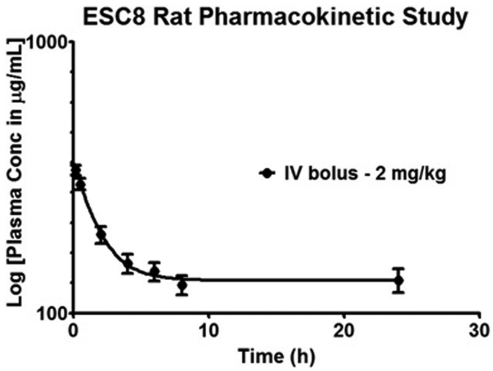

Figure 6. Pharmacokinetic studies of ESC8 solution in Sprague–Dawley rats. ESC8 was administered by intravenous bolus injection (2.0 mg/kg) in rats (n = 3). Blood sample collection was done up to 24 h, and plasma was separated. ESC8 was extracted by ethanol precipitation and separated on a C18 symmetry column under isocratic conditions with ethanol/water (7:3 ratio) at a flow rate of 0.5 mL/min by reverse-phase HPLC. ESC8 plasma concentration was interpolated from rat plasma calibration standards and a concentration–time plot obtained. First-order input, one-compartment distribution, and first-order elimination curve fitting was performed using WinNonlin software, and pharmacokinetic parameters were estimated. Results are presented as mean ± SD (n = 3) of plasma–drug concentration vs time.

Table 4. Pharmacokinetic Parameters of ESC8 Following Intravenous Administration in Sprague–Dawley Rats[a]

pharmacokinetic parameter	ESC8 solution (IV)
$dose_{IV}$ (mg/kg)	2.0
elimination rate, K (h^{-1})	0.048 ± 0.01
elimination half-life, $T_{1/2}$ (h)	14.63 ± 2.95
clearance (L/h/kg)	0.91 ± 0.24
V_{ss} (L/kg)	1.93 ± 0.35
AUC ($\mu g \cdot h/mL$)	5469.60 ± 783.62
AUMC ($\mu g \cdot h^2/mL$)	115484.14 ± 16292.31
MRT (h)	21.11 ± 3.86

[a]Curve fitting of concentration–time plot of ESC8 intravenous bolus in rat was done using WinNonlin. ESC8 was administered to Sprague–Dawley rats (n = 3) by intravenous bolus injection (2 mg/kg). Plasma concentration data was modeled by assuming first-order input, one-compartment distribution, and first order elimination (where, K10 = K01) [condition number = 17.24; AIC criteria = 36.53; SC criteria = 36.42]. V_{ss} = volume of distribution at steady state concentration; AUC = area under the concentration–time curve for drug in plasma after intravenous dose administration. AUMC = area under the first-moment curve of the plasma drug concentration–time curve from time zero to infinity; MRT = mean residence time.

formulations following gavage of SD rats (20 mg/kg dose for ESC8-liposome, ESC8-SLN, and ESC8-NLC groups and 20 mg/kg dose for ESC8-Corn oil group) is presented in Figure 7. One-compartment analyses were performed using WinNonlin to obtain the pharmacokinetic parameters following oral administration (Table 5). ESC8-corn oil attained maximum concentration of 543.70 ± 58.73 at 8.50 ± 0.72 h. ESC8 was eliminated at a rate of 0.12 ± 0.02 h^{-1} with an elimination half-life of 5.89 ± 0.51 h. The volume of distribution was 8.60 ± 1.06 mL, and the rate of clearance was 1.10 ± 0.14 L/h. The $AUC_{0-\infty}$ and $AUMC_{0-\infty}$ were 12357.10 ± 1408.14 $\mu g \cdot h/mL$ and 105057.59 ± 12119.20 $\mu g \cdot h^2/mL$, respectively, with a mean residence time ($MRT_{0-\infty}$) of 8.50 ± 1.33 h. The bioavailability of ESC8-corn oil was 9.04 ± 1.16%. ESC8-liposome and ESC8-SLN recorded maximum concentrations of 486.53 ± 55.36 and 890.62 ± 62.47 $\mu g/mL$ at 6.80 ± 0.69 and 7.32 ± 0.82 h, respectively. The respective elimination rates and elimination half-lives were 0.15 ± 0.01 h^{-1} and 4.71 ± 0.62 h for ESC8-liposome; and 0.14 ± 0.01 h^{-1} and 5.08 ± 0.68 h for ESC8-SLN. ESC8-liposome and ESC8-SLN were distributed in a volume of 3.78 ± 0.41 and 2.07 ± 0.47 mL with clearance rates of 0.56 ± 0.13 and 0.28 ± 0.09 L/h, respectively. The respective $AUC_{0-\infty}$ and $AUMC_{0-\infty}$ were 8991.76 ± 1022.62 $\mu g \cdot h/mL$ and 61131.38 ± 8602.56 $\mu g \cdot h^2/mL$ for ESC8-liposome; and 17728.97 ± 1962.05 $\mu g \cdot h/mL$ and 129834.57 ± 14932.31 $\mu g \cdot h^2/mL$ for ESC8-SLN; $MRT_{0-\infty}$ was 6.80 ± 1.02 and 7.32 ± 1.21 h, respectively. The absolute bioavailability of ESC8-liposome and ESC8-SLN were 16.45 ± 2.22 and 32.41 ± 3.49%, respectively. ESC8-NLC reached maximum concentration of 792.53 ± 75.98 at 7.45 ± 0.86 h. Elimination was at a rate of 0.13 ± 0.02 h^{-1} with an elimination half-life of 5.16 ± 0.44 h. Volume of distribution of ESC8-NLC was 2.32 ± 0.36 mL with a rate of clearance of 0.31 ± 0.12 L/h. The $AUC_{0-\infty}$ and $AUMC_{0-\infty}$ were 16047.25 ± 2070.29 $\mu g \cdot h/mL$ and 119532.76 ± 16042.14 $\mu g \cdot h^2/mL$, respectively, with a $MRT_{0-\infty}$ of 7.45 ± 1.05 h. The absolute bioavailability was 29.33 ± 4.83%.

3.9. ESC8 Inhibits Breast Tumor Growth. Figure 8 shows a plot of change in tumor volume (percentage of initial) vs treatment in a mouse model of breast cancer. The mean change in tumor volume (% of initial) after 14 days treatment with (i) no treatment, (ii) blank SLN, (iii) Cisplatin (2 mg/kg, 2×/week, IP injection), (iv) ESC8-SLN (10 mg/kg/day), (v) ESC8-SLN (20 mg/kg/day), and ESC8-SLN (10 mg/kg/day) + Cisplatin (2 mg/kg, 2×/week, IP injection) were 242.15 ± 32.81, 223.19 ± 18.33, 179 ± 15.72, 63.45 ± 8.29, 55.47 ± 7.06, and 38.74 ± 6.91%, respectively. Analysis of differences in change in tumor volume was done using GraphPad Prism 5.0 and statistical differences estimated by one-way ANOVA (***P < 0.0001) followed by Turkey's multiple compartment test. The differences in the means were not significant for untreated vs blank SLN group (P = 0.2447; Figure 6A). Similarly, no significant differences were observed between ESC8-SLN (10 mg/kg/day) and ESC8-SLN (20 mg/kg/day) (P = 0.1029; Figure 6B). However, the difference in tumor volume between ESC8-SLN (10 mg/kg/day) and Cisplatin (2 mg/kg, 2×/week) was significant (P < 0.0001; Figure 6C). The decrease in tumor volume in ESC8-SLN (10 mg/kg/day) and ESC8-SLN (10 mg/kg/day) + Cisplatin (2 mg/kg, 2×/week, IP injection) groups was significant (P = 0.0002). Overall, the rank in tumor growth inhibition followed the order ESC8-SLN (10 mg/kg/day) + Cisplatin (2 mg/kg, 2×/week, IP injection) ≫ ESC8-SLN (10 mg/kg/day) and ESC8-SLN (20 mg/kg/day) ≫ Cisplatin (2 mg/kg, 2×/week) ≫ controls.

3.10. Biodistribution of Orally Administered ESC8 in Xenograft Tumors. Results for the tumor distribution studies of ESC8 lipid nanocarriers are as shown in Table 6. At 10 mg/kg dose of ESC8 base from lipid formulations, there was 32.2 ± 4.63, 28.5 ± 5.16, 61.9 ± 4.96, and 59.3 ± 5.32 ng of ESC8 from corn oil, liposome, SLN, and NLC, respectively, retained per mg of tumor tissue in 8 h. The respective concentrations represent 12.88%, 11.4%, 24.76%, and 23.72% of ESC8 from corn oil, liposome, SLN, and NLC per loading dose of 250 μg per mice.

3.11. ESC8 Induces p21 Expression in Xenograft Tumors. Protein expression of p21, Caspase-9, EGFR, p-Akt1, Slug, Vimentin, NFkβ, and IKKγ are shown in Figures 9

DOI: 10.1021/mp5008629
Mol. Pharmaceutics 2015, 12, 1105–1120

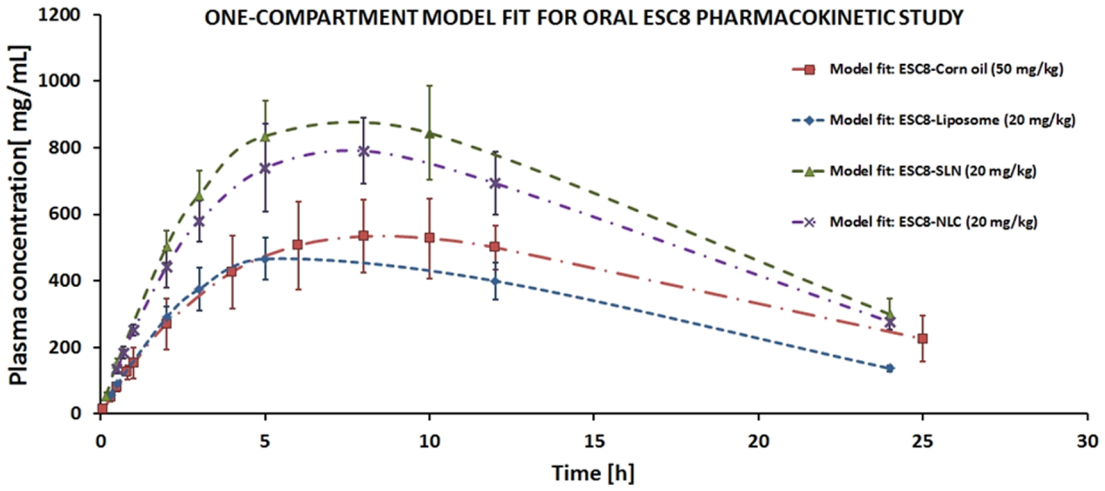

Figure 7. Pharmacokinetic studies of ESC8 nanoparticles in Sprague–Dawley rats. ESC8 was formulated as liposomes and solid lipid nanoparticles and administered to rats at a 20 mg/kg dose by oral gavage. Blood samples were collected up to 24 h and the plasma separated. ESC8 was extracted by ethanol precipitation and separated on a C18 symmetry column under isocratic conditions with ethanol/water (7:3 ratio) at a flow rate of 0.5 mL/min. ESC8 plasma concentration was interpolated from rat plasma calibration standards and a concentration–time plot obtained. First-order input, one-compartment distribution, and first-order elimination curve fitting was performed using WinNonlin software, and pharmacokinetic parameters were estimated. Data presented is the mean ± SD (n = 3) of plasma–drug concentration vs time for each group.

Table 5. Pharmacokinetic Parameters of ESC8 Formulations Obtained by One-Compartment Analysis of Plasma–Drug Concentration Data Following Oral Administration in Sprague–Dawley Rats[a]

pharmacokinetic parameter	ESCS-corn oil	ESC8-liposome	ESC8-SLN	ESC8-NLC
$dose_{PO}$ (mg/kg)	50	20	20	20
C_{max} (μg/mL)	534.70 ± 58.73	486.53 ± 55.36	890.62 ± 62.47[b,c]	792.53 ± 75.98[d,e]
T_{max} (h)	8.50 ± 0.72	6.80 ± 0.69[f]	7.32 ± 0.82	7.45 ± 0.86
K_{el} (r^{-1})	0.12 ± 0.02	0.15 ± 0.01	0.14 ± 0.01	0.13 ± 0.02
$T_{1/2}$ (h)	5.89 ± 0.51	4.71 ± 0.62	5.08 ± 0.68	5.16 ± 0.44
V_d/F (mL)	8.60 ± 1.06	3.78 ± 0.41[g]	2.07 ± 0.47[h,i]	2.32 ± 0.36[j,k]
Cl/F (L/h/kg)	1.01 ± 0.14	0.56 ± 0.13[l]	0.28 ± 0.09[m,n]	0.31 ± 0.12[o]
$AUC_{0-\infty}$ (μg·h/mL)	12357.10 ± 1408.14	8991.76 ± 1022.62[p]	17728.97 ± 1962.05[q,r]	16047.25 ± 2070.29[s]
$AUMC_{0-\infty}$ (μg·hr^2/mL)	105057.59 ± 12119.20	61131.38 ± 8602.56[t]	129834.57 ± 14932.31[u]	119532.76 ± 16042.14[v]
$MRT_{0-\infty}$ (h)	8.50 ± 1.33	6.80 ± 1.02[w]	7.32 ± 1.21[x,y]	7.45 ± 1.05[z,aa]
bioavailabilty, F (%)	9.04 ± 1.16	16.45 ± 2.22	32.41 ± 3.49	29.33 ± 4.83

[a]Sprague–Dawley rats (average weight of 0.25 kg) were dosed with ESC8 formulated as (a) dispersions in corn oil (50 mg/kg), (b) liposomes (20 mg/kg), (c) solid lipid nanoparticles (20 mg/kg), and (d) nanostructured lipid carriers (20 mg/kg) (n = 3 per group). Plasma samples were taken at different time points and assayed for ESC8 using an HPLC method. Plasma concentration–time course data were fitted into a first-order input, one-compartment distribution, and first-order elimination pharmacokinetic model using WinNonlin software. Pharmacokinetic parameters were estimated and the data presented as mean ± SD (n = 3). C_{max} = maximum plasma concentration of drug; T_{max} = time for drug concentration to reach C_{max}; K_{el} = elimination rate constant; half-life, $T_{1/2}$ = time for plasma–drug concentration to fall to half the initial concentration during the elimination phase; V_d/F = volume of distribution of fraction of drug absorbed. Cl/F = clearance of fraction of drug absorbed. $AUC_{0-\infty}$ = area under the plasma concentration–time curve measured through infinity; $AUMC_{0-\infty}$ = area under the concentration times the time versus time curve measured through infinity; $MRT_{0-\infty}$ = mean residence time through infinity; bioavailability, F = fraction of drug absorbed. Statistical analyses: unpaired t test with two-tailed P value [b]C_{max}: ESC8-SLN vs ESC8-corn oil (**P = 0.0022). [c]ESC8-SLN vs ESC8-liposome (**P = 0.0011). [d]ESC8-NLC vs ESC8-corn oil ($^{\#}P$ = 0.0109). [e]ESC8-NLC vs ESC8-liposome ($^{\#\#}P$ = 0.0049). [f]T_{max}: ESC8-liposome vs ESC8-corn oil ($^{¥}P$ = 0.0401). [g]V_d/F: ESC8-liposome vs corn oil ($^{¥¥}P$ = 0.0018). [h]ESC8-SLN vs ESC8-corn oil (***P = 0.0006). [i]ESC8-SLN vs ESC8-liposome (**P = 0.0090). [j]ESC8-NLC vs ESC8-corn oil ($^{\#\#\#}P$ = 0.0006). [k]ESC8-NLC vs ESC8-liposome ($^{\#\#}P$ = 0.0098): [l]Cl/F: ESC8-liposome vs ESC8-corn oil ($^{¥}P$ = 0.0159). [m]ESC8-SLN vs ESC8-corn oil (**P = 0.0016). [n]ESC8-SLN vs ESC8-liposome (*P = 0.374). [o]ESC8-NLC vs ESC8-corn oil ($^{\#\#}P$ = 0.0028). [p]AUC: ESC8-liposome vs ESC8-corn oil ($^{¥}P$ = 0.0286). [q]ESC8-SLN vs ESC8-corn oil (*P = 0.0183). [r]ESC8-SLN vs ESC8-liposome (**P = 0.0024). [s]ESC8-NLC vs ESC8-liposome ($^{\#\#}P$ = 0.0061). [t]AUMC: ESC8-liposome vs ESC8-corn oil ($^{¥¥}P$ = 0.0069). [u]ESC8-SLN vs ESC8-liposome (**P = 0.0023). [v]ESC8-NLC vs ESC8-liposome ($^{\#\#\#}P$ = 0.0003). [w]Bioavailability, F: ESC8-liposome vs ESC8-corn oil ($^{¥¥}P$ = 0.0069). [x]ESC8-SLN vs ESC8-corn oil (***P = 0.0004). [y]ESC8-SLN vs ESC8-liposome (**P = 0.0025). [z]ESC8-NLC vs ESC8-corn oil ($^{\#\#}P$ = 0.0021). [aa]ESC8-NLC vs ESC8-liposome ($^{\#}P$ = 0.0137).

through 12. Protein expression was normalized against β-actin, and the results are presented as mean protein/β-actin ratio with treatment. Elevated levels of p21 were found in all treatment groups compared to the controls. The relative expression of p21 in ESC8-SLN (10 mg/kg) (0.330 ± 0.047) and ESC8-SLN (20 mg/kg) (0.359 ± 0.051) was not considered to be significant between the two groups (P = 0.3388), but were significant when compared to the control groups (P < 0.0001) (Figure 9). Additionally, ESC8-SLN at 20 mg/kg mediated a significantly higher (P < 0.001) p21 expression compared to Cisplatin at 2 mg/kg (0.197 ± 0.014). Combination treatment with ESC8 (10 mg/kg) + Cisplatin (2 mg/kg), however,

DOI: 10.1021/mp5008629
Mol. Pharmaceutics 2015, 12, 1105–1120

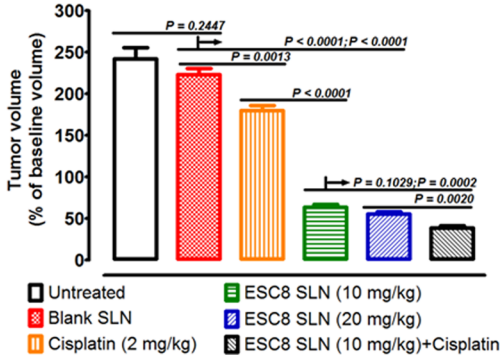

Figure 8. ESC8-SLN formulations inhibit tumor growth in a mouse xenograft model of triple negative breast cancer. Mice were inoculated with MDA-MB-231 cells in the mammary fat pad and treated as described under Materials and Methods. Tumor volume at the end of the treatment period was normalized against the initial volume at the start of treatment and expressed as percentage mean ± SD (n = 4). Tumor volumes were compared between (i) untreated vs blank SLN controls (n = 4); (ii) blank SLN control vs ESC8-SLN (10 mg/kg) vs ESC8-SLN (20 mg/kg) (n = 4); (iii) blank SLN control vs Cisplatin (2 mg/kg, 2× per week, i.p.) vs ESC8-SLN (10 mg/kg) (n = 4); and (iv) blank SLN control vs ESC8-SLN (10 mg/kg) vs ESC8-SLN (10 mg/kg) + Cisplatin (2 mg/kg, 2× per week, i.p.) (n = 4). Statistical analysis of differences in percentage of mean tumor volume was performed using unpaired t test with two-tailed P-value. $P < 0.05$ was considered significant.

Table 6. Biodistribution of ESC8 in Xenograft Tumors[a]

ESC8 formulation [10 mg/kg]	tumor concentration of ESC8 [ng/mg]
ESC8-corn oil	32.2 ± 4.63
ESC8-liposome	28.5 ± 5.16
ESC8-SLN	61.9 ± 4.96
ESC8-NLC	59.3 ± 5.32

[a]ESC8 biodistribution into MDA-MB-231 tumors was investigated following treatment of ESC8 lipid nanocarriers in athymic nude mice bearing MDA-MB-231 cells as xenografts. Mice were given 10 mg/kg single dose of ESC8 as ESC8-corn oil, ESC8-liposome, ESC8-SLN, and ESC8-NLC (n = 2 per group) as described in Materials and Methods. Tumors were excised and ESC8 extracted per unit of tumor tissue. The concentration of ESC8 was estimated from HPLC standard plot interpolations, and the results presented as tumor concentration of ESC8 (ng/mg). Differences between groups were analyzed by one-way ANOVA; (P = 0.58, ESC8-SLN vs ESC8-NLC; $P < 0.05$, ESC8-SLN vs ESC8-corn oil, and ESC8-NLC vs ESC8-corn oil).

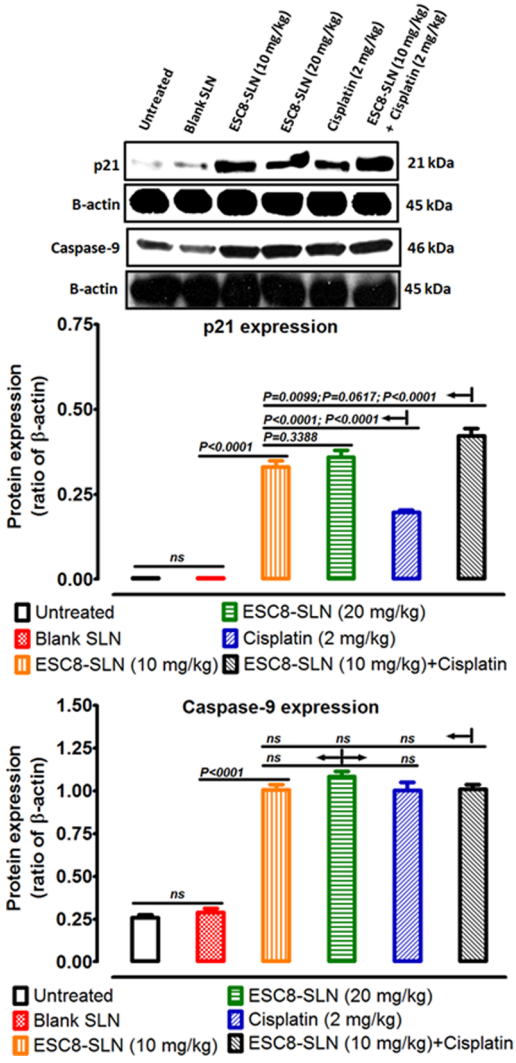

Figure 9. ESC8 formulation inhibits tumor growth by promoting the expression of tumor suppressor and apoptotic markers. Tumor xenografts were resected from mice bearing MDA-MB-231 cells and total protein extracted as described in Materials and Methods. Proteins were separated by SDS-PAGE and probed for markers of tumor suppression (p21) and apoptosis (Caspase-9). Protein expression was quantitated by densitometry using the ImageJ software and normalized with β-actin (internal control), and the results were presented as mean ± SD. Data analysis was done using GraphPad Prism 5.0 and the differences in means with treatment analyzed by unpaired t test. Results are representative of at least triplicates of two determinations.

mediated a greater induction of p21 expression (0.422 ± 0.053) compared to the single treatments (P = 0.0099 vs ESC8, 10 mg/kg; $P < 0.0001$ vs Cisplatin, 2 mg/kg; and P = 0617 vs ESC8, 20 mg/kg). Significant ($P < 0.0001$) increases in Caspase-9 expression of 1.007 ± 0.074, 1.083 ± 0.074, 1.001 ± 0.115, and 1.011 ± 0.066 were observed in the ESC8-SLN (10 mg/kg), ESC8-SLN (20 mg/kg), Cisplatin (2 mg/kg), and ESC8-SLN (10 mg/kg) + Cisplatin (2 mg/kg) groups, respectively, compared to control groups (Figure 9). The differences observed between treatment groups were not significant although ESC8 (20 mg/kg) exhibited a greater expression. Figure 10 shows EGFR expression with significant decreases in all treatment groups compared to the controls ($P <$ 0.0001). ESC8-SLN (10 mg/kg; 0.217 ± 0.009) was superior to ESC8-SLN (20 mg/kg; 0.290 ± 0.006) and Cisplatin (2 mg/kg; 0.259 ± 0.011) in inducing EGFR expression. However, the greatest inhibition was observed in the combination group (0.163 ± 0.009), which was significant compared to each of the single treatments ($P < 0.0001$). Phospho-Akt1 expression (Figure 10) was significantly ($P < 0.05$) decreased in ESC8-SLN (10 mg/kg) (0.348 ± 0.05; P = 0.0051), ESC8-SLN (20 mg/kg) (0.379 ± 0.05; P = 0.0422), and ESC8-SLN (10 mg/kg) + Cisplatin (2 mg/kg) (0.00 ± 0.00; $P < 0.0001$) groups compared to control groups. Phospho-Akt1 expression was, however, elevated in the Cisplatin (2 mg/kg) (0.500 ± 0.06) group, which was significant when compared to ESC8-SLN (10 mg/kg) (P = 0.0008), ESC8-SLN (20 mg/kg) (P = 0.0049), and ESC8-SLN (10 mg/kg) + Cisplatin (2 mg/kg) ($P <$ 0.0001) groups.

In Figure 11, Slug expression was not affected by the lower dose of ESC8-SLN (0.616 ± 0.015) compared to control groups. However, ESC8-SLN (20 mg/kg) and Cisplatin (2 mg/

DOI: 10.1021/mp5008629
Mol. Pharmaceutics 2015, 12, 1105−1120

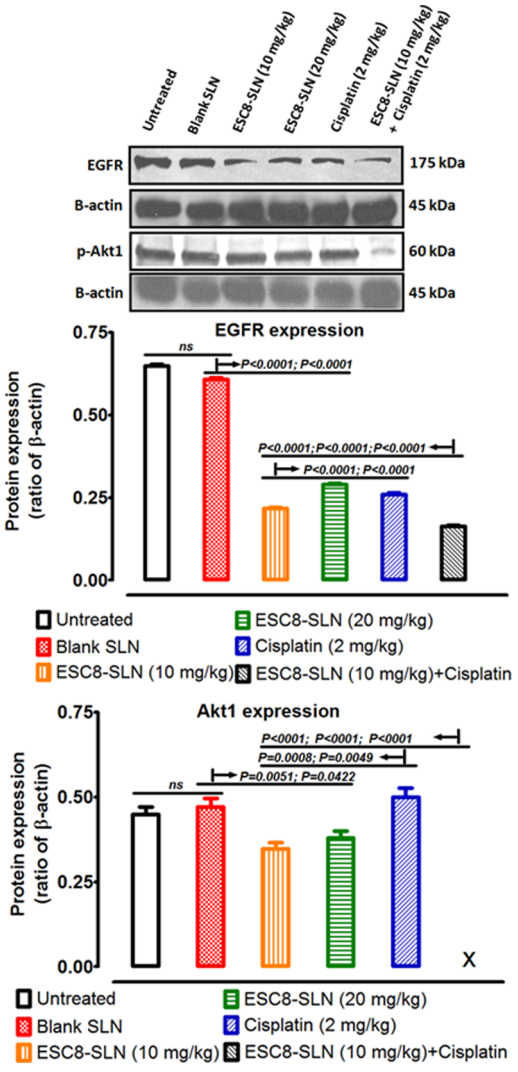

Figure 10. ESC8 formulation inhibits breast tumor growth by inhibiting EGFR and p-Akt1 expression. Tumor xenografts were resected from mice bearing MDA-MB-231 cells and total protein extracted as described in Materials and Methods. Proteins were separated by SDS-PAGE and probed for EGFR and p-Akt1. Protein expression was estimated by densitometry using the ImageJ software and normalized with β-actin. Data analysis was done using GraphPad Prism 5.0, and the differences in means with treatment were analyzed by unpaired t test. Results are representative of at least triplicates of two determinations.

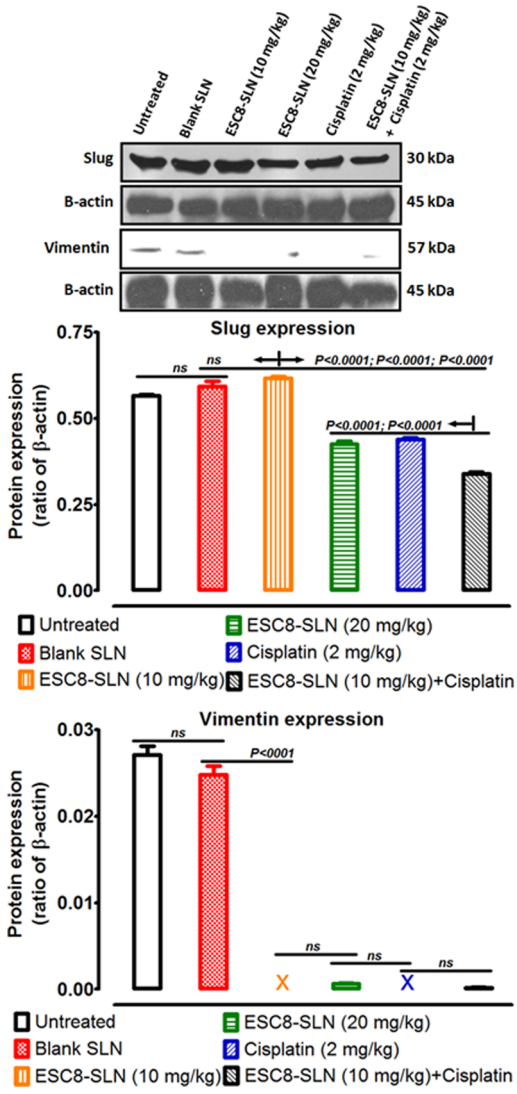

Figure 11. ESC8 formulation inhibits breast tumor growth by inhibiting Slug and Vimentin expression. Tumor xenografts were resected from mice bearing MDA-MB-231 cells and total protein extracted as described in Materials and Methods. Proteins were separated by SDS-PAGE and probed for Slug and Vimentin. Protein expression was estimated by densitometry using the ImageJ software and normalized with β-actin. Data analysis was done using GraphPad Prism 5.0, and the differences in means with treatment were analyzed by unpaired t test. Results are representative of at least triplicates of two determinations.

kg), although comparable, produced significant decreases in Slug expression (0.426 ± 0.017 and 0.439 ± 0.012, respectively) compared to the controls. Consistent with the possibility of an additive interaction, the combination treatment of ESC8-SLN (10 mg/kg) + Cisplatin (2 mg/kg) produced the greatest effect (0.338 ± 0.012) of inhibiting Slug expression compared to all treatment groups (P < 0.0001). Vimentin expression was decreased significantly by 96−100% in all treatment groups compared to the controls (P < 0.0001); however, the differences between the treatment groups were not significant (Figure 11). NFkβ expression was unchanged between ESC8-SLN (10 mg/kg) and ESC8-SLN (20 mg/kg) groups (0.572 ± 0.083 and 0.591 ± 0.082, respectively); they were, however, significantly lower (P = 0.0177 and P = 0.0323, respectively) than the control groups (Figure 12). NFkβ expression levels in ESC8-SLN (10 mg/kg) and ESC8-SLN (20 mg/kg) groups were significantly decreased (P = 0.0223 and P = 0.0471, respectively) relative to the Cisplatin group (0.684 ± 0.059). The decreased NFkβ levels in the ESC8-SLN (10 mg/kg) + Cisplatin (2 mg/kg) group (0.507 ± 0.061) was considered significant when compared to Cisplatin (2 mg/kg) and ESC8-SLN (20 mg/kg) (P = 0.0004 and P = 0.00692, respectively); however, the difference between the combination group and ESC8-SLN (10 mg/kg) group was not significant (P = 0.1474). IKKγ expression was unchanged in ESC8-SLN (10 mg/kg) group (0.828 ± 0.07) compared to controls (0.838 ± 0.01 and 0.851 ± 0.10) (Figure 12). IKKγ expression was, however, decreased significantly in ESC8-SLN (20 mg/kg) (0.503 ± 0.05), Cisplatin (2 mg/kg) (0.636 ± 0.05), and ESC8-SLN (10 mg/kg) + Cisplatin (2 mg/kg) (0.003 ± 0.00) compared to control groups (P < 0.0001, P = 0.0003, and P <

DOI: 10.1021/mp5008629
Mol. Pharmaceutics 2015, 12, 1105−1120

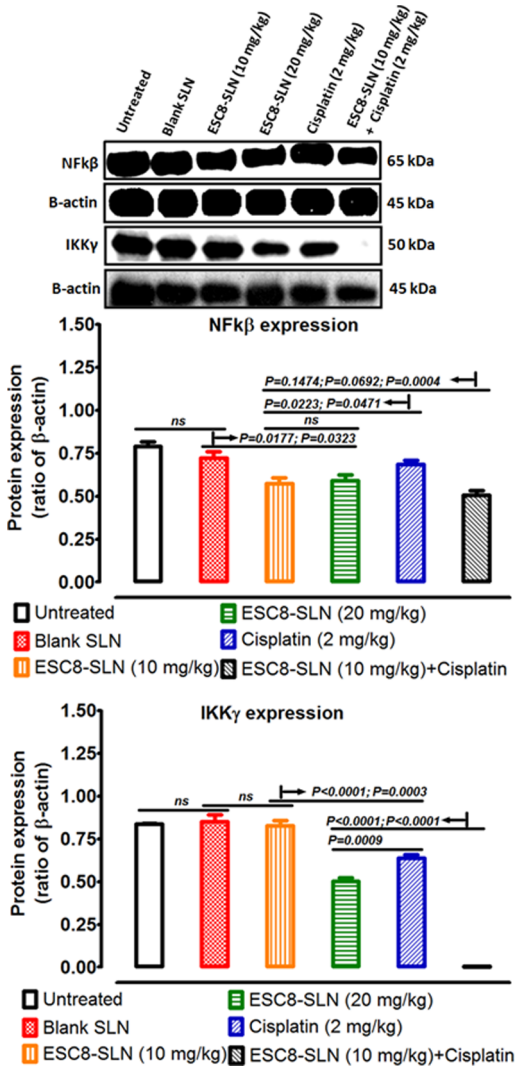

Figure 12. ESC8 formulation inhibits breast tumor growth by inhibiting NFkβ and IKKγ expression. Tumor xenografts were resected from mice bearing MDA-MB-231 cells and total protein extracted as described in Materials and Methods. Proteins were separated by SDS-PAGE and probed for NFkβ and IKKγ. Protein expression was estimated by densitometry using the ImageJ software and normalized with β-actin. Data analysis was done using GraphPad Prism 5.0, and the differences in means with treatment were analyzed by unpaired t test. Results are representative of at least triplicates of two determinations.

0.0001, respectively). IKKγ expression was reduced by 96% in ESC8-SLN (10 mg/kg) + Cisplatin (2 mg/kg) combination compared to the single treatment groups.

4. DISCUSSION

Challenges associated with safe and effective cancer therapy epitomized by the burgeoning of acquired tumor resistance to many anticancer drugs continue to plague cancer treatment. For triple negative breast cancer (TNBC) in particular, the lack of estrogen receptors (ER), progesterone receptors (PR), and human epidermal growth factor receptor 2 receptors (HER2) limits the potential of many prospective candidate drugs for hormone therapy. For this reason, the use of drugs such as tamoxifen, a selective estrogen receptor modulator that is useful in ER-positive breast cancers, is otherwise of little benefit in TNBCs. Therefore, our discovery of a safe cationic lipid-conjugated estrogenic derivative (ESC8) with potent anticancer activity across TNBC and non-TNBC cells (Figure 1) is a promising approach. ESC8 was several folds superior to tamoxifen in invoking potent anticancer responses in MDA-MB-231 cells (Figure 2).[17] We had previously shown that ESC8 induced significant breast tumor regression by combined apoptotic and autophagic mechanisms involving caspase and mTOR signaling, respectively.[17]

We proposed a combinational neoadjuvant chemotherapy approach to treating TNBC-bearing mice using ESC8 (p.o.) and Cisplatin (2 mg/kg, 2×/week, i.p.) for 2 weeks in this study. We justified our approach on the basis of the benefit of neoadjuvant chemotherapy (NACT) in TNBC from various clinical trials.[23,24] Significantly, combination of carboplatin and/or bevacizumab to NACT comprising paclitaxel−doxorubicin−cyclophosphamide increased the pathologic complete response (pCR) rates compared to NACT alone in a randomized controlled trial of Stage II and III TNBC.[24] However, therapeutic responses were associated with marked hematologic and cardiovascular toxicities. Cisplatin, an antineoplastic platinum compound, induces apoptosis and inhibition of cell growth by facilitating DNA cross-linking and DNA−protein complexation.[25,26] However, its usefulness is limited by acquired tumor resistance.[26] Although Cisplatin is being investigated in clinical trials in combination therapies against TNBC,[9,27] it is yet to receive approval for use in breast cancer.[9,15] As expected, Cisplatin inhibited cell growth by inhibiting entry of cells into G_2-phase of the cell cycle *in vitro*; in contrast, ESC8 did not result in any observable cell cycle arrest (Figure 3). This was significant for the combination approach with Cisplatin and ESC8 in terms of the anticipated composite induction of cell death via mutually exclusive mechanisms.[17,28] Investigating cell cycle dynamics was anticipated to afford authors an idea of other mechanisms of action (i.e., cytostasis) of ESC8 in MDA-MB-231 cells. Previously, ESC8 had demonstrated simultaneous apoptotic and autophagic effects (the latter, challenging the conventional association of autophagy with prosurvival of cancer cells).[17] Further, distinct mechanisms of the combination drugs are typically associated with additivity and synergism, and are a safeguard against potential cross-acquired chemoresistance, which has plagued Cisplatin use clinically. In the present study, the authors set out to explore the possibility of ESC8 having cytostatic properties; hence, the investigation of cell cycle changes with ESC8 treatment.

In this study, we examined the feasibility of oral delivery of ESC8 formulated in a lipidic carrier to abrogate tumor growth in a xenograft mouse tumor model of TNBC. Oral delivery is the most popular and convenient route of administration, given the advantages of overcoming limitations including extravasation of drug or blood, catheter infections, and thrombosis associated with intravenous administration.[29−31] Specifically, innovations in nanodelivery systems have enhanced the therapeutic applications of many anticancer drugs.[32] First generation colloidal delivery vehicles such as polymeric nanoparticles, liposomes, micelles, and self-(micro/nano)-emulsifying drug delivery systems (SM/NEDDS) have proved variously useful in enhancing the delivery of poorly bioavailable drugs. However, biocompatibility (polymeric nanoparticles) and stability (liposomes, micelles, and SM/NEDDS) have limited their applications.[33,34] ESC8 is a highly amphiphilic compound with a gummy consistency and undergoes self-assembly in the presence of a surfactant in aqueous media.[17,35]

DOI: 10.1021/mp5008629
Mol. Pharmaceutics 2015, 12, 1105−1120

Thus, we hypothesized that a formulation of ESC8 in a self-nanoemulsifying delivery system will be stable, biocompatible, and orally bioavailable. Many steroids have been shown to be substrates of multidrug resistance proteins including P-glycoprotein (P-gp), which is expressed on the apical side of the intestines and in many tumors.[36−38] However, initial investigation of the possible involvement of P-gp in the transport of ESC8 across Caco-2 monolayer using the P-gp inhibitor verapamil did not support a significant role of P-gp-mediated ESC8 transport (Table 1). We initially optimized ESC8 in a self-nanoemulsifying delivery system (SNEDD) from ternary phase diagrams using soybean oil, Tween 80/transcutol P, and vitamin E TPGS (as oil, surfactant, and cosurfactant, respectively); the SNEDDs exhibited high *in vitro* permeability across the Caco-2 monolayer (data not shown). However, *in vivo* bioavailability of the ESC8-SNEDD was poor due to high ESC8-serum binding (evident from serum-binding immunoassay and pharmacokinetic profile), possibly stemming from instability resulting in SNEDD inversion and/or drug precipitation in plasma.[39] Thus, an alternative delivery system with high stability was necessary.

Second generation colloidal systems such as SLNs and NLCs are more versatile due to their relative stability and biocompatibility.[40] Nanovehicles such as liposome and SLNs have been shown to enhance the oral bioavailability and anticancer efficacies of many antineoplastics.[41,42] Our initial observation with 1,2-dipalmitoyl-*sn*-glycero-phosphatidylethanolamine (DPPE)-polyethylene glycol (PEG)-17β-estradiol (ES) complex formulated as liposomes revealed efficient targeting of estrogen receptor.[35] Sufficient *in vitro* kinetics was attained for near-infrared DiR-labeled cationic liposomes entrapping Annexin A2 shRNA in a lung tumor model in nude mice resulting in 75% tumor growth inhibition.[20] We successfully increased the oral bioavailability of ESC8 formulated as liposomes, nanostructured lipid carriers (NLCs), and solid lipid nanoparticles (SLNs) in rats (Table 4). SLNs exhibited superior drug release properties and a better pharmacokinetic profile compared to the NLCs, liposomes, and corn oil (Figure 5) in keeping with previous findings.[33] Size stability profiles of the formulations were not impacted greatly with time, and while lipid nanocarriers have been shown to exhibit instability overtime, they can be stabilized by lyophilization or adsorption onto a solid matrix.[43] Further, tumor biodistribution studies of the ESC8 lipid nanocarriers showed superior tumor uptake of ESC8 from SLN (Table 6). Therefore, on the basis of a superior drug release, tumor uptake, and pharmacokinetic profiles, we proceeded to investigate the antitumor response of ESC8-SLN in mice bearing TNBC cells as xenografts. Orally bioavailable ESC8-SLN was well tolerated in mice and inhibited tumor growth at doses of 10 mg/kg/day ($P < 0.0001$, vs blank SLN) and 20 mg/kg/day ($P < 0.0001$, vs blank SLN) given for 14 days; and in combination with Cisplatin given intraperitoneally, ESC8-SLN significantly inhibited tumor growth ($P < 0.0001$).

Previously, we had shown that ESC8 induced cell death via apoptosis and autophagy, the latter being facilitated through inhibition of PI3K-Akt-mTOR signaling.[17] The epidermal growth factor receptor (EGFR) is overexpressed in TNBCs and is a promising therapeutic target.[44] The putative ligand of EGFR, the epidermal growth factor (EGF), is involved in normal cellular functions including wound healing and cell growth but has been found to be overexpressed in many cancers.[45,46] EGF-mediated activation of EGFR-PI3K-Akt-mTOR signaling has been shown in many types of cancers.[47−49] ESC8 treatment was accompanied by reduced expression of EGFR closely correlated with reduced Akt1 activation in tumor xenografts and might define the upstream initiation of autophagy (Figure 10). Overexpression of EGFR was associated with reduced expression or mutation in the (wild-type) p53 tumor suppressor, and p53 mutation led to acquired oncogenic phenotype resulting in EGFR recycling and a more aggressive TNBC.[50] However, the induction of p21 and inhibition of EGFR and phospho-Akt1 expression by ESC8 progressed independent of the p53 expression level although a p53 mutated status was very likely.[51,52] Stimulation of p21 expression by p53 results in the inhibition of cyclin-dependent kinases (CDKs) involved in promoting cell cycle, thereby inhibiting both G_1-S phase and G_2-mitosis transitions.[52,53] The p53/p21-mediated inhibition of cell cycle progression may be accompanied by apoptosis induction, and the induction of Caspase-9 expression through extrinsic apoptotic mechanisms is necessary for the proteolytic activation of Caspases-3, -6, and -7 to induce apoptosis.[54] Vimentin is a protein expressed in mesenchymal cells, is well appreciated as a marker for epithelial-to-mesenchymal transition (EMT), and whose expression was decreased significantly in all treatment groups.[55] Additionally, Slug, a transcriptional protein associated with EMT through inhibition of E-cadherin and found overexpressed in many tumor types, was reduced by ESC8.[53] ESC8 was, therefore, sufficiently capable of perturbing EMT through inhibition of Slug and Vimentin expression although the delineation of the extent of EMT reversal was outside the scope of the present study.

In conclusion, our study demonstrates the broad anticancer properties of ESC8 in triple negative and nontriple negative breast cancer. Significantly, tailoring ESC8 for oral administration was achieved by formulating them into SLN with translational relevance as demonstrated by the inhibition of tumor growth either as a single treatment or with Cisplatin. The molecular mechanisms defining these anticancer effects were outlined and show the promising prospect of ESC8-SLN as a candidate for adjuvant and/or neoadjuvant therapy in triple negative breast cancer.

AUTHOR INFORMATION

Corresponding Author

*Address: Department of Pharmaceutics, Florida A&M University, 1520 South Martin Luther King Jr. Boulevard, Dyson Pharmacy Building, Room 021, Tallahassee, Florida 32307, United States. Tel: 850-345-2754. Fax: 850-599-3813. E-mail: mandip.sachdeva@famu.edu.

Author Contributions

⊥These authors contributed equally to this work.

Notes

The authors declare no competing financial interest.

ACKNOWLEDGMENTS

This research was supported with funding from the National Institutes of Health's Minority Biomedical Research Support (MBRS)-SC1 program [Grant # SC1 GM092779-01; to M.S.]; the National Institute on Minority Health and Health Disparities (NIMHD) P20 program [Grant # 1P20 MD006738-03; to M.S.]; and the Department of Defense (DOD) Breast Cancer Program [Grant # W81XWH-11-1-0211]. G.S. thanks Council of Scientific and Industrial Research

DOI: 10.1021/mp5008629
Mol. Pharmaceutics 2015, 12, 1105−1120

(CSIR), Govt. of India for his doctoral fellowship. R.B. thanks CSIR Network project CSC0302 and DST [SR/S1/OC-64/2008], Govt. of India for research support.

REFERENCES

(1) Al-Hajj, M.; Wicha, M. S.; Benito-Hernandez, A.; Morrison, S. J.; Clarke, M. F. Prospective identification of tumorigenic breast cancer cells. *Proc. Natl. Acad. Sci. U.S.A.* **2003**, *100*, 3983−3988.

(2) Koboldt, D. C.; Fulton, R. S.; McLellan, M. D.; Schmidt, H.; Kalicki-Veizer, J.; McMichael, J. F.; Fulton, L. L.; Dooling, D. J. Comprehensive molecular portraits of human breast tumours. *Nature* **2012**, *490*, 61−70.

(3) American Cancer Society. Cancer Facts & Figures 2014. http://www.cancer.org/research/cancerfactsstatistics/cancerfactsfigures2014/index (accessed September 2, 2014).

(4) Siegel, R.; Naishadham, D.; Jemal, A. Cancer statistics, 2013. *Cancer J. Clin.* **2013**, *63*, 11−30.

(5) Bhat-Nakshatri, P.; Goswami, C. P.; Badve, S.; Sledge, G. W., Jr.; Nakshatri, H. Identification of FDA-approved drugs targeting breast cancer stem cells along with biomarkers of sensitivity. *Sci. Rep.* **2013**, *3*, 2530.

(6) Joensuu, H.; Gligorov, J. Adjuvant treatments for triple-negative breast cancers. *Ann. Oncol* **2012**, *23* (Suppl 6), vi40−45.

(7) Jelovac, D.; Emens, L. A. HER2-directed therapy for metastatic breast cancer. *Oncology* **2013**, *27*, 166−175.

(8) Azzam, D. J.; Zhao, D.; Sun, J.; Minn, A. J.; Ranganathan, P.; Drews-Elger, K.; Han, X.; Picon-Ruiz, M.; Gilbert, C. A.; Wander, S. A.; Capobianco, A. J.; El-Ashry, D.; Slingerland, J. M. Triple negative breast cancer initiating cell subsets differ in functional and molecular characteristics and in gamma-secretase inhibitor drug responses. *EMBO Mol. Med.* **2013**, *5*, 1502−1522.

(9) Baselga, J.; Gomez, P.; Greil, R.; Braga, S.; Climent, M. A.; Wardley, A. M.; Kaufman, B.; Stemmer, S. M.; Pego, A.; Chan, A.; Goeminne, J. C.; Graas, M. P.; Kennedy, M. J.; Ciruelos Gil, E. M.; Schneeweiss, A.; Zubel, A.; Groos, J.; Melezinkova, H.; Awada, A. Randomized phase II study of the anti-epidermal growth factor receptor monoclonal antibody cetuximab with cisplatin versus cisplatin alone in patients with metastatic triple-negative breast cancer. *J. Clin. Oncol.* **2013**, *31*, 2586−2592.

(10) Bayraktar, S.; Gluck, S. Molecularly targeted therapies for metastatic triple-negative breast cancer. *Breast Cancer Res. Treat.* **2013**, *138*, 21−35.

(11) Sorlie, T.; Perou, C. M.; Tibshirani, R.; Aas, T.; Geisler, S.; Johnsen, H.; Hastie, T.; Eisen, M. B.; van de Rijn, M.; Jeffrey, S. S.; Thorsen, T.; Quist, H.; Matese, J. C.; Brown, P. O.; Botstein, D.; Lonning, P. E.; Borresen-Dale, A. L. Gene expression patterns of breast carcinomas distinguish tumor subclasses with clinical implications. *Proc. Natl. Acad. Sci. U.S.A.* **2001**, *98*, 10869−10874.

(12) Yin, S.; Xu, L.; Bonfil, R. D.; Banerjee, S.; Sarkar, F. H.; Sethi, S.; Reddy, K. B. Tumor-initiating cells and FZD8 play a major role in drug resistance in triple-negative breast cancer. *Mol. Cancer Ther.* **2013**, *12*, 491−498.

(13) Liu, P.; Kumar, I. S.; Brown, S.; Kannappan, V.; Tawari, P. E.; Tang, J. Z.; Jiang, W.; Armesilla, A. L.; Darling, J. L.; Wang, W. Disulfiram targets cancer stem-like cells and reverses resistance and cross-resistance in acquired paclitaxel-resistant triple-negative breast cancer cells. *Br. J. Cancer* **2013**, *109*, 1876−1885.

(14) Hurley, J.; Reis, I. M.; Rodgers, S. E.; Gomez-Fernandez, C.; Wright, J.; Leone, J. P.; Larrieu, R.; Pegram, M. D. The use of neoadjuvant platinum-based chemotherapy in locally advanced breast cancer that is triple negative: retrospective analysis of 144 patients. *Breast Cancer Res. Treat.* **2013**, *138*, 783−794.

(15) Kim, E. M.; Mueller, K.; Gartner, E.; Boerner, J. Dasatinib is synergistic with cetuximab and cisplatin in triple-negative breast cancer cells. *J. Surg. Res.* **2013**, *185*, 231−239.

(16) Lee, J.; Gollahon, L. Nek2-targeted ASO or siRNA pretreatment enhances anticancer drug sensitivity in triplenegative breast cancer cells. *Int. J. Oncol.* **2013**, *42*, 839−847.

(17) Sinha, S.; Roy, S.; Reddy, B. S.; Pal, K.; Sudhakar, G.; Iyer, S.; Dutta, S.; Wang, E.; Vohra, P. K.; Roy, K. R.; Reddanna, P.; Mukhopadhyay, D.; Banerjee, R. A lipid-modified estrogen derivative that treats breast cancer independent of estrogen receptor expression through simultaneous induction of autophagy and apoptosis. *Mol. Cancer Res.* **2011**, *9*, 364−374.

(18) Foulon, V.; Schoffski, P.; Wolter, P. Patient adherence to oral anticancer drugs: an emerging issue in modern oncology. *Acta Clin. Belg.* **2011**, *66*, 85−96.

(19) Andey, T.; Patel, A.; Jackson, T.; Safe, S.; Singh, M. 1,1-Bis (3′-indolyl)-1-(p-substitutedphenyl)methane compounds inhibit lung cancer cell and tumor growth in a metastasis model. *Eur. J. Pharm. Sci.* **2013**, *50*, 227−241.

(20) Andey, T.; Marepally, S.; Patel, A.; Jackson, T.; Sarkar, S.; O'Connell, M.; Reddy, R. C.; Chellappan, S.; Singh, P.; Singh, M. Cationic lipid guided short-hairpin RNA interference of annexin A2 attenuates tumor growth and metastasis in a mouse lung cancer stem cell model. *J. Controlled Release* **2014**, *184*, 67−78.

(21) Chougule, M. B.; Patel, A. R.; Jackson, T.; Singh, M. Antitumor activity of Noscapine in combination with Doxorubicin in triple negative breast cancer. *PLoS One* **2011**, *6*, e17733.

(22) Lee, S. O.; Andey, T.; Jin, U. H.; Kim, K.; Singh, M.; Safe, S. The nuclear receptor TR3 regulates mTORC1 signaling in lung cancer cells expressing wild-type p53. *Oncogene* **2012**, *31*, 3265−3276.

(23) Liedtke, C.; Mazouni, C.; Hess, K. R.; Andre, F.; Tordai, A.; Mejia, J. A.; Symmans, W. F.; Gonzalez-Angulo, A. M.; Hennessy, B.; Green, M.; Cristofanilli, M.; Hortobagyi, G. N.; Pusztai, L. Response to neoadjuvant therapy and long-term survival in patients with triple-negative breast cancer. *J. Clin. Oncol.* **2008**, *26*, 1275−1281.

(24) Sikov, W. M.; Berry, D. A.; Perou, C. M.; Singh, B.; Cirrincione, C. T.; Tolaney, S. M.; Kuzma, C. S.; Pluard, T. J.; Somlo, G.; Port, E. R.; Golshan, M.; Bellon, J. R.; Collyar, D.; Hahn, O. M.; Carey, L. A.; Hudis, C. A.; Winer, E. P. Impact of the addition of carboplatin and/or bevacizumab to neoadjuvant once-per-week paclitaxel followed by dose-dense doxorubicin and cyclophosphamide on pathologic complete response rates in stage II to III triple-negative breast cancer: CALGB 40603 (Alliance). *J. Clin Oncol* **2015**, *33*, 13−21.

(25) Ivy, K. D.; Kaplan, J. H. A re-evaluation of the role of hCTR1, the human high-affinity copper transporter, in platinum-drug entry into human cells. *Mol. Pharmacol.* **2013**, *83*, 1237−1246.

(26) Germa-Lluch, J. R.; Piulats, J. M. [Molecular bases of platinum-resistance in testicular cancer]. *Arch. Esp. Urol.* **2013**, *66*, 524−535.

(27) Erten, C.; Demir, L.; Somali, I.; Alacacioglu, A.; Kucukzeybek, Y.; Akyol, M.; Can, A.; Dirican, A.; Bayoglu, V.; Tarhan, M. O. Cisplatin plus gemcitabine for treatment of breast cancer patients with brain metastases; a preferential option for triple negative patients? *Asian Pac. J. Cancer Prev.* **2013**, *14*, 3711−3717.

(28) Otto, A. M.; Paddenberg, R.; Schubert, S.; Mannherz, H. G. Cell-cycle arrest, micronucleus formation, and cell death in growth inhibition of MCF-7 breast cancer cells by tamoxifen and cisplatin. *J. Cancer Res. Clin. Oncol.* **1996**, *122*, 603−612.

(29) Roger, E.; Lagarce, F.; Benoit, J. P. Development and characterization of a novel lipid nanocapsule formulation of Sn38 for oral administration. *Eur. J. Pharm. Biopharm* **2011**, *79*, 181−188.

(30) Mazzaferro, S.; Bouchemal, K.; Ponchel, G. Oral delivery of anticancer drugs III: formulation using drug delivery systems. *Drug Discovery Today* **2013**, *18*, 99−104.

(31) Mazzaferro, S.; Bouchemal, K.; Ponchel, G. Oral delivery of anticancer drugs II: the prodrug strategy. *Drug Discovery Today* **2013**, *18*, 93−98.

(32) Saremi, S.; Dinarvand, R.; Kebriaeezadeh, A.; Ostad, S. N.; Atyabi, F. Enhanced oral delivery of docetaxel using thiolated chitosan nanoparticles: preparation, in vitro and in vivo studies. *Biomed. Res. Int.* **2013**, *2013*, 150478.

(33) Shidhaye, S. S.; Vaidya, R.; Sutar, S.; Patwardhan, A.; Kadam, V. J. Solid lipid nanoparticles and nanostructured lipid carriers–innovative generations of solid lipid carriers. *Curr. Drug Delivery* **2008**, *5*, 324−331.

DOI: 10.1021/mp5008629
Mol. Pharmaceutics 2015, 12, 1105−1120

(34) Puri, A.; Loomis, K.; Smith, B.; Lee, J. H.; Yavlovich, A.; Heldman, E.; Blumenthal, R. Lipid-based nanoparticles as pharmaceutical drug carriers: from concepts to clinic. *Crit. Rev. Ther. Drug Carrier Syst.* **2009**, *26*, 523−580.
(35) Reddy, B. S.; Banerjee, R. 17Beta-estradiol-associated stealth-liposomal delivery of anticancer gene to breast cancer cells. *Angew. Chem., Int. Ed.* **2005**, *44*, 6723−6727.
(36) Oka, A.; Oda, M.; Saitoh, H.; Nakayama, A.; Takada, M.; Aungst, B. J. Secretory transport of methylprednisolone possibly mediated by P-glycoprotein in Caco-2 cells. *Biol. Pharm. Bull.* **2002**, *25*, 393−396.
(37) Kim, W. Y.; Benet, L. Z. P-glycoprotein (P-gp/MDR1)-mediated efflux of sex-steroid hormones and modulation of P-gp expression in vitro. *Pharm. Res.* **2004**, *21*, 1284−1293.
(38) Rao, U. S.; Fine, R. L.; Scarborough, G. A. Antiestrogens and steroid hormones: substrates of the human P-glycoprotein. *Biochem. Pharmacol.* **1994**, *48*, 287−292.
(39) Pouton, C. W. Lipid formulations for oral administration of drugs: non-emulsifying, self-emulsifying and 'self-microemulsifying' drug delivery systems. *Eur. J. Pharm. Sci.* **2000**, *11* (Suppl 2), S93−98.
(40) Neves, A. R.; Lucio, M.; Martins, S.; Lima, J. L.; Reis, S. Novel resveratrol nanodelivery systems based on lipid nanoparticles to enhance its oral bioavailability. *Int. J. Nanomed.* **2013**, *8*, 177−187.
(41) Zhang, Z.; Mei, L.; Feng, S. S. Paclitaxel drug delivery systems. *Expert Opin. Drug. Delivrey* **2013**, *10*, 325−340.
(42) Nekkanti, V.; Venkateswarlu, V.; Ansari, K. A.; Pillai, R. Development and pharmacological evaluation of a PEG based nanoparticulate camptothecin analog for oral administration. *Curr. Drug Delivery* **2011**, *8*, 661−666.
(43) Huang, X.; Chen, Y. J.; Peng, D. Y.; Li, Q. L.; Wang, X. S.; Wang, D. L.; Chen, W. D. Solid lipid nanoparticles as delivery systems for Gambogenic acid. *Colloids Surf., B* **2013**, *102*, 391−397.
(44) Secq, V.; Villeret, J.; Fina, F.; Carmassi, M.; Carcopino, X.; Garcia, S.; Metellus, I.; Boubli, L.; Iovanna, J.; Charpin, C. Triple negative breast carcinoma EGFR amplification is not associated with EGFR, Kras or ALK mutations. *Br. J. Cancer* **2014**, *110*, 1045−1052.
(45) Al-Ejeh, F.; Shi, W.; Miranda, M.; Simpson, P. T.; Vargas, A. C.; Song, S.; Wiegmans, A. P.; Swarbrick, A.; Welm, A. L.; Brown, M. P.; Chenevix-Trench, G.; Lakhani, S. R.; Khanna, K. K. Treatment of triple-negative breast cancer using anti-EGFR-directed radioimmunotherapy combined with radiosensitizing chemotherapy and PARP inhibitor. *J. Nucl. Med.* **2013**, *54*, 913−921.
(46) Goncalves, A.; Sabatier, R.; Charafe-Jauffret, E.; Gilabert, M.; Provansal, M.; Tarpin, C.; Extra, J. M.; Viens, P.; Bertucci, F. Triple-negative breast cancer: histoclinical and molecular features, therapeutic management and perspectives. *Bull. Cancer* **2013**, *100*, 453−464.
(47) Guo, D.; Hildebrandt, I. J.; Prins, R. M.; Soto, H.; Mazzotta, M. M.; Dang, J.; Czernin, J.; Shyy, J. Y.; Watson, A. D.; Phelps, M.; Radu, C. G.; Cloughesy, T. F.; Mischel, P. S. The AMPK agonist AICAR inhibits the growth of EGFRvIII-expressing glioblastomas by inhibiting lipogenesis. *Proc. Natl. Acad. Sci. U.S.A.* **2009**, *106*, 12932−12937.
(48) Faber, A. C.; Li, D.; Song, Y.; Liang, M. C.; Yeap, B. Y.; Bronson, R. T.; Lifshits, E.; Chen, Z.; Maira, S. M.; Garcia-Echeverria, C.; Wong, K. K.; Engelman, J. A. Differential induction of apoptosis in HER2 and EGFR addicted cancers following PI3K inhibition. *Proc. Natl. Acad. Sci. U.S.A.* **2009**, *106*, 19503−19508.
(49) Huang, L.; Wong, C. C.; Mackenzie, G. G.; Sun, Y.; Cheng, K. W.; Vrankova, K.; Alston, N.; Ouyang, N.; Rigas, B. Phospho-aspirin (MDC-22) inhibits breast cancer in preclinical animal models: an effect mediated by EGFR inhibition, p53 acetylation and oxidative stress. *BMC Cancer* **2014**, *14*, 141.
(50) Shapira, I.; Lee, A.; Vora, R.; Budman, D. R. P53 mutations in triple negative breast cancer upregulate endosomal recycling of epidermal growth factor receptor (EGFR) increasing its oncogenic potency. *Crit. Rev. Oncol. Hematol.* **2013**, *88*, 284−292.
(51) Russo, D.; Ottaggio, L.; Foggetti, G.; Masini, M.; Masiello, P.; Fronza, G.; Menichini, P. PRIMA-1 induces autophagy in cancer cells carrying mutant or wild type p53. *Biochim. Biophys. Acta* **2013**, *1833*, 1904−1913.
(52) Cao, D.; Bromberg, P. A.; Samet, J. M. Diesel particle-induced transcriptional expression of p21 involves activation of EGFR, Src, and Stat3. *Am. J. Respir. Cell Mol. Biol.* **2010**, *42*, 88−95.
(53) Zeng, Q.; Li, W.; Lu, D.; Wu, Z.; Duan, H.; Luo, Y.; Feng, J.; Yang, D.; Fu, L.; Yan, X. CD146, an epithelial-mesenchymal transition inducer, is associated with triple-negative breast cancer. *Proc. Natl. Acad. Sci. U.S.A.* **2012**, *109*, 1127−1132.
(54) Chougule, M.; Patel, A. R.; Sachdeva, P.; Jackson, T.; Singh, M. Anticancer activity of Noscapine, an opioid alkaloid in combination with Cisplatin in human non-small cell lung cancer. *Lung Cancer* **2011**, *71*, 271−282.
(55) Gomez-Casal, R.; Bhattacharya, C.; Ganesh, N.; Bailey, L.; Basse, P.; Gibson, M.; Epperly, M.; Levina, V. Non-small cell lung cancer cells survived ionizing radiation treatment display cancer stem cell and epithelial-mesenchymal transition phenotypes. *Mol. Cancer* **2013**, *12*, 94.

DOI: 10.1021/mp5008629
Mol. Pharmaceutics 2015, 12, 1105−1120

Journal of Controlled Release 213 (2015) 18–26

Contents lists available at ScienceDirect

Journal of Controlled Release

journal homepage: www.elsevier.com/locate/jconrel

Evaluation of self-emulsified DIM-14 in dogs for oral bioavailability and in Nu/nu mice bearing stem cell lung tumor models for anticancer activity

Apurva R. Patel [a,1], Ravi Doddapaneni [a,1], Terrick Andey [a], Heather Wilson [b], Stephen Safe [b,c], Mandip Singh [a,*]

[a] College of Pharmacy and Pharmaceutical Sciences, Florida A&M University, Tallahassee, FL 32307, USA
[b] Institutes of Biosciences and Technology, Houston, TX 77843, USA
[c] Texas A & M Health Sciences Center, Houston, TX 77030, USA

ARTICLE INFO

Article history:
Received 21 May 2015
Accepted 11 June 2015
Available online 14 June 2015

Keywords:
Self-emulsifying drug delivery
DIM-14
H1650 stem cell
Anti-cancer activity

ABSTRACT

3, 3-Diindolylmethane-14 (DIM-14), a novel lipophilic derivative of DIM, has demonstrated anticancer activity in different types of cancers. However, poor solubility and low oral bioavailability of DIM-14 limit its translational benefits in vivo. This study was carried out to improve the oral bioavailability of DIM-14 via self-emulsifying drug (SED) delivery system in dogs and to evaluate pharmacodynamic characteristics of SED against H1650 stem cell tumor models. DIM-14 was incorporated into an oil, surfactant, and co-surfactant mixture using labrafil and tween-80 to obtain SED. SED were characterized by droplet size, polydispersitiy index (PDI), zeta potential, entrapment efficiency (EE), in vitro permeability and drug release (investigated with Caco-2 monolayers and dissolution apparatus respectively). Pharmacokinetic parameters in dogs were evaluated and analyzed using Winonlin. Anti-tumor activity was carried out in H1650 lung tumor model. Particle size of SED was between 230 and 246 nm and surface charge was negative and ranged from 26.50 to 28.69 mV. Entrapment efficiency of SED was 85%. Pharmacokinetic evaluation in dogs showed increased Cmax (39.18 ± 7.34 vs 21.68 ± 6.3 μg·dL-1), higher AUC0–t (34,481.34 ± 1125.46 vs 14,159.53 ± 702.20 μg·min·dL-1) and improved absorption with 3 times more bioavailability of SED compared to DIM-14 solution. SED showed ~30–59% tumor volume/weight reduction in H1650 tumor model compared to DIM-P solution. Our studies demonstrate the potential application of self-emulsifying drug delivery system (SEDDS), that enhances oral absorption of DIM-14 and increased anti-tumor activity against lung tumor models.

Published by Elsevier B.V.

1. Introduction

Lung cancer is one of the leading causes of cancer-related deaths worldwide and most of lung cancer cases (85%) belong to the non-small-cell lung cancer (NSCLC) type [1,40]. Despite significant advances in our knowledge about lung cancer, effective therapies to combat lung cancer are still in infancy. Although the use of targeted therapies for lung cancer has been reported, patients are yet to benefit from them. Recent reports have demonstrated that tumors contain a small subpopulation of cells, termed cancer stem cells (CSCs), which exhibit pro-tumorigenic characteristics including high proliferation capacity, multipotent differentiation, drug resistance and long life span relative to other cells. The survival rate of lung cancer patients is very low due to the acquisition of resistance to systemic treatment regimens, which in turn may be due to the presence of cancer stem cells within the primary tumor. One new therapeutic avenue that is currently being tested in preclinical experiments for a variety of solid tumors is targeting CSCs which are thought to be responsible for tumor initiation and recurrence after chemotherapy [2]. A major challenge for treating this type of cancer due to CSCs is that, these are naturally resistant to the cytotoxic effect of radio-chemotherapy because of slow cell cycling, lower proliferation, and increased expression of DNA repair and anti-apoptosis genes [3,4]. This has led to hypothesis that targeting CSC populations is essential for an effective treatment, but this issue has not yet been experimentally tested.

New therapies using novel mechanisms to induce tumor cell death are required and natural products due to their potential anticancer compounds play a crucial role in envisaging new therapies. 3,3-Diindolylmethane (DIM) is a natural product derived from indole-3-carbinol (I3C) which is present in cruciferous vegetables such as Brussels sprouts, broccoli and cauliflower. DIM has generated much interest in cancer research because of its low toxicity and cytotoxic effects on cancer cells in vitro and inhibition of tumor growth in vivo [5]. A series of novel synthetic 1,1-bis(3-indolyl)-1-(p-substituted phenyl) methane analogs (C-DIMs) induced expression of cell cycle inhibitors such as p21 and p27, downregulated-cyclin proteins including cyclin D1, decreased

* Corresponding author.
E-mail address: mandip.sachdeva@gmail.com (M. Singh).
[1] Equal Contribution.

http://dx.doi.org/10.1016/j.jconrel.2015.06.014
0168-3659/Published by Elsevier B.V.

expression of survival and anti-apoptotic proteins including survivin, bcl-2, bax and induced poly (ADP-Ribose) polymerase (PARP) cleavage, mitochondrial cytochrome c release and procaspase cleavage [6–8,41–43]. C-DIMs, are also potent anticancer agents and their activities are structure-dependent [9–11]. Considering that CSCs may be key mediators of metastasis, we hypothesized that targeting CSCs with DIM-14 would increase the anti-tumor potential.

Approximately 40% of new active pharmaceutical agents have poor aqueous solubility and their oral delivery is often associated with low bioavailability. Various formulation strategies which can be explored to develop oral delivery of poorly soluble drugs include utilization of surfactants, lipids, permeation enhancers, micronization, salt formation, β-cyclodextrins complexes, nanocarriers, solid dispersions, spray drying and self-emulsifying drug delivery systems (SEDDS). SEDDS are mixtures of oils, surfactants, solvents and co-solvents that create fine oil-in-water emulsions upon mild stirring in aqueous media. SEDDS offer several advantages which includes their spontaneous formation, thermodynamic stability, improved bioavailability [12] and ease of manufacturing. Following their oral administration, these systems rapidly disperse in gastrointestinal fluids to yield micro or nano emulsions and are rapidly absorbed through the lymphatic pathway [13]. Various bioavailability studies have reported that lipophilic compounds, such as, simvastatin and halofantrine, are more efficiently taken up from gastrointestinal tract when administered in SEDDS [14–16].

DIM-14 has showed anticancer activity in lung tumor cell lines in vitro and in vivo. Further, even though DIM-14 is a desirable anticancer agent, its activity as a single agent is limited due to its poor oral bioavailability. To address this hypothesis, we investigated the anti-tumor efficacy of the DIM-14 and SED formulations in the lung tumor models. The objective of this study was designed to evaluate SED (self-emulsifying DIM-14) in dogs for pharmacokinetic analysis and asses their anticancer activity in H1650 mice lung cancer model.

2. Materials and methods

2.1. Chemicals

DIM-14 was prepared as described [5]. All culture media contained antibiotic-antimycotic solution PSN mix by Gibco-Invitrogrn (Grand Island, NY, USA). Laminin, accutase, poly-D-lysine, epidermal growth factor, and fibroblast growth factor were purchased from Sigma Aldrich (St. Louis, MO); labrafil M1944 and labrasol from Gattefosse (Paramus, NJ). Kolliphor™ TPGS (pharma grade) was purchased from BASF fine chemicals. All other chemicals used were of analytical grade.

2.2. Source of cells

H1650 parent cells and side population cells (SP)/cancer stem cells (CSCs) were generously donated by Dr. Srikumar Chellappan of the H. Lee Moffitt Cancer Center and Research Institute (Tampa, FL) and Caco-2 cells were obtained from American Type Culture Collection (Rockville, MD, USA). H1650 CSCs were cultured in DMEM:F12 base medium enriched with fibroblast and epidermal growth factors (10 μg/ml) and 2% PSN cocktail. Cells were maintained at 37 °C under an atmosphere of 95% air and 5% CO2. H1650 CSCs were cultured on a basement membrane-coated matrix consisting of immobilized laminin on a poly-D-lysine layer.

2.3. Animals

Nu/nu mice (20–30 g) were used for the current studies. The protocols were approved by the Institutional Animal Care and Use Committee, Florida A & M University. Animals were maintained on standard animal diet, in a controlled room (22 ± 1 °C @ 35–50% RH) for a week prior to experiments. Eighteen month old female intact Labrador retriever dogs were acquired from an internal canine breeding colony maintained at Texas A&M, College of Veterinary Medicine. All canine protocols were approved by the Institutional Animal Care and Use Committee at Texas A&M University. Dogs were housed in large runs and allowed outdoor play time and toys for enrichment. They were fed standard dog chow and water ad libitum for the duration of the study.

2.4. H1650 SP cell viability

H1650 SP cells were seeded in a 96-well format (1×10^4 per well) and incubated for 16–18 h. Treatment was carried out for 72 h with different concentrations of DIM-14. The cells were washed with PBS 2× and fixed in 0.1 ml glutaraldehyde solution (0.025% w/v) and incubated at 37 °C for 30 min. Glutaraldehyde was aspirated and 0.1 ml crystal violet solution (0.01% w/v) added and incubated at room temperature for 15 min. Crystal violet solution was aspirated followed by 2 washes with PBS; the plates were air-dried and disodium hydrogen phosphate solution added to dissolve the crystal violet. The absorbance of crystal violet was read at 540 nm and the cell viability calculated as a percentage of the control. Determinations of cell viability were made at least 3× and the data presented as mean ± SD.

2.5. Preparation of liquid self-emulsifying system and SB DIM-P

The liquid self-emulsified (SE) formulations were prepared as previously reported [17]. Initially, solubility of DIM-14 was determined in different oils and surfactants to select the suitable oil to be used for the formulation. The mixture of oils, surfactants and co-surfactants was optimized by DOE analysis. Briefly, DIM-14 was dissolved into the mixture of oil, surfactant, and co-surfactant with help of heating at 50 °C in a water bath and vortexed until a clear solution was obtained. Then it was kept at room temperature for 24 h and examined for stability parameters such as turbidity/phase separation. Optimized concentrations of Enova oil, TPGS, surfactant (tween 80) and co-surfactant (labarafil) were determined from QbD design. The optimized composition is showed in Table 1.

2.6. Characterization of self-emulsified spray dried formulations

2.6.1. Emulsification time

The emulsification time (the time for a pre-concentrate to form a homogeneous mixture upon dilution) was monitored by visually observing the disappearance of SED and the final appearance of the emulsion in triplicate. A dissolution apparatus (Dissolution Tester USP, Type-II) was used at a paddle speed of 50 rpm with 200 ml buffer medium at 37 °C. The SED (1 g) was added slowly to the medium and time required for the disappearance of SED was recorded.

2.6.2. Droplet size and zeta potential determination

Five milligrams of the SED formulation was diluted with water to 10 ml in a flask and gently mixed. The droplet size distribution and zeta potential of the resultant emulsion was determined by laser diffraction analysis using a particle size analyzer (Nicomp Zetasizer, US). The sizing of the emulsion droplet was determined in a small volume module. Particle size was calculated from the volume size distribution. All studies were replicated ($n = 3$) and statistically analyzed ($P < 0.05$).

Table 1
Optimize ingredients of DIM-14 as self-emulsified drug delivery system (SEDDS).

Ingredients	Composition of SEDDS (% w/w)
DIM-14	20
Enova oil	50
TPGS	10
Labrafil 1944	20

2.6.3. Dilution studies/robustness on dilution

A dilution study was done to access the effect of dilution on the SED pre-concentrate. In this study, the optimized formulation was subjected to various dilutions (i.e., 1:50, 1:100 and 1:500) with various diluents (i.e., water, 0.1 N HCl, phosphate buffer pH 7.5) and the droplet size was recorded.

2.6.4. Determination of drug content

DIM-14 from an SED formulation was extracted in acetonitrile using the sonication technique. The extract was analyzed for DIM-14 content by HPLC method already established in our laboratory [18]. Entrapment efficiency was estimated using the formula:

$$\text{Entrapment efficiency, } EE(\%) = [(Wn - Wr)/Wn] \times 100$$

where, Wn = weight of DIM-14 in SED, and Wr = weight of DIM-14 in filtrate.

2.6.5. In vitro release studies

DIM-14 release from SED formulations were performed using USP XXIII, dissolution apparatus II with 200 ml of distilled water as dissolution medium at 37 ± 5 °C with paddle speed at 50 rpm. SED formulation equivalent to 2 mg of DIM-14 was introduced into the dissolution tester. At predetermined time intervals, an aliquot of 1 ml was collected, filtered, and analyzed for the content of DIM-14 by HPLC. An equivalent volume (1 ml) of fresh dissolution medium was replaced to compensate the loss due to sampling.

2.7. Caco-2 permeability studies of DIM-14

Single cell suspensions (10^5 cells per ml) were seeded in the apical compartment of a Costar® Transwell® permeable support with a polycarbonate membrane (0.4 μm pore size) in a 12-well plate format in a 0.5 ml volume. The cells were maintained for 21 days with media changes done on alternate days for 14 days and daily subsequently. Formation and integrity of Caco-2 monolayer and tight junctions were monitored by the transepithelial electrical resistance (TEER). Permeation studies were done by adding buffer (HBSS-HEPES buffer) to the donor (pH 6.5) and acceptor (pH 7.4) compartments for 5 min at 37 °C. An absorptive permeability study was done by adding sample solution to the donor compartment (pH 6.5) and free buffer to the acceptor compartment (pH 7.4). Sampling was carried out from the acceptor compartment at 15, 30, 45, 60, 90, and 120 min under sink condition. Secretory studies were carried out by adding the sample to the acceptor chamber (pH 7.4) and sampling from the donor chamber (pH 6.5). Samples were eluted by HPLC and amount of DIM-14 was obtained by interpolating the peak area from a standard plot of area versus amount of DIM-14. The apparent permeability (Papp) of DIM-14 was computed using the formula:

$$\text{Papp(cm/s)} = [Q/(Ci * T * A)],$$

where Q = amount of DIM-14 in receiver (μg); Ci = initial concentration of DIM-14 (g/cm^3), T = time (sec), and A = Area of insert (cm2).

2.8. Bioavailability of DIM-14 and SED

2.8.1. Bioavailability in dogs

Pharmacokinetic profile of DIM-14 in Dogs was determined following IV and oral administration. Animals were randomly distributed into three experimental groups (n = 3). DIM-14 was formulated as described earlier for intravenous administration and for oral solution; DIM-14 was dissolved in corn oil. The oral treatment groups were given 3.33 mg/kg of DIM-14 solution and SED equivalent to 3.33 mg/kg of DIM-P was administered orally by syringe. Each dog had a central venous catheter (long saphenous) placed on the day of the study. The third group was given DIM-14 (0.5 mg/kg) intravenously. Dogs were fasted overnight before the start of pharmacokinetic studies. Blood samples were collected from the venous catheters into heparinized tubes. Samples were collected at baseline, and at 15, 30, 60, 120, 180, 240, 360, 480, 600, 720, 1440 min after administration of a single dose of DIM-14 solution and SED. Blood samples were immediately centrifuged and plasma was collected and stored at −80 °C until analysis. At the end of the study, major organs were collected for further evaluation.

2.8.2. Data analysis

Pharmacokinetic parameters were determined using non-compartmental techniques with WinNonlin® 5.0 software (Pharsight Corporation, Mountain View, CA, USA). SHAM analysis (i.e., Slope, Height, Area, and Moment) [19] utilized plasma concentration-time data to estimate the area under the curve (AUC), terminal elimination half-life (t1/2), and the area under the first moment of the plasma concentration-time curve (AUMC). The AUC was calculated for each animal using the piecewise log trapezoidal areas. The non-compartmental parameters were calculated for each rat before averaging dose groups.

2.9. In vivo anticancer evaluation in lung cancer models

2.9.1. H1650 cancer stem cell xenograft tumor model

H1650 CSCs at 80–90% confluency were harvested using accutase (Sigma-Aldrich, St. Louis, MO) (Bajpai, Lesperance et al. 2008) and washed 2× with PBS. Cells were counted (1 × 106) and suspended as single cells in 50 μl serum-free DMEM:F12 media and diluted in matrigel (3 mg/ml) to a final volume of 300 μl on ice. Cell suspension in matrigel (300 μl) was injected on the right flank of mice using a pre-chilled 24-gauge needle and syringe. Animals were maintained under standard husbandry for xenografts to develop.

2.9.2. H1650 cancer stem cell orthotopic lung tumor model

Mice were placed under isoflurane-induced anesthesia under aseptic conditions. The left lateral chest was doused with iodine and cleaned with an alcohol swab. A small lateral incision (~5 mm) was made to the left chest in plane of the left fore-limb just below the scapula. A cell suspension-filled B-D® 1 ml latex free syringe connected to a 27-gauge Surflo® winged infusion set was used to deliver an inoculum of 1×10^4 cells (in a 0.1 ml volume of serum-free DMEM:F12 base media) through the sixth intercostal space into the left lung. Incisions were closed with surgical skin clips and animals observed for full motor and cognitive recovery. Mice were maintained for 30 days for development of lung tumor verified by dissection of a random mouse for anatomical observation.

2.10. Treatment of animals

Mice were randomly divided into the following groups (n = 12) to receive DIM-14 formulations by oral gavage. The control group received vehicle (No DIM-14); the second group received DIM-14 (20 mg/kg) solution every other day; the third group received SED (20 mg/kg). To check for evidence of toxicity, the animals were weighed twice weekly. At the end of study, all animals were sacrificed by exposure to a lethal dose of carbon dioxide. After dissection and removal of the lungs, the lungs and tumor mass were washed in sterile PBS and weighed. The lung weights and tumor volume were used for assessment of the therapeutic activity of the treatments.

2.11. Western blot analysis

Protein was extracted from tumor nodules collected from control-untreated and treated tumors using RIPA buffer (50 mM Tris–HCL, pH 8.0, with 150 mM sodium chloride, 1.0% Igepal CA-630 (NP-40), 0.5% sodium deoxychlorate, and 0.1% sodium dodecyl sulfate) with

protease inhibitor. The lysate from normal lung tissues was also prepared in a similar manner as described above. Protein content was measured using BCA Protein Assay Reagent Kit (PIERCE, Rockford, IL). Equal amounts of supernatant protein (50 μg) from the control and different treatment groups were denatured by boiling for 5 min in sample buffer, separated by 10% SDS-PAGE, transferred to nitrocellulose membranes for immunoblotting. Membranes were blocked with 5% skim milk in Tris-buffered saline with Tween 20 and probed with antibodies against ER stress markers and β-actin (1:1000) (Santa Cruz Biotechnology, Santa Cruz, CA). Horseradish peroxidase-conjugated secondary antibodies (Santa Cruz Biotechnology, Santa Cruz, CA) were used. Proteins were visualized using enhanced chemiluminescent solution (Pierce, Rockford, IL) and exposed to Kodak X-OMAT AR autoradiography film (Eastman Kodak, Rochester, NY).

2.12. Statistical analysis

Results obtained were analyzed using GraphPad Prism 5.0 (GraphPad Software, Inc.). Statistical significance in differences in cell viability and migration were determined by unpaired t-test (***$P < 0.0001$); and one-way analysis of variance (ANOVA) followed by Bonferroni's multiple comparison test (***$P < 0.05$); tumor weight and lung weight (*$P < 0.05$) by one-way ANOVA followed by Tukey's post-test (***$P < 0.0001$; **$P < 0.05$). Results are presented for at least three determinations and presented as mean ± SD.

3. Results

3.1. H6150 SP cells are resistant to chemotherapy

The IC50 of DIM-14 in H1650 and H1650 SP cells were 8.70 ± 0.13 nM and 33.75 ± 3.65 nM respectively. The concentration of drug treatment resulting in 50% cell death (IC50) was estimated from cell viability data using linear regression analysis.

3.2. Characterization of SED DIM-14

3.2.1. Droplet size, zeta potential determination and drug content

The formulation composition ratio in Table 1 gave the particle size (240 ± 24.23 nm, mean ± SD, n = 3) than other SED formulations. The PDI (polydispersity index) was 0.11 ± 0.02. Also, the coefficient of variance (COV) for the measurement set was less than 5%. The charge of oil droplets in SED was negative due to the presence of free fatty acids and the zeta potential of the formulation was −28.9 ± 0.42 (mean ± SD, n = 3). We have measured the particle size and zeta potential aging after 24 of dispersion and it was found that there was no statistical differences compare to time zero readings. Drug content of the formulation was found to be 85.34 ± 0.42% (mean ± SD, n = 3).

3.2.2. Release studies

At initial 12 h, SED formulation released 99% of DIM-14. Fig. 1 reveals the in vitro drug release profiles of DIM-14 from free drug and solution with ~10% and ~40% of drug release in 24 h. The release profile of optimized formulation was found to release more than 50% of DIM-14 within 4 h from the SED formulation, indicating a highly desirable release profile.

3.2.3. Caco-2 permeability studies of DIM-14

The TEER values of >400 $\Omega \cdot cm^2$ and mean permeability values of paracellular control Lucifer Yellow of $< 0.15 \times 10^{-6}$ cm/s were within normal limits, thus confirming paracellular integrity of monolayers. The average Peff, A–B assay for DIM-14 was approximately 0.26 ± 0.05×10^{-6} cm/s, and B–A was 0.41 ± 0.09×10^{-6} cm/s. The TEER values of monolayers were indicative of tight junction integrity, and TEER values did not significantly change throughout the experiment. The A–B apparent permeability (Papp) values using the Caco-2 assay for SED were 9.45 ± 0.07×10^{-6} cm/s and 10.95 ± 0.08×10^{-6} cm/s respectively for unstirred and stirred water layers respectively.

3.3. Optimization of SED using desirability function

The contour plots and the prediction profiler of interactions between independent variables are shown in Fig. 2. Using the desirability function, all measured responses were combined into a single response. The optimized batch was identified with a desirability value of 0.757 for SED. Individual and overall desirability for all measured responses were evaluated.

3.4. Bioavailability studies of SED

3.4.1. Bioavailability in dogs

The plasma concentration-time profiles of DIM-14 formulations in dogs are shown in Fig. 3. The concentration-time plot of DIM-14 in dog plasma followed a single i.v. bolus injection which was estimated from peak area of HPLC chromatograms of injected plasma samples (Fig. 3A). Non-compartmental pharmacokinetic parameters were

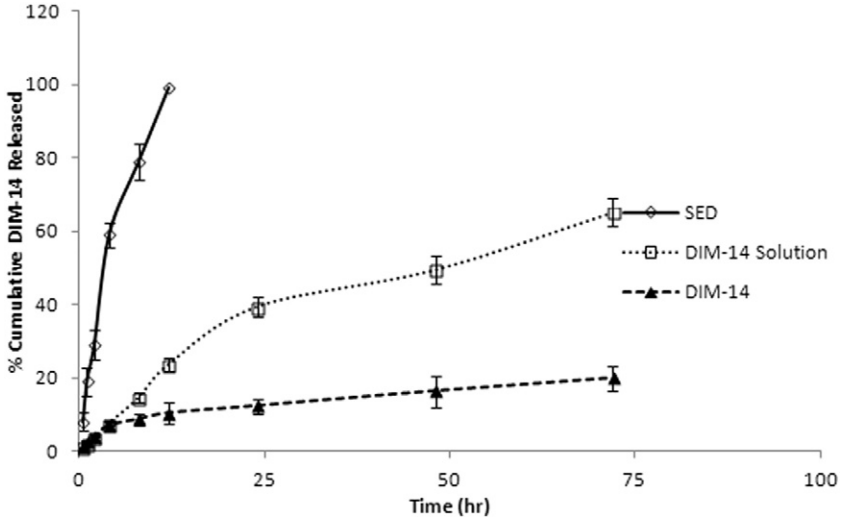

Fig. 1. In-vitro release study of DIM-14 free drug, DIM-14 solution and SED formulation.

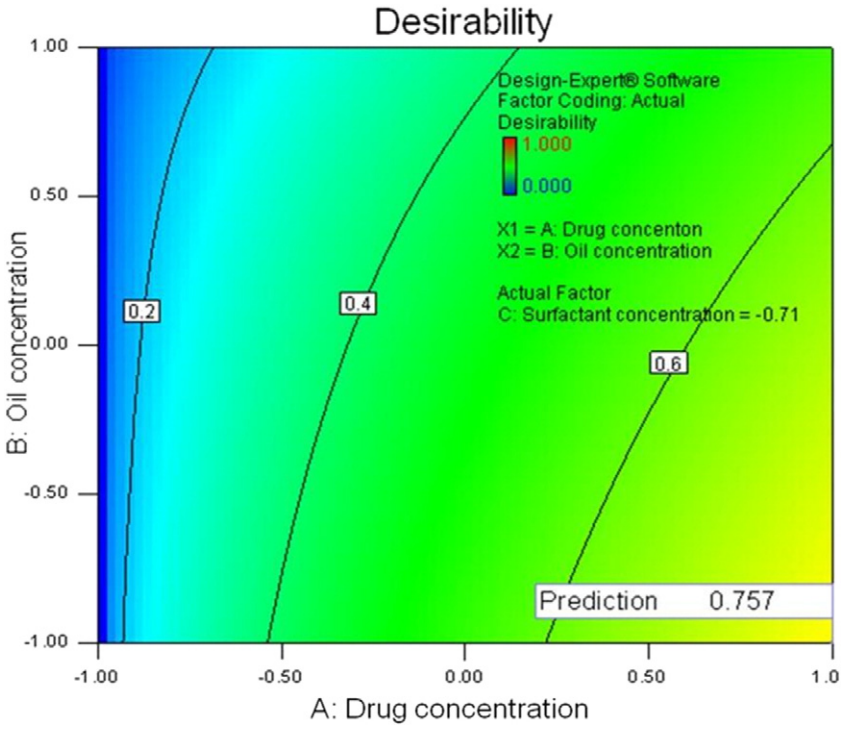

Fig. 2. Contour plots showing the effect of independent variables on desirability and dependent variables during process design SED.

measured. Curve fitting into a two-compartment model was done using the WinNonlin software. Following intravenous bolus injection, there was a rapid distribution of drug into peripheral tissues (K12 = 0.39 l/h) and a comparatively slow distribution from the peripheral compartment to the central compartment (K21 = 0.15 l/h), and a slower elimination from the central compartment (K10 = 0.003 l/h). Volume of distribution (Vd) of DIM-14 was 0.321 l/kg and remained unchanged at steady state (Vdss = 0.319 l/kg).

AUC was calculated by trapezoidal methods ($P < 0.05$), and secondary parameters were calculated. Oral delivery of DIM-14 (3.33 mg/kg) showed poor bioavailability (<10%) and a shorter plasma half-life compared to that of SED. However, the half-life for SED was increased by ~3 h with increase in bioavailability by ~25%. Pharmacokinetic evaluation in dogs showed improved absorption of SED formulations compared to solution; increased Cmax (39.18 ± 7.34 vs 21.68 ± 6.3 μg dL-1) and higher AUC0–t (34,481.34 ± 1125.46 vs 14,159.53 ± 702.20 μg min dL-1). The relative oral bioavailability of SED calculated on the basis of AUC0–t was about 3 fold more as compared to solution.

3.5. In vivo anticancer activity of oral DIM-P

3.5.1. H1650 cancer stem cell xenograft tumor model

The results in Fig. 4 showed that lung tumor weights were significantly (*, $P < 0.001$) decreased by 30 and 64% after treatment with DIM-14 and SED respectively compared to vehicle control. In mice treated with the DIM-14 and SED, lung tumor volumes were decreased by 29 and 61% respectively. A non-significant ($P > 0.05$) change in average number of tumor nodules was observed among central, mid and peripheral regions of harvested lungs from each of the treated groups (Fig. 4). DIM-14 and SED treatment showed significant (*, $P < 0.001$) decrease in average number of tumor nodules by 29 and 56% respectively compared

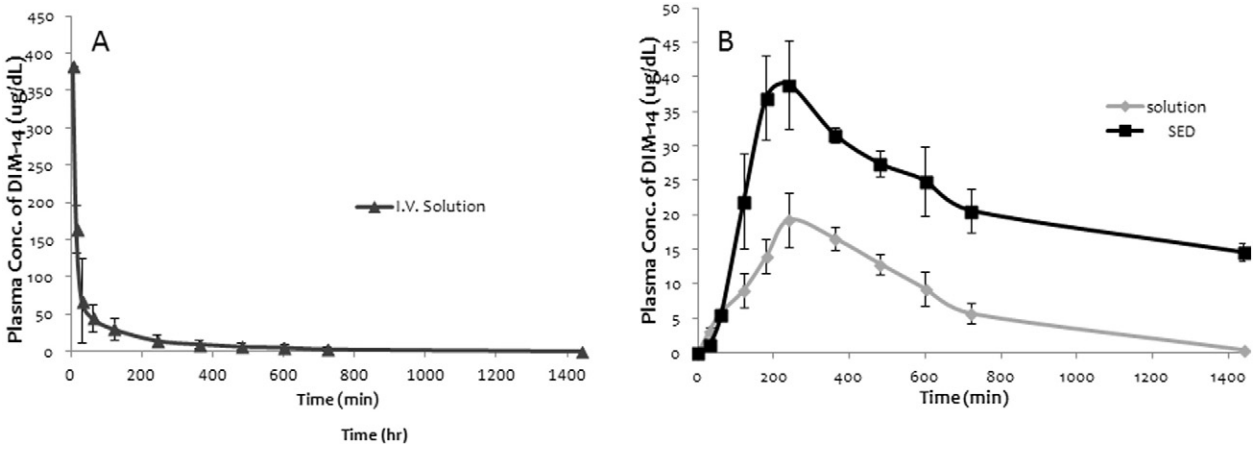

Fig. 3. A) Plasma concentration (μg/dL) vs time profile (hr) following intravenous administration of DIM-14 (0.5 mg/kg), B) plasma concentration (μg/dL) vs time profile (hr) following oral administration of DIM-14 solution (3.33 mg/kg) and self-emulsified formulation of DIM-14 (3.33 mg/kg) (SED) in dogs (n = 4).

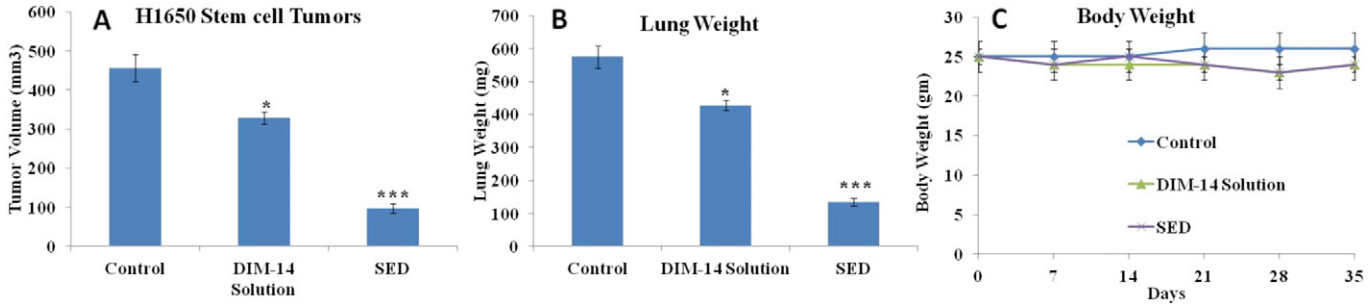

Fig. 4. Effects of DIM-14 solution and SED on H1650 stem cell xenograft lung tumor volume (a); tumor weight (b); mice body weight (c). Lung weights and tumor volumes were determined for measurement of therapeutic activity of the treatments. One-way ANOVA followed by post Tukey test was used for statistical analysis. $P < 0.05$ (*, significantly different from untreated controls; **, significantly different from DIM-P solution). Data presented are means ± SD (n = 12).

to control groups. We did not observe any weight loss or other signs of toxicity in mice treated with DIM-14.

3.5.2. H1650 cancer stem cell orthotopic lung tumor model

Treatment was started ten days after tumor implantation and continued for a total of 30 days. Ten days after inoculation with tumor cells, the average lung weights and tumor volumes were 198 ± 17.25 mg and 87 ± 18.87 mm^3, respectively (Based on pilot study). The results (Fig. 5) showed that lung tumor weights were significantly (*, $P < 0.001$) decreased by 24 and 59% after treatment with DIM-14 and SED respectively compared to vehicle control. In mice treated with the SED& DIM-14, lung tumor volumes were decreased by 67 and 34% respectively. A non-significant ($P > 0.05$) change in average number of tumor nodules was observed among central, mid and peripheral regions of harvested lungs from each of the treated groups (Fig. 5). DIM-14 and SED treatment showed significant (*, $P < 0.001$) decrease in average number of tumor nodules by 22 and 49% respectively compared to control groups. We did not observe any weight loss or other signs of toxicity in mice treated with DIM-14.

3.6. Hematoxylin and eosin staining

The lung tumor histology was evaluated by H & E staining of lung tumor tissue. DIM-14 and SED treated tumors exhibited only occasional, isolated microvessels, while tumors from untreated mice had well-formed capillaries surrounding nests of tumor cells. Histological examination of the lungs and tracheobronchial epithelium showed no signs of inflammation or edema among all groups which suggests a safer toxicity profile for both DIM-14 and SED therapy.

3.7. Anti-tumor activity of DIM-14 and SED formulations

Western blot analysis of Bcl-2 expression suggested that the anti-apoptotic marker, Bcl-2, was significantly down regulated in SED group compared to untreated control and DIM-14 treated groups (Fig. 6). The densitometric analysis of western blot bands revealed that β-actin relative Bcl-2 expression was reduced 1.8 and 4.2 fold, respectively in DIM-14 and SED groups compared to untreated control tumors. The SED produced 2.4 fold higher repression in the Bcl-2 expression compared to DIM-14, suggesting the superior anticancer effects of SED in lung cancer stem cell model. Similarly, the expression of cell survival marker survivin was also significantly down regulated (0.9 and 2.1 fold) in DIM-14 and SED groups compared to control groups (Fig. 6). Typical properties of CSCs include their capacities for self-renewal and differentiation, in vivo tumorigenic potential and resistance to chemotherapy. The stem cell self-renewal marker SOX2 expressions was found to be higher in control tumor lysates. Treatment with SED formulation resulted in significant down regulation of SOX2.

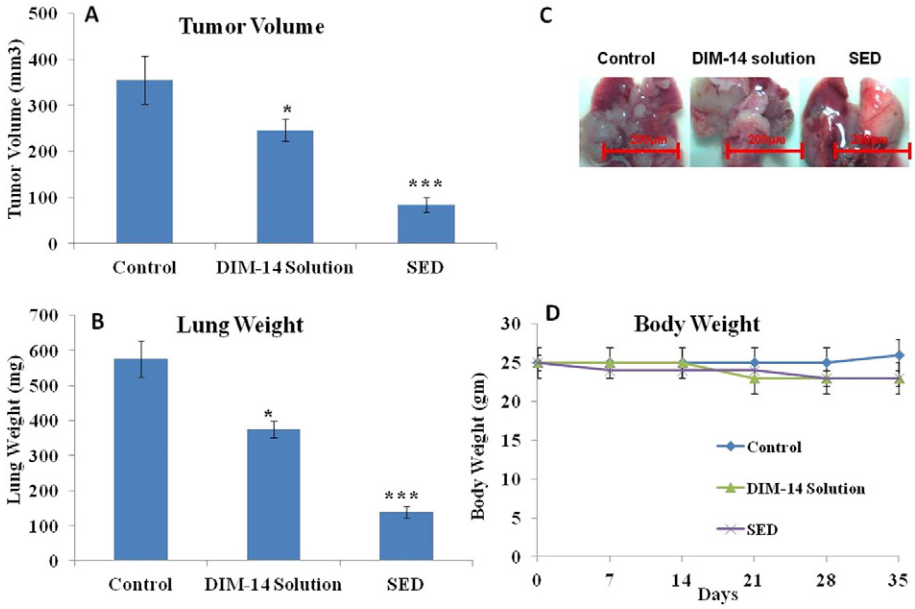

Fig. 5. Effects of DIM-14 solution and SED on H1650 stem cell orthotopic lung tumor volume (a); tumor weight (b); lung tumor tissues (c); mice body weight (D). Lung weights and tumor volumes were determined for measurement of therapeutic activity of the treatments. One-way ANOVA followed by post Tukey test was used for statistical analysis. $P < 0.05$ (*, significantly different from untreated controls; **, significantly different from DIM-P solution). Data presented are means ± SD (n = 12).

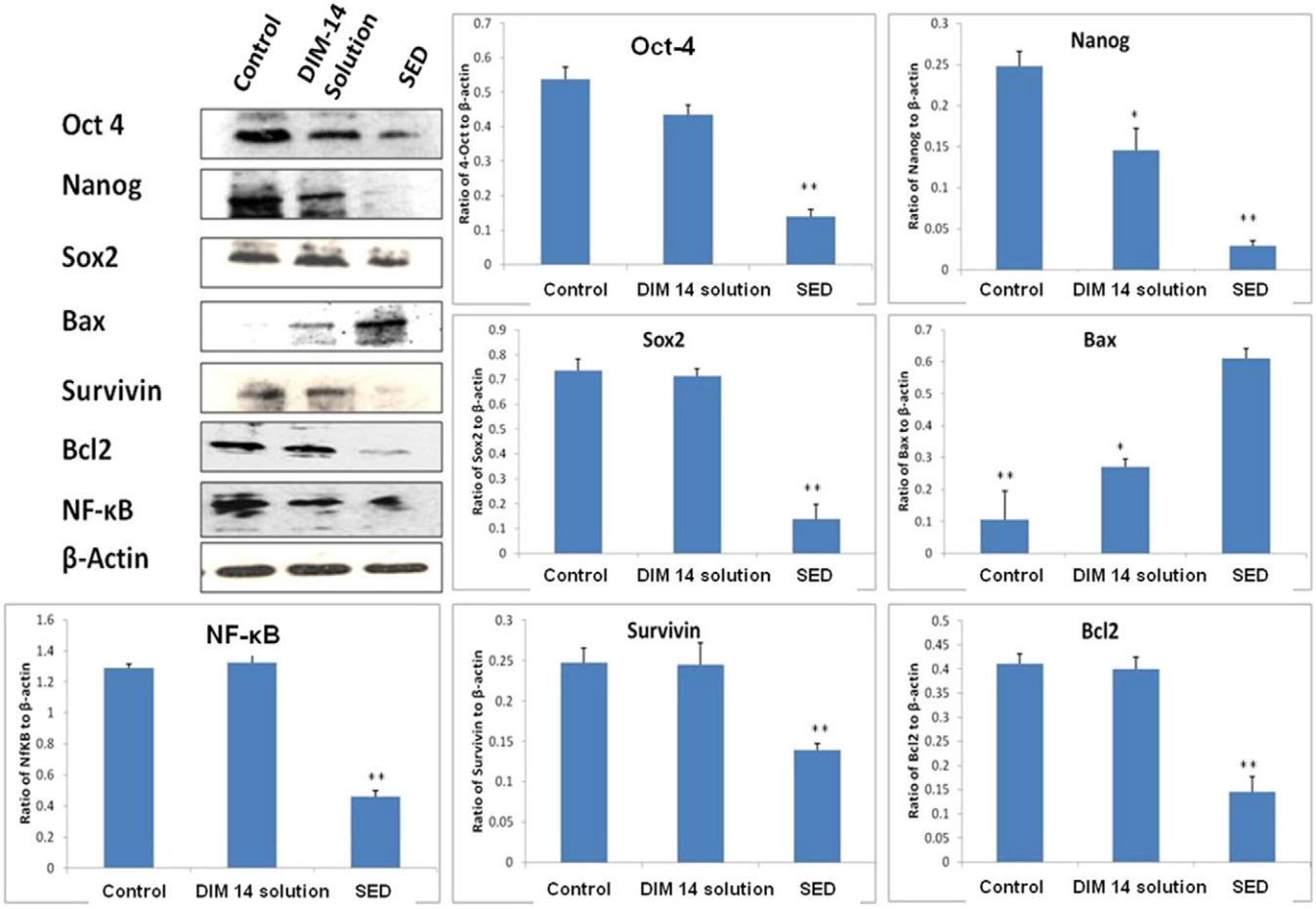

Fig. 6. Western blot analysis of different proteins in tumor lysates from control-untreated and treated groups. Lane 1 = control; Lane 2 = DIM-14 solution; Lane 3 = SED. Protein expression levels (relative to β-actin) were determined. Mean ± SEM for three replicate determinations. One-way ANOVA followed by post Tukey test was used for statistical analysis. $P < 0.01$ (*, significantly different from untreated controls; **, significantly different from single treatments).

The relative expressions were found to be reduced 1.9 and 4.8 fold significantly in DIM-14 and SED formulations respectively compared to untreated control tumor lysates (Fig. 6). Also, the stem cell marker Nanog indicated the promising anticancer effects of both DIM-14 and SED formulations. Compared to untreated control, the relative expression of Nanog was decreased (2.4 and 5.5 fold) in DIM-14 and SED groups respectively; SED produced 2.8 fold decreased Nanog expression compared to DIM-14 (Fig. 6). The expression of another stem cell marker, Oct4, was significantly decreased in SED formulation compared to untreated control and DIM-14 treated groups, with 2.16 and 3.50 fold reduction respectively (Fig. 6). The expression of NF-κB was also significantly down regulated in both DIM-14 and SED formulation treated tumors (Fig. 6). All these results suggest that SED formulation showed superior anticancer effects than DIM-14 treated groups, suggesting its superior anticancer activity.

4. Discussion

DIM-14, in its native state exhibits poor aqueous solubility and less oral bioavailability with no detectable toxicity. Different analogs of DIM have been synthesized in order to enhance its clinical usefulness [10,11,20–23]. However, low bioavailability properties of these DIMs preclude their translational utility outside of cultured cells. Various drug delivery approaches using carriers aimed at increasing oral bioavailability have shown some promise [24–27]. In the current study, first time we developed DIM-14 into a self-emulsified drug delivery system and explored its ability to overcome its solubility and bioavailability related problems [18,44].

For development of SED formulations, the selection of suitable oil is crucial because it solubilizes the lipophilic drug and increases its transport via the intestinal lymphatic system, thus enhancing its absorption from GIT. Based on our solubility screening, since both sesame and corn oil had the maximum solubility for DIM-14, Enova oil was selected as oil phase because it contains higher amount of triglycerides with medium chain fatty acids; which have lower interfacial tension, better water solubility and partitioning ability as an emulsifier than triglycerides with long chain fatty acids [28]. We also screened various non-ionic surfactants with HLB values >10 for their efficiency as emulsifier and Tween 20 (HLB 16) was selected as the surfactant for preparation of the binary mixture. In SED, the primary means of self-emulsification assessment were visual estimation and rate of emulsification (index for the assessment of the efficiency of emulsification). The emulsification time study showed that the optimized formulation employed could emulsify within 55 s (rapidity of the formulation). The SED formulation was optimized using desirability functions such as droplet size and drug release. It was found that the theoretical (predicted) and observed (experimental) values were in close agreement. Higher values of correlation coefficient (R2) for the dependent variables indicated a good fit for SED experimental model.

In-vivo pharmacokinetic analysis with the desired formulation in dogs showed significantly ($P < 0.05$) higher absolute oral bioavailability of ~25% compared to DIM-14 solution. The increased AUC and C_{max} values with SED formulation demonstrated the superior

oral performance of our formulation compared to drug in free form. The relative bioavailability of the SED was 3 fold higher in dogs compared to DIM-14 alone. These support the hypothesis that SED is effective in improving the oral bioavailability of DIM-14.

The plasma concentration of the DIM-14 solution reached Cmax within 360 min after oral administration. Compared with the plasma concentration profile of the DIM-14 solution, the plasma concentration profile of the SED was a little faster during the first 120 min, and was stabilized in sustained fashion over 720 min, followed by rapid decline in DIM-14 plasma concentration, resulting in sustained release effect of SED formulation. Since this is the first study of DIM-14 in dogs, we do not have any previous information on bio-distribution of DIM-14 but we observed three compartment distribution for DIM-P previously [18]. Oral bioavaibility of DIM-5, DIM-7, DIM-8 and DIM-12 was found to be 39, 30, 6 and 42% respectively by De Miranda et al. [29]. Pharmacokinetic profile for all of them was found to be similar expect DIM-8 having the high first pass metabolism. The time for each DIMs to reach Cmax (Tmax) after oral gavage administration was about 60 min for DIM-8 and 120 min for all others, which is similar to DIM-14. Similarly, Clearance as a function of bioavailability, extrapolated volume of distribution, and mean resonance time were dependent on DIMs structure and route of administration.

In the present case, an increase in the AUC of DIM-14 was observed with SED and results revealed that the SED significantly promoted and sustained DIM-14 absorption. One unique property of SED is that it has superior absorption in the gastrointestinal tract when loaded with lipophilic drugs. The small droplet size (in the range of 500 nm) of the microemulsions may penetrate the absorption site via the transcellular pathway, and could protect the drug from enzyme degradation. Therefore, the higher bioavailability of DIM-14 through SED may be due to the enhanced absorption through the lymphatic pathway, as previously reported [30,31]. A relatively high ratio of emulsifier in SED may also contribute to the increased permeability by disturbing the cell membrane [32].

For the first time in the current study, we evaluated the effect of DIM-14 against H650 lung cancer stem cells. This evaluation of DIM-14 SED as potential anticancer agent in H1650 lung cancer mice model highlighted the significant increase in anticancer activity in SED than that of the DIM-14 solution. This is expected because of the improved oral absorption and increased half-life of SED. The improved oral bioavailability of DIM-14 in SED is further complemented by the increased apoptosis compared to DIM-14 solution at the same dose of 20 mg/kg.

An effective therapeutic approach against cancers should focus on elimination of pool of CSCs which are quiescent or slowly replicating and thus more resistant to apoptosis induced by current cytotoxic regiments [2]. So far, very few drugs have been reported to exhibit CSCs inhibitory activity. One such drug, salinomycin, a potassium ionophore used as an agricultural antibiotic, reduced the proportion of CSCs by more than 100-fold relative to paclitaxel [3]. In the same study, nigericin, structural similarity to salinomycin, also exhibited selective toxicity on breast CSCs, suggesting that salinomycin killing CSCs may be due to its action as a potassium ionophore [3]. Metformin, a standard agent for diabetes, selectively killed cancer stem cells in several breast cancer cell lines in vitro and in vivo [4]. Unfortunately, salinomycin is very toxic to humans that prevent its clinical use [33]. Metformin, on the other hand, is not very potent; against CSCs it works only at high concentrations of 100–300 μM, which is beyond physiologically achievable limit. This served as the basis for our study to look for new agents that could selectively target CSC.

DIM-14 in the current study depicted potential anticancer activities as it was able to suppress various molecular markers associated with cancer expression. Anticancer activity could be correlated with decrease in the levels of BCL-2 and survivin in lung cancer stem cell tumor animal models. There are several reports suggesting the relation between CSCs and BCL2 level. Madjd et al. [34] showed that BCL-2 was highly expressed in breast CSCs and potentially affects the chemo-resistance by inducing other signaling pathways required for CSC survival. Lagadinou et al. [35] reported that BCL-2 inhibition reduced oxidative phosphorylation and selectively eradicated quiescent LSCs (Leukemia stem cells). In addition to BCL2 suppression, inhibition of survivin — an inhibitor of apoptosis protein, could potentiate the anticancer activity of DIM-14 and SED. Survivin is generally highly expressed in most cancers and expected to play a significant role in chemotherapy resistance, increased tumor recurrence, and shorter patient survival [36].

To date, very little is known regarding how Oct4, Sox2 and Nanog contribute to CSC properties at the molecular level. For the first time we report the effect of DIM derivatives on expression of these stemness factors. DIM-14 was found to efficiently impair the growth of LCSCs by reducing the expression of pluripotent stem cell transcription factors (Oct4, Sox2, Nanog). These factors are called as stemness factor because of their ability to determine the fate to stem cells. Inappropriate time and level of expression of these transcription factors would result in cancer stem cells rather than normal pluripotent stem cells or differentiated somatic cells. Upregulation of Oct4, Sox2 and Nanog, is correlated with poor survival outcome of patients with various types of cancer [37,38]. Interestingly, levels of inflammatory marker NF-kB were also found to be decreased in DIM-14 and SED treated stem cell lung cancer model. This indicates that DIM-14 could have inhibited the inflammatory pathway necessary for transformation and lung cancer stem cell formation. Along with suppression or inhibition of all above mentioned CSCs markers, DIM was also found to reverse the drug resistance of CSC as well as decrease their self-renewal potential of CSC in several carcinoma and melanoma cell lines [39]. Semov et al. [39], demonstrated that DIM is a selective and potent inhibitor of CSCs and pre-treatment of tumor spheres with DIM before implantation to mice significantly retarded the growth of primary tumors compared to tumors formed by untreated tumor spheres. These factors make DIM-14 a potential candidate of choice to be implemented in lung cancer prevention and therapy.

Our study attains significance because of the new potential applications attached to DIM-14 in cancer therapy. The unique ability of DIM-14 to eliminate cancer stem cells highlights its potential to use as a medium to bring about a dual therapeutic effect when combined along with conventional cancer treatment regimen consisting chemotherapeutic agents or irradiation. While a bulk of cancer non-stem cells in tumor can be efficiently eliminated by conventional cytotoxic agent or by irradiation, DIM-14 can selectively eliminate cancer stem cells. This dual therapeutic treatment of cancers by application of DIM-14 along with conventional treatment has the enormous potential to rule out the development of chemo-resistance, metastases and most importantly, tumor recurrence. Thus our unique in vivo model successfully establishes the potential application of DIM-14 to inhibit lung cancer stem cells and paves ways for other researchers to evaluate its application in other types of cancers also.

5. Conclusion

The improved oral bioavailability and superior anticancer effect of DIM-14 in lung cancer model through the self-emulsified formulation, gives a novel opportunity and technology to deal with poorly water soluble and low oral bioavailable drugs. Based on superior pharmacokinetic and pharmacodynamic profile, DIM-14 can be a potential anticancer drug to treat/prevent different cancer types by oral administration. In addition, DIM-14 SED in the current study was shown to be effective against lung cancer stem cells as well. In conclusion, this unique approach of drug formulation has numerous industrial applications and provides an effective alternative to deal with poorly water soluble, gastric acid sensitive, first pass metabolizing drugs.

Acknowledgement

The authors acknowledge the financial assistance of this research from the National Institute on Minority Health and Health

Disparities (NIMHD) P20 program [Grant # 1P20MD006738-03; to M.S.]; and the Department of Defense (DOD) Breast Cancer Program [Grant # W81XWH-11-1-0211] and the National Institutes of Health (NIH-NCI) [1R21CA175618-01A1 to M.S.]. The authors thank Dr. Srikumar Chellappan, (Professor, H. Lee Moffitt cancer center and research institute, Tampa, Florida) for the kind gift of lung cancer stem cells for our work.

References

[1] N. Ichite, M.B. Chougule, T. Jackson, S.V. Fulzele, S. Safe, M. Singh, Enhancement of docetaxel anticancer activity by a novel diindolylmethane compound in human non-small cell lung cancer, Clin. Cancer Res. 15 (2) (2009) 543–552.
[2] J. Wang, Z.H. Li, J. White, L.B. Zhang, Lung cancer stem cells and implications for future therapeutics, Cell Biochem. Biophys. 69 (3) (2014) 389–398.
[3] P.B. Gupta, T.T. Onder, G. Jiang, K. Tao, C. Kuperwasser, R.A. Weinberg, E.S. Lander, Identification of selective inhibitors of cancer stem cells by high-throughput screening, Cell 138 (4) (2009) 645–659.
[4] H.A. Hirsch, D. Iliopoulos, P.N. Tsichlis, K. Struhl, Metformin selectively targets cancer stem cells, and acts together with chemotherapy to block tumor growth and prolong remission, Cancer Res. 69 (19) (2009) 7507–7511.
[5] C. Qin, D. Morrow, J. Stewart, K. Spencer, W. Porter, R. Smith III, T. Phillips, M. Abdelrahim, I. Samudio, S. Safe, A new class of peroxisome proliferator-activated receptor gamma (PPARgamma) agonists that inhibit growth of breast cancer cells: 1,1-Bis(3′-indolyl)-1-(p-substituted phenyl)methanes, Mol. Cancer Ther. 3 (3) (2004) 247–260.
[6] S. Chintharlapalli, R. Smith III, I. Samudio, W. Zhang, S. Safe, 1,1-Bis(3′-indolyl)-1-(p-substitutedphenyl)methanes induce peroxisome proliferator-activated receptor gamma-mediated growth inhibition, transactivation, and differentiation markers in colon cancer cells, Cancer Res. 64 (17) (2004) 5994–6001.
[7] Y. Su, K. Vanderlaag, C. Ireland, J. Ortiz, H. Grage, S. Safe, A.E. Frankel, 1,1-Bis(3′-indolyl)-1-(p-biphenyl)methane inhibits basal-like breast cancer growth in athymic nude mice, Breast Cancer Res. 9 (4) (2007) R56.
[8] N. Ichite, M. Chougule, A.R. Patel, T. Jackson, S. Safe, M. Singh, Inhalation delivery of a novel diindolylmethane derivative for the treatment of lung cancer, Mol. Cancer Ther. 9 (11) (2010) 3003–3014.
[9] S. Chintharlapalli, S. Papineni, S.J. Baek, S. Liu, S. Safe, 1,1-Bis(3′-indolyl)-1-(p-substitutedphenyl)methanes are peroxisome proliferator-activated receptor gamma agonists but decrease HCT-116 colon cancer cell survival through receptor-independent activation of early growth response-1 and nonsteroidal anti-inflammatory drug-activated gene-1, Mol. Pharmacol. 68 (6) (2005) 1782–1792.
[10] S. Chintharlapalli, S. Papineni, S. Safe, 1,1-Bis(3′-indolyl)-1-(p-substitutedphenyl)methanes inhibit growth, induce apoptosis, and decrease the androgen receptor in LNCaP prostate cancer cells through peroxisome proliferator-activated receptor gamma-independent pathways, Mol. Pharmacol. 71 (2) (2007) 558–569.
[11] P. Lei, M. Abdelrahim, S.D. Cho, X. Liu, S. Safe, Structure-dependent activation of endoplasmic reticulum stress-mediated apoptosis in pancreatic cancer by 1,1-bis(3′-indolyl)-1-(p-substituted phenyl)methanes, Mol. Cancer Ther. 7 (10) (2008) 3363–3372.
[12] K. Kohli, S. Chopra, D. Dhar, S. Arora, R.K. Khar, Self-emulsifying drug delivery systems: an approach to enhance oral bioavailability, Drug Discov. Today 15 (21-22) (2010) 958–965.
[13] B. Singh, S. Bandopadhyay, R. Kapil, R. Singh, O. Katare, Self-emulsifying drug delivery systems (SEDDS): formulation development, characterization, and applications, Crit. Rev. Ther. Drug Carrier Syst. 26 (5) (2009) 427–521.
[14] P. Zhang, Y. Liu, N. Feng, J. Xu, Preparation and evaluation of self-microemulsifying drug delivery system of oridonin, Int. J. Pharm. 355 (1-2) (2008) 269–276.
[15] N.S. Barakat, Enhanced oral bioavailability of etodolac by self-emulsifying systems: in-vitro and in-vivo evaluation, J. Pharm. Pharmacol. 62 (2) (2010) 173–180.
[16] P. Patil, V. Patil, A. Paradkar, Formulation of a self-emulsifying system for oral delivery of simvastatin: in vitro and in vivo evaluation, Acta Pharm. 57 (1) (2007) 111–122.
[17] P. Balakrishnan, B.J. Lee, D.H. Oh, J.O. Kim, Y.I. Lee, D.D. Kim, J.P. Jee, Y.B. Lee, J.S. Woo, C.S. Yong, H.G. Choi, Enhanced oral bioavailability of Coenzyme Q10 by self-emulsifying drug delivery systems, Int. J. Pharm. 374 (1-2) (2009) 66–72.
[18] A.R. Patel, S.D. Spencer, M.B. Chougule, S. Safe, M. Singh, Pharmacokinetic evaluation and in vitro-in vivo correlation (IVIVC) of novel methylene-substituted 3,3′ diindolylmethane (DIM), Eur. J. Pharm. Sci. 46 (1-2) (2012) 8–16.
[19] W.J. Jusko, J.J. Schentag, W.E. Evans, W.J. Jusko, Applied Pharmacokinetics, Applied Therapeutics, Inc., San Francisco, 1980.
[20] S. Chintharlapalli, S. Papineni, S. Safe, 1,1-Bis(3′-indolyl)-1-(p-substituted phenyl)methanes inhibit colon cancer cell and tumor growth through PPARgamma-dependent and PPARgamma-independent pathways, Mol. Cancer Ther. 5 (5) (2006) 1362–1370.
[21] T. Inamoto, S. Papineni, S. Chintharlapalli, S.D. Cho, S. Safe, A.M. Kamat, 1,1-Bis(3′-indolyl)-1-(p-chlorophenyl)methane activates the orphan nuclear receptor Nurr1 and inhibits bladder cancer growth, Mol. Cancer Ther. 7 (12) (2008) 3825–3833.
[22] P. Lei, M. Abdelrahim, S.D. Cho, S. Liu, S. Chintharlapalli, S. Safe, 1,1-Bis(3′-indolyl)-1-(p-substituted phenyl)methanes inhibit colon cancer cell and tumor growth through activation of c-jun N-terminal kinase, Carcinogenesis 29 (6) (2008) 1139–1147.
[23] P. Lei, M. Abdelrahim, S. Safe, 1,1-Bis(3′-indolyl)-1-(p-substituted phenyl)methanes inhibit ovarian cancer cell growth through peroxisome proliferator-activated receptor-dependent and independent pathways, Mol. Cancer Ther. 5 (9) (2006) 2324–2336.
[24] M.D. Moretti, E. Gavini, C. Juliano, G. Pirisino, P. Giunchedi, Spray-dried microspheres containing ketoprofen formulated into capsules and tablets, J. Microencapsul. 18 (1) (2001) 111–121.
[25] S. Nazzal, M.A. Khan, Controlled release of a self-emulsifying formulation from a tablet dosage form: stability assessment and optimization of some processing parameters, Int. J. Pharm. 315 (1-2) (2006) 110–121.
[26] S. Nazzal, M. Nazzal, Y. El-Malah, A novel texture-probe for the simultaneous and real-time measurement of swelling and erosion rates of matrix tablets, Int. J. Pharm. 330 (1-2) (2007) 195–198.
[27] V. Nekkanti, P. Karatgi, R. Prabhu, R. Pillai, Solid self-microemulsifying formulation for candesartan cilexetil, AAPS PharmSciTech 11 (1) (2010) 9–17.
[28] D.F. Driscoll, J. Nehne, H. Peterss, R. Franke, B.R. Bistrian, W. Niemann, The influence of medium-chain triglycerides on the stability of all-in-one formulations, Int. J. Pharm. 240 (1-2) (2002) 1–10.
[29] B.R. De Miranda, J.A. Miller, R.J. Hansen, P.J. Lunghofer, S. Safe, D.L. Gustafson, D. Colagiovanni, R.B. Tjalkens, Neuroprotective efficacy and pharmacokinetic behavior of novel anti-inflammatory para-phenyl substituted diindolylmethanes in a mouse model of Parkinson's disease, J. Pharmacol. Exp. Ther. 345 (1) (2013) 125–138.
[30] N.L. Trevaskis, C.L. McEvoy, M.P. McIntosh, G.A. Edwards, R.M. Shanker, W.N. Charman, C.J. Porter, The role of the intestinal lymphatics in the absorption of two highly lipophilic cholesterol ester transfer protein inhibitors (CP524,515 and CP532,623), Pharm. Res. 27 (5) (2010) 878–893.
[31] Z. Zhang, L. Ma, S. Jiang, Z. Liu, J. Huang, L. Chen, H. Yu, Y. Li, A self-assembled nanocarrier loading teniposide improves the oral delivery and drug concentration in tumor, J. Control. Release 166 (1) (2013) 30–37.
[32] E. Scott Swenson, W.J. Curatolo, (C) Means to enhance penetration: (2) Intestinal permeability enhancement for proteins, peptides and other polar drugs: mechanisms and potential toxicity, Adv. Drug Deliv. Rev. 8 (1) (1992) 39–92.
[33] P. Story, A. Doube, A case of human poisoning by salinomycin, an agricultural antibiotic, N. Z. Med. J. 117 (1190) (2004) U799.
[34] Z. Madjd, A.Z. Mehrjerdi, A.M. Sharifi, S. Molanaei, S.Z. Shahzadi, M. Asadi-Lari, CD44+ cancer cells express higher levels of the anti-apoptotic protein Bcl-2 in breast tumours, Cancer Immun. 9 (2009) 4.
[35] E.D. Lagadinou, A. Sach, K. Callahan, R.M. Rossi, S.J. Neering, M. Minhajuddin, J.M. Ashton, S. Pei, V. Grose, K.M. O'Dwyer, J.L. Liesveld, P.S. Brookes, M.W. Becker, C.T. Jordan, BCL-2 inhibition targets oxidative phosphorylation and selectively eradicates quiescent human leukemia stem cells, Cell Stem Cell 12 (3) (2013) 329–341.
[36] K.M. Rahman, S. Banerjee, S. Ali, A. Ahmad, Z. Wang, D. Kong, W.A. Sakr, 3,3′-Diindolylmethane enhances taxotere-induced apoptosis in hormone-refractory prostate cancer cells through survivin down-regulation, Cancer Res. 69 (10) (2009) 4468–4475.
[37] M.L. Wang, S.H. Chiou, C.W. Wu, Targeting cancer stem cells: emerging role of Nanog transcription factor, Onco Targets Ther. 6 (2013) 1207–1220.
[38] K. Liu, B. Lin, M. Zhao, X. Yang, M. Chen, A. Gao, F. Liu, J. Que, X. Lan, The multiple roles for Sox2 in stem cell maintenance and tumorigenesis, Cell. Signal. 25 (5) (2013) 1264–1271.
[39] A. Semov, L. Iourtchenco, L.F. Liu, S. Li, Y. Xu, X. Su, E. Muyjnek, V. Kiselev, V. Alakhov, Diindolilmethane (DIM) selectively inhibits cancer stem cells, Biochem. Biophys. Res. Commun. 424 (1) (2012) 45–51.
[40] S.V. Fulzele, A. Chatterjee, M.S. Shaik, T. Jackson, N. Ichite, M. Singh, 15-Deoxy-Delta12,14-prostaglandin J2 enhances docetaxel anti-tumor activity against A549 and H460 non-small-cell lung cancer cell lines and xenograft tumors. Anticancer Drugs 18 (2007) 65–78.
[41] M. Chougule, A.R. Patel, P. Sachdeva, T. Jackson, M. Singh, Anticancer activity of Noscapine, an opioid alkaloid in combination with Cisplatin in human non-small cell lung cancer. Lung Cancer 71 (2011) 271–282.
[42] S.V. Fulzele, A. Chatterjee, M.S. Shaik, T. Jackson, M. Singh, Inhalation delivery and anti-tumor activity of celecoxib in human orthotopic non-small cell lung cancer xenograft model. Pharm Res 23 (2006) 2094–2106.
[43] A. Haynes, M.S. Shaik, A. Chatterjee, M. Singh, Evaluation of an aerosolized selective COX-2 inhibitor as a potentiator of doxorubicin in a non-small-cell lung cancer cell line. Pharm Res 20 (2003) 1485–1495.
[44] A.R. Patel, C. Godugu, H. Wilson, S. Safe, M. Singh, Evaluation of Spray BIO-Max DIM-P in Dogs for Oral Bioavailability and in Nu/nu Mice Bearing Orthotopic/Metastatic Lung Tumor Models for Anticancer Activity. Pharm Res 32 (2015) 2292–2300.

Drug Delivery

ISSN: 1071-7544 (Print) 1521-0464 (Online) Journal homepage: http://www.tandfonline.com/loi/idrd20

Tumor neovasculature-targeted cationic PEGylated liposomes of gambogic acid for the treatment of triple-negative breast cancer

Ravi Doddapaneni, Ketan Patel, Ibtisam Hasan Owaid & Mandip Singh

To cite this article: Ravi Doddapaneni, Ketan Patel, Ibtisam Hasan Owaid & Mandip Singh (2016) Tumor neovasculature-targeted cationic PEGylated liposomes of gambogic acid for the treatment of triple-negative breast cancer, Drug Delivery, 23:4, 1232-1241, DOI: 10.3109/10717544.2015.1124472

To link to this article: https://doi.org/10.3109/10717544.2015.1124472

Published online: 24 Dec 2015.

Drug Delivery

http://informahealthcare.com/drd
ISSN: 1071-7544 (print), 1521-0464 (electronic)

Drug Deliv, 2016; 23(4): 1232–1241
 DOI: 10.3109/10717544.2015.1124472

Taylor & Francis
Taylor & Francis Group

RESEARCH ARTICLE

Tumor neovasculature-targeted cationic PEGylated liposomes of gambogic acid for the treatment of triple-negative breast cancer

Ravi Doddapaneni[1], Ketan Patel[1], Ibtisam Hasan Owaid[2], and Mandip Singh[1]

[1]College of Pharmacy and Pharmaceutical Sciences, Florida A&M University, Tallahassee, FL, USA and [2]John D. Dingell VA Medical Center, Detroit, MI, USA

Abstract

Gambogic acid (GA) is a naturally derived potent anticancer agent with extremely poor aqueous solubility. In the present study, positively charged PEGylated liposomal formulation of GA (GAL) was developed for parenteral delivery for the treatment of triple-negative breast cancer (TNBC). The GAL was formulated with a particle size of 107.3 ± 10.6 nm with +32 mV zeta potential. GAL showed very minimal release of GA over 24 h period confirming the non-leakiness and stability of liposomes. *In vitro* cytotoxicity assays showed similar cell killing with GA and GAL against MDA-MB-231 cells but significantly higher inhibition of HUVEC growth was observed with GAL. Furthermore, GAL significantly ($p < 0.05$) inhibited the MDA-MB-231 orthotopic xenograft tumor growth with >50% reduction of tumor volume and reduction in tumor weight by 1.7-fold and 2.2-fold when compared to GA and controls, respectively. Results of western blot analysis indicated that GAL significantly suppressed the expression of apoptotic markers, bcl2, cyclinD1, survivin and microvessel density marker-CD31 and increased the expression of p53 and Bax compared to GA and control. Collectively, these data provide further support for the potential applications of cationic GAL in its intravenous delivery and its significant role in inhibiting angiogenesis against TNBC.

Keywords

Angiogenesis, cationic liposome, enhanced permeation and retention, gambogic acid, triple-negative breast cancer

History

Received 2 October 2015
Revised 18 November 2015
Accepted 22 November 2015

Introduction

Currently, patients with triple-negative breast cancer (TNBC) have neither effective targeted therapy nor do the breast cancer clinicians have a biomarker to identify aggressive and recurrent TNBC. To date, TNBCs are managed with standard chemotherapy but consequently, relapses are high due to acquired resistance and over 522 000 deaths per year from breast cancer worldwide as a direct result of this disease (Tao et al., 2014). TNBC accounts for 15% of all invasive breast cancers. It is a higher grade cancer and occurs at higher rates in young and African-American women (Palmer et al., 2014). Moreover, unlike the other type of solid tumor, TNBC patients have susceptibility toward the development of visceral metastases early in the course of the disease. Developments of effective approaches with improved treatment potential against these cancers are critical as the survival rate of patients with metastatic TNBC is very few months (Bonotto et al., 2014). Very poor prognosis and limited treatment options due to lack to typical breast cancer markers are the two basic factors compromising the cure of TNBC today. Therefore, there is an urgent need to develop new drugs or novel formulation strategy to potentiate the therapeutic outcome to combat TNBC.

Gambogic acid (GA) is a recently explored polyprenylated xanthene from the *Garcinia hanburryi* tree for its multiple therapeutic actions. GA has demonstrated significant anticancer activity against various cancers, both *in vitro* and *in vivo* conditions (Wang & Chen, 2012). GA was reported to act via multiple mechanisms promoting the tumor growth which involves apoptosis, cell cycle arrest, telomerase inhibition, anti-angiogenesis activity and an anti-metastasis effect (Zou et al., 2012). Lu et al. (2007) have reported that GA possesses both anticancer and anti-angiogenesis activity. As like other potent natural origin anticancer drugs (paclitaxel, doxorubicin, camptothecin, etc.), in future GA could transfer to clinical studies.

The major hurdle for clinical application of GA would be its extremely poor water solubility (<5 ppm) and very short biological half-life (less than 1 h in dogs and less than 20 min in rats) (Liu et al., 2006). It has been demonstrated that, by using surfactant micelles, the solubility of GA was increased and which results in enhanced *in vivo* anticancer activity. For preclinical studies, it has served the purpose but such surfactant have one or the multiple side effects, such as life-threatening hypersensitivity reactions, vascular stimulation, hemolytic toxicity, neurotoxicity, nephrotoxicity and cardiotoxicity, which discourage its application for the clinical purpose (Qi et al., 2008b). Similar problems are observed

Address for correspondence: Mandip Singh, College of Pharmacy and Pharmaceutical Sciences, Florida A&M University, Tallahassee, FL 32307, USA. Tel: (850) 561-2790. Fax: (850) 599-3813. Email: mandip.sachdeva@famu.edu

with the existing taxane formulations, and extensive research has been carried out to develop a safe and effective parenteral formulation with extended half-life.

PEGylated liposomes could be the most suitable formulation approach for parenteral delivery of GA because of lipophilic nature of GA and superior *in vivo* biocompatibility of PEGylated liposomes (Adlakha-Hutcheon et al., 1999; Chang & Yeh, 2012). The liposomal formulation is a safe, industry feasible and therapeutically superior alternative to solvent and surfactant-based formulation approach. There are several reports on supporting encapsulation of various anticancer drugs (doxorubicin, mitoxantrone, paclitaxel, docetaxel, etc.) into liposomes (Immordino et al., 2006; Deshpande et al., 2013). Many liposomal drugs are already approved for clinical formulations, such as AmBisome®, Doxil®, DaunoXome® and Marqibo® while others are under clinical trial (Chang & Yeh, 2012). Nanocarriers-based solubilization approach is preferred over other approaches because of additional advantages of nanocarriers in facilitating tumor uptake of the drug. Nanocarriers are passively accumulated into tumor because of enhanced permeation and retention (EPR) effect of leaky neovasculature of the tumor which minimizes the off-target side effects of the anticancer drugs. Doxorubicin-loaded liposomes showed a significant reduction in cardiotoxicity side effect of the drug and provides better therapeutic effect at a low dose (Xing et al., 2015). Surface PEGylation plays a crucial role in prolonging the circulation life of cationic liposome in blood circulation. It helps in two ways; enhance the probability of accumulation into the tumor by EPR effect and provide prolong exposure of drug to cancer cells. It has also been demonstrated that positively charged nanocarriers were preferentially bound to angiogenic blood vessels of the tumor and enhances intracellular uptake of the drug in cancer cells (Sawant & Torchilin, 2012). Due to more negative charge of neovasculature compared to healthy vasculature, cationic PEGylated liposomes will be of paramount significance to target the tumor more efficiently. Endothelial cells targeting of tumor can be achieved without anchoring a ligand on the liposomal surface. Targeting tumor endothelium could help in inhibiting the tumor growth at a reduced dose. GA is an ideal candidate for cationic PEGylated delivery because it has both anticancer and antiangiogenic effects. Such surface modifications are very facile in liposomal formulation compared to other type of nanocarriers.

In the present study, GA-loaded positively charged PEGylated liposomes were developed and characterized for parenteral delivery of GA and to achieve tumor neovasculature specific delivery. The formulation could be a potentially viable clinical approach for the treatment of TNBC.

Materials and methods

Chemicals and drugs

GA was purchased from Santa Cruz Biotechnology (Ann Arbor, MI) and dimethyl sulfoxide (DMSO) was purchased from Sigma-Aldrich (St. Louis, MO). Fetal bovine serum (FBS) from Invitrogen (Grand Island, NY) and an antibiotic mixture containing penicillin (5000 U/ml), streptomycin (0.1 mg/ml) and neomycin (0.2 mg/ml) from Sigma-Aldrich. Dulbecco's modified Eagle's medium (DMEM)/F-12 medium from Invitrogen and HUVEC cells and other cell culture materials like endothelial growth media and growth factors were purchased from Lonza (Basel, Switzerland). N-[1-(2,3-dioleoyloxy)propyl]-N, N, N-trimethylammonium methyl-sulfate (DOTAP), dipalmitoyl phosphatidylcholine (DPPC) and N-(carbonyl-methoxy polyethylene glycol 2000)-1,2-distearoyl-sn-glycero-3-phosphoethanolamine, sodium salt (DSPE-PEG-2000) were purchased from Lipoid (Ludwigshafen, Germany).

HPLC analysis

HPLC-UV method was developed to analyze GA for release studies. Chromatographic separation was achieved on Waters 717 instrument equipped with a Waters symmetry (250 mm/4.6 mm/5 μm) column using ACN:phosphate buffer pH 3 (90:10) as mobile phase with a flow rate of 1 ml/min, detected at 290 nm. The retention time of GA was 14.7 ± 0.15 min.

Cell culture

MDA-MB-231, Hep G2 and MIA PaCa-2 cells were obtained from American Type Culture Collection and maintained in DMEM (Sigma-Aldrich) nutrient mixture supplemented with 10% FBS and antibiotic-antimycotic mixture comprising penicillin (5000 U/ml), streptomycin (0.1 mg/ml) and neomycin (0.2 mg/ml) at 37 °C. When cells became approximately 80–90% confluent, cells lines were subcultured with 0.25% trypsin-EDTA (Invitrogen).

Animals

Female Nu/Nu mice (six-weeks old from Harlan, Indianapolis, IN) were grouped and housed ($n = 5$ per cage) in sterile microisolator caging unit supplied with autoclaved Tek-Fresh bedding. The animals were housed at Florida A&M University in accordance with the standards of the Guide for the Care and Use of Laboratory Animals and the Association for Assessment and Accreditation of Laboratory Animal Care.

Preparation and characterization of liposomes containing gambogic acid (GAL)

Different batches of GAL were prepared using ethanol injection – ultrasonication method. Briefly, GA, DPPC, cholesterol, DOTAP and DSPE-PEG 2000 in 1:14:6:2:0.6 molar ratios were dissolved in absolute ethanol and injected into water at 55 °C with constant stirring. After a minute, the mixture was sonicated for 2 min using a probe sonicator at 400 W, 30% amplitude (Branson, Danbury, CT) to reduce the particle size. Liposomes were further stirred for 1 h at 55 °C to evaporate the ethanol. The weight ratio of GA to phospholipids was varied to optimize the GA loading and particle size. We have used the lowest amount of ethanol because ethanol is difficult to evaporate and affect the long-term physical stability of liposomes. Further, sonication was done to achieve particle size around 100 nm. Release study of GA loaded liposomes and GA solution in DMSO was carried out by dialysis bag method. Drug release study was performed at 37 °C under shaking (100 rpm) which was monitored using a dialysis bag containing phosphate-buffered saline (PBS)

with the addition of 0.5% Tween-80 as a sink solution at pH 7.4. GA solution was prepared by dissolving 20 mg of GA in 1 ml of ethanol:Tween-80 (1:1) solution. For animal study, it was diluted appropriately with water for injection. Data are calculated from triplicate experiments and presented as mean, and error bars refer to SD.

In vitro cytotoxicity of GA and GAL

MDA-MB-231, HepG2 and MIA Paca-2 cells were seeded at a density of 10 000 cells/well in 96-well plates and allowed to adhere for 24 h. Cells were exposed to different concentration of GA and GAL for 48 h in triplicate. Cytotoxicity was assessed at the end of drug exposure using crystal violet assay. Absorbance was measured at 545 nm using a microplate reader (ChroMate 4300, Palm city, FL). Untreated cells were used as control and results were expressed as the relative percentage of absorbance compared to control. Half-maximal inhibitory concentration (IC50) was calculated using Sigma Plot software, version 9.0 (SYSTAT Software, San Jose, CA).

Western blot analysis

For *in vitro* experiments, 3.2 μm of GA and 3.8 μm of GAL were used to prepare protein lysates for immunoblotting. The dose of GA 10 mg/kg was used for all the *in vivo* experiments. Protein samples for western blot analysis were extracted from MDA-MB-231 cells and tumor tissues by using RIPA lysis buffer according to Godugu et al. (2014). Protein concentration was estimated by using BCA protein assay reagent kit. Equal amounts of 50 μg protein from different groups were denatured by heating for 5 min in SDS sample buffer and protein samples were separated by 10% SDS-PAGE. The protein samples separated on SDS-PAGE were transferred to nitrocellulose membranes for immunoblotting. After blocking, the membranes were incubated with skim milk (5% skim milk in 10 mm Tris-HCl (pH 7.6), 150 mm NaCl and 0.5% Tween-20) and probed with primary antibodies. The primary antibodies such as bcl-2, survivin, Bax, cyclin D1, p53, CD31 and β-actin were used in 1:1000 dilutions. The horse radish peroxidase (HRP)-conjugated secondary antibodies were used. Evaluation of expression of each protein was calculated in comparison to the expression of β-actin.

Analysis of miR-224 and miR-34b expression

MDA-MB-231 cells were treated with GA (3.2 μm) and GAL (3.8 μm) for microRNA analysis. miR-224 and 34b expression was carried out using 2 μg of total RNA for polyadenylation reaction analysis according to the manufacturer's protocol (ABI Systems, Green Island, NY). At 37 °C for 30 min, the reaction mixture was incubated and the reaction tubes were immediately transferred to the ice to proceed for first-strand cDNA synthesis (ABI Systems) according to the manufacturer's protocol. The target transcript levels (miR-224 and miR-34b) were normalized against U6 snRNA expression. Untreated cells were used as a control and compared the expression level of these miRNA's to the control samples according to the Doddapaneni et al. (2013). The data of qRT-PCR are expressed as the mean ± standard deviation (SD). All the experiments were carried out in triplicates.

In vitro HUVEC tube formation assay

HUVECs were grown in epithelial basal medium supplemented with 10% FBS at 37 °C and 5% CO_2. Keeping 24-well culture plates on the ice, added chilled corning matrigel matrix (10 mg/ml) according to the manufacturer's instructions. Briefly, plates were incubated at 37 °C for 30–60 min. The remaining liquid was carefully removed (medium) from the cultureware without disturbing the layer of corning matrigel matrix just before use. Endothelial cell suspensions was prepared by trypsinization and resuspending the cells in culture medium at 4×10^5 cells/ml. In order to study the effect, GA and GAL were added to the wells. HUVECs were suspended in EGM-2 medium containing various growth factors and drugs were seeded onto the matrigel. The effect of DTX on angiogenesis was also evaluated as a positive control by tube formation assay. After 12 h, cells were labeled by adding 300 μl/well of 8 μg/ml corning calcein AM in Hank's balanced salt solution and plates were incubated for 30 min at 37 °C, 5% CO_2. The cells were washed twice with PBS and photographed. Tube formation was calculated as follows: a three branch point event was taken as one tube and percentage inhibition expressed using untreated wells at 100%. This assay was repeated three times.

Anticancer studies in MDA-MB-231 cells induced breast cancer models

Triple-negative MDA-MB-231 breast carcinoma subcutaneous xenograft model was used for anticancer evaluations of GA PEGylated liposomes. MDA-MB-231 cells (1 million in 100 μl of phosphate buffer) were subcutaneously injected into the right flank of the mice. Two weeks after the tumor cells implantation, GA and GAL treatment was started and tumor sizes were measured using vernier caliper. At the time of the first dose of drug administration, the tumor volumes were approximately 100 mm^3. Mice were randomly divided into three groups ($n = 6$ for each group) to receive IV injection of saline (control group), GA solution (10 mg/kg) and GAL (10 mg/kg). The therapy was continued six times at 2 d intervals through IV injection. The greatest longitudinal diameter (length) and the greatest transverse diameter (width) were measured. Tumor volumes were monitored every alternate day till the termination of the study.

Immunohistochemistry of CD31 expression in xenograft breast tumor model

Paraffin-embedded tumor tissues were deparaffinized and blocked for peroxidase activity for CD31 expression. Washed specimens with PBS twice, then specimens were incubated in normal goat serum according to the manufacturer's instructions (Santa Cruz Biotechnology, Santa Cruz, CA). The section slides were washed with PBS twice and incubated with primary antibody against CD31 overnight at 4 °C. The HRP-conjugated secondary antibody was applied to locate the primary antibody (Santa Cruz Biotechnology). After three washes with PBS, the section slides were stained with Nova Red stain and counterstained with hematoxylin. The Olympus BX40 light microscope equipped with a computer-controlled

digital camera (DP71, Olympus Center Valley, PA) was used to visualize the images on the slides.

Statistics

All data are presented as the mean ± SD or mean ± standard error of mean (SEM). The significance of the difference in treatment groups was determined using one-way ANOVA and Tukey's multiple comparison test using GraphPad prism version 5.0 (San Diego, CA), where the value of $p < 0.05$ between the groups was considered as statistically significant difference between these groups.

Results

Preparation, characterization and *in vitro* drug release profile of liposomes

Different batches of GAL were prepared using ethanol injection – ultrasonication method. Particle size, entrapment efficiency and drug loading were optimized. Finally, optimized batch of GAL had a particle size of 107.3 ± 10.6 nm and 0.158 polydispersity index. The surface charge of GAL was positive with an average zeta potential of + 32 mV. Gel permeation chromatography showed 92.1 ± 2.7% entrapment efficiency of GA within liposomes. Drug loading did not show a remarkable difference in particle size. However, liposomes prepared with more than 10% w/w GA loading and 1.5 mg/ml final GA concentration were not stable for more than 2 h at room temperature. The *in vitro* release behavior of the GAL is shown in Figure 1. GA solution showed the immediate and complete release of GA in release medium within 1 h. GAL showed much sustained and minimal release of GA. Only 11.65% of GA release was observed over the period of 24 h.

In vitro cytotoxicity of GA and GAL

In vitro cytotoxicity studies with GA against MDA-MB-231, Hep G2 and MIA PaCa-2 cells showed IC50 values of 3.2 ± 0.28, 4.06 ± 0.41 and 5.29 ± 0.53 µm, respectively (Table 1). The GAL treated MDA-MB-231, HepG2 and MIA PaCa-2 cells were showed IC50 values of 3.8 ± 0.34, 4.35 ± 0.48 and 5.61 ± 0.30 µm, respectively. All three cell lines showed more potency toward GA and GAL with little variations between their potencies. There was no significant difference between cytotoxicity of GA-free drug and GAL because permeability was similar for both free drug and liposome. Highly metastatic MDA-MB-231 human carcinoma cells were, however, selected for further studies as an *in vitro* model to study the effect of GA and GAL on TNBC.

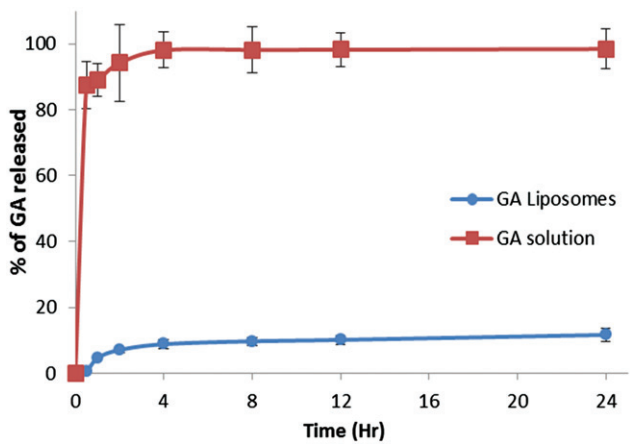

Figure 1. *In vitro* release profile of GA and GAL. GAL showed very minimal release of GA in 48 h.

Analysis of apoptotic and survival markers

Western blot analysis of the antiapoptotic marker bcl-2 significantly ($p < 0.01$) down regulated in GAL-treated cells when compared to untreated control and GA-free drug-treated cells (Figure 2A and B). As shown in Figure 2B, expression of bcl-2 was found to be reduced (1.33-fold) in comparison to untreated control cells. The GAL resulted in a 0.81-fold higher repression in the bcl-2 expression compared to GA-free drug, suggesting the superior anticancer effects of GAL in breast cancer. The expression of survivin protein was significantly ($p < 0.05$) decreased (0.72 and 1.25-fold) in GA-free drug and GAL-treated cells compared to control cells, respectively (Figure 2B). The cell proliferating related protein cyclin D1 expressions were found to be higher in MDA-MB-231 control lysates. On treatment with GAL formulation, cyclin D1 was significantly ($p < 0.01$) down regulated. The relative expressions of cyclin D1 were found to be reduced 0.51 and 0.71-fold significantly in GA-free drug and GAL formulations, respectively compared to untreated control lysates (Figure 2B). The relative expression of p53 was increased in GA-free drug- (1.08-fold) and GAL- (2.30-fold) treated cells compared to control. In GA- and GAL-treated groups, Bax expression was increased significantly ($p < 0.01$) compared to untreated control cells, thus highlighting the potential of GAL inducing apoptosis in breast cancer cells (Figure 2B).

Real-time PCR analysis

The study was carried out to gain additional insights into the mechanisms/crucial factors regulating GA and GAL induced anticancer effects. We examined the expression pattern of miR-224 and miR-34b in MDA-MB-231 cells. A down-regulation of miR-224 (Figure 3) and up-regulation of miR-34b (Figure 3) expression was observed in cells treated with GA and GAL. As our primary data, the miR-224 was downregulated (1-fold) and miR-34 was up-regulated (1.7-fold) significantly ($p < 0.05$) in cells treated with GAL as compared with control cells which were treated with PBS (Figure 3). However, miR-34b expression was significantly

Table 1. IC50 values of MDA-MB-231, Hep G2 and MIA PaCa-2 cells treated by GA and GAL for 48 h. Data represent mean ± SD ($n = 3$).

Cell lines	IC 50 (µm)
GA MDA-MB-231	3.2 ± 0.28
GA Hep G2	4.06 ± 0.41
GA MIA PaCa-2	5.29 ± 0.53
GAL MDA-MB-231	3.8 ± 0.34
GAL Hep G2	4.35 ± 0.48
GAL MIA PaCa-2	5.61 ± 0.30

($p < 0.05$) increased compared to control. Thus, these findings espouse the role of miR-224 and miR-34 in GA induction of anticancer effects.

Anti-angiogenic effect

Compared to control group, a decrease in capillary tube branch point formations were observed in GA and GAL group (Figure 4C and D). We observed that an extensive meshwork of branched capillary-like tubules having multicentric junctions in the control group (Figure 4A). GAL (Figure 4D) showed remarkable inhibition of branching point of HUVEC at as low as 50 nm concentration compared with docetaxel (Figure 4B). Effect of GAL was more pronounced with >90% inhibition of branching point compared to control while positive control docetaxel (20 nm) showed 80.0% inhibition (Figure 4E).

Antitumor activity of GA and GAL *in vivo*

The *in vivo* antitumor efficacy of GAL was investigated in MDA-MB-231 orthotropic xenograft tumor-bearing nude mice and compared with GA solution. As illustrated in Figure 5A and B, the treatment group showed significant tumor growth inhibition compared to the control group. In particular, the tumor volumes in the GAL group were much smaller than those of GA solution group ($p < 0.05$), indicating a statistically improved antitumor effect of GAL compared to the free drug group. Compared to untreated control groups, 1.31- and 2.0-fold, respective decrease in the tumor volume in

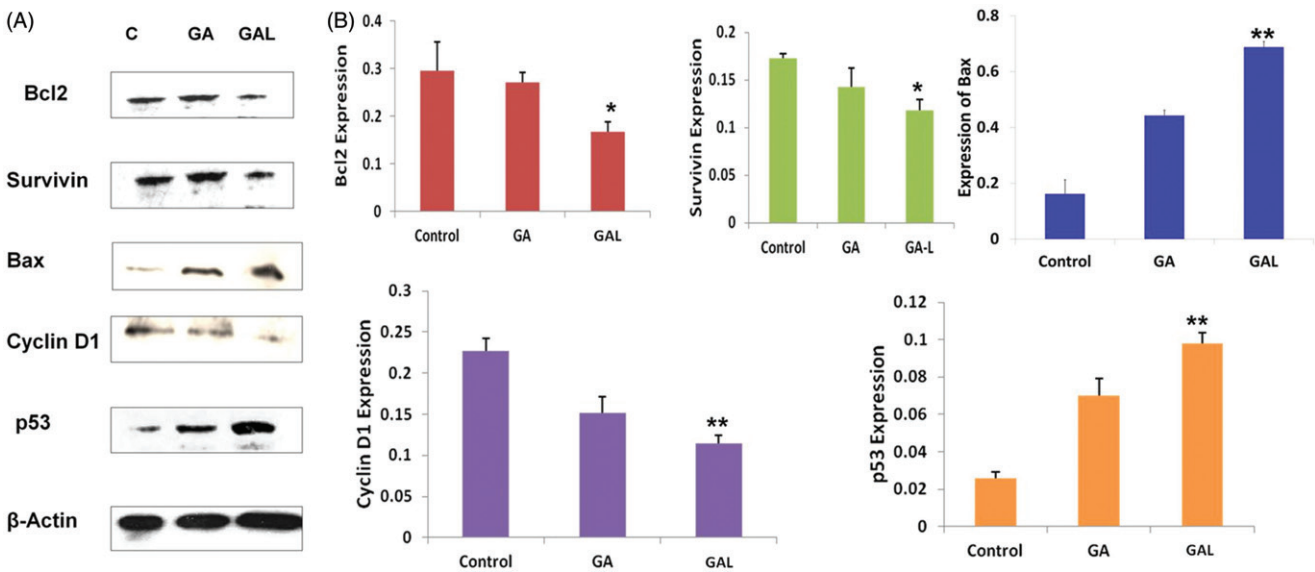

Figure 2. Determination of protein expression levels by western blot**.** (A) Expression of bcl2, survivin, Bax, cyclin D1 and p53 in comparison to the control β-actin in GA- and GAL-treated MDA-MB-231 cells by western blot. Untreated cells were used as control. (B) Western blot analysis of expression of different proteins up/downregulated significantly in GAL treated cells. Data are calculated from triplicate experiments and presented as mean, and error bars refer to SD, $*p < 0.05$, $**p < 0.01$ compared with control.

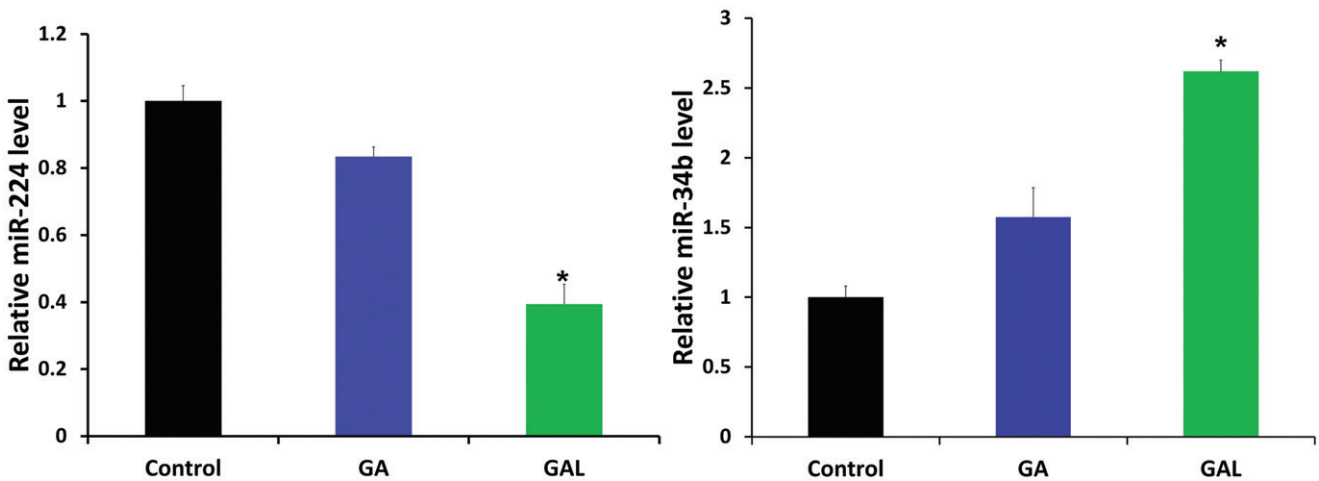

Figure 3. Quantification of microRNA-224 and microRNA-34b expression by real-time PCR. MDA-MB-231 cells were treated with GA and GAL and quantified the expression of miR-224 and miR-34b. Each experiment was performed in triplicate. The expression level of each gene was normalized by snRNA and then compared to control cells. The means of the normalized microRNA expression values were calculated for each time point and expressed as relative fold changes (mean ± SD). $*p < 0.05$, compared with control.

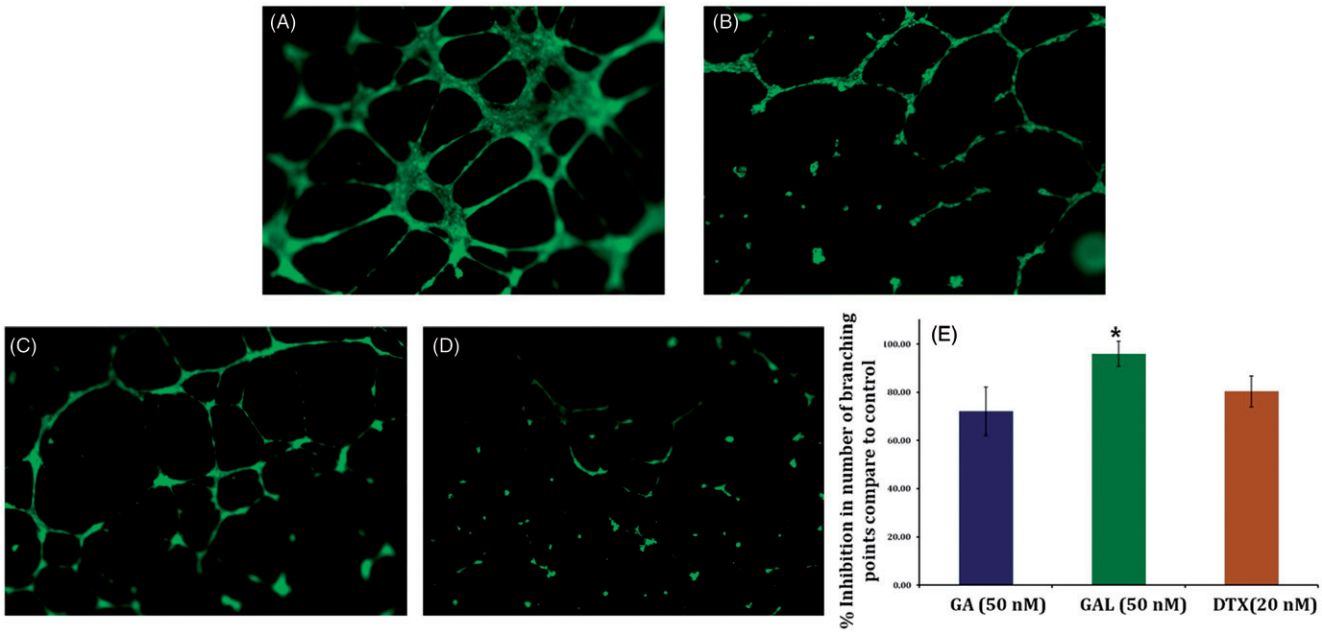

Figure 4. Effect of GA and GAL on angiogenesis by tube formation assay. HUVEC cells were treated with (A) no treatment, control (B) Docetaxel (C) GA and (D) GAL at indicated concentrations and docetaxel used as a positive control. (E) Analysis of percentage inhibition of angiogenesis by calculating branch points in GA and GAL-treated cells. Data are calculated from triplicate experiments and presented as mean, and error bars refer to SD, $*p<0.05$ compared with control.

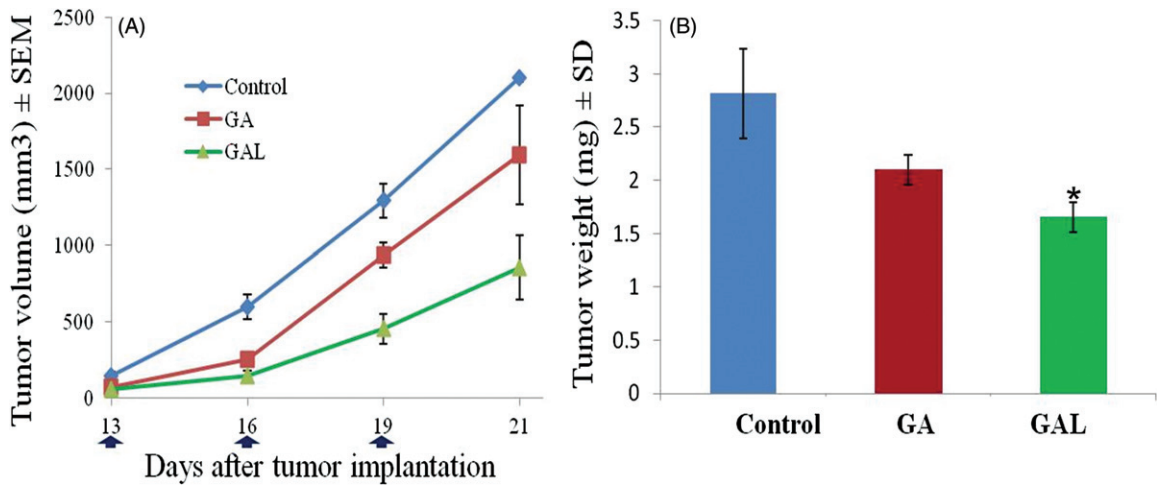

Figure 5. *In vivo* efficacy of GA and GAL. (A) Tumor growth kinetics with dosing every other day for five times. (B) Relative tumor weight of mice after the treatment. Data are expressed as mean ± SEM ($n=6$). $*p<0.05$ compared with control.

GA-free drug and GAL-treated tumor groups was observed (Figure 5A). Similarly, the tumor weights of mice treated with GAL were significantly ($p<0.05$) lower compared to GA-free solution (Figure 5B). There was no statistically significant change in the body weights of the animals treated with GA (25 ± 2.3 g) and GAL (25 ± 1.9 g) groups, suggesting the safety of the GA and GAL.

Antitumor and anti-angiogenic effects of GA and GAL in xenograft breast tumors

Next, we conducted the mechanistic studies to confirm the superior anticancer effects of GAL compared to GA-free drug-treated groups *in vivo* (Figure 6). As shown by western blot analysis in Figure 6, in GA-free drug and GAL groups, Bcl-2 expressions were found to be decreased (0.9 and 1.6-fold) significantly ($p<0.01$), respectively compared to untreated control tumors. The GAL produced 0.7-fold higher repression in the bcl-2 expression compared to GA-free drug, suggesting the superior anticancer effects of GAL in breast cancer. Similarly, the cell survival marker survivin expression was also significantly ($p<0.05$) down regulated to 0.6- and 1.79-fold in GA-free drug and GAL groups compared to the control group, respectively (Figure 6). In regressed tumors, the GA and GAL treatments significantly ($p<0.05$) decreased cyclin D1 expressions to a 0.8- and 1.4-fold, respectively, of controls. The tumor suppressor protein p53 levels also indicated the promising anticancer effects of GA in both free drug and liposome formulations. GA and GAL-treated groups significantly ($p<0.05$) increased p53 expression to 1.51 and 2.36-fold, in regressed tumor samples compared to control. Similarly, the expression of Bax also increased

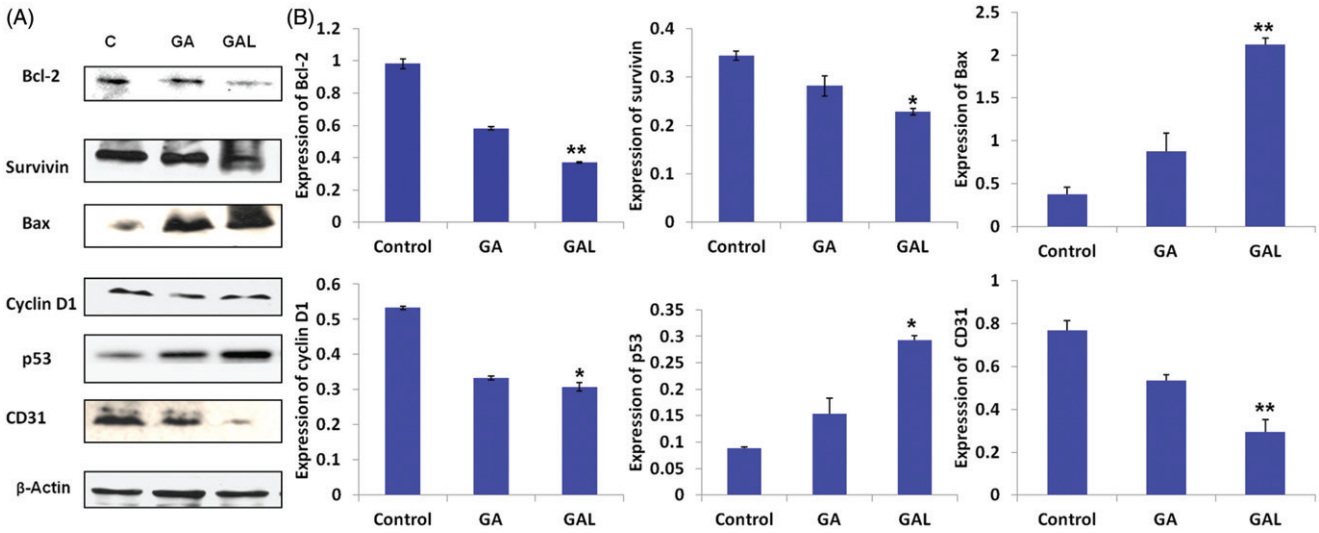

Figure 6. *In vivo* apoptotic activity of GA and GAL in Balb/c nu/nu mice by western blot. (A) Expression of Bcl2, survivin, Bax, cyclin D1, p53 and CD31 in comparison to the control β-actin in GA and GAL-treated tumor tissues by western blot. The untreated animal group were maintained as control. (B) Western blot analysis of expression of different proteins up/downregulated in GA-treated cells. Data are calculated from triplicate experiments and presented as mean, and error bars refer to SD, $*p<0.05$, $**p<0.01$ compared with control.

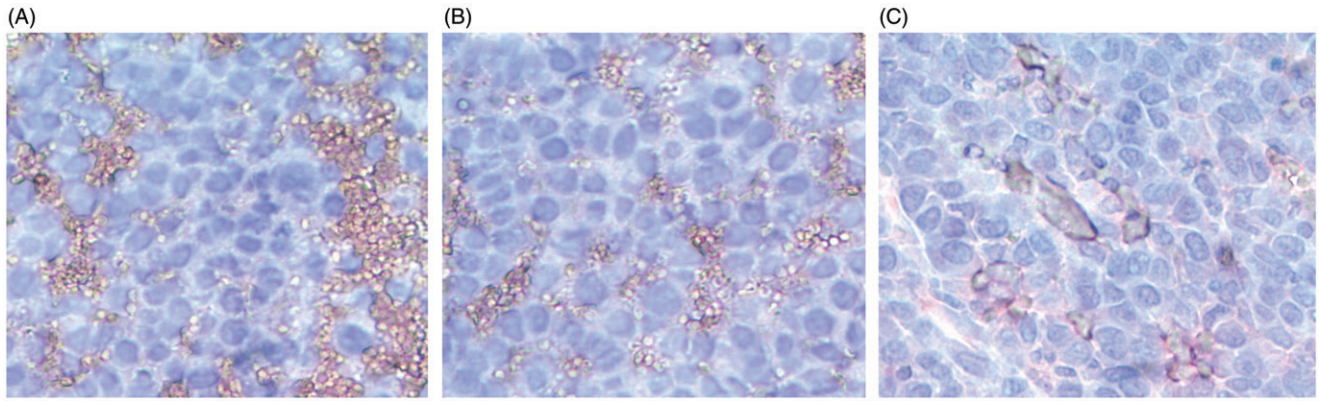

Figure 7. Analysis of CD31 expression by immunohistochemistry. Immunohistochemical peroxidase staining of CD31 in xenograft breast tumors of (A) Control, (B) GA and (C) GAL treatment groups. Presence of dark stain indicated positive staining for the primary antibody.

significantly ($p<0.01$) in GAL-treated groups than GA-free drug and control, thus providing the further evidence that GAL inducing apoptosis of breast cancer cells through bcl2/Bax. CD31 (platelet endothelial cell adhesion molecule-1) expression was significantly ($p<0.01$) decreased in GAL-treated group than control or GA-treated group (Figure 6).

Further, the expression of CD31 was also confirmed by immunohistochemistry. The highest expression of CD31 was seen in tumor tissues harvested from untreated mice (Figure 7A). Decreased CD31 staining was observed in tumors treated with GAL (Figure 7C) compared to tumors treated with GA alone (Figure 7B). All these results revealed that GA in free drug form and in liposome form significantly produced anticancer effects. Moreover, GAL formulation showed better anticancer and antiangiogenic effects than GA-free drug treated groups, which suggest the superior anticancer potential of our liposome formulation.

Discussion

Breast carcinoma is the leading cause of cancer-related death in women. The poor prognosis in breast carcinoma is due to its resistance to current therapies and to tumor metastasis (André & Zielinski, 2012). Development of an effective chemotherapeutic agent with the potential to trigger cancer cell death to prevent tumor invasion and metastasis is highly essential to prevent this form of cancer. Although GA potency as an anti-tumor agent has been demonstrated (Zou et al., 2012), the antitumor and antiangiogenic activities of GAL have not been explored yet. To the best of our knowledge, this is the first study concerning the use of GA loaded in cationic liposomes in TNBC therapy *in vivo*.

The high amount of organic solvent and surfactant are needed for parenteral delivery of GA because of its extremely poor aqueous solubility (<0.5 μg/ml) (Cai et al., 2014). For preclinical and clinical studies, we need at least 0.5 mg/ml solubility and physically stable solution in water for injection or saline. That means, 1000 times higher solubility, which can be achieved using solvent and surfactants. However, parenterally accepted non-ionic surfactants like polysorbate 80 and cremophor EL have severe life-threatening side effects. Therefore, there is a huge demand of solvent and surfactant-free formulations of existing anticancer molecules like paclitaxel and docetaxel as well (Patel et al., 2013). The

liposomal formation is a safe, industry feasible and therapeutically superior alternative to solvent and surfactant-based formulation approach. GA is a highly lipophilic molecule with a log *p* of 7.6, so liposomal formulation could be the most appropriate choice for parenteral delivery. We used ethanol for liposomal preparation; but ethanol is difficult to evaporate, so we kept the formulation for a long time on the heated stirrer. Importantly, a marketed formulation like taxol and taxotere contains 2–3 ml of ethanol/dose, and thus it is very safe solvent for parenteral use. Hence, a trace amount of ethanol will not harm at all. GA can be easily solubilized and stabilized by entrapping within lipid bilayers of liposomes. The release profile of GAL depicted that GA was confined to lipid bilayers of liposomes and as long as the liposomes are stable release of GA would be difficult. Such release profile is very desirable for targeted drug delivery since drug will release only on liposomal disintegration after cellular internalization. It helps in minimizing the systemic exposure of drug and related side effects.

In vitro cytotoxicity studies showed that GAL retained the cytotoxicity of GA against MDA-MB-231 cell line. Once internalized, liposomes are degraded in endosomes and release the drug into the cytoplasm. Hence, the difference in the cytotoxicity between free GA and GAL was found to be negligible *in vitro*. In similar observations with our study, Saxena & Hussain (2012) demonstrated that GA encapsulated in poloxamer 407/TPGS showed comparable *in vitro* cytotoxicity than free GA in breast cancer MCF-7 cells (Saxena & Hussain, 2012).

Interestingly, a huge difference in anti-angiogenic activity of free GA and GAL was observed in HUVEC study. Angiogenic endothelial cells are negatively charged which might affect their interaction with the chemical nature of drug and nanocarrier. As GA is an anionic molecule while GAL has cationic charge. We can assume that intracellular GA concentration would be much higher when given as GAL compared to free GA solution. Lu et al. (2007) showed that GA inhibits angiogenesis and secretion of VEGF reduced from tumor cells. Furthermore, Qi et al. (2008a) reported that when the cells were treated with GA *in vitro,* expression of extracellular matrix proteins (like MMP-2 and MMP-9) was decreased. To study the possible mechanisms involved in the enhanced cytotoxicity of GA-free drug and GAL, we evaluated apoptosis and HUVEC tube formation of tumor cells. It has been suggested that apoptosis may represent a protective mechanism against neoplastic development as it eliminates genetically damaged cells or excess cells that have improperly been induced to proliferate (Vaseva & Moll, 2009; Andreopoulou et al., 2015). Zhai et al. (2008) have shown that induced cell apoptosis by repressing bcl2 expression by GA. Low concentrations of GA have no obvious inhibitory effect on cell viability or apoptosis-inducing effect (Li et al., 2011). Moreover, we observed that *in vitro* treatment with GA significantly ($p < 0.05$) up-regulates the expression of the pro-apoptotic protein Bax and down-regulated the expression of the anti-apoptotic protein Bcl-2 in MDA-MB-231 cells at the protein level. It is not known whether GA affects other genes in addition to Bax and Bcl-2, how it affects, and also if other mechanisms may contribute to changes in cell apoptosis. This would like to explore in future in our laboratory.

Previous studies have demonstrated the anti-angiogenic potential of GA-free drug on HUVEC (Lu et al., 2013). There has been no study so far that evaluated the effect of GA loaded in cationic liposomes on HUVEC tube formation. GAL treatment showed linear structures of the network were significantly ($p < 0.01$) disrupted compared to GA-free drug treatment or control. GA-free drug and GAL exhibited anti-angiogenic activity by inhibition of tube formation compared to control (Figure 4). In a similar study, Lu et al. (2007) showed that GA has potential to inhibit angiogenesis *in vitro* and *in vivo* via suppressing phosphorylation of VEGFR2 selectively and reduction of the VEGF secretion from tumor cell. In our study, we observed a significantly potent inhibition in GAL-treated cells compared to GA-free drug. Our study demonstrates that GA and GAL directly reduce HUVEC proliferation and tube formation on matrigel. In the present study, we provide evidence for the first time that GAL has a potent anti-angiogenic activity. The dual anti-tumor and anti-angiogenic activities of GAL are consistent with those of some other conventional anticancer drugs such as docetaxel, paclitaxel and camptothecin, and thus suggest its potential use as anti-tumor agents as well as its efficacy to be included in tumor therapy (Patel et al., 2014).

Due to the observed *in vitro* anti-angiogenic and apoptotic activity, we were interested in evaluating the expression of microRNAs involved in the apoptosis. In this study, our microarray data analysis (data not shown) and validation by qRT-PCR revealed that miR-34b and 224 expressions positively correlates with the expression of the apoptotic genes *Bcl2, p53* and *Bax,* which are known to induce apoptosis. But the strength of the conclusions of this study was hampered as these results are based on *in vitro* experiments. In order to assess the functional role of miR-34b and miR-224, further studies should be done using animal models. Also, studies of miR-34b and miR-224 with gene targets in TNBC are of further importance. Our study provided an addition confirmation that miR-34b has an anti-tumor function in TNBC. Findings from our study by both microarray and real-time PCR analysis indicated that these microRNAs act as tumor suppressors. In addition to miR-34b and miR-224, supporting our data, other miRs like miR-335, miR-206 and miR-126 have also been identified as human breast cancer metastasis suppressor miRs (Misso et al., 2014).

The anticancer effect of GAL may be induced by inhibiting angiogenesis and directly killing tumor cells. Our *in vivo* studies demonstrated that administration of the GAL did not lead to any abnormal behavioral changes in these animals, suggesting that the GA-free drug and nanosized assemblies of GAL are safe for parenteral administration. However, due to the presence of non-ionic surfactant in a free drug solution, administration in human may cause severe toxicities. In the *in vivo* study, Yao et al. (2014) demonstrated that GA loaded hyaluronic acid nanoparticles exhibited therapeutic efficacy with reduced toxicity. Encouragingly, we also observed these findings in the GAL-treated group, suggesting that the GAL did not have toxicity in mice. *In vivo* anticancer efficacy study of intravenously administered GA on MDA-MB-231 bearing balb/c nude mice was also carried out in this study. However, no description of solubilizer or formulation was given in the report. We assume that author may have used ethanol and

surfactant based formulation. In spite of injecting less number of cells (1.5 million/animal) compared to Li et al. (2012) (2 million/animal), a significant difference in tumor progression was observed for GA in TNBC tumor bearing mice. In that study, average tumor volume in the animals of control group attained 2000 mm^3 in 10 weeks while in our study the same volume was achieved within just 21 d. Further, the author showed that anticancer efficacy of GA was observed for 7 weeks after the first dose. It is noteworthy that in that report, animals were given about 25 doses of GA by IV route every other day. While in our study only three doses were administered every third day and the study was terminated after 21 d. In both the studies, cell line, type of animals and organ of injection are same, but tumor development and growth rate is very different. The possible reason for such variation could be the passage number of injected MDA-MB-231 cells. We have injected the cells which were freshly cultivated from tumor tissue of MDA-MB-231 tumor-bearing mice. Generally, tumor cells obtained by this method are very aggressive in proliferation and invasionConsidering the results of our study and previously reported studies on anticancer efficacy of GA against TNBC, we can conclude that liposomal formulation prepared in our laboratory has some salient advantages over solution-based formulation: (a) liposomal formulation requires significantly less number of doses for inhibiting tumor growth; (b) formulating cationic charged liposomes of GA could potentially helpful in targeting angiogenesis; (c) organic solvents and surfactants are not required to deliver GA.

One of the widely accepted mechanism of tumor development is apoptotic inhibition and to inhibit the carcinogenic process, numerous chemopreventive agents have been shown to act through the induction of apoptosis (Naithani et al., 2008). Our observations in the current study also support that GA-free drug and GAL act by the induction of apoptosis. We observed in the current study that GA-free drug and GAL treatment decreases the expression of survivin in breast tumors (Figure 5). Survivin, an inhibitor of apoptosis protein, is highly expressed in most of the cancers and associated with chemotherapy resistance (Pereira & Amarante-Mendes, 2011). Therefore, our observed down-regulation of survivin expression results in activation of caspases and thereby induces apoptosis in tumor cells. Expression of p53 plays a vital role in regulating tumor cell response to drugs and modulate the effect of downstream effectors like Bax and p21 (Xu et al., 2013). In our study, found that Bax was activated in GA-free drug and GA cationic liposomes treatment group leading to apoptosis in breast tumors. Our observations were similar to Gu et al. (2009) reported that GA *in vitro* (at a concentration of 4 μm) induces apoptosis of non-metastatic breast cancer MCF-7 cells by reducing Bcl2 expression via p53 in a time- and concentration-dependent fashion. To sum up, our findings in the current study suggests that mechanism of action of GA to induce apoptosis mediated via down-regulation of antiapoptotic Bcl_2 and upregulation of proapoptotic Bax. Our immunohistochemical analysis also found that the expression of CD31 was decreased in GAL group compared to GA-free drug and control groups which clearly indicated that microvessel density and neovascularization was significantly affected by GAL treatment. The superior antitumor activity of GAL was expected to majorly contribute by its preferential interaction and consequent disruption of neovasculature.

Conclusion

Solvent and non-ionic surfactant-free delivery system of GA was developed for parenteral administration. Cationic PEGylated liposome enhanced the anti-angiogenic efficacy of GA by facilitating preferential interaction with endothelial cells of tumor neovasculature. Significant reduction in tumor volume and alteration in apoptosis and angiogenic markers were attributed to enhanced delivery of GA to tumor tissues due to long circulation and positive surface charge of liposomes. Similar to TNBC, GA-loaded cationic PEGylated liposome could be useful in the treatment of other solid tumor with extensive angiogenesis.

Declaration of interest

This research was supported with funding from the National Institutes of Health's Minority Biomedical Research Support (MBRS)-SC1 program [Grant # SC1 GM092779-01]; the National Institute on Minority Health and Health Disparities (NIMHD) P20 program [Grant # 1P20 MD006738-03] and the Department of Defense (DOD) Breast Cancer Program [Grant # W81XWH-11-1-0211].

References

Adlakha-Hutcheon G, Bally MB, Shew CR, Madden TD. (1999). Controlled destabilization of a liposomal drug delivery system enhances mitoxantrone antitumor activity. Nat Biotechnol 17:775–9.

André F, Zielinski CC. (2012). Optimal strategies for the treatment of metastatic triple-negative breast cancer with currently approved agents. Ann Oncol 23:vi46–51.

Andreopoulou E, Schweber SJ, Sparano JA, McDaid HM. (2015). Therapies for triple negative breast cancer. Expert Opin Pharmacother 16:983–98.

Bonotto M, Gerratana L, Poletto E, et al. (2014). Measures of outcome in metastatic breast cancer: insights from a real-world scenario. Oncologist 19:608–15.

Cai L, Qiu N, Xiang M, et al. (2014). Improving aqueous solubility and antitumor effects by nanosized gambogic acid-$mPEG_{2000}$ micelles. Int J Nanomedicine 9:243–55.

Chang HI, Yeh MK. (2012). Clinical development of liposome-based drugs: formulation, characterization, and therapeutic efficacy. Int J Nanomedicine 7:49–60.

Deshpande PP, Biswas S, Torchilin VP. (2013). Current trends in the use of liposomes for tumor targeting. Nanomedicine (Lond) 8:1509–28.

Doddapaneni R, Chawla YK, Das A, et al. (2013). Overexpression of microRNA-122 enhances *in vitro* hepatic differentiation of fetal liver-derived stem/progenitor cells. J Cell Biochem 114:1575–83.

Godugu C, Patel AR, Doddapaneni R, et al. (2014). Approaches to improve the oral bioavailability and effects of novel anticancer drugs berberine and betulinic acid. PLoS One 9:e89919.

Gu H, Rao S, Zhao J, et al. (2009). Gambogic acid reduced bcl-2 expression via p53 in human breast MCF-7 cancer cells. J Cancer Res Clin Oncol 135:1777–82.

Immordino ML, Dosio F, Cattel L. (2006). Stealth liposomes: review of the basic science, rationale, and clinical applications, existing and potential. Int J Nanomedicine 1:297–315.

Li C, Lu N, Qi Q, et al. (2011). Gambogic acid inhibits tumor cell adhesion by suppressing integrin β1 and membrane lipid rafts-associated integrin signaling pathway. Biochem Pharmacol 82: 1873–83.

Li C, Qi Q, Lu N, et al. (2012). Gambogic acid promotes apoptosis and resistance to metastatic potential in MDA-MB-231 human breast carcinoma cells. Biochem Cell Biol 90:718–30.

Liu YT, Hao K, Liu XQ, Wang GJ. (2006). Metabolism and metabolic inhibition of gambogic acid in rat liver microsomes. Acta Pharmacol Sin 27:1253–8.

Lu N, Hui H, Yang H, et al. (2013). Gambogic acid inhibits angiogenesis through inhibiting PHD2-VHL-HIF-1α pathway. Eur J Pharm Sci 49: 220–6.

Lu N, Yang Y, You QD, et al. (2007). Gambogic acid inhibits angiogenesis through suppressing vascular endothelial growth factor-induced tyrosine phosphorylation of KDR/Flk-1. Cancer Lett 258:80–9.

Misso G, Di Martino MT, De Rosa G, et al. (2014). Mir-34: a new weapon against cancer? Mol Ther Nucleic Acids 3:e194. doi: 10.1038/mtna.2014.47.

Naithani R, Huma LC, Moriarty RM, et al. (2008). Comprehensive review of cancer chemopreventive agents evaluated in experimental carcinogenesis models and clinical trials. Curr Med Chem 15: 1044–71.

Palmer JR, Viscidi E, Troester MA, et al. (2014). Parity, lactation, and breast cancer subtypes in African American women: results from the AMBER Consortium. J Natl Cancer Inst 106:dju237. doi: 10.1093/jnci/dju237.

Patel K, Patil A, Mehta M, et al. (2013). Medium chain triglyceride (MCT) rich, paclitaxel loaded self nanoemulsifying preconcentrate (PSNP): a safe and efficacious alternative to Taxol. J Biomed Nanotechnol 9:1996–2006.

Patel K, Patil A, Mehta M, et al. (2014). Oral delivery of paclitaxel nanocrystal (PNC) with a dual Pgp-CYP3A4 inhibitor: preparation, characterization and antitumor activity. Int J Pharm 472:214–23.

Pereira WO, Amarante-Mendes GP. (2011). Apoptosis: a programme of cell death or cell disposal? Scand J Immunol 73:401–7.

Qi Q, Gu H, Yang Y, et al. (2008a). Involvement of matrix metalloproteinase 2 and 9 in gambogic acid induced suppression of MDA-MB-435 human breast carcinoma cell lung metastasis. J Mol Med (Berl) 86:1367–77.

Qi Q, You Q, Gu H, et al. (2008b). Studies on the toxicity of gambogic acid in rats. J Ethnopharmacol 117:433–8.

Sawant RR, Torchilin VP. (2012). Challenges in development of targeted liposomal therapeutics. AAPS J 14:303–15.

Saxena V, Hussain MD. (2012). Poloxamer 407/TPGS mixed micelles for delivery of gambogic acid to breast and multidrug-resistant cancer. Int J Nanomedicine 7:713–21.

Tao Z, Shi A, Lu C, et al. (2014). Breast cancer: epidemiology and etiology. Cell Biochem Biophys 72:333–8.

Vaseva AV, Moll UM. (2009). The mitochondrial p53 pathway. Biochim Biophys Acta 1787:414–20.

Wang X, Chen W. (2012). Gambogic acid is a novel anti-cancer agent that inhibits cell proliferation, angiogenesis and metastasis. Anticancer Agents Med Chem 12:994–1000.

Xing M, Yan F, Yu S, Shen P. (2015). Efficacy and cardiotoxicity of liposomal doxorubicin-based chemotherapy in advanced breast cancer: a meta-analysis of ten randomized controlled trials. PLoS One 10:e0133569. doi: 10.1371/journal.pone.0133569.

Xu J, Zhou M, Ouyang J, et al. (2013). Gambogic acid induces mitochondria-dependent apoptosis by modulation of Bcl-2 and Bax in mantle cell lymphoma JeKo-1 cells. Chin J Cancer Res 25:183–91.

Yao J, Li Y, Sun X, et al. (2014). Nanoparticle delivery and combination therapy of gambogic acid and all-trans retinoic acid. Int J Nanomedicine 9:3313–24.

Zhai D, Jin C, Shiau CW, et al. (2008). Gambogic acid is an antagonist of antiapoptotic Bcl-2 family proteins. Mol Cancer Ther 7:1639–46.

Zou ZY, Wei J, Li XL, et al. (2012). Enhancement of anticancer efficacy of chemotherapeutics by gambogic acid against gastric cancer cells. Cancer Biother Radiopharm 27:299–306.

Research Article

For reprint orders, please contact: reprints@futuremedicine.com

Nanomedicine

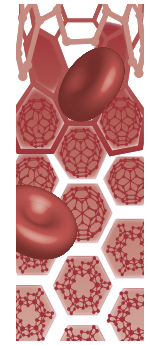

Tumor stromal disrupting agent enhances the anticancer efficacy of docetaxel loaded PEGylated liposomes in lung cancer

Ketan Patel[1], Ravi Doddapaneni[1], Nusrat Chowdhury[1], Cedar HA Boakye[1], Gautam Behl[1] & Mandip Singh*,[1]

[1]College of Pharmacy & Pharmaceutical Sciences, Florida A&M University, Tallahassee, FL 32307, USA

*Author for correspondence:
Tel.: + 850 561 2790
Fax: +1 850 599 3813
mandip.sachdeva@famu.edu

Aim: Therapeutic efficacy of anticancer nanomedicine is compromised by tumor stromal barriers. The present study deals with the development of docetaxel loaded PEGylated liposomes (DTXPL) and to investigate the effect of tumor stroma disrupting agent, telmisartan, on anticancer efficacy of DTXPL. **Methods:** DTXPL was prepared using proprietary modified hydration method. Effect of oral telmisartan treatment on tumor uptake of coumarin-6 liposomes and anticancer efficacy of DTXPL was evaluated in orthotopic xenograft lung tumor bearing mice. **Results:** DTXPL (105.7 ± 3.8 nm) showed very high physical stability, negligible hemolysis, 428% enhancement in bioavailability with significantly higher intratumoral uptake. Marked reduction in collagen-I, MMP2/9 and lung tumor weight were observed in DTXPL+telmisartan group. **Conclusion:** Combination of DTXPL with telmisartan could significantly enhance clinical outcome in lung cancer.

First draft submitted: 16 November 2015; Accepted for publication: 9 March 2016; Published online: 12 May 2016

Keywords: cancer nanomedicine • docetaxel • orthotopic lung cancer • pegylated liposome • solid tumor targeting • tumor fibrosis • tumor stroma

Lung cancer is by far the most common cause of cancer related mortality in both men and women. Non-small-cell lung cancer (NSCLC) accounts for 87% of total cases of lung cancer with overall 5-year survival rate less than 18.2% [1,2]. Depending on the stage of lung cancer and condition of patients, the chemotherapeutic regimen for lung cancer includes following drugs: Cisplatin/carboplatin or paclitaxel/docetaxel, etoposide, vinorelbine, erlotinib or other tyrosine kinase inhibitors, gemcitabine and pemetrexed. Despite recent advances in diagnosis and treatment, the clinical outcome amongst NSCLC patients is still not impressive. Docetaxel (DTX) is one the most widely used for drug for the treatment of various types of solid tumor including ovarian, breast, lung and head/neck cancers. Docetaxel has extremely poor water solubility and rapid precipitation tendency, which necessitates very high concentration of ethanol and surfactant for its intravenous injection. Tween 80 in Taxotere® formulation is responsible for severe life threatening hypersensitivity and peripheral neuropathy [3,4]. A safer formulation to enhance patient compliance and therapeutic efficacy of DTX is always in demand. As a result, current research is mainly focused on developing nanomedicinal formulation such as liposomes, polymeric micelles, albumin nanoparticles, polymer drug conjugates, etc. Liposomes are the most versatile nanocarrier with superior biocompatibility and large scale manufacturing feasibility compared to other types of nanocarrier. Abraxane®, Doxil®, Depocyt®, Myocet®, DaunoXome®, Marqibo®, etc. are commercially available anticancer nanoformulations for parenteral administration. It is noteworthy that all of them are liposomal formulations except Abraxane® [5].

Future Medicine part of fsg

In spite of enormous preclinical research on development of nanocarriers for taxanes and liposomal formulations for variety of drugs, there is no liposomal formulation of docetaxel available in the market. There are few research papers describing the parenteral delivery of DTX using PEGylated nanocarriers (PLGA, caprolactone or gold nanoparticle) and even fewer reports on docetaxel loaded PEGylated liposomes [6–9]. Surprisingly, none of the reports have demonstrated the physicochemical stability of DTX nanocarriers. Poor physical stability of DTX encapsulated liposomes is the major limiting factor for its clinical development. Usually, formulations developed for preclinical research purposes have stability sufficient enough to carry out animal studies but for clinical application, long term stability is indispensable. Therefore, an innovative liposomal preparation method is required to formulate DTX liposomes with an extended stability. PEGylated liposomes of DTX could potentially serve these purposes by improving the solubility of DTX without using ethanol or surfactant, enhancing the pharmacokinetic of DTX due to prolong plasma circulation and enhancing the anticancer efficacy because of enhanced permeation and retention (EPR) mediated higher intratumoral uptake.

Poor diffusion and penetration of drug into solid tumors owing to high interstitial pressure or tumor stromal barriers, is a serious issue limiting the efficacy of existing chemotherapeutic agents [10]. Leaky neovasculature, abnormal lymphatic system and perivascular fibrosis are associated with high interstitial fluid pressure. Matrix rigidity and fibroblast contractility in solid tumor result in increased fiber tension which leads to decreased convection and transcapillary transport of anticancer drugs to deep tumor regions. Therapeutic outcome of cancer chemotherapy has been significantly improved by use of nanocarriers due to their ability to delivery of anticancer drugs selectively to tumor tissues with limited accumulation in healthy tissues [5,10,11]. However, mere development of nanocarriers of chemotherapeutic drugs and reliance on EPR effect for its intratumoral uptake is not adequate to achieve desired anticancer effect. EPR mediated passive targeting and tumor surface antigen directed active targeting lead to higher accumulation of drug into tumor tissues [12]. However, irrespective of the surface characteristics and targeting nature of the nanocarriers, their distribution within solid tumor matrix is severely hindered by dense collagen network and very high interstitial tumor pressure due to highly fibrous interstitium in solid tumors. Collagen rich network embedded in hyaluronan of tumor stroma significantly impede the penetration of drug and nanoparticles into tumors. The extracellular matrix (ECM) creates both a physical and hydrodynamic barrier in the form of high intratumoral pressure which prevents most therapeutics and nanoparticles from reaching the tumor foci [11,13,14]. Thus, disruption of tumor ECM is very important for enhanced delivery of drug and nanoparticles in solid tumors. Recently, there is a huge interest in drug or enzyme reducing the collagen density in tumor, which has the collateral effect of decreasing tumor interstitial fluid pressure (TIFP) thereby facilitating higher drug/nanocarrier penetration. Few researchers have showed enhanced uptake of antibody, virus or nanocarriers in tumor tissues by disrupting stromal barrier using bacterial collagenase, relaxin or TGF-β1 inhibitors [15–17]. In our previous report, we have demonstrated that inhalable telmisartan reduced collagen level in lung tumors and enhanced uptake of fluorescent polystyrene nanoparticles. Telmisartan is an angiotensin receptor blocker used for the treatment of hypertension. In our earlier published work, we have studied that TGF-β1 inhibition was the primary mechanism for antifibrotic activity of inhalable telmisartan in lung tumors [13].

In this paper, a modified hydration method was proposed to produce a stable DTX loaded PEGylated liposomes (DTXPLs) and compared with conventional liposomes. Thereafter, the effect of oral telmisartan treatment on tumor stromal disruption, uptake of liposomes in tumors and anticancer efficacy of DTXPLs in orthotropic lung tumor bearing athymic nude mice was evaluated.

Experimental

Chemicals & drugs

Docetaxel was purchased from AK scientific (CA, USA). Phospholipids were purchased from Lipoid (Germany). All other chemicals and HPLC solvents were purchased from Sigma-Aldrich (MO, USA). DMEM-F12K medium, fetal bovine serum and other cell culture materials were purchased from Lonza (Basel, Switzerland). Primary antibodies were purchased from cell signaling technology (USA).

HPLC analysis

Reverse phase HPLC-UV method was used to analyze DTX for stability, release and pharmacokinetic studies. Chromatographic separation was achieved on Waters 717 instrument equipped with waters symmetry (250 mm/4.6 mm/5 µm) column using ACN:Phosphate buffer pH 3 (55:45) as mobile phase with flow rate of 0.55 ml/min, detected at 227 nm. Plasma DTX analysis was achieved at same chromatographic conditions. Retention time of DTX was 13.9 ± 0.15 min. Salting-out Liquid-Liquid Extraction (SALLE) method was used to extract DTX from plasma. For DTX extrac-

tion, 250 µl Acetonitrile was added to 150 µl plasma samples followed addition of 100 mg NaCl to separate acetonitrile and plasma layer. Samples were vigorously stirred and centrifuged at 5000 rpm for 10 min at 10°C. Supernatant was mixed with 50 µl of Milli-Q water. Samples were directly loaded to HPLC auto-sampler for analysis.

Animals

Sprague–Dawley rats were purchased from Harlan Inc. (Indianapolis, IN). The rats were housed and maintained in specific pathogen-free conditions in a facility approved by the American Association for Accreditation of Laboratory Animal Care (AALAC). Food and water were provided ad libitum to the animals in standard cages. Animals were maintained at standard conditions of 37°C and 60% humidity. All experiments were done in accordance with the guidelines of the Institutional Animal Care and Use Committee (IACUC) at Florida A&M University.

Female, 6-week old, athymic Nu/nu mice were purchased from Harlan Inc. (IN, USA). The mice were housed and maintained in specific pathogen-free conditions in a facility approved by the American Association for Accreditation of Laboratory Animal Care. Food and water were provided ad libitum to the animals in standard cages. Animals were maintained at standard conditions of 37°C and 60% humidity. All experiments were done in accordance with the guidelines of the Institutional Animal Care and Use Committee (IACUC) at Florida A&M University. Animals were acclimatized for 1 week prior to the tumor studies.

Preparation of liposomes

Liposomes were prepared using modified hydration method. Briefly, phospholipids, cholesterol, PEGylated phospholipid and DTX were dissolved in chloroform. The solution was drop wise added to mannitol at 45°C with constant stirring and left overnight for evaporation of chloroform. Resultant powder was dispersed into water and sonicated for 4 min using probe sonicator (Branson Probe Sonicator, USA). Molar ratio of DTX to phospholipids and processing parameters were optimized on the basis of physical stability. Taxotere was prepared using same formula as marketed docetaxel formulation – Taxotere® (Sanofi-Aventis, USA). For ethanol injection method, phospholipids and DTX were dissolved in absolute ethanol and injected into water at 55°C [18]. Batches of thin film hydration method were prepared by vacuum evaporating chloroform solution containing phospholipids and DTX in round bottom flask followed by hydration with water at 55°C.

Particle size, zeta potential & entrapment efficiency

Hydrodynamic diameter of formulation was analyzed by dynamic light scattering (DLS) using Nicomp PSS particle size analyzer (PSS Systems, USA). Formulation was diluted into HPLC grade water to achieve concentration of 0.1 mg/ml of DTX. Entrapment efficiency was analyzed using gel permeation chromatography using Sephadex G50 column (Sigma Aldrich, USA).

Scanning electron microscopy (SEM) analysis

The SEM pictures of liposomes were taken on a FEI Nova NanoSEM 400 machine fitted with a tungsten (W) filament. The air dried liposomes samples were mounted on a metal stub using double sided carbon tape followed by coating with 8 nm thick layer of iridium (Ir) by sputter coating for 30 min. Finally the pictures were taken at an accelerating voltage of 5 kV and observed using 3 µm scale bars.

In vitro release

DTX release from taxotere and liposomes was evaluated by a dialysis bag method using phosphate buffer pH 7.4 with 0.2% w/v tween 80 as release medium. The dialysis bag (MWCO 50 kD, Spectrum Lab, USA) filled with 1 ml of DTX formulation was tied to the paddle of USP dissolution apparatus I (50 rpm, 37°C). Samples were withdrawn at 0.5, 1, 2, 4, 8, 12 and 24 h and DTX content was analyzed by HPLC.

In vitro hemolysis study

In vitro hemolysis study was carried out using human red blood cells (RBCs) as per the procedure reported earlier [19]. Briefly, blood cells were separated from plasma by centrifugation at 5000 rpm for 10 min followed by discarding the supernatant and resuspending cell pellet into equivalent ml of HBSS to achieve the same hematocrit. Taxotere and DTXPL were dispersed in HBSS to prepare 0.5 mg/ml solution of DTX. Appropriate quantity of this stock solution was added to 1 ml of RBC dispersion to achieve 50, 25 and 10 µg/ml DTX concentrations. The samples were incubated for 30 min at 37°C and centrifuged at 5000 rpm for 10 min and the supernatants were subjected to analysis. Hemoglobin release was determined by UV spectrophotometer at 550 nm. HBSS was used as the negative control and sodium dodecyl sulphate solution was used as positive control (100% hemoglobin release). % hemolysis was calculated by following formula:

% hemolysis = (absorbance of test sample – absorbance of negative control)/(absorbance of positive control – absorbance of negative control) × 100

Plasma-to-blood ratio

Plasma-to-blood ratio (PBR) of taxotere and DTXPL were analyzed in human blood [19]. Taxotere and DTXPL were diluted with phosphate buffer to prepare DTX concentrations of 250 µg/ml each. 20 µl of this solution was added to 980 µl of human blood to prepare final concentration of 5 µg/ml of DTX in blood (n = 6). After a 30 min incubation period at 37°C, three samples from each set were centrifuged (5000 rpm, 10 min) while other three samples were frozen at -80°C for complete hemolysis. Plasma was separated from centrifuged samples. DTX concentration in plasma and hemolysed blood was calculated by HPLC method.

In vivo pharmacokinetic in rats

In vivo pharmacokinetic study of taxotere and DTXPL was performed in Sprague–Dawley rats. After 1 week of acclimatization, animals were divided into two groups – six animals in each group. Taxotere and DTXPL were diluted with saline and 5 mg/kg DTX dose was administered via tail vein. Blood samples were collected via tail vein at 0.066, 0.5, 1, 2, 4 and 8 h post dosing. Blood samples were centrifuged at 10,000 rpm at 4°C for 10 min to separate plasma. DTX plasma concentration data after intravenous administration was analyzed by Kinetica 5® (Thermofisher, USA).

Inoculation of A549 in mice

A549 cells were grown in DMEM-F12K Media containing 10% FBS and standard antibiotic mix at 5 % CO_2 and 37°C. For orthotopic lung tumor model, mice were anesthetized with isoflurane and a 5 mm skin incision was made to the left chest, 5 mm below the scapula. Hamilton syringe with 28-gauge hypodermic needles was used to inject A549 cells through the sixth intercostal space into the left lung. The needle was quickly advanced to a depth of 3 mm and removed after the injection of the cells (2 million per mouse) suspended in 100 µL PBS (pH 7.4) into the lung parenchyma. Wounds from the incisions were closed with surgical skin clips. Animals were observed for 45 to 60 min until fully recovered. The animals develop lung tumor within 14 days after the cell inoculation [2,20,21].

Antitumor study

After 14 days, animals were randomly divided into four groups (Saline solution, Taxotere, DTXPL and DTXPL + telmisartan) of 12 animals each. Telmisartan treatment was started on 15th day of cell inoculation while DTX treatment was started from 17th day. Dose of DTX (intravenous) and telmisartan (oral) was 5 mg/kg body weight. Six doses of DTX formulations were given biweekly for 3 weeks. Two doses of telmisartan were given at 24 h and 48 h before each DTX dose. Six animals from each group were sacrificed (carbon dioxide inhalation), 3 days after the last dose of DTX formulation. Lungs were collected, weighted and observed for lung tumor growth using a stereomicroscope (Olympus, USA). The same tumors were used for immunohistochemistry (IHC) and western blot analysis. Study was continued till 45 days with remaining animals to observe the survival rates over the period of time.

Coumarin-6 liposome uptake in lung tumor

After 21 days of A549 inoculation, animals were divided into two groups: control and telmisartan. Control group received saline solution and telmisartan group received two doses of telmisartan (5 mg/kg, once a day) by oral route. On 24th day, both the group received coumarin-6 liposomes (1 mg/kg) via tail vein injection. Animals were sacrificed (carbon dioxide inhalation) after 1 h and lungs were collected. Cryosection (40 µm thickness) of part of lung bearing tumor nodules was carried out and immediately observed under fluorescence microscope. Intensity of green color as a measurement of coumarin-6 uptake in normal lung and tumor tissue was carried out using ImageJ software. The tumor sections were also stained with picrosirius red (Abcam, USA) to evaluate the collagen density.

Western blot analysis

Protein samples for western blot analysis were extracted from lung tumor tissues using RIPA lysis buffer containing protease inhibitors and 500 mM phenyl methyl sulfonyl fluoride (PMSF). Protein concentration was estimated using BCA protein assay reagent kit. Equal amounts (50 µg) of protein from different groups were denatured by heating for 5 min in SDS sample buffer and separated using 10% SDS-PAGE. The protein samples separated on SDS-PAGE were transferred to nitrocellulose membranes for immunoblotting. After blocking, the membranes with skim milk (5% skim milk in 10 mM Tris-HCl (pH 7.6), 150 mM NaCl, and 0.5% Tween 20) probed with primary antibodies. The primary antibodies such as survivin, MMP-2, MMP-9 and β-actin were used in 1:1000 dilutions. HRP-conjugated secondary antibodies were used. The detail procedure for western blotting was followed according to our published methods.

Immunohistochemistry of CD31 expression

Paraffin-embedded tumor tissues were deparaffinized and blocked for peroxidase activity for CD31 expression. The specimens were washed with PBS twice and then incubated in normal goat serum according to the

manufacturer's instructions (Santa Cruz Biotechnology, CA, USA). Subsequently, the sections were incubated with CD31 antibody, at 4°C overnight, followed by a 30 min treatment with HRP secondary antibody (Santa Cruz Biotechnology). After three washes with PBS, the sections were developed with diaminobenzidene-hydrogen peroxidase substrate and images were taken microscopically. The number of CD31 positive endothelial cells and/or the number of blood vessels were counted in four different high power fields per section (400×). The average number of microvessels per high power field was examined as described earlier [22].

Statistics

All data are presented as the mean ± standard deviation (SD). The significance of difference in treatment groups was determined using Student's *t*-test or one-way ANOVA using GraphPad prism version 5.0 (CA, USA), where value of $p < 0.05$ between the groups was considered as statistically significant difference between these groups.

Results

Formulation development & characterization

Physical instability within short period of time and poor drug loading are the two major issues in developing formulation of DTX. Therefore, our focus was to develop a novel formulation with high DTX loading and long term physical stability. Results of liposomal DTX batches prepared using various methods are given in Table 1. Initially, methods of liposome preparation were compared and optimized on the basis of physical stability. Ethanol injection and thin film hydration are most widely used and industry accepted methods of manufacturing liposomes for various preclinical and clinical studies. As shown in Table 1, DTX-loaded liposomes prepared using ethanol injection showed very rapid precipitation of DTX while thin film hydration showed marginally better stability depending on type of phospholipids used.

Unsaturated phospholipid (DOPC) showed fivefold higher stability compared with the liposomes prepared using saturated lipid (DPPC). However, particle size of liposomes prepared using both the lipids were nearly similar. Liposomes prepared using DOPC gave particle size of 132.6 ± 12.7 nm while DPPC gave slightly lower size of 114.2 ± 8.5 nm. DTXPL prepared using modified hydration method showed significantly higher stability compared with conventional methods like ethanol injection and thin film hydration. Initially, on dispersion into water, 20–30 µm sized multilamellar liposomes were formed. Ultrasonication has significantly reduced the liposome size in the range of 100 nm. Effect of cholesterol, mannitol, and type of phospholipids, hydration temperature, DTX loading and DTX concentration on physical stability of DTXPL was analyzed to optimize the formulation.

Amount of cholesterol has critical role in DTX precipitation. Batch prepared using DOPC and 3 mole percent DTX with 15 mole percent of cholesterol showed maximum stability for 3–4 days as shown in Table 1. Batches with same composition prepared using higher or 0% cholesterol content showed lesser stability. Cholesterol content above 40 mole percent of the batch showed rapid precipitation within 2–3 h. Thus, further batches were prepared using 15 mole percent of cholesterol, in other words, DTX:cholesterol weight ratio around 1:3 was optimized. We have observed that approximately 100 nm sized DTX liposomes formed after sonication step were stable for longer period of time when passed through sephadex G50 column. Extraliposomal mannitol was adversely affecting the physical stability of liposomes. Mannitol free batches showed stability for 3–4 days while unprocessed batches were found to be stable for 2 days only. Physical stability data mentioned in Table 1 represent the results of various batches after mannitol separation. Batches prepared with saturated phospholipids like DSPC and DPPC become unstable within 2–4 h, while batches prepared with DOPC (unsaturated phospholipid) were much more stable. Hydration temperature of proliposomal powder composed of phospholipid, DTX, cholesterol and mannitol was playing crucial role. Batches hydrated with water at 10 and 25°C showed nearly similar stability for up to 2–3 days while the batches hydrated at 45°C showed higher physical stability for 4 days.

DTX loading was found to be the most critical parameter affecting the stability. Drastic reduction in stability was observed with small increment in DTX loading from 3 to 5 mole percent as shown in Table 1. All the batches described in Table 1 have final DTX concentration of 1 mg/ml. Batches with higher DTX concentration 1.5 and 2 mg/ml with same DTX mole percent loading showed inferior stability compared with 1 mg/ml batches. The effect of final DTX concentration on physical stability was less significant compared with DTX loading. Various excipients – solubilizer, surfactant, salt and albumin were added in DTXPL to investigate the effect of those excipients on stability. List of excipients and concentration are described in Table 1. Surprisingly, all the excipients were found to be adversely affecting the stability, in other words, facilitating the DTX precipitation rate instead of slowing it down. Therefore, an alternative strategy was explored to enhance the stability of parent DTXPL. Blank liposomes (BL) of DOPC and DSPC were prepared using ethanol injection method. Appro-

Table 1. Composition and results of DTXPL batches prepared using different methods.

Method	DTX loading (mole percent)	Phospholipid	Excipient added after DTXPL preparation	Physical stability at room temperature
Ethanol injection	3	DOPC	–	Immediate precipitation
Ethanol injection	3	DPPC	–	Immediate precipitation
Thin film hydration	3	DOPC	–	Stable for 10–12 h
Thin film hydration	3	DPPC	–	Stable for 2–3 h
Modified hydration	3	DPPC	–	Immediate precipitation
Modified hydration	3	POPC	–	Stable for 12 h
Modified hydration	3	DOPC	–	Stable for 4 days
Modified hydration	4	DOPC	–	Precipitated within 24 h
Modified hydration	5	DOPC	–	Precipitated within 4 h
Modified hydration	3	DOPC	TPGS (0.5% w/v) Sodium Citrate (0.5% w/v) Hydroxy propyl β cyclodextrin (0.2% w/v) PEG 400 (1% w/v) Tween 80 (0.5% w/v) Albumin (1% w/v)	Reduced the stability of parent liposomes. Formed large agglomerates of DTX
Modified hydration	3	DOPC	Blank liposomes of DOPC	Stable for 2 weeks 7–8-fold enhancement in stability
Modified hydration	3	DOPC	Blank liposomes of DSPC	Stable for 6–7 days twofold enhancement in stability

priate amount of BL was added to DTXPL containing 3.5 mole percent DTX at 1.2 mg/ml DTX concentration to achieve final loading of 3 mole percent DTX at 1 mg/ml DTX concentration. Addition of DSPC-BL led to twofold enhancement in stability while addition of DOPC-BL resulted in 7–8-fold higher stability at room temperature. Particle size and entrapment efficiency was not significantly affected by drug loading and drug concentration. We observed that physical stability was roughly 8- to 10-times higher at 2–8°C than room temperature for all the batches. Finally, optimized formulation was composed of mixture of DTXPL+DOPC-BL with DTX loading of 3 and 1 mg/ml DTX concentration. It was found to be physically and chemically stable for 2 months at 2–8°C. The average particle size and zeta potential of finally optimized batch was 105.7 ± 3.8 nm and -12.4 mv, respectively. Entrapment efficiency was found to be 97.4%, which confirmed that DTX was confined to liposomal bilayers.

The SEM analysis of the liposomes revealed almost spherical morphology and the structures observed were in agreement with SEM images of liposomal formulation reported earlier [23]. Interestingly, SEM image of the liposomes prepared with thin film hydration methods showed large crystals (Figure 1B) of DTX while no such crystals were observed in SEM images of liposomes prepared using modified hydration method (Figure 1A).

In vitro release

Sustained release of DTX was one of the desired parameters. As shown in Figure 2, taxotere showed complete release of DTX within first 2 h whereas DTXPL showed sustained release of DTX over the period of 48 h. Release of DTX from taxotere was following first order release kinetic while DTXPL exhibited 0 order release profile. DTXPL showed mere 40% DTX release in 48 h. However, complete release is expected *in vivo* due to degradation of liposomes in extracellular and intracellular milieu *in vivo*.

In vitro hemolysis study and PBR

Effect of DTXPL formulation on Human RBC was evaluated by incubating various concentration of formulation with RBC suspension. Both hemolysis and redispersion of RBC were evaluated and compared with taxotere. As shown in Figure 3A, negligible hemolysis was observed even at highest concentration of DTX. Further, very quick and complete redispersion of

RBC suggested that DTXPL did not alter the surface characteristics of RBC (Figure 3B & D). Contrary, taxotere formulation showed 22.7% hemolysis at 25 µg/ml DTX concentration and more importantly redispersion of RBC was very poor on inversion (Figure 3C). Taxotere showed PBR of 1.09 ± 0.08 while DTXPL showed higher PBR of 1.42 ± 0.12. It has indicated that liposomes were intact and DTX was preferentially confined to liposomal bilayer instead of partitioning into RBC.

Pharmacokinetic study

The plasma concentration profiles and pharmacokinetic parameters of DTX after intravenous injection of taxotere and DTXPL are depicted in Figure 4 and Table 2, respectively. As expected, there was a significant difference in pharmacokinetic profile of DTX. Noncompartment, one compartment and two compartment analysis of pharmacokinetic profile was carried out to understand the distribution and elimination pattern of liposomal DTX versus taxotere. Noncompartment analysis showed that the MRT of taxotere (1.99 h) was much low when compared with the DTXPL (8.08 h). DTXPL showed very low clearances rate of 0.35 (mg)/(µg/ml)/h when compared with taxotere, 1.63 (mg)/(µg/ml)/h. Liposomal formulation showed higher C_{max} and AUC compared with taxotere which is a micellar formulation of DTX. Importantly, DTXPL showed 428% enhancement in bioavailability of DTX compared with taxotere. Long circulation and extended release of DTX from liposomes have collectively contributed to higher AUC. In one compartment analysis of the plasma concentration vs time data, the drug loaded liposome cleared faster from plasma than the taxotere, which suggested that the liposomes are getting distributed toward the more perfused organs. MRT of DTX was lower for DTXPL (0.35 h) compared with taxotere (0.53 h). The two compartment analysis demonstrated that the DTXPL were quickly removed from the circulating system (Cl = 0.33 (mg)/(µg/ml)/h) with rapid distribution ($t_{1/2\ alpha}$ = 0.044 h) and slow terminal elimination phase ($t_{1/2\ beta}$ = 7.83 h) compared with taxotere ($t_{1/2\ alpha}$ = 0.35 h and $t_{1/2\ beta}$ = 3.27 h).

Uptake of coumarin-6 PEGylated liposomes in lung tumor

Coumarin-6 PEGylated liposomes were injected to observe their distribution in normal lung vs tumor tissue. Cryosection of lungs of control and telmisartan treated animals are shown in Figure 5A. Intensity of green fluorescence in normal lung tissue is nearly equal in both the groups but it was significantly higher in tumor in telmisartan treated group. Further, green fluorescence intensity of normal lung part and tumor part calculated using ImageJ software has clearly suggested the enhanced uptake of coumarin-6 in telmisartan treated group (Figure 5B).

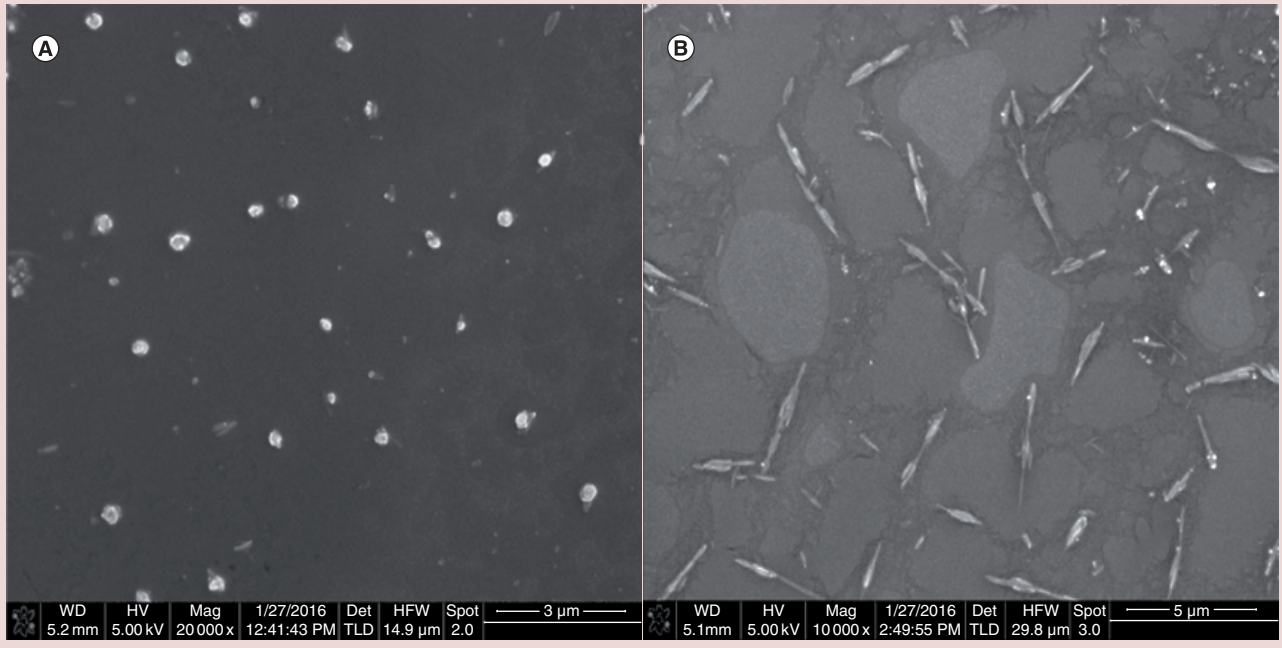

Figure 1. Scanning electron microscopy analysis of DTX-loaded liposomes prepared using modified hydration method (A) and thin film hydration method (B).

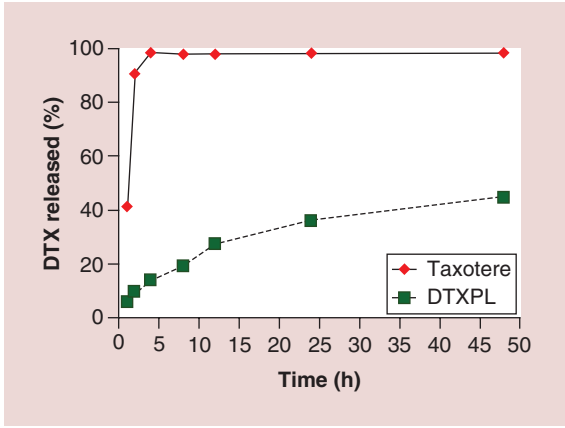

Figure 2. *In vitro* release of DTX from taxotere and DTXPL. Release study was carried out in USP apparatus II using dialysis bag (MWCO 50 kD) in phosphate buffer pH 7.4 with 0.2% w/v tween 80 at 37°C.

Anticancer study in orthotopic lung tumor bearing athymic nude mice

Picrosirius red stained of lung sections of control and telmisartan treated animals are shown in Figure 6A. Control showed bright red collagen fibers while reduced amount of red fibers were observed in telmisartan treated group. As shown in Figure 6B, lungs were completely covered with tumor growth in control group while partially covered in taxotere and DTXPL treated group. Interestingly, significant inhibition of tumor growth was observed in DTXPL + telmisartan group. The same results were reflected in lung tumor weight analysis (Figure 6C). There was no statistically significant difference observed in the tumor growth and lung tumor weight between taxotere and DTXPL treated animals. Results of taxotere and DTXPL were very surprising because both the group showed marginal improvement and nearly similar anticancer efficacy despite of significantly different in their pharmacokinetic profile. Oral telmisartan did not show any inhibition of lung tumor growth (data not shown). Interestingly, lung tumor weight of DTXPL in oral telmisartan pretreated group was 14 and 10.87-fold lower than control and only DTXPL treated group, respectively. Moreover, lung integrity was mostly intact and regular in DTXPL+telmisartan treated animals. Results of survival study were in complete agreement with tumor inhibition data (Figure 6D). DTXPL+Telmisartan group showed 80% survival at the end of 45 days, while other groups showed less than 50% survival at the same time. All the animals in control group showed complete mortality within 40 days.

CD31 immunostaining confirmed the significantly lower microvessel density in combination group compared with DTXPL alone group (Figure 7A). Western blot analysis further confirmed the superior anticancer and antifibrotic effects of DTX+Telmisartan liposome compared with DTX alone. Immuno blot analysis for survivin expression suggested that the antiapoptotic marker survivin was decreased in DTXPL+telmisartan group (Figure 7B). Quantitative analysis of western blot images suggested that in DTXPL and DTXPL+telmisartan groups showed 0.91- and 2.10-fold reduction of survivin expression compared with untreated control tumors. Significant ($p < 0.01$) down regulation of MMP9 and MMP2 expression was observed in DTXPL+telmisartan treated tumors (Figure 7C & D).

Discussion

This is the first report demonstrating the improved delivery of DTX liposomes to lung tumors by using oral telmisartan as an antifibrotic agent. Development of long circulating DTX liposomes with extended stability profile is very challenging task. DTXPLs were

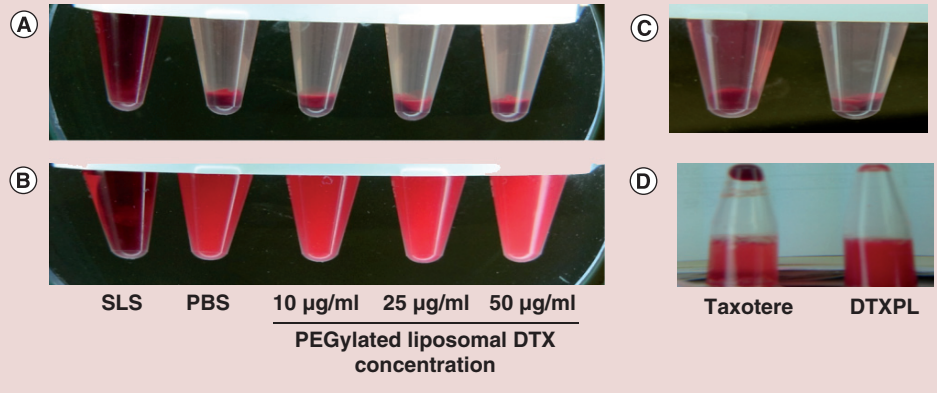

Figure 3. *In vitro* hemolysis study of DTXPL at various DTX concentrations was carried out on human RBC. DTXPL showed no hemolysis **(A)** and no aggregation on redispersion **(B)** even at very highest concentration of DTX. Taxotere showed hemolysis **(C)** and aggregation of RBC **(D)** at 25 µg/ml DTX concentration.

successfully prepared using an innovative modified hydration method developed in our laboratory. The physical stability of DTXPLs was successively increased by exploring various strategies with simultaneously understanding their role in modulating the stability of liposomes. There is no previous report investigating the pharmacodynamics profile of PEGylated liposomal DTX against orthotopic lung tumor bearing athymic nude mice. Second, collagen rich tumor stroma poses a significant hurdle in efficient delivery of nanocarrier to the majority of the tumors. Only long plasma circulation is not enough to deliver the drug to deeper layers of lung tumor. Therefore, in present study, telmisartan was used as an oral antifibrotic agent to disrupt the tumor stroma to enhance the permeation of DTXPLs.

Ethanol injection and thin film hydration are widely adopted methods reported in literature. However, DTX liposomal batches prepared by both the methods showed very poor physical stability. Both the drugs of taxane class, paclitaxel and docetaxel are very difficult to solubilize and stabilize in aqueous system [3,24]. DTX is quite a bulky molecule compared with the head-chain structure of phospholipids. The insertion of DTX into the bilayer would take more space and push the phospholipid molecule to be closer to each other. However, intermolecular force between lipids would try to resist the insertion of DTX. This intermolecular force rises with more DTX incorporated into the lipid bilayer. Feng *et al.* have performed studies on interaction of paclitaxel (DTX is a semisynthetic derivative of paclitaxel) with phospholipids and reported that paclitaxel is miscible with the lipid but there is a repulsive interaction between them. Our results with DTXPL are in agreement with their hypothesis [25].

Noteworthy, novel modified hydration method developed in our lab is very suitable to entrap such molecules with very poor dynamic and kinetic solubility, for example, paclitaxel, docetaxel. In modified hydration method, the lipid film is prepared over mannitol and the duration of hydration step is much shorter (1 min) compared with thin film hydration method (45 min). However, separation of soluble carrier, mannitol, is an additional step required in modified hydration method. We can hypothesize that distribution of DTX in inner

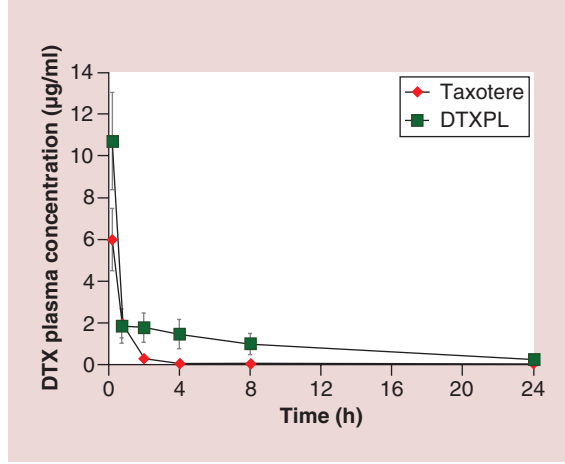

Figure 4. Pharmacokinetic profile of taxotere and DTXPL in SD rats (n = 6). DTXPL showed higher plasma concentration of DTX at all the time points.

leaflet of liposome bilayer could be higher when prepared using modified hydration method compared with thin film hydration method. Bilayer packing and membrane curvature of small unilamellar vesicles (SUVs) result in a large area and low density of the outer layer while the inner layer has increased packing density [26]. Inner layer is less hydrated/polar compared with outer layer and therefore drug entrapped within outer layer is transferred to aqueous layer much faster than drug entrapped within the inner layer [26,27]. High amount of mannitol or resultant osmotic pressure might be responsible for inner layer favored distribution of DTX during hydration step. However, presence of high amount of mannitol in external phase led to enhance precipitation rate and therefore mannitol was immediately removed after sonication step. Liposomes prepared using DOPC showed better stability compared with DPPC. DOPC forms less ordered bilayer with high cross sectional area due to presence of double bond which might help in encapsulating DTX for longer period of time. Also, possibility of interdigitation-mediated drug precipitation is negligible with DOPC compared with DPPC [28].

Though, modified hydration method produced DTX liposome with improved stability compared with conventional methods, the stability was not sufficient enough for clinical purpose. The main reason behind

Table 2. Pharmacokinetic parameters.

	Taxotere	Liposomes
C_{max} (µg/ml)	6.1 ± 1.7	10.68 ± 2.9
AUC (µg.h/ml)	5.29 ± 1.1	22.65 ± 4.3
$T_{1/2}$ (h)	6.67 ± 1.6	7.39 ± 1.8
MRT	1.99 ± 0.36	8.08 ± 2.5
Relative BA	–	428%

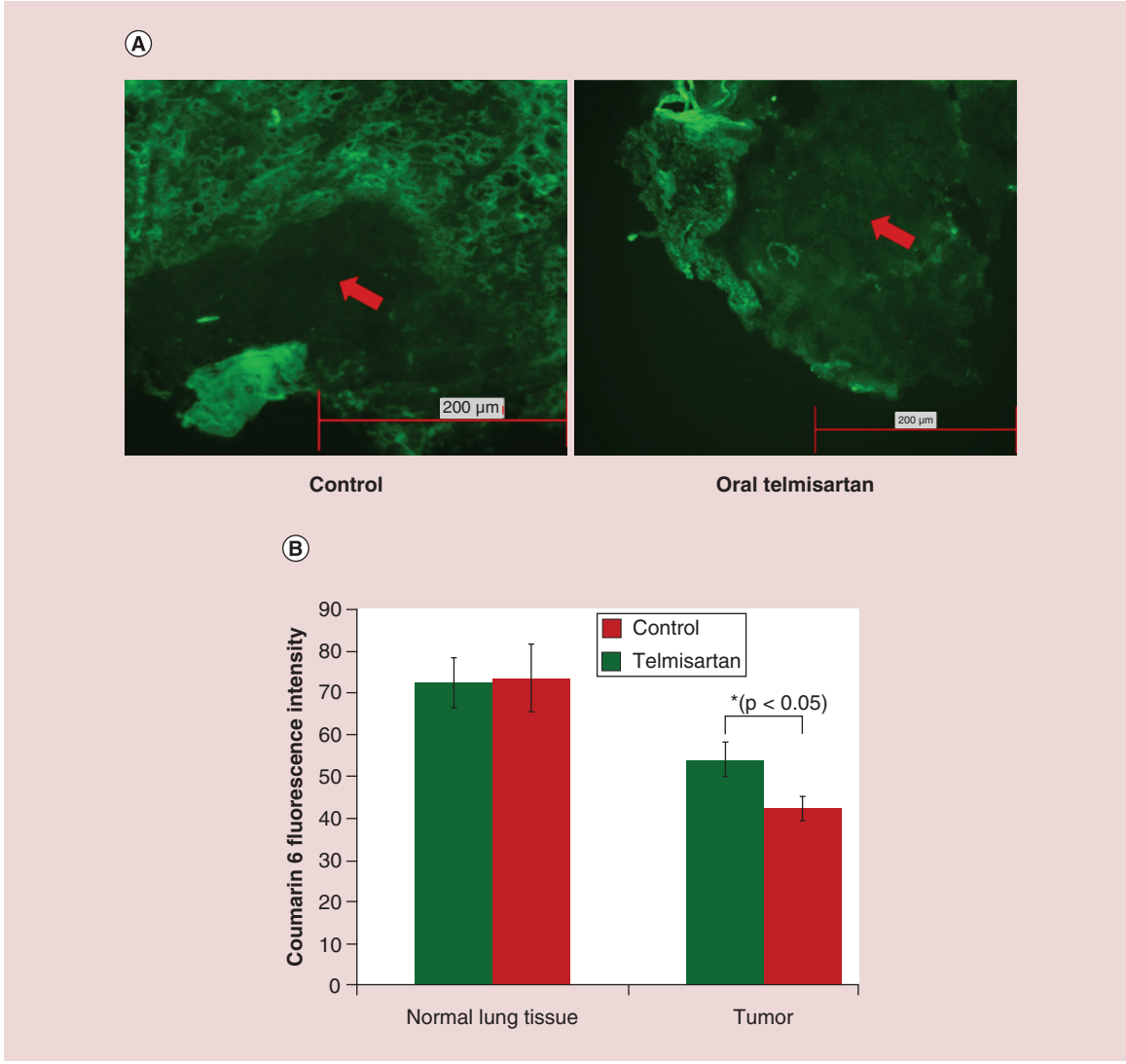

Figure 5. Distribution of coumarin-6 liposomes in tumor bearing lung. (A) Fluorescence images of lung sections of control and telmisartan treated animals. Red arrow indicates the tumor region. **(B)** Green fluorescence intensity in normal and cancerous lung was calculated and expressed as mean ± SD. p-values were calculated using *t*-test and $p < 0.05$ considered as significant. Normal lung tissue showed similar fluorescence but telmisartan treated group showed higher fluorescence in tumor region as shown in graph.

destabilization is the transfer of DTX from liposomal bilayer to aqueous phase, where it leads to aggregation and precipitation of DTX at very rapid rate. We have hypothesized that addition of various solubilizer, surfactant or albumin may reduce the amount of free DTX in aqueous phase and attenuate the precipitation process but results were completely opposite to our hypothesis. Presence of these excipients in the external phase of DTXPL, resulted in more hydrophilic and hydroxyl group rich environment. Thus, additions of hydrophilic excipients were found to adversely affect the stability by promoting the transfer in aqueous phase followed by rapid precipitation. DTX can be transferred to other liposomes by collision between the liposomes or by passive diffusion through aqueous phase [29,30]. Based on this, we hypothesized that addition of blank liposomes might be helpful in inhibiting DTX precipitation. There was a remarkable enhancement in stability of DTXPL was observed after addition of blank liposomes of DOPC or DSPC. Blank DOPC liposomes showed even better stability profile compared with DSPC blank liposomes. Difference in membrane fluidity and permeability due to difference in phase transition temperature (DOPC: -17°C; DSPC: 55°C) of both the lipids could be the main reason for this behavior [26]. Blank liposomes proved to be the most appropriate reservoir system to maintain sink conditions, irrespective of DTX transfer mecha-

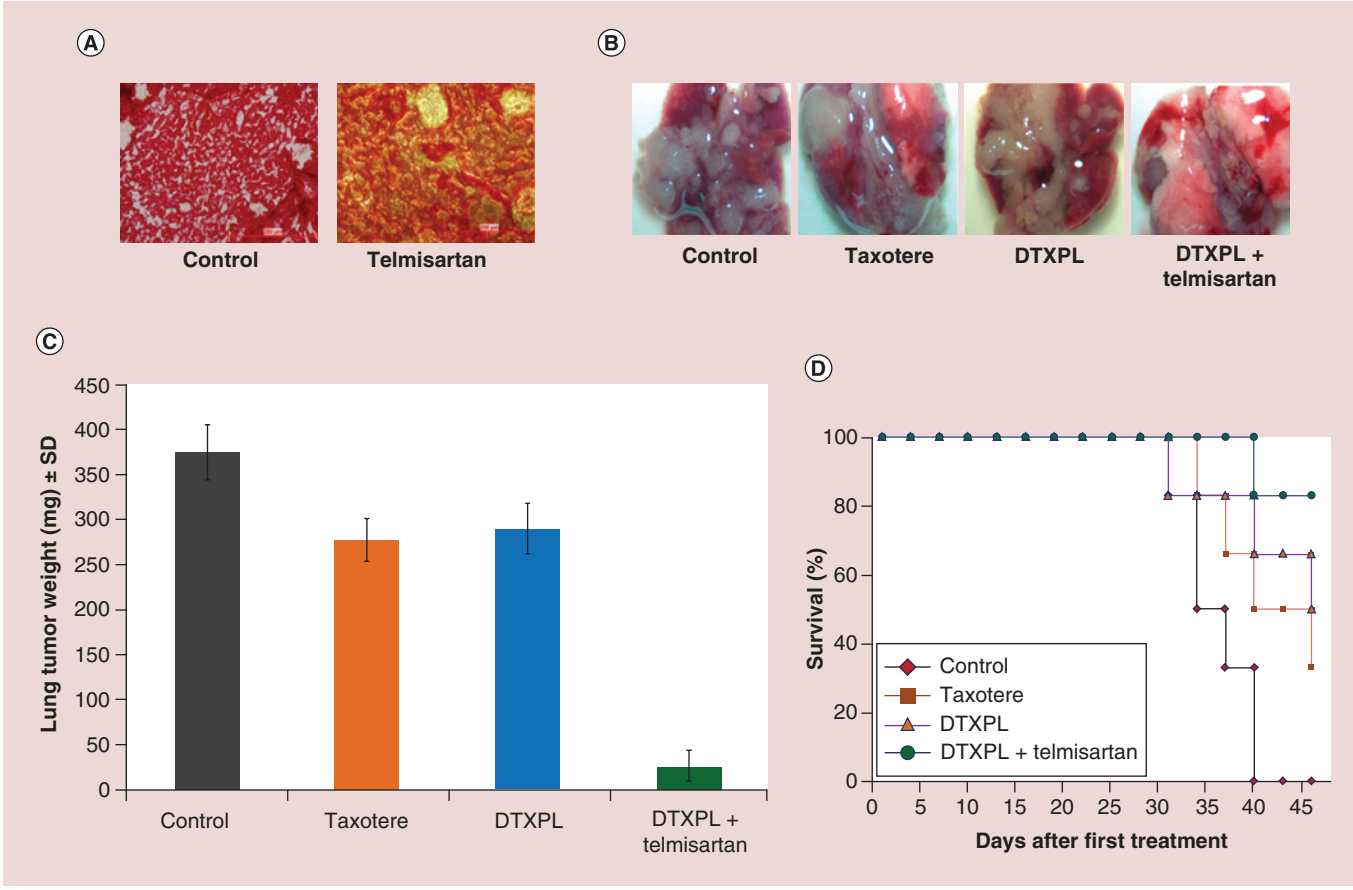

Figure 6. *In vivo* studies in A549 orthotopic lung tumor bearing nude mice. (A) Picrosirius red staining of lung tumor of control and telmisartan treated animals. Telmisartan treated animals showed significant reduction in collagen I fibers. **(B)** Orthotopic growth of untreated and treated xenografts. Lungs were collected 3 days after the last dose of DTX formulation. Lung integrity was severely compromised in untreated group. **(C)** Lung tumor weight (mg ± SD) of control and various treatment groups. **(D)** Kaplan–Meier survival plot.

nism. At both the storage conditions, in other words, room temperature and 2–8°C, DSPC liposomes are in gel phase indicating condensed and structurally well organized-somewhat rigid arrangement of hydrocarbon chains. However, DOPC liposomes are in liquid crystalline phase at both the storage conditions. We can assume that reversible transfer of DTX between DTXPL and DOPC blank liposomes could be easier than DSPC blank liposomes.

The negative surface charge of DTXPL could be contributed by negatively charged phosphate group of PEG-DSPE which is in accordance with the previous report [31]. Sustained release of DTX from stable and long circulating liposomes is extremely important to achieve EPR dependent passive targeting of tumor [32–34].

The pharmacokinetic profile of DTX liposomes was very much in correlation with the data of *in vitro* release profile and blood to plasma DTX ratio. The longer $t1/2$ in the PEGylated liposomes is related to the reduced uptake of liposomal drug by the elements of the reticuloendothelial system (RES) [12]. Prolong circulation enhance the chance of extravasation in leaky tumor vasculature and also provide long term exposure of drug to cancer cells. Taxotere maintained the therapeutic concentration of DTX only for short duration while DTXPL released drug in a controlled manner which maintained the DTX concentration within therapeutic window for prolonged period. The lower V_{ss} of DTXPL suggested that the liposomes controlled the distribution of DTX to unwanted tissues and resulted in long circulation in blood stream.

Another important aspect of this work was to investigate the effect of tumor stroma disruption (reduction in tumors fibrosis) on permeation of PEGylated liposomes and efficacy of DTXPL. Therapeutic benefit of EPR effect mediated tumor uptake of nanocarriers is limited by poor penetration to deeper regions in tumor. Of course, EPR helps in preferential passive uptake but further access into tumor tissue is minimized by tumor stroma. It was reported that stromal depletion results in improved tumor perfusion and a lower TIFP [35]. We have already demonstrated that telmisartan admin-

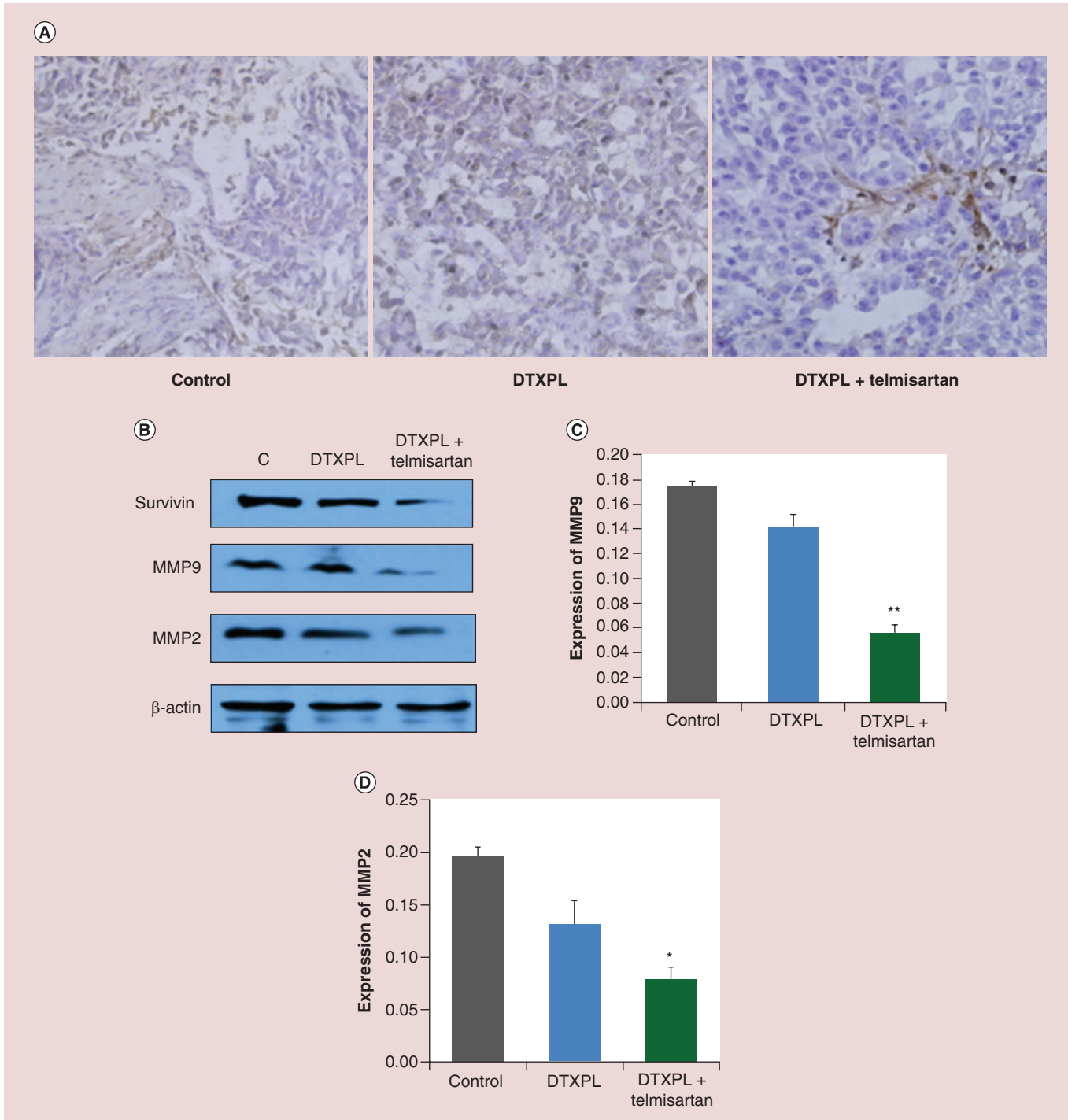

Figure 7. Immunohistochemistry (IHC) and western blot analysis of lung tumor. **(A)** IHC of lung tumor section for microvessel density using CD31 staining. CD31 stained tumor section of DTXPL+telmisartan treated animal showed marked reduction in microvessels. **(B)** Western Blot analysis of orthotopic lung tumor lysates. Western blot images of different protein expressions in tumor lysates. Quantitative analysis of expressions of **(C)** MMP9 and **(D)** MMP2.
*$p < 0.05$; **$p < 0.01$.

istered by inhalation route showed higher accumulation of fluorescent polystyrene nanoparticle in tumor region [12]. Since, oral route has very high patient compliance over aerosol based inhalation route, in the present study telmisartan was administered by oral route. Further, use of fluorescent PEGylated liposome (Coumarin-6 as fluorescent probe) could be a superior choice over fluorescent polystyrene nanoparticles. Therefore,

use of coumarin-6 loaded PEGylated liposomes to investigate tumor uptake is more relevant than using fluorescent polystyrene nanoparticles. Higher uptake of coumarin-6 can be correlated with the disruption of collagen network and tumor stroma by telmisartan. In this report for the first time we are showing simultaneous distribution of PEGylated coumarin-6 liposomes between healthy and cancerous tissue. Though there are several reports describing the use of coumarin-6 liposomes to investigate the cellular uptake but these studies have been limited to *in vitro* imaging only [36–38].

The restrictive tumor microenvironment can be 'normalized' by pretreatment of agents that interfere with vascular growth factors (e.g., TGF-β, VEGF, etc.) or agents promoting the degradation of ECM components [13]. In our earlier report, we have shown that telmisartan reduced the expression of Collagen-1, TGF-β1, cleaved caspase-3, Vimentin and E-Cadherin expression in lung tumor [13]. In this paper, we have investigated the effect of telmisartan treatment on level of MMPs. In solid tumors, MMPs expression is regulated by TGF-β, while MMPs, are produced either by cancer or stromal cells, activate latent TGF-β in the ECM, together facilitating the enhancement of tumor progression. MMPs are mostly involved in the recycling of ECM as well as in releasing cytokines and growth factors from ECM. Tumor stromal cells express high levels of MMP2 at the advancing tumor front and are responsible for invasion and metastases. Although, there are homologies between functional domains among the MMPs, only MMP2 and MMP9, contain collagen binding domains (CBDs) formed by three-tandem fibronectin type II-like modules. MMP2 is a key component of cancer cell migration across collagen by a mechanism involving CBD-mediated MMP2 interactions with collagen. As shown in results, DTX+telmisartan combination significantly inhibited the MMP2 and MMP9 expression. As mentioned earlier, tumor extracellular matrix (ECM) is mainly composed of a dense collagen network embedded in the gel of glycosaminoglycans (GAGs), primarily hyaluronan. A number of studies demonstrating the use of collagenase, hyaluronidase and lysyl oxidase to degrade tumor ECM, as a means to improve the delivery of various therapeutics have been published in last decade [39,40]. Collagenase labeled gold nanoparticle exhibited 35% higher tumor accumulation compared with unlabeled gold nanoparticles [17]. Also, it has been shown that liposomes injected 1 h after the collagenase injection, led to approximately 1.5-fold increase in tumor uptake. Further, pretreatment with collagenase and hyaluronidase were found to enhance the transfection efficiency of plasmid DNA in subcutaneous tumor [39].

However, orally bioavailable small molecular inhibitors should be preferred over intravenous injection of proteolytic enzymes for disrupting the tumor stroma. Recently, losartan has been reported to reduce stromal collagen and hyaluronan production, associated with decreased expression of profibrotic signals including TGF-β1 [41]. There are few small and large molecular (lerdelimumab and metelimumab) TGF-β inhibitiors currently under preclinical or clinical trial showing antifibrotic activity in cancer, glaucoma and other fibrosis related disorders [42]. Liu *et al.* reported that TGF-β inhibition improves the distribution and efficacy of therapeutics in breast carcinoma by normalizing the tumor stroma [15]. In a pancreatic tumor model, a small molecule TGF-β receptor I inhibitor (LY364947) showed enhanced uptake of the nanoliposomes–Doxil® and polymeric micelles (30 and 70 nm), but did not affect distribution of small molecular weight chemotherapeutic agent [43]. Further, TGF-β type I receptor inhibition resulted in decreased pericyte coverage of the endothelial cells in tumor neovasculature and promoted higher accumulation of nanomedicines [43]. Most of these studies reported the use of novel TGF-β inhibitor while we have used a low dose of a well-established drug to minimize the risk of possible side effects and toxicity. Simultaneous delivery of PEGylated formulation with antifibrotic therapy was further reflected in orthotopic xenograft tumor bearing nude mice model. Significantly higher tumor survival, intact lung structure and lung tumor weight similar to normal mice at the end of animal study clearly indicated the promising potential of DTX+telmisartan treatment. Superior pharmacodynamics activity was contributed by oral telmisartan mediated enhanced uptake of DTXPL in tumor region over healthy lung tissue. The strategy of using tumor stromal disrupting agents prior to the treatment with anticancer drug loaded nanocarrier has a promising translational potential. Therapeutic efficacy of various types of nanomedicine (liposomes, polymer-drug conjugates, polymeric micelles) can be significantly enhanced by disrupting tumor stroma using a small molecule antifibrotic agent. Since there are many nanomedicinal products for the delivery of drugs, DNA, siRNA, diagnostic agents or imaging agents will probably be commercialized in the near future; this approach has potential clinical applications. Moreover, DTXPL has potential for clinical application due to its facile and scale up feasible technology, long term stability compared with liposomal formulations and enhanced efficacy of docetaxel.

Future perspective

Pretreatment with antifibrotic agent prior to the treatment of anticancer nanomedicine will be integral part of cancer chemotherapy in future. Nanomedicine is future of cancer treatment and most of the nanoformu-

lations under preclinical or clinical trial are designed for taxane (paclitaxel or docetaxel) delivery. In such scenario, there is a need to explore means to enhance the delivery of nanoparticle to deeper layer of tumors. Therapeutic efficacy of various types of nanomedicine (liposomes, polymer–drug conjugates, polymeric micelles) can be significantly enhanced by disrupting tumor stroma using a small molecular antifibrotic agent. Further, our novel modified hydration method has huge scope of commercialization for clinical use due to its several advantages over conventional method.

Conclusion

Modified hydration is a superior method to prepare stable liposomes of drugs with severe solubility and precipitation issues. Addition of small amount of blank liposomes leads to remarkable enhancement in physical stability of DTXPL. This method has a huge scope for commercialization due to its facile and scale up feasible manufacturing technology, long term stability and high drug loading capacity. PEGylation driven prolong circulation, improved pharmacokinetics, EPR facilitated passive accumulation and telmisartan mediated deeper penetration of DTXPL have collectively contributed to superior anticancer efficacy of DTX. Enhancement of intratumoral deposition of nanocarrier by oral telmisartan treatment could be a simple and extremely beneficial approach in improving the clinical outcome of existing and upcoming anticancer nanoformulations.

Acknowledgements

We are thankful to Eric Lochner, Department of Physics, The Florida State University, Tallahassee, FL, USA for helping us in SEM analysis of liposomes.

Financial & competing interests disclosure

This research was supported with funding from the National Institutes of Health's Minority Biomedical Research Support (MBRS)-SC1 program (grant no. SC1 GM092779-01); Cancer Institute of the National Institutes of Health under Award Number R21CA175618; National Institute on Minority Health and Health Disparities (NIMHD) P20 program (grant #1P20 MD006738-03) and the Department of Defense (DOD) Breast Cancer Program (grant no. W81XWH-11-1-0211). The authors have no other relevant affiliations or financial involvement with any organization or entity with a financial interest in or financial conflict with the subject matter or materials discussed in the manuscript apart from those disclosed.

No writing assistance was utilized in the production of this manuscript.

Ethical conduct of research

The authors state that they have obtained appropriate institutional review board approval or have followed the principles outlined in the Declaration of Helsinki for all human or animal experimental investigations. In addition, for investigations involving human subjects, informed consent has been obtained from the participants involved.

Executive summary

Preparation of docetaxel-loaded PEGylated liposomes using modified hydration method

- Docetaxel liposome prepared using modified hydration method (developed in our laboratory) showed very high stability compared with liposomes prepared using conventional (ethanol injection or thin film hydration) methods.
- Modified hydration technique was found to be the most suitable method to develop stable PEGylated liposomes of drug with severe solubility and precipitation problem, for example, paclitaxel or docetaxel.

Strategies to prevent docetaxel precipitation

- Blank liposomes composed of unsaturated phospholipids serve as a reservoir system to subside the docetaxel precipitation rate while hydrophilic solubilizers and surfactants enhanced the docetaxel precipitation.

Pharmacokinetic studies in rats

- The pharmacokinetic profile of DTX liposomes was very much in correlation with the data of *in vitro* release profile and blood to plasma DTX ratio. The longer *t*1/2 in the PEGylated liposomes is related to the reduced uptake of liposomal drug by the elements of the reticuloendothelial system (RES).

Uptake of coumarin-6 PEGylated liposomes in lung tumor

- Significantly higher uptake of liposomes in tumoral vs healthy tissues was observed in telmisartan pretreated animals suggesting the compromised tumor stromal barrier in telmisartan treated animals.

Anticancer study in orthotopic lung tumor-bearing nude mice

- Picrosirius red staining showed a significantly lower collagen I in the tumor of telmisartan-treated animals.
- Significantly higher tumor survival, intact lung structure and lung tumor weight similar to normal mice at the end of animal study clearly indicated the promising potential of DTX+Telmisartan treatment.
- Superior pharmacodynamics activity is contributed by telmisartan mediated TGF-β and other cytokines modulatory effects in disrupting tumor ECM and enhancing DTXPL uptake in tumor region over healthy lung tissue.

References

1 Desantis CE, Lin CC, Mariotto AB *et al.* Cancer treatment and survivorship statistics, 2014. *CA Cancer J. Clin.* 64(4), 252–271 (2014).

2 Ichite N, Chougule MB, Jackson T, Fulzele SV, Safe S, Singh M. Enhancement of docetaxel anticancer activity by a novel diindolylmethane compound in human non-small cell lung cancer. *Clin. Cancer. Res.* 15(2), 543–552 (2009).

3 Joshi M, Liu X, Belani CP. Taxanes, past, present, and future impact on non-small cell lung cancer. *Anticancer Drugs* 25(5), 571–583 (2014).

4 Patel K, Chowdhury N, Doddapaneni R, Boakye CH, Godugu C, Singh M. Piperlongumine for enhancing oral bioavailability and cytotoxicity of docetaxel in triple-negative breast cancer. *J. Pharm. Sci.* 104(12), 4417–4426 (2015).

5 Jin SE, Jin HE, Hong SS. Targeted delivery system of nanobiomaterials in anticancer therapy: from cells to clinics. *BioMed Res. Int.* 2014 814208 (2014).

6 Noori Koopaei M, Khoshayand MR, Mostafavi SH *et al.* Docetaxel loaded PEG-PLGA nanoparticles: optimized drug loading, in vitro cytotoxicity and in vivo antitumor effect. *Iran. J. Pharm. Res.* 13(3), 819–833 (2014).

7 Palma G, Conte C, Barbieri A *et al.* Antitumor activity of PEGylated biodegradable nanoparticles for sustained release of docetaxel in triple-negative breast cancer. *Int. J. Pharm.* 473(1–2), 55–63 (2014).

8 De Oliveira R, Zhao P, Li N *et al.* Synthesis and *in vitro* studies of gold nanoparticles loaded with docetaxel. *Int. J. Pharm.* 454(2), 703–711 (2013).

9 Patel AR, Chougule M, Singh M. EphA2 targeting pegylated nanocarrier drug delivery system for treatment of lung cancer. *Pharm. Res.* 31(10), 2796–2809 (2014).

10 Jain RK, Stylianopoulos T. Delivering nanomedicine to solid tumors. *Nat. Rev. Clin. Oncol.* 7(11), 653–664 (2010).

11 Lammers T, Kiessling F, Hennink WE, Storm G. Drug targeting to tumors: principles, pitfalls and (pre-) clinical progress. *J. Control. Release* 161(2), 175–187 (2012).

12 Bae YH, Park K. Targeted drug delivery to tumors: myths, reality and possibility. *J. Control. Release* 153(3), 198–205 (2011).

13 Godugu C, Patel AR, Doddapaneni R, Marepally S, Jackson T, Singh M. Inhalation delivery of telmisartan enhances intratumoral distribution of nanoparticles in lung cancer models. *J. Control. Release* 172(1), 86–95 (2013).

14 Netti PA, Berk DA, Swartz MA, Grodzinsky AJ, Jain RK. Role of extracellular matrix assembly in interstitial transport in solid tumors. *Cancer Res.* 60(9), 2497–2503 (2000).

15 Liu J, Liao S, Diop-Frimpong B *et al.* TGF-beta blockade improves the distribution and efficacy of therapeutics in breast carcinoma by normalizing the tumor stroma. *Proc. Natl Acad. Sci. USA* 109(41), 16618–16623 (2012).

16 Papageorgis P, Stylianopoulos T. Role of TGFbeta in regulation of the tumor microenvironment and drug delivery (review). *Int. J. Oncol.* 46(3), 933–943 (2015).

17 Murty S, Gilliland T, Qiao P *et al.* Nanoparticles functionalized with collagenase exhibit improved tumor accumulation in a murine xenograft model. *Part. Part. Syst. Charact.* 31(12), 1307–1312 (2014).

18 Doddapaneni R, Patel K, Owaid IH, Singh M. Tumor neovasculature-targeted cationic PEGylated liposomes of gambogic acid for the treatment of triple-negative breast cancer. *Drug Deliv.* doi:10.3109/10717544.2015.1124472 1–10 (2015) (Epub ahead of print).

19 Patel K, Patil A, Mehta M, Gota V, Vavia P. Medium chain triglyceride (MCT) rich, paclitaxel loaded self nanoemulsifying preconcentrate (PSNP): a safe and efficacious alternative to Taxol. *J. Biomed. Nanotechnol.* 9(12), 1996–2006 (2013).

20 Jackson T, Chougule MB, Ichite N, Patlolla RR, Singh M. Antitumor activity of noscapine in human non-small cell lung cancer xenograft model. *Cancer Chemother. Pharmacol.* 63(1), 117–126 (2008).

21 Fulzele SV, Chatterjee A, Shaik MS, Jackson T, Singh M. Inhalation delivery and anti-tumor activity of celecoxib in human orthotopic non-small cell lung cancer xenograft model. *Pharm. Res.* 23(9), 2094–2106 (2006).

22 Weidner N, Folkman J, Pozza F *et al.* Tumor angiogenesis: a new significant and independent prognostic indicator in early-stage breast carcinoma. *J. Natl. Cancer Inst.* 84(24), 1875–1887 (1992).

23 Ruozi B, Belletti D, Tombesi A *et al.* AFM, ESEM, TEM, and CLSM in liposomal characterization: a comparative study. *Int. J. Nanomed.* 6 557–563 (2011).

24 Patel K, Patil A, Mehta M, Gota V, Vavia P. Oral delivery of paclitaxel nanocrystal (PNC) with a dual Pgp-CYP3A4 inhibitor: preparation, characterization and antitumor activity. *Int. J. Pharm.* 472(1–2), 214–223 (2014).

25 Zhao L, Feng SS. Effects of lipid chain length on molecular interactions between paclitaxel and phospholipid within model biomembranes. *J. Colloid Interface Sci.* 274(1), 55–68 (2004).

26 Liu XY, Yang Q, Kamo N, Miyake J. Effect of liposome type and membrane fluidity on drug-membrane partitioning analyzed by immobilized liposome chromatography. *J. Chromatogr. A* 913(1–2), 123–131 (2001).

27 Chiantia S, Klymchenko AS, London E. A novel leaflet-selective fluorescence labeling technique reveals differences between inner and outer leaflets at high bilayer curvature. *Biochim. Biophys. Acta* 1818(5), 1284–1290 (2012).

28 Kurniawan Y, Venkataramanan KP, Scholz C, Bothun GD. n-Butanol partitioning and phase behavior in DPPC/DOPC membranes. *J. Phys. Chem. B* 116(20), 5919–5924 (2012).

29 Loew S, Fahr A, May S. Modeling the release kinetics of poorly water-soluble drug molecules from liposomal nanocarriers. *J. Drug. Deliv.* 2011 376548 (2011).

30 Hefesha H, Loew S, Liu X, May S, Fahr A. Transfer mechanism of temoporfin between liposomal membranes. *J. Control. Release* 150(3), 279–286 (2011).

31 Nag OK, Awasthi V. Surface engineering of liposomes for stealth behavior. *Pharmaceutics* 5(4), 542–569 (2013).

32 Maruyama K. Intracellular targeting delivery of liposomal drugs to solid tumors based on EPR effects. *Adv. Drug Deliv. Rev.* 63(3), 161–169 (2011).

33 Kobayashi H, Watanabe R, Choyke PL. Improving conventional enhanced permeability and retention (EPR) effects; what is the appropriate target? *Theranostics* 4(1), 81–89 (2013).

34 Paolino D, Cosco D, Racanicchi L *et al.* Gemcitabine-loaded PEGylated unilamellar liposomes vs GEMZAR: biodistribution, pharmacokinetic features and *in vivo* antitumor activity. *J. Control. Release* 144(2), 144–150 (2010).

35 Lammerts E, Roswall P, Sundberg C *et al.* Interference with TGF-beta1 and -beta3 in tumor stroma lowers tumor interstitial fluid pressure independently of growth in experimental carcinoma. *Int. J. Cancer* 102(5), 453–462 (2002).

36 Wei M, Xu Y, Zou Q *et al.* Hepatocellular carcinoma targeting effect of PEGylated liposomes modified with lactoferrin. *Eur. J. Pharm. Sci.* 46(3), 131–141 (2012).

37 Muthu MS, Kulkarni SA, Xiong J, Feng SS. Vitamin E TPGS coated liposomes enhanced cellular uptake and cytotoxicity of docetaxel in brain cancer cells. *Int. J. Pharm.* 421(2), 332–340 (2011).

38 Li RJ, Ying X, Zhang Y *et al.* All-trans retinoic acid stealth liposomes prevent the relapse of breast cancer arising from the cancer stem cells. *J. Control. Release* 149(3), 281–291 (2011).

39 Cemazar M, Golzio M, Sersa G *et al.* Hyaluronidase and collagenase increase the transfection efficiency of gene electrotransfer in various murine tumors. *Hum. Gene Ther.* 23(1), 128–137 (2012).

40 Kanapathipillai M, Mammoto A, Mammoto T *et al.* Inhibition of mammary tumor growth using lysyl oxidase-targeting nanoparticles to modify extracellular matrix. *Nano Lett.* 12(6), 3213–3217 (2012).

41 Chauhan VP, Martin JD, Liu H *et al.* Angiotensin inhibition enhances drug delivery and potentiates chemotherapy by decompressing tumour blood vessels. *Nat. Commun.* 4, 2516 (2013).

42 Akhurst RJ, Hata A. Targeting the TGFbeta signalling pathway in disease. *Nat. Rev. Drug Discov.* 11(10), 790–811 (2012).

43 Meng H, Zhao Y, Dong J *et al.* Two-wave nanotherapy to target the stroma and optimize gemcitabine delivery to a human pancreatic cancer model in mice. *ACS Nano* 7(11), 10048–10065 (2013).

NR4A1 Antagonists Inhibit β1-Integrin-Dependent Breast Cancer Cell Migration

Article *in* Molecular and Cellular Biology · February 2016

DOI: 10.1128/MCB.00912-15

5 authors, including:

Erik Hedrick
Cleveland Clinic
21 PUBLICATIONS **157** CITATIONS
SEE PROFILE

Stephen Safe
Texas A&M University System
527 PUBLICATIONS **28,040** CITATIONS
SEE PROFILE

AMERICAN SOCIETY FOR MICROBIOLOGY | Molecular and Cellular Biology

NR4A1 Antagonists Inhibit β1-Integrin-Dependent Breast Cancer Cell Migration

Erik Hedrick,[a] Syng-Ook Lee,[b] Ravi Doddapaneni,[c] Mandip Singh,[c] Stephen Safe[a]

Department of Veterinary Physiology and Pharmacology, Texas A&M University, College Station, Texas, USA[a]; Department of Food Science and Technology, Keimyung University, Daegu, Republic of Korea[b]; Department of Pharmaceutics, College of Pharmacy and Pharmaceutical Sciences, Florida A&M University, Tallahassee, Florida, USA[c]

Overexpression of the nuclear receptor 4A1 (NR4A1) in breast cancer patients is a prognostic factor for decreased survival and increased metastasis, and this has been linked to NR4A1-dependent regulation of transforming growth factor β (TGF-β) signaling. Results of RNA interference studies demonstrate that basal migration of aggressive SKBR3 and MDA-MB-231 breast cancer cells is TGF-β independent and dependent on regulation of β1-integrin gene expression by NR4A1 which can be inhibited by the NR4A1 antagonists 1,1-bis(3′-indolyl)-1-(*p*-hydroxyphenyl)methane (DIM-C-pPhOH) and a related *p*-carboxymethylphenyl [1,1-bis(3′-indolyl)-1-(*p*-carboxymethylphenyl)methane (DIM-C-pPhCO$_2$Me)] analog. The NR4A1 antagonists also inhibited TGF-β-induced migration of MDA-MB-231 cells by blocking nuclear export of NR4A1, which is an essential step in TGF-β-induced cell migration. We also observed that NR4A1 regulates expression of both β1- and β3-integrins, and unlike other β1-integrin inhibitors which induce prometastatic β3-integrin, NR4A1 antagonists inhibit expression of both β1- and β3-integrin, demonstrating a novel mechanism-based approach for targeting integrins and integrin-dependent breast cancer metastasis.

Cell adhesion and attachment are essential for tissue integrity and cellular homeostasis, and the heterodimeric integrin cell surface receptors play a critical role in these processes (1–3). There are 18 different α subunits and 8 different β subunits that form 24 αβ-integrin receptor heterodimers, and the large 12-member β1-integrin subgroup bind multiple extracellular matrix (ECM) molecules to activate multiple intracellular pathways and also induce cross talk with other signaling systems (1–3). The functions of integrin heterodimers are highly tissue specific, and many human pathologies also involve integrin signaling (reviewed in references 4 and 5). β1-Integrin is highly expressed in most tumors and is associated with a negative prognostic significance such as overall and disease-free survival, recurrence, and metastasis for head and neck and squamous cell carcinoma, melanoma, lung, breast, prostate, laryngeal, and pancreatic cancers (6–17). A recent immunostaining study of 225 breast invasive ductal carcinomas (IDCs) showed that β1-integrin was overexpressed in 32.8% of patients with IDCs (13). Numerous studies show that focal adhesion kinase (FAK) which is downstream from β1-integrin is also a negative prognostic factor for breast cancer patients (18–20). The important functional role of β1-integrin has been demonstrated in mouse models expressing *erbB2* under the control of the mouse mammary tumor virus and crossed with mammary tissue-specific β1-integrin-deficient mice. These mice exhibit a decrease in tumor volume, increased apoptosis, and decreased lung metastasis compared to animals expressing wild-type β1-integrin (21–23). Although small molecules, peptides, and antibodies that inhibit β1-integrin signaling have been developed, clinical agents that target β1-integrin for cancer chemotherapy are not currently available.

The orphan nuclear receptor 4A1 (NR4A1) (also called TR3 or Nur77) is overexpressed in breast cancer and other tumors, and functional studies show that NR4A1 exhibits prooncogenic activity (reviewed in reference 24). Studies in this laboratory have characterized a series of 1,1-bis(3′-indolyl)-1-(*p*-substituted phenyl) methane (C-DIM) analogs that bind NR4A1 and act as receptor antagonists to inhibit growth and induce apoptosis in several cancer cell lines and in tumors from mouse xenografts (25–30). A recent study demonstrated functional interactions between NR4A1 and transforming growth factor β (TGF-β) and in estrogen receptor (ER)-negative MDA-MB-231 cells, knockdown of NR4A1 decreased migration and also inhibited TGF-β-induced migration of this cell line (31). Results of gene array studies in pancreatic cancer cells identified *β1-integrin* as a potential NR4A1-regulated gene (27). In this study, we demonstrate that NR4A1 regulates β1-integrin expression and β1-integrin-dependent migration of breast cancer cells, and this is accompanied by decreased expression of β3-integrin. In MDA-MB-231 cells, results of our studies show that both constitutive and TGF-β-induced migration are dependent on nuclear and extranuclear NR4A1-regulated pathways, respectively. C-DIM/NR4A1 antagonists inhibit NR4A1-dependent expression of β1- and β3-integrins and other prooncogenic NR4A1-regulated genes and pathways and represent a novel class of mechanism-based anticancer agents.

MATERIALS AND METHODS

Cell lines and antibodies. SKBR3, MDA-MB-231, and MCF-7 breast cancer cells were purchased from American Type Culture Collection (Manassas, VA). The cells were maintained at 37°C in the presence of 5% CO_2 in Dulbecco's modified Eagle's medium (DMEM)–Ham's F-12 medium with 10% fetal bovine serum with antibiotic. NR4A1 antibody was pur-

Received 30 September 2015 **Returned for modification** 21 December 2015
Accepted 24 February 2016
Accepted manuscript posted online 29 February 2016
Citation Hedrick E, Lee S-O, Doddapaneni R, Singh M, Safe S. 2016. NR4A1 antagonists inhibit β1-integrin-dependent breast cancer cell migration. Mol Cell Biol 36:1383–1394. doi:10.1128/MCB.00912-15.

Address correspondence to Stephen Safe, ssafe@cvm.tamu.edu.

Supplemental material for this article may be found at http://dx.doi.org/10.1128/MCB.00912-15.

chased from Novus Biologicals (Littleton, CO). TGF-β was purchased from BD Biosystems (Bedford, MA). β-Actin antibody, Dulbecco's modified Eagle's medium, RPMI 1640 medium, and 36% formaldehyde were purchased from Sigma-Aldrich (St. Louis, MO). Hematoxylin was purchased from Vector Laboratories (Burlingame, CA). β3-Integrin, phosphorylated focal adhesion kinase (p-FAK), FAK, axin 2, leptomycin B, and NR4A1 immunofluorescent antibody were purchased from Cell Signaling Technologies (Manassas, VA). β1-Integrin antibody was purchased from Santa Cruz Biotech (Santa Cruz, CA), p84 antibody was purchased from GeneTex (Irvine, CA), and glyceraldehyde-3-phosphate dehydrogenase (GAPDH) antibody was purchased from Biotium (Hayward, CA).

Cell adhesion assay. SKBR3, MDA-MB-231, and MCF-7 cancer cells (3.0×10^5 per well) were seeded in Dulbecco's modified Eagle's medium–Ham's F-12 medium supplemented with 2.5% charcoal-stripped fetal bovine serum and were allowed to attach for 24 h. The cells were seeded and subsequently treated with various concentrations of 1,1-bis(3′-indolyl)-1-(*p*-hydroxyphenyl)methane (DIM-C-pPhOH) or *p*-carboxymethylphenyl (1,1-bis(3′-indolyl)-1-(*p*-carboxymethylphenyl)methane [DIM-C-pPhCO_2Me]) for 24 h or 1 h prior to treatment with TGF-β (5 ng/ml) (4-h cotreatment) or without TGF-β or with 100 nM siβ1-integrin (small interfering RNA against β1-integrin) or siNR4A1 for 48 h. The cells were trypsinized, counted, and then placed for 90 min on BD BioCoat human fibronectin cellware 24-well plates (BD Biosciences, Bedford, MA). The medium was then aspirated, and the wells were gently washed with phosphate-buffered saline (PBS) and stained with 0.5% crystal violet stain. The cells were then counted for adhesion to fibronectin. Wells coated with bovine serum albumin (BSA) and poly-L-lysine were used as negative controls.

Boyden chamber assay. SKBR3, MDA-MB-231, and MCF-7 cancer cells (3.0×10^5 per well) were seeded in Dulbecco's modified Eagle's medium–Ham's F-12 medium supplemented with 2.5% charcoal-stripped fetal bovine serum and were allowed to attach for 24 h. The cells were seeded and subsequently treated with various concentrations of DIM-C-pPhOH or DIM-C-pPhCO_2Me for 24 h or 1 h prior to treatment with TGF-β (5 ng/ml) (4 h cotreatment) or without TGF-β or with 100 nM siβ1-integrin, siNR4A1, siSp1 (Sp1 stands for specificity protein 1), or sip300 for 48 h. The cells were trypsinized, counted, placed in 24-well 8.0-μm-pore ThinCerts from BD Biosciences (Bedford, MA), allowed to migrate for 24 h, fixed with formaldehyde, and then stained with hematoxylin. Cells that migrated through the pores were then counted.

Real-time PCR. RNA was isolated using Zymo Research *Quick-RNA* MiniPrep kit (Irvine, CA). Quantification of mRNA (β1-integrin, β3-integrin) was performed using Bio-Rad iTaq universal SYBR green one-step kit (Richmond, CA) using the manufacturer's protocol with real-time PCR. TATA binding protein (TBP) mRNA was used as a control to determine relative mRNA expression.

Immunoprecipitation. MDA-MB-231 cancer cells (3.0×10^5 per well) were seeded in Dulbecco's modified Eagle's medium–Ham's F-12 medium supplemented with 2.5% charcoal-stripped fetal bovine serum and allowed to attach for 24 h. The medium was then changed to DMEM–Ham's F-12 medium containing 2.5% charcoal-stripped fetal bovine serum, and either dimethyl sulfoxide (DMSO) or TGF-β (5 ng/ml) was added for 4 h (after pretreatment with leptomycin B [20 nM] for 24 h or pretreatment with 20 μM DIM-C-pPhOH or DIM-C-pPhCO_2Me or no pretreatment). Protein A Dynabeads were prepared, and binding of antibody with protein and protein-protein interactions were isolated by Life Technologies immunoprecipitation kit using Dynabeads coated with protein A (Grand Island, NY) following the manufacturer's protocol. Protein-protein interactions of interest were determined by Western blot analysis.

Chromatin immunoprecipitation. The chromatin immunoprecipitation (ChIP) assay was performed using the ChIP-IT Express magnetic chromatin immunoprecipitation kit (Active Motif, Carlsbad, CA) according to the manufacturer's protocol. SKBR3 and MDA-MB-231 cells were treated with DMSO, DIM-C-pPhOH, or DIM-C-pPhCO_2Me (15 or 20 μM) for 24 h. The cells were then fixed with 1% formaldehyde, and the cross-linking reaction was stopped by the addition of 0.125 M glycine. After the cells were washed twice with phosphate-buffered saline, the cells were scraped and pelleted. Collected cells were hypotonically lysed, and nuclei were collected. Nuclei were then sonicated to the desired chromatin length (~200 to 1,500 bp). The sonicated chromatin was immunoprecipitated with normal IgG, p300 (Santa Cruz), siSp1 (Abcam), NR4A1 (Novus Biologicals), or RNA polymerase II (Pol II) (Active Motif) antibodies and protein A-conjugated magnetic beads at 4°C overnight. After the magnetic beads were extensively washed, protein-DNA cross-links were reversed and eluted. DNA was prepared by proteinase K digestion followed by PCR amplification. The primers for detection of the β1-integrin promoter region were 5′-TCACCACCCTTCGTGACAC-3′ (sense) and 5′-GAGATCCTGCATCTCGGAAG-3′ (antisense), and the primers for detection of the β3-integrin promoter region were 5′-TCTC AGGCGCAGGGTCTAGAGAA-3′ (sense) and 5′-TCGCGGCGCCCAC CGCCTGCTCTACGCT-3′ (antisense). PCR products were resolved on a 2% agarose gel in the presence of RGB-4103 GelRed nucleic acid stain.

Nuclear/cytosolic extraction. MDA-MB-231 cancer cells (3.0×10^5 per well) were seeded in Dulbecco's modified Eagle's medium–Ham's F-12 medium supplemented with 2.5% charcoal-stripped fetal bovine serum and were allowed to attach for 24 h. The medium was then changed to DMEM–Ham's F-12 medium containing 2.5% charcoal-stripped fetal bovine serum, and either DMSO or TGF-β (5 ng/ml) was added for 4 h (after pretreatment with 20 nM leptomycin B for 24 h or pretreatment with 20 μM DIM-C-pPhOH or DIM-C-pPhCO_2Me or no pretreatment). Nuclear and cytosolic fractions were then isolated using Thermo Scientific NE-PER nuclear and cytoplasmic extraction kit (Rockford, IL) according to the manufacturer's protocol. Fractions were then analyzed by Western blotting. GAPDH and p84 were used as cytoplasmic and nuclear positive controls, respectively.

Immunofluorescence. MDA-MB-231 (1.0×10^5 per well) were seeded in two-well Nunc Lab-Tek chambered borosilicate cover glass slides (no. 1 borosilicate cover glass) from Thermo Scientific and were allowed to attach for 24 h. The medium was then changed to DMEM–Ham's F-12 medium containing 2.5% charcoal-stripped fetal bovine serum, and either DMSO or TGF-β (5 ng/ml) was added for 4 h (after pretreatment with leptomycin B [20 nM] for 24 h or pretreatment with 20 μM DIM-C-pPhOH or DIM-C-pPhCO_2Me or no pretreatment). The cells were then treated with fluorescent NR4A1 primary antibody [Nur77 (D63C5) XP], and immunofluorescence was observed according to Cell Signaling Technology's immunofluorescence protocol. 4′,6′-Diamidino-2-phenylindole (DAPI) staining was observed using Hoechst staining according to Biotium's apoptotic and necrotic assay kit by following the manufacturer's protocol. The cells were visualized by microscopy (Advanced Microscopy), and NR4A1 localization was determined by green fluorescence. DAPI was used to stain the nucleus, and images were taken sequentially of NR4A1, DAPI, and then merged (28–30).

Western blot analysis. SKBR3, MDA-MB-231, and MCF-7 cancer cells (3.0×10^5 per well) were seeded in Dulbecco's modified Eagle's medium–Ham's F-12 medium supplemented with 2.5% charcoal-stripped fetal bovine serum and were allowed to attach for 24 h. The cells were transfected with 100 nM siβ1-integrin, siNR4A1, siSp1, or sip300 for 72 h or treated with various C-DIM compounds. Cell lysates were analyzed by Western blotting as described previously (28–30).

Small interfering RNA interference assay. Small interfering RNA (siRNA) experiments were conducted as described previously (28–30). The siRNA complexes used in the study are as follows: siGL2-5′, CGU ACG CGG AAU ACU UCG A; siNR4A1, SASI_Hs02_00333289[1], SASI_Hs02_00333290[2]; siβ1-integrin, SASI_Hs02_00333437[1], SASI_Hs01_00159474; siSp1, SASI_Hs02_003; sip300, SASI_Hs01_00052818.

Triple-negative breast cancer (TNBC) orthotopic xenograft studies. Female BALB/c nude mice (6 to 8 weeks old) were obtained (Charles River Laboratory, Wilmington, MA) and maintained and treated as previously

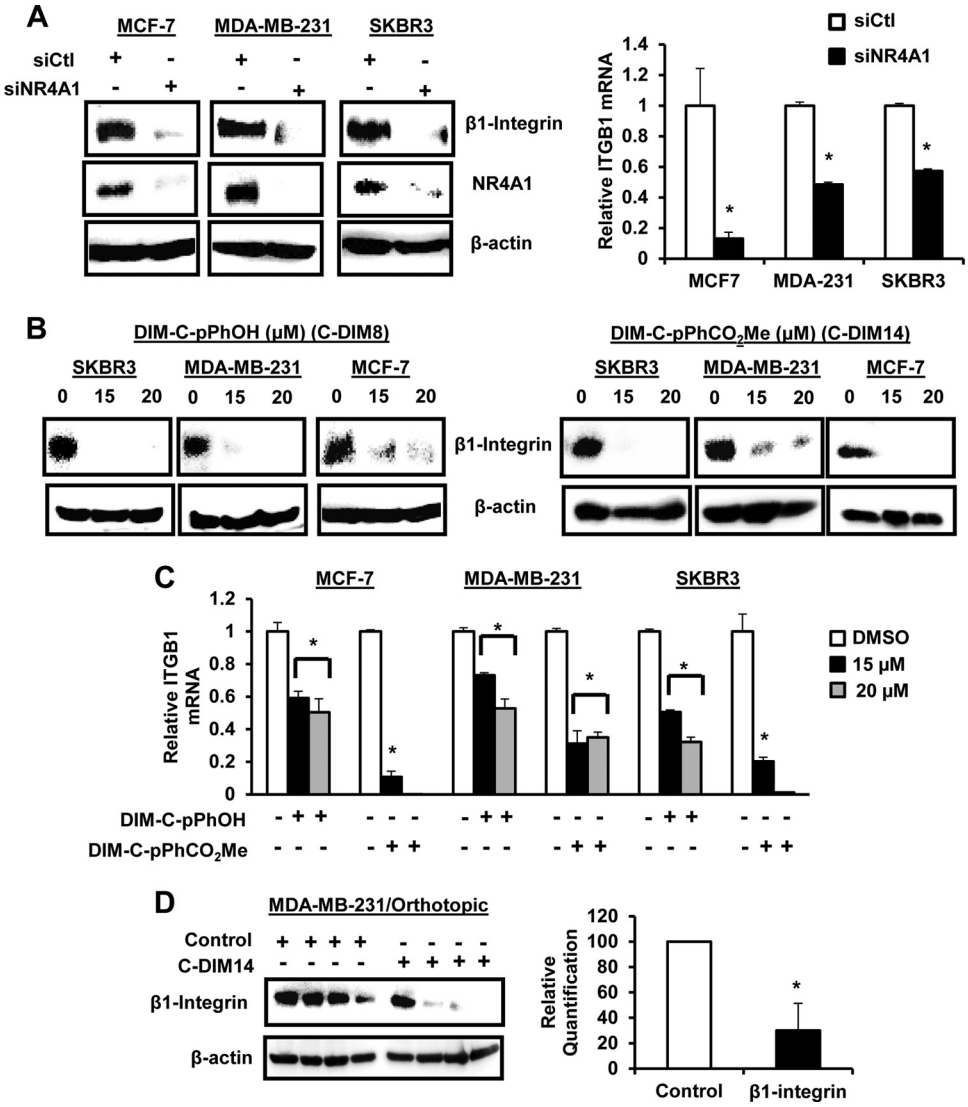

FIG 1 NR4A1 regulates β1-integrin expression in breast cancer cells and tumors. (A) Breast cancer cells were transfected with siNR4A1, and cell extracts were analyzed for protein and mRNA expression by Western blotting or real-time PCR, respectively, as outlined in Materials and Methods. (B and C) Breast cancer cells were treated with DMSO, DIM-C-pPhOH, or DIM-C-pPhCO$_2$Me for 24 h, and extracts were analyzed for protein (B) or mRNA (C) levels by Western blotting and real-time PCR, respectively, as outlined in Materials and Methods. (D) Cell lysates from tumors (MDA-MB-231 orthotopic) (30) derived from animals treated with corn oil (control) or DIM-C-pPhCO$_2$Me (C-DIM-14; 40 mg/kg of body weight/day) were analyzed by Western blotting, and decreased protein expression was determined and normalized against the β-actin protein loading control. Quantified data are presented as means plus standard errors (SE) (error bars) (at least three replicates), and significant ($P < 0.05$) decreases are indicated by an asterisk.

described (30). Tumor volumes and tumor weights were determined as previously described (30). Tumor lysates were obtained and analyzed by Western blotting.

Statistical analysis. Statistical significance of differences between the treatment groups was determined by Student's *t* test. The results are expressed as means with error bars representing 95% confidence intervals (95% CIs) for at least three experiments for each group unless otherwise indicated. A *P* value of <0.05 was considered statistically significant. All statistical tests were two sided.

RESULTS

NR4A1 regulates β1-integrin expression. β1-Integrin is expressed in ER-positive MCF-7, ER-negative MDA-MB-231, and *erbB2*-overexpressing SKBR3 breast cancer cells, and knockdown of NR4A1 (siNR4A1) by RNA interference (RNAi) decreased expression of β1-integrin protein and mRNA (Fig. 1A). Previous studies identified 1,1-bis(3′-indolyl)-1-(*p*-hydroxyphenyl)methane (DIM-C-pPhOH; C-DIM8) and 1,1-bis(3′-indolyl)-1-(*p*-carboxymethylphenyl)methane (DIM-C-pPhCO$_2$Me; C-DIM14) as NR4A1 ligands that act as antagonists in breast and other cancer cell lines (25–30), and both compounds also decreased expression of β1-integrin protein (Fig. 1B) and mRNA (Fig. 1C) in MCF-7, MDA-MB-231, and SKBR3 cells. Moreover, Western blot analysis of tumor lysates from mice bearing MDA-MB-231 cells (orthotopic) (30) showed that DIM-C-pPhCO$_2$Me significantly decreases β1-integrin protein expression (Fig. 1D). β1-Integrin regulates phosphorylation of FAK (p-FAK), and transfection of MCF-7, MDA-MB-231, and SKBR3 cells with siNR4A1 (Fig. 2A) or treatment with DIM-CpPhOH (Fig. 2B) or DIM-C-

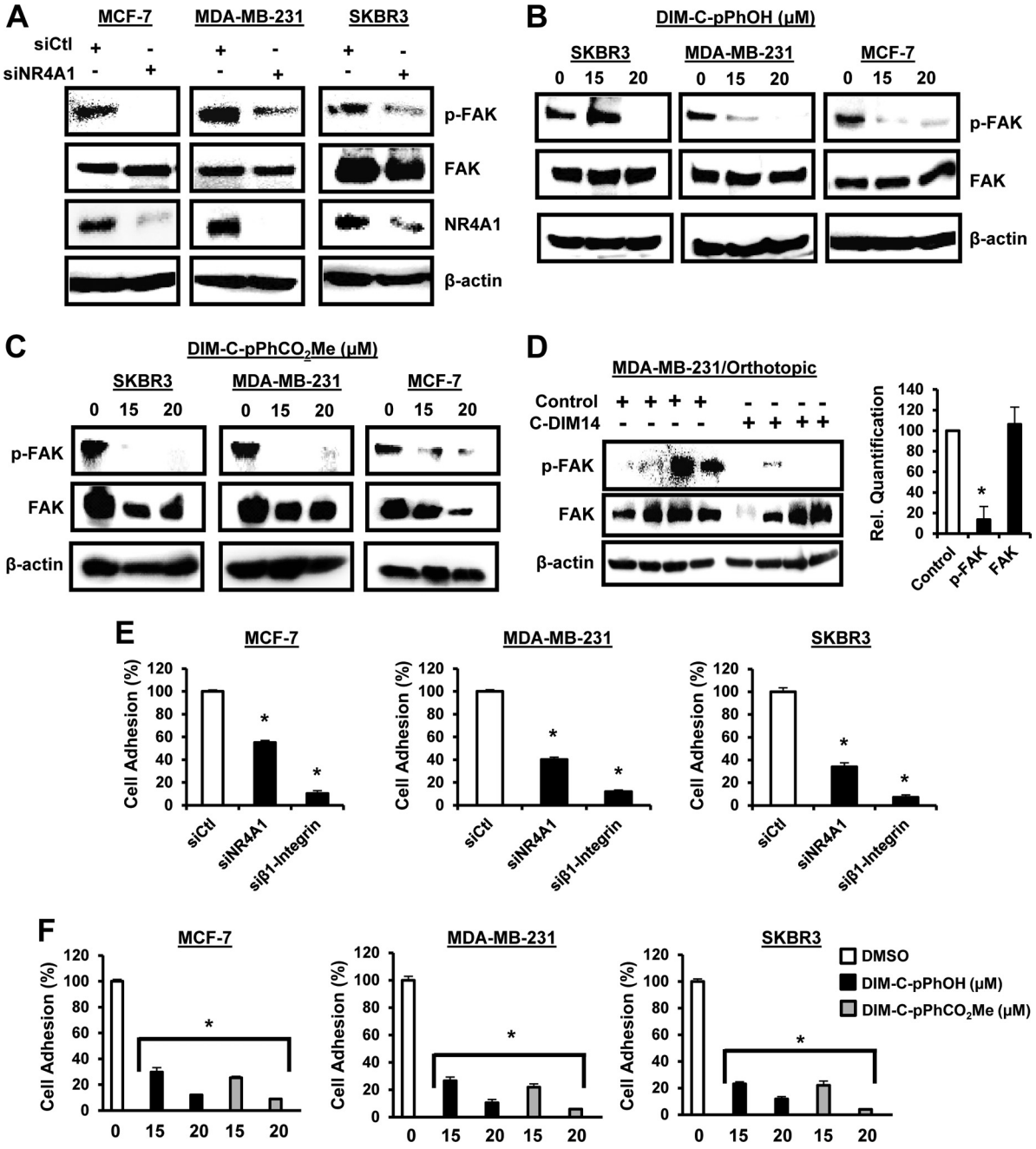

FIG 2 NR4A1 regulates β1-integrin-dependent responses. Breast cancer cells were transfected with siNR4A1 (A), treated with DMSO and DIM-C-pPhOH (B) or DIM-C-pPhCO$_2$Me (C) for 24 h, and whole-cell lysates were analyzed by Western blotting as outlined in Materials and Methods. (D) Tumor lysates from mice (MDA-MB-231 orthotopic-derived [30]) treated with corn oil or DIM-C-pPhCO$_2$Me (40 mg/kg/day) were analyzed by Western blotting and quantitated as outlined in the legend to Fig. 1D. (E and F) The effects of siNR4A1 and siβ1-integrin (E) or DIM-C-pPhOH and DIM-C-pPhCO$_2$Me (F) on fibronectin-induced adhesion of breast cancer cells was determined as outlined in Materials and Methods. Results in panels D to F are means plus SE (error bars) (at least three replicates), and a significant ($P < 0.05$) decrease is indicated by an asterisk. Western blots in Fig. 1 and 2 were derived from the same experiment showing effects on β1-integrin (Fig. 1) and β1-integrin-regulated responses (Fig. 2).

pPhCO$_2$Me (Fig. 2C) decreased phosphorylation of FAK. In addition, results from the *in vivo* orthotopic study (30) showed that p-FAK is decreased in tumors from mice bearing MDA-MB-231 cells and treated with DIM-C-pPhCO$_2$Me (Fig. 2D). Fibronectin-induced cell adhesion is also a prototypical β1-integrin-regulated response, and cell adhesion was significantly decreased in MCF-7, MDA-MB-231, and SKBR3 cells after transfection with siNR4A1 (Fig. 2E) or after treatment with DIM-C-pPhOH or DIM-C-pPhCO$_2$Me (Fig. 2F). For a positive control, we showed that knockdown of β1-integrin (siβ1-integrin) by RNA also decreased cell adhesion (Fig. 2E) (see Fig. S1 in the supplemental material).

Mechanisms of NR4A1 regulation of β1-integrin and β3-integrin. NR4A1 regulates gene expression through direct interactions with genomic nerve growth factor Bα (NGFBα) response

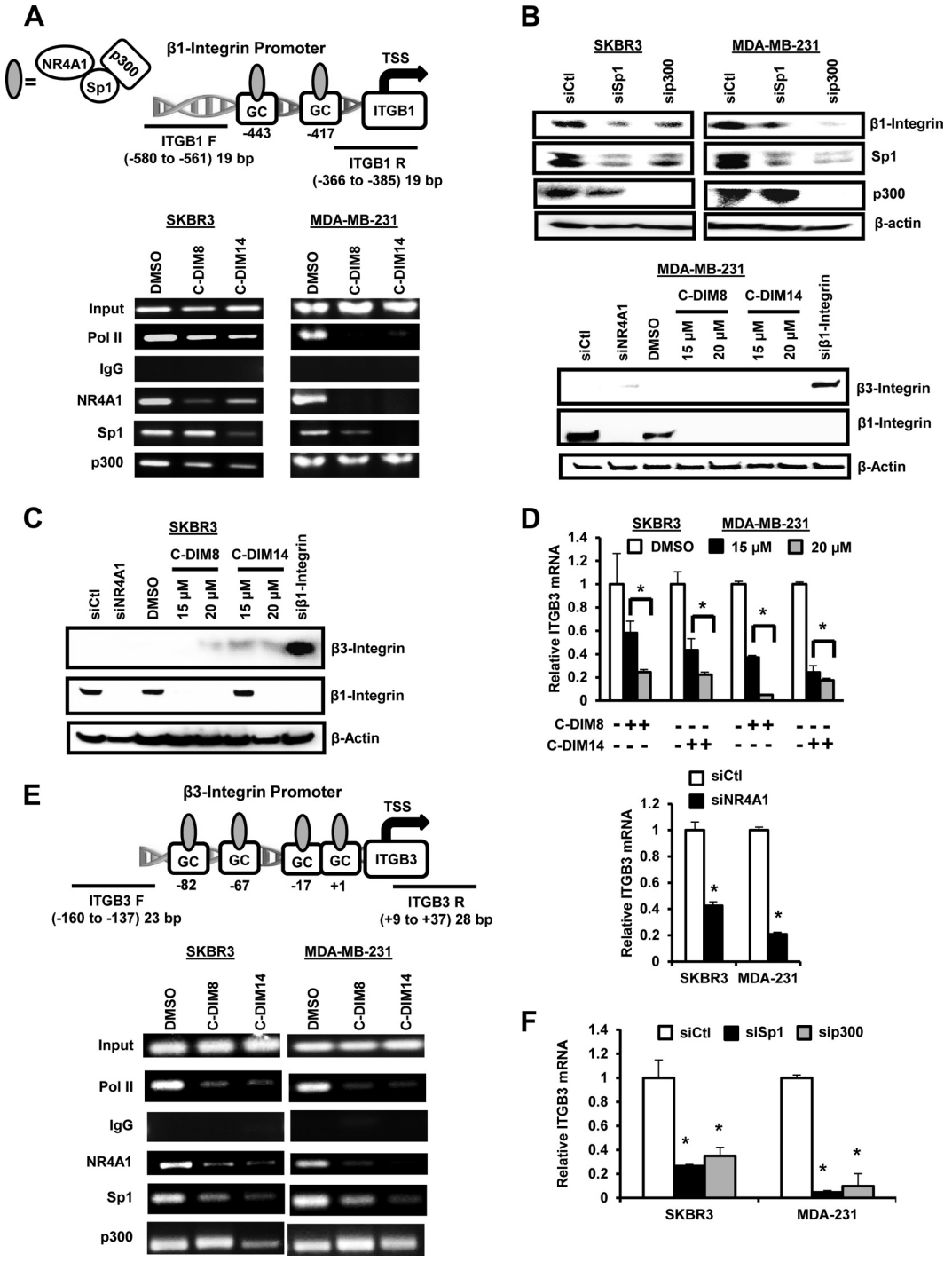

FIG 3 Role of NR4A1/p300/Sp1 in regulation of β1- and β3-integrin. (A) Analysis of Pol II, NR4A1, Sp1, and p300 binding to the β1-integrin promoter was determined in a ChIP assay using the indicated primers (ITGB1 F [ITGB1 stands for β1-integrin and F stands for forward] and ITGB1 R [R stands for reverse]). TSS, transcription start site. (B) Cells were treated with oligonucleotides that knock down Sp1 (siSp1) and p300 (sip300), and whole-cell lysates were analyzed by Western blotting as outlined in Materials and Methods. (C) Cells were transfected with siNR4A1 or treated with DIM-C-pPhOH (C-DIM8) or DIM-C-pPhCO$_2$Me (C-DIM14), and whole-cell lysates were analyzed by Western blotting as outlined in Materials and Methods. (D) Cells were transfected with siNR4A1 or treated with C-DIM8 or C-DIM14, and their effects on β3-integrin (ITGB3) mRNA levels were determined. The treatments significantly ($P < 0.05$) decrease mRNA levels. (E) Analysis of Pol II, NR4A1, Sp1, and p300 binding to the proximal GC-rich region of the β3-integrin promoter was determined in a ChIP assay as outlined in Materials and Methods. (F) Cells were transfected with siSp1 and sip300 and analyzed by real-time PCR for β3-integrin mRNA levels. Both oligonucleotides significantly ($P < 0.05$) decreased β3-integrin mRNA levels.

elements (NBRE) and Nur response elements (NuRE) or by interactions with specificity protein 1 (Sp1) bound to GC-rich promoter elements (32, 33). NBRE and NuRE were not identified in the β1-integrin promoter, whereas two GC-rich sequences were located at −760 and −676 in the proximal region of the β1-integrin promoter (Fig. 3A). Previous studies show that NR4A1, Sp1, and the nuclear coregulatory gene p300 interact with the GC-rich region of the survivin promoter to regulate survivin gene expression (25). Using the more aggressive SKBR3 and MDA-MB-231 cells as models, cells were treated with dimethyl sulfoxide (DMSO), DIM-C-pPhOH, or DIM-C-pPhCO_2Me and analyzed in a chromatin immunoprecipitation (ChIP) assay using primers targeted to the GC-rich region of the β1-integrin promoter. The results show that Pol II, NR4A1, Sp1, and p300 interact with the GC-rich promoter regions, and after treatment with DIM-C-pPhOH or DIM-C-pPhCO_2Me for 24 h, the band for Pol II was decreased in both cell lines (Fig. 3A), and this was consistent with decreased β1-integrin expression. Ligand-induced inactivation of NR4A1 also decreased NR4A1 binding to the promoter; however, changes in the Sp1 and p300 bands were somewhat variable and dependent on cell context and ligand. For example, the loss of p300 was observed in SKBR3 cells but not MDA-MB-231 cells, and it is possible that p300 was interacting with the *trans*-acting factors in the proximal region of the β1-integrin promoter. We further investigated the roles of Sp1 and p300 in regulating β1-integrin expression in SKBR3 and MDA-MB-231 cells by RNAi, and knockdown of Sp1 (siSp1) and p300 (sip300) also decreased β1-integrin expression (Fig. 3B), suggesting that like survivin (25), NR4A1 regulates β1-integrin expression through a NR4A1/p300/Sp1 complex. p300 knockdown also decreases Sp1 expression, suggesting that p300 plays a role in regulating expression of this gene. These results do not exclude a role for other factors in NR4A1 regulation of β1-integrin, and this is currently being investigated.

Previous reports show that inhibition of β1-integrin by RNAi or other β1-integrin inhibitors increases expression of β3-integrin resulting in enhanced metastasis (34–36). The β3-integrin promoter is also GC rich (37), and therefore, we investigated the possible regulation of β3-integrin by NR4A1. Western blot analysis showed that constitutive β3-integrin protein levels were barely detectable and remained low after treatment with C-DIM/NR4A1 antagonists or siNR4A1 (Fig. 3C), whereas knockdown of β1-integrin by RNAi increased β3-integrin protein as previously reported (36). There was more robust expression of β3-integrin mRNA in MDA-MB-231 and SKBR3 cells, and transfection of siNR4A1 or treatment with C-DIM/NR4A1 antagonists significantly decreased β3-integrin mRNA levels (Fig. 3D). ChIP assays showed that NR4A1, Sp1, and p300 bound the proximal GC-rich region of the β3-integrin gene, and treatment with DIM-C-pPhOH or DIM-C-pPhCO_2Me decreased binding of Pol II, NR4A1, and Sp1 but differentially affected p300 binding to the promoter. In addition, we also observed that knockdown of Sp1 (siSp1) or p300 (sip300) in MDA-MB-231 and SKBR3 cells decreased β3-integrin mRNA levels (Fig. 3E). These results demonstrate that NR4A1 regulates both β1- and β3-integrin expression, and in contrast to β1-integrin-specific inhibitors, NR4A1 antagonists downregulate expression of both β1- and β3-integrin.

Migration of MDA-MB-231 and SKBR3 cells: roles of NR4A1 and β1-integrin. Both MDA-MB-231 and SKBR3 cells undergo migration (constitutive) in a Boyden chamber assay in the absence of a stimulus. Transfection of these cells with siNR4A1 (Fig. 4A) or siβ1-integrin (Fig. 4B) decreased migration of both cell lines, and similar results were observed with two oligonucleotides targeting NR4A1 and β1-integrin. Treatment of SKBR3 and MDA-MB-231 cells with DIM-C-pPhOH (CDIM8) or DIM-C-pPhCO_2Me (CDIM14) also decreased migration (Fig. 4C), and the effects of DIM-C-pPhOH as an inhibitor of cell migration was not affected by cotreatment with leptomycin B (LMB), confirming that the inhibitory effects of this NR4A1 antagonist did not require nuclear export (25). We also investigated the role of NR4A1 in mediating DIM-C-pPhCO_2Me-dependent inhibition of migration of MDA-MB-231 and SKBR3 cells by knocking down NR4A1 and then treating with the NR4A1 antagonist DIM-C-pPhcO_2Me (Fig. 4E). Treatment of the NR4A1-depleted cells with DIM-C-pPhCO_2Me resulted in minimal inhibition of cell migration. Similar results were observed after treatment of β1-integrin-depleted cells with DIM-C-pPhCO_2Me, and we also observed that DIM-C-pPhOH did not inhibit invasion in cells depleted of NR4A1 or β1-integrin (see Fig. S2 in the supplemental material). This would suggest that induction of β3-integrin after knockdown of β1-integrin (Fig. 3B) does not play a very significant role in cell migration using the Boyden chamber assay. Thus, inhibition of breast cancer cell migration by C-DIMs/NR4A1 antagonists is dependent on both NR4A1 and β1-integrin and consistent with regulation of β1-integrin by NR4A1. Overexpression of β1-integrin in SKBR3 and MDA-MB-231 cells slightly increases cell migration, and in NR4A1-depleted cells which exhibit decreased migration, overexpression of β1-integrin significantly reverses this response (Fig. 4F). In addition, NR4A1 ligand-mediated inhibition of breast cancer cell migration was also rescued by β1-integrin overexpression (Fig. 4G), further confirming that β1-integrin-mediated migration is NR4A1 dependent. Thus, the constitutive or basal migration of SKBR3 and MDA-MB-231 cells in the absence of endogenous stimuli is linked to nuclear NR4A1 regulation of β1-integrin.

TGF-β-induced migration of MDA-MB-231 cells: role of extranuclear NR4A1. A recent study reported that TGF-β-induced migration of MDA-MB-231 cells was also NR4A1 dependent and involved a pathway associated with SMAD7 degradation resulting in activation of TGF-βR receptor 1 (TGF-βR1) (31). Treatment of MDA-MB-231 cells with 5 ng/ml TGF-β significantly induced cell migration (Fig. 5A) as previously described (31), and knockdown of NR4A1 or treatment with DIM-C-pPhOH or DIM-C-pPhCO_2Me blocked TGF-β-induced migration and significantly decreased overall migration, similar to that observed after knockdown of NR4A1 or treatment with the NR4A1 antagonists alone (Fig. 4A to C). TGF-β-induced migration was inhibited after cotreatment with the TGF-βR1 inhibitor ALK5i and also the nuclear export inhibitor LMB, and ALK5i had no effect on endogenous cell migration (data not shown). Analysis of cytosolic and nuclear extracts show that TGF-β induced expression and nuclear export of NR4A1 which was blocked by LMB (Fig. 5B) indicating that TGF-β-induced migration requires cytosolic NR4A1, whereas constitutive migration which is not inhibited by ALK5i is due to nuclear NR4A1-dependent regulation of β1-integrin. We also examined SMAD7 expression and observed minimal endogenous expression in MDA-MB-231 and SKBR3 cells, and TGF-β increased SMAD7 only in SKBR3 cells (Fig. 5C). In contrast, cotreatment with TGF-β plus LMB, CDIM8, or CDIM14 dramatically increased SMAD7 protein expression of both cell lines, suggesting that nuclear localization of NR4A1 inhibits degradation of

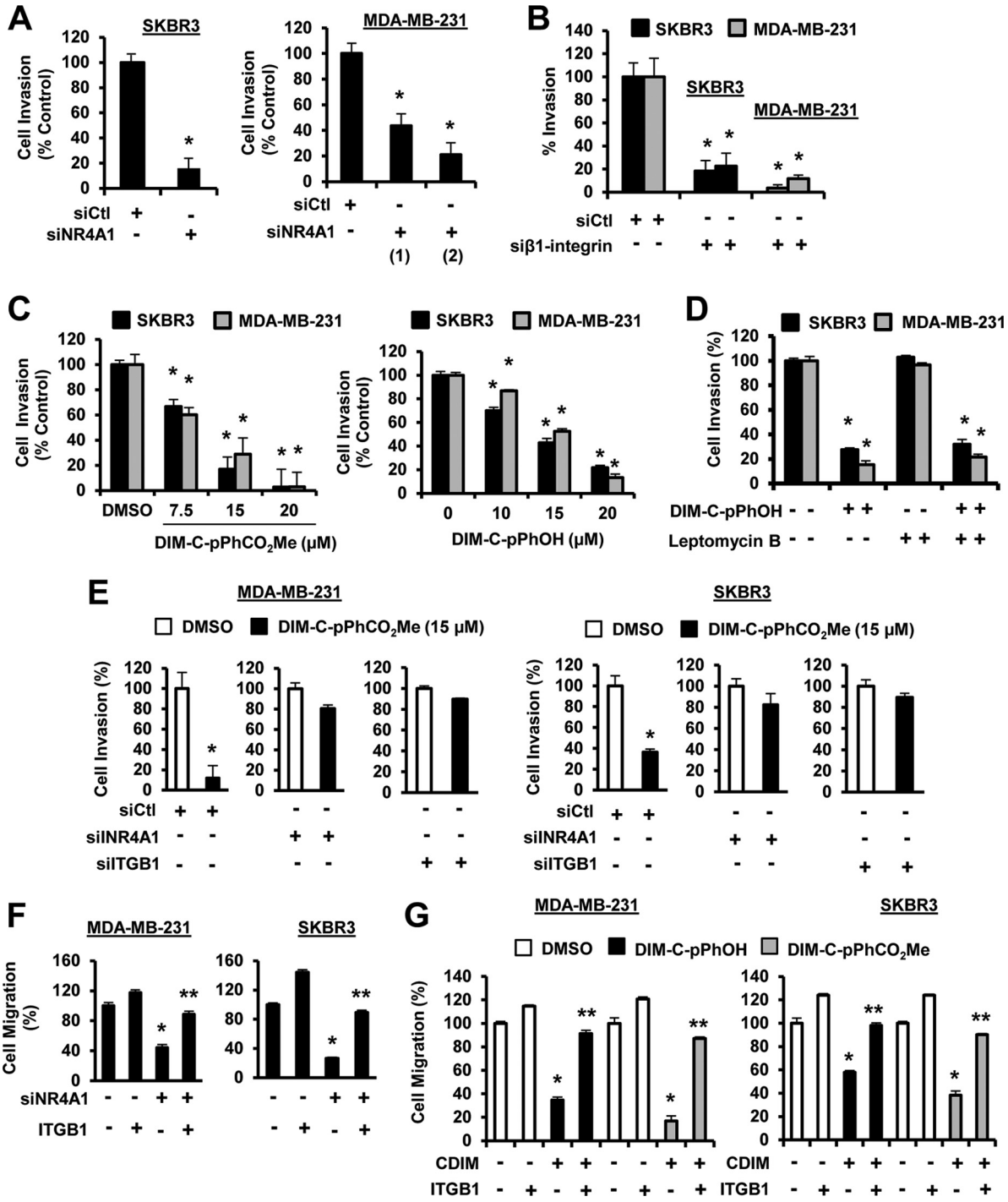

FIG 4 NR4A1 regulates β1-integrin-dependent breast cancer cell migration. (A to D) Cells were transfected with siNR4A1 (A) or siβ1-integrin (B) or treated with DIM-C-pPhOH and DIM-C-pPhCO$_2$Me (C) and DIM-C-pPhOH with or without leptomycin B (LMB) (D), and breast cancer cell migration was determined in a Boyden chamber assay as outlined in Materials and Methods. (E) Cells were transfected with a nonspecific oligonucleotide (siCtl), siNR4A1, or siβ1-integrin and treated with DIM-C-pPhCO$_2$Me, and cell migration was determined in a Boyden chamber assay as outlined in Materials and Methods. (F and G) Cells were transfected with siNR4A1 alone (F) or treated with DIM-C-pPhOH/DIM-C-pPhCO$_2$Me (G) in combination with a β1-integrin (ITGB1) expression plasmid, and effects on cell migration were determined in a Boyden chamber assay as outlined in Materials and Methods. Results are expressed as means plus SE (error bars) for at least three replicates for each treatment group, and significantly ($P < 0.05$) decreased migration (*) or rescue by β1-integrin overexpression (**) is indicated.

SMAD7, which is a cytosolic protein. These results are consistent with previous studies, suggesting that NR4A1 (cytosolic) plays a role in proteasome-dependent degradation of SMAD7 (31). Immunostaining of NR4A1 in MDA-MB-231 cells confirms that NR4A1 is nuclear, and treatment with TGF-β induces nuclear export of this receptor, and this is blocked by LMB (Fig. 5C).

Since C-DIM/NR4A1 antagonists act through binding nuclear NR4A1, we examined the effects of short-term (4-h) treatment of

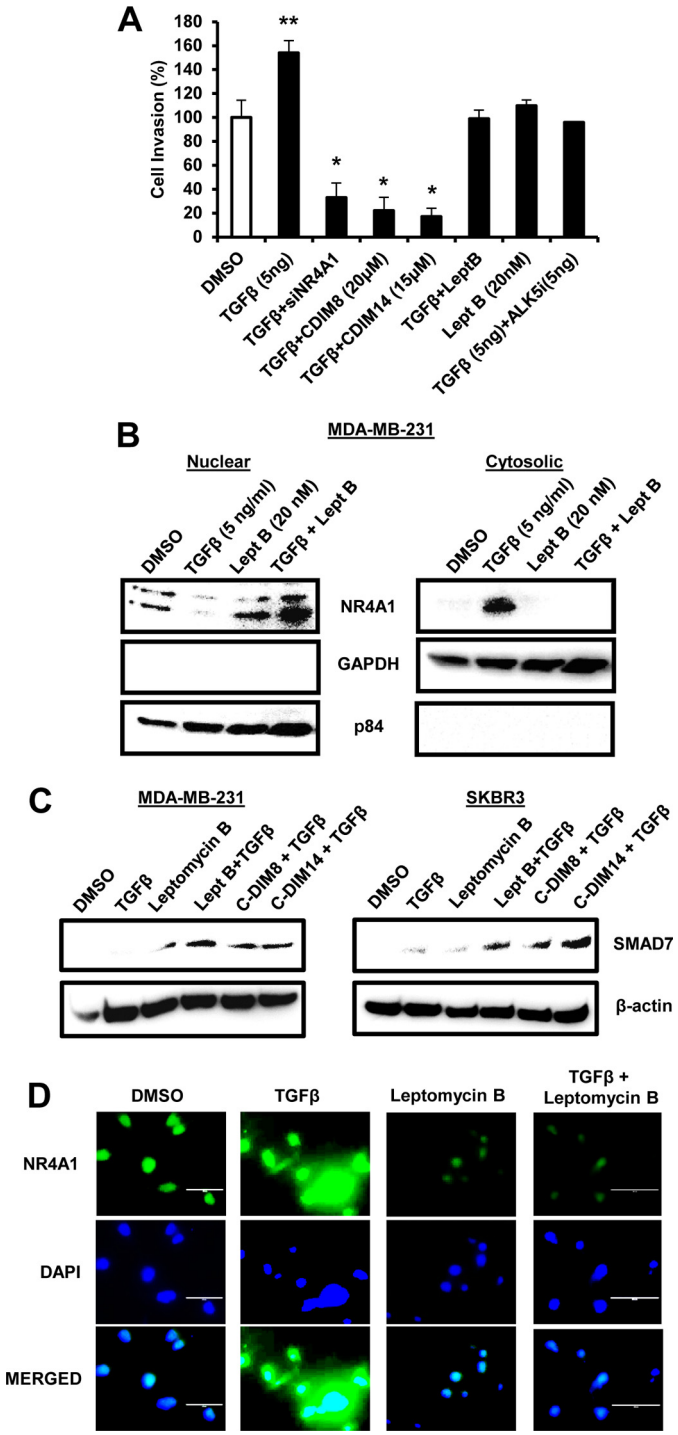

FIG 5 Role of NR4A1 on TGF-β-induced migration of MDA-MB-231 cells. (A) MDA-MB-231 cells were treated with TGF-β alone for 4 h or in combination with siNR4A1, DIM-C-pPhOH, and DIM-C-pPhCO$_2$Me (24-h treatment), LMB and ALK5i, and LMB (alone). Cell migration was determined in a Boyden chamber assay. (B) MDA-MB-231 cells were treated with DMSO, TGF-β, and LMB (alone) and in combination for 4 h. Nuclear and cytosolic extracts were analyzed by Western blotting using nuclear (p84) and cytosolic (GADPH) loading controls. (C) Cells were treated with DMSO, TGF-β, LMB alone, and TGF-β in combination with LMB, DIM-C-pPhOH (CDIM8), or DIM-C-pPhCO$_2$Me (CDIM14) for 4 h, and whole-cell lysates were analyzed for SMAD7 expression by Western blot analysis. (D) Cells were treated with DMSO, 5 ng/ml TGF-β, LMB, and LMB plus TGF-β for 4 h and immunostained with both NR4A1 antibodies and DAPI as outlined in Materials and Methods.

MDA-MB-231 with DIM-C-pPhOH or DIM-C-pPhCO$_2$Me on TGF-β-induced migration. Like LMB, both compounds blocked TGF-β-induced migration (Fig. 6A), and this was accompanied by inhibition of TGF-β-induced nuclear export of NR4A1 (Fig. 6B) and paralleled results observed for LMB (Fig. 5A and B). The inhibitory effects observed after treatment with the C-DIM/NR4A1 ligands for 4 h were not due to decreased β1-integrin expression (Fig. 6C), suggesting that bound NR4A1 was resistant to TGF-β-induced nuclear export, and the factors that regulate nuclear export are currently being investigated. A previous report showed that TGF-β-induced NR4A1 interacts with axin 2 and other factors (e.g., E3 ligases Arkadia and RNF12) to form a polyubiquitination complex (31), and after treatment of MDA-MB-231 cells with TGF-β, LMB, C-DIMs, and their combinations, Western blot analysis of the cytosolic fraction immunoprecipitated with axin 2 antibodies gave a strong band for NR4A1 only in cells treated with TGF-β alone (Fig. 6D). In contrast, treatment with DIM-C-pPhOH, DIM-C-pPhCO$_2$Me, or LMB, which inhibit TGF-β-induced nuclear export of NR4A1, resulted in decreased intensities of cytosolic NR4A1 bands associated with the axin 2 antibody immunoprecipitates. The results demonstrate that NR4A1 plays an important role in breast cancer cell migration by regulation of β1-integrin (endogenous activity) and TGF-β-induced migration which is dependent on NR4A1 nuclear export (Fig. 6E).

DISCUSSION

The NR4A family of orphan nuclear receptors NR4A1, NR4A2, and NR4A3 were initially identified as stress-induced immediate early genes with a characteristic domain structure observed for nuclear receptors. NR4A receptors have both unique and overlapping functions, and there is increasing evidence that they play an important role in cellular homeostasis and diseases associated with metabolism, cardiovascular and neurological functions, inflammation, and the immune system (38–40). Endogenous ligands for NR4A1 have not been identified; however, synthetic ligands that are structurally related to cytosporone B have been developed (41–43) and have potential clinical applications. For example, ethyl[2,3,4-trimethoxy-6-(*i*-octanoyl)phenyl]acetate is an NR4A1 ligand that acts as a receptor antagonist to decrease NR4A1-dependent hepatic gluconeogenesis and lower blood glucose levels in a rodent model for type 2 diabetes (43). NR4A1 is also overexpressed in solid tumors including both ER-positive and ER-negative breast tumors and is a negative prognostic factor for lung, colon, and breast cancer patients (26, 31, 44).

Initial studies targeting NR4A1 for cancer chemotherapy showed that cell death observed in some cancer cell lines treated with several apoptosis agents was due to nuclear export of NR4A1 and the subsequent interactions of NR4A1 with bcl-2 to form a proapoptotic complex that disrupted mitochondria (45, 46). The proapoptotic effects were also observed using peptides and paclitaxel that mimic NR4A1 interactions with bcl-2 (42, 47). Studies in this laboratory have identified C-DIMs as NR4A1 ligands that act as antagonists in cancer cell lines, and previous studies have demonstrated that C-DIM/NR4A1 antagonists inhibit growth and induce cell death through inactivation of nuclear NR4A1-dependent prooncogenic pathways in pancreatic, lung, colon, kidney, and breast cancer cell lines (24–30).

A recent report showed that high expression of NR4A1 in breast tumors correlated with decreased relapse-free survival, and this was linked to the role of NR4A1 in TGF-β and TGF-β/cyto-

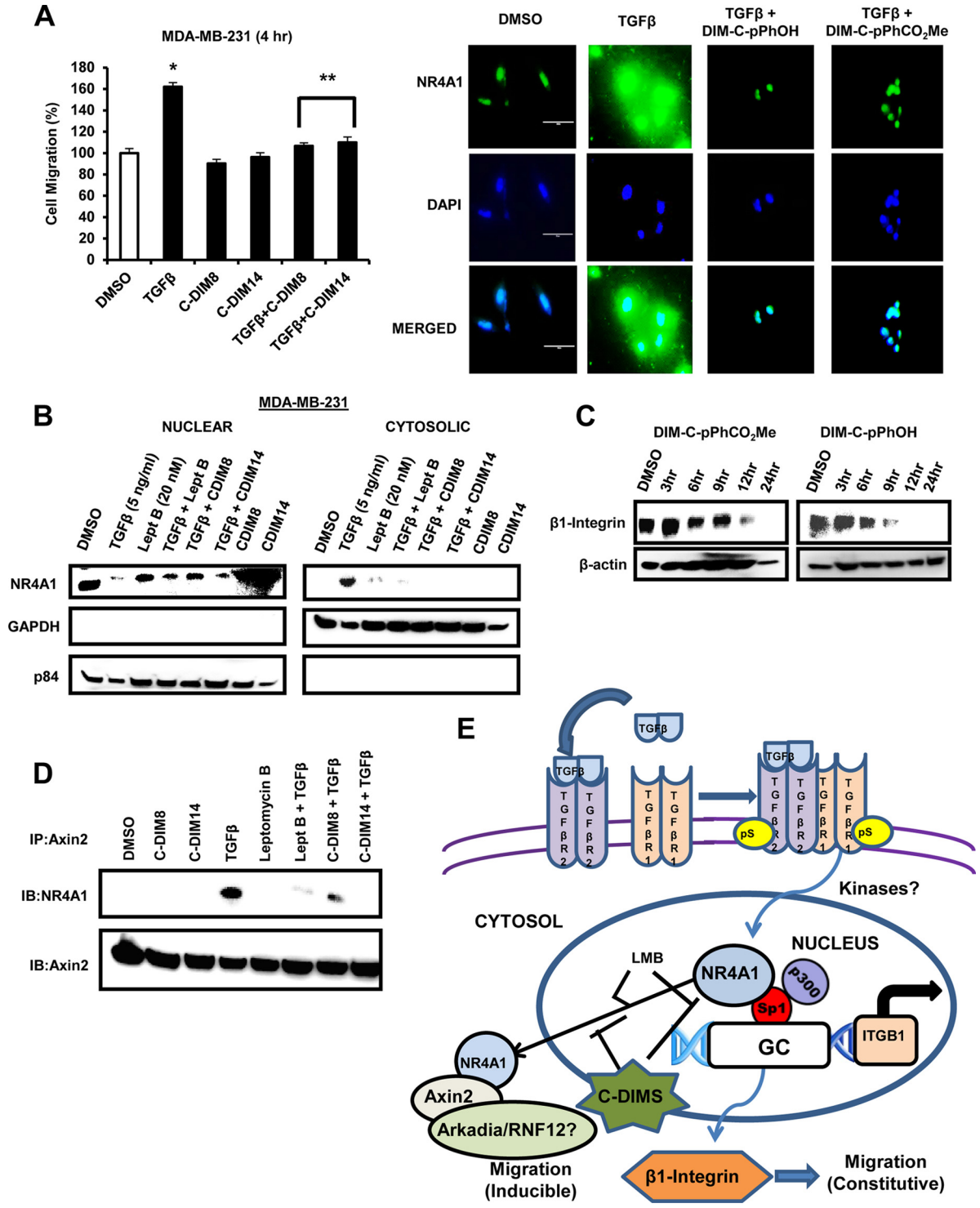

FIG 6 (A) MDA-MB-231 cells were treated with TGF-β, DIM-C-pPhOH, and DIM-C-pPhCO$_2$Me alone and TGF-β plus C-DIMs for 4 h, and cell migration was determined in a Boyden chamber assay and immunostaining (NR4A1) and DAPI staining was determined as outlined in the legend to Fig. 5C. (B) Cells were treated as described in the legend to Fig. 5B, and the cytosolic and nuclear extracts were further examined by Western blot analyses. (C) MDA-MB-231 cells were treated with DIM-C-pPhCO$_2$Me or DIM-C-pPhOH for different times, and whole-cell lysates were analyzed by Western blotting for β1-integrin expression. (D) Cells were treated as outlined above for panel B, and whole-cell lysates were immunoprecipitated with axin 2 antibodies (IP:Axin2) and analyzed by Western blotting (immunoblotting [IB]). (E) Schematic outline of the role of NR4A1 in constitutive and TGF-β-induced migration in breast cancer cells.

kine-induced migration/invasion and metastasis (31). Results of ongoing genomic and functional studies in several cancer cell lines identified β-*integrin* as a possible NR4A1-regulated promigration/invasion gene, and this correlated with previous *in vivo* studies showing that β1-integrin was important for metastasis of mammary tumors overexpressing the *erbB2* oncogene (9, 21–23). Results in Fig. 1, 2, and 4 demonstrate that knockdown of NR4A1 or treatment with the NR4A1 antagonists DIM-C-pPhOH and DIM-C-pPhCO$_2$Me decreased expression of β1-integrin protein and mRNA and β1-integrin-dependent responses in MCF7, MDA-MB-231, and SKBR3 cells and also inhibited migration of the latter two cell lines.

The mechanism of NR4A1 regulation of β-integrin in SKBR3 and MDA-MB-231 cells did not involve direct binding to *cis*-acting genomic sequences but through an indirect mechanism in which NR4A1/p300 act as a coregulatory complex to activate Sp1-regulated genes. The ChIP assays show that NR4A1, Sp1, and p300 interacted at the GC-rich region of the β*1-integrin* gene promoter (Fig. 3), and knockdown of any one of these factors or treatment with C-DIM/NR4A1 antagonists resulted in decreased β1-integrin expression. These results are similar to those previously observed for NR4A1/p300/Sp1-mediated regulation of survivin in pancreatic cancer cells (25) and are consistent with other reports showing that other nuclear receptors also regulate expression of other Sp-dependent genes through NR4A1/Sp1 complexes (48–50). Previous studies show that knockdown or inhibition of β1-integrin in breast cancer cells results in the expression of β3-integrin, and this "integrin-switching" enhances TGF-β-induced metastasis (34–36), which presents a problem for applications of β1-integrin inhibitors in treatment of breast cancer. Like β1-integrin, the 5′-promoter region of the β3-integrin gene contains GC-rich sequences (37), and our results demonstrate that NR4A1 also regulates β3-integrin expression, and NR4A1 antagonists or NR4A1 knockdown decreases expression of both genes (Fig. 3). Thus, coregulation of β1- and β3-integrin by NR4A1 negates the "integrin-switching" phenomena (34–36) and further demonstrates that the C-DIM/NR4A1 antagonists represent a novel therapeutic approach for inhibiting β1/β3-integrin-induced signaling and metastasis in breast cancer cells.

MDA-MB-231 and SKBR3 cells readily migrate in the absence of TGF-β or cytokine stimulus, and results of RNAi studies show that inhibition of cell migration by C-DIM/NR4A1 antagonists was observed only in cells expressing NR4A1 or β1-integrin (Fig. 4). Moreover, since the inhibitory effects of C-DIMs were similar in the presence or absence of the nuclear export inhibitor LMB (Fig. 4F), our results indicate that constitutive migration of these cells was due to nuclear NR4A1-dependent regulation of β1-integrin. This is also supported by the observation that the TGF-β receptor inhibitor ALK5i inhibits TGF-β-induced migration but does not affect the high rate of constitutive migration of MDA-MB-231 cells (Fig. 5A). A recent study showed that NR4A1 was also required for TGF-β-induced migration of MDA-MB-231 and other cell lines, and this was due to interactions of NR4A1, axin 2, and E3 ligases which enhanced SMAD7 degradation, resulting in activation of the TGF-βR1 pathway (31). We also observed that TGF-β induced NR4A1 expression and migration of MDA-MB-231 cells; however, the key essential element in this pathway was that TGF-β induced nuclear export of NR4A1 (Fig. 5B and D and 6C). Moreover, inhibition of nuclear export by the NR4A1 ligands (DIM-C-pPhOH or DIM-C-pPhcO$_2$Me) or LMB also blocked TGF-β-induced migration and enhanced SMAD7 expression (Fig. 5C). Previous studies on SMAD7 degradation in MDA-MB-231 cells used transfected FLAG-SMAD7 (31), whereas in this study, we observed low to nondetectable SMAD7 expression in MDA-MBA-231 and SKBR3 cells. However, LMB, DIM-C-pPhOH, and DIM-C-pPhCO$_2$Me which prevent NR4A1 export also increased SMAD7 expression in cells cotreated with these compounds plus TGF-β (Fig. 5C), and this is consistent with a role for cytosolic NR4A1 in SMAD7 degradation as previously reported (31). Thus, TGF-β-induced migration of MDA-MB-231 cells is due to nuclear export of NR4A1, and the C-DIM/NR4A1 antagonist blocks this pathway presumably by inhibiting factors/pathways required for nuclear export, and these factors/pathways are currently being investigated.

In summary, results of this study show that nuclear NR4A1 regulates β1-integrin expression in breast cancer cells, and C-DIM/NR4A1 antagonists inhibit expression of β1-integrin and β1-integrin-mediated responses, including cell migration, and the antagonists also inhibit NR4A1-regulated expression of β3-integrin. In contrast, TGF-β-induced migration of MDA-MB-231 cells requires nuclear export of NR4A1 which is inhibited not only by LMB but also by C-DIM/NR4A1 antagonists. Thus, constitutive migration and TGF-β-induced migration are dependent on nuclear and extranuclear NR4A1, respectively, and the C-DIM/NR4A1 antagonists inhibit both pathways by decreasing NR4A1-dependent expression of β1-integrin and by inhibition of TGF-β-induced nuclear export of NR4A1 (Fig. 6E). This study expands on the prooncogenic functions of NR4A1 and indicates that C-DIM compounds and other NR4A1 antagonists represent an important new class of mechanism-based anticancer drugs for treating patients with tumors overexpressing this receptor.

ACKNOWLEDGMENTS

The financial assistance of the National Institutes of Health (P30-ES023512, S. Safe), the DOD-CDRMP (BC103116, M. Singh), Texas AgriLife Research and Sid Kyle endowment, is gratefully acknowledged.

E.H. carried out the *in vitro* studies and assisted in writing the manuscript. S.-O.L. carried out some of the *in vitro* studies and initially identified β1-integrin as an NR4A1-regulated gene. R.D. carried out the *in vivo* studies. M.S. supervised the *in vivo* studies and carried out data analysis. S.S. developed the C-DIMs as NR4A1 antagonists, supervised the studies, and wrote the manuscript.

We declare that we have no conflicts of interest that would prejudice the impartiality of this research.

FUNDING INFORMATION

This work, including the efforts of Mandip Singh, was funded by DOD | Congressionally Directed Medical Research Programs (CDMRP) (BC103116). This work, including the efforts of Stephen Safe, was funded by HHS | NIH | National Institute of Environmental Health Sciences (NIEHS) (P30-ES023512). This work, including the efforts of Stephen Safe, was funded by Texas AgriLife Research.

The funders had no role in study design, data collection and interpretation, or the decision to submit the work for publication.

REFERENCES

1. **Shattil SJ, Kim C, Ginsberg MH.** 2010. The final steps of integrin activation: the end game. Nat Rev Mol Cell Biol **11:**288–300. http://dx.doi.org/10.1038/nrm2871.
2. **Arnaout MA, Goodman SL, Xiong JP.** 2007. Structure and mechanics of integrin-based cell adhesion. Curr Opin Cell Biol **19:**495–507. http://dx.doi.org/10.1016/j.ceb.2007.08.002.

3. **Hynes RO.** 2002. Integrins: bidirectional, allosteric signaling machines. Cell **110:**673–687. http://dx.doi.org/10.1016/S0092-8674(02)00971-6.
4. **Goodman SL, Picard M.** 2012. Integrins as therapeutic targets. Trends Pharmacol Sci **33:**405–412. http://dx.doi.org/10.1016/j.tips.2012.04.002.
5. **Desgrosellier JS, Cheresh DA.** 2010. Integrins in cancer: biological implications and therapeutic opportunities. Nat Rev Cancer **10:**9–22. http://dx.doi.org/10.1038/nrc2748.
6. **Brakebusch C, Fassler R.** 2005. β1-Integrin function in vivo: adhesion, migration and more. Cancer Metastasis Rev **24:**403–411. http://dx.doi.org/10.1007/s10555-005-5132-5.
7. **Barkan D, Chambers AF.** 2011. β1-Integrin: a potential therapeutic target in the battle against cancer recurrence. Clin Cancer Res **17:**7219–7223. http://dx.doi.org/10.1158/1078-0432.CCR-11-0642.
8. **Howe GA, Addison CL.** 2012. β1 Integrin: an emerging player in the modulation of tumorigenesis and response to therapy. Cell Adh Migr **6:**71–77. http://dx.doi.org/10.4161/cam.20077.
9. **Lahlou H, Muller WJ.** 2011. Beta1-integrins signaling and mammary tumor progression in transgenic mouse models: implications for human breast cancer. Breast Cancer Res **13:**229. http://dx.doi.org/10.1186/bcr2905.
10. **Wang D, Muller S, Amin AR, Huang D, Su L, Hu Z, Rahman MA, Nannapaneni S, Koenig L, Chen Z, Tighiouart M, Shin DM, Chen ZG.** 2012. The pivotal role of integrin beta1 in metastasis of head and neck squamous cell carcinoma. Clin Cancer Res **18:**4589–4599. http://dx.doi.org/10.1158/1078-0432.CCR-11-3127.
11. **Oshita F, Kameda Y, Hamanaka N, Saito H, Yamada K, Noda K, Mitsuda A.** 2004. High expression of integrin beta1 and p53 is a greater poor prognostic factor than clinical stage in small-cell lung cancer. Am J Clin Oncol **27:**215–219. http://dx.doi.org/10.1097/01.COC.0000054894.64867.80.
12. **Yao ES, Zhang H, Chen YY, Lee B, Chew K, Moore D, Park C.** 2007. Increased beta1 integrin is associated with decreased survival in invasive breast cancer. Cancer Res **67:**659–664. http://dx.doi.org/10.1158/0008-5472.CAN-06-2768.
13. **dos Santos PB, Zanetti JS, Ribeiro-Silva A, Beltrao EI.** 2012. Beta 1 integrin predicts survival in breast cancer: a clinicopathological and immunohistochemical study. Diagn Pathol **7:**104. http://dx.doi.org/10.1186/1746-1596-7-104.
14. **Wei G, Du Y, Yang C, Zhang X.** 2008. The expression and significance of integrin beta1 and focal adhesion kinase and its clinical value in laryngeal carcinoma. Lin Chung Er Bi Yan Hou Tou Jing Wai Ke Za Zhi **22:**1112–1114. (In Chinese.)
15. **Nikkola J, Vihinen P, Vlaykova T, Hahka-Kemppinen M, Heino J, Pyrhonen S.** 2004. Integrin chains beta1 and alphav as prognostic factors in human metastatic melanoma. Melanoma Res **14:**29–37.
16. **Pontes-Junior J, Reis ST, de Oliveira LC, Sant'anna AC, Dall'oglio MF, Antunes AA, Ribeiro-Filho LA, Carvalho PA, Cury J, Srougi M, Leite KR.** 2010. Association between integrin expression and prognosis in localized prostate cancer. Prostate **70:**1189–1195. http://dx.doi.org/10.1002/pros.21153.
17. **Bottger TC, Maschek H, Lobo M, Gottwohl RG, Brenner W, Junginger T.** 1999. Prognostic value of immunohistochemical expression of beta-1 integrin in pancreatic carcinoma. Oncology **56:**308–313. http://dx.doi.org/10.1159/000011984.
18. **Luo M, Guan JL.** 2010. Focal adhesion kinase: a prominent determinant in breast cancer initiation, progression and metastasis. Cancer Lett **289:**127–139. http://dx.doi.org/10.1016/j.canlet.2009.07.005.
19. **Theocharis SE, Klijanienko JT, Padoy E, Athanassiou S, Sastre-Garau XX.** 2009. Focal adhesion kinase (FAK) immunocytochemical expression in breast ductal invasive carcinoma (DIC): correlation with clinicopathological parameters and tumor proliferative capacity. Med Sci Monit **15:**BR221–BR226.
20. **Yom CK, Noh DY, Kim WH, Kim HS.** 2011. Clinical significance of high focal adhesion kinase gene copy number and overexpression in invasive breast cancer. Breast Cancer Res Treat **128:**647–655. http://dx.doi.org/10.1007/s10549-010-1150-2.
21. **Lahlou H, Sanguin-Gendreau V, Zuo D, Cardiff RD, McLean GW, Frame MC, Muller WJ.** 2007. Mammary epithelial-specific disruption of the focal adhesion kinase blocks mammary tumor progression. Proc Natl Acad Sci U S A **104:**20302–20307. http://dx.doi.org/10.1073/pnas.0710091104.
22. **White DE, Kurpios NA, Zuo D, Hassell JA, Blaess S, Mueller U, Muller WJ.** 2004. Targeted disruption of beta1-integrin in a transgenic mouse model of human breast cancer reveals an essential role in mammary tumor induction. Cancer Cell **6:**159–170. http://dx.doi.org/10.1016/j.ccr.2004.06.025.
23. **Huck L, Pontier SM, Zuo DM, Muller WJ.** 2010. β1-Integrin is dispensable for the induction of ErbB2 mammary tumors but plays a critical role in the metastatic phase of tumor progression. Proc Natl Acad Sci U S A **107:**15559–15564. http://dx.doi.org/10.1073/pnas.1003034107.
24. **Safe S, Jin UH, Hedrick E, Reeder A, Lee SO.** 2014. Role of orphan nuclear receptors in cancer and potential as drug targets. Mol Endocrinol **28:**157–172. http://dx.doi.org/10.1210/me.2013-1291.
25. **Lee SO, Abdelrahim M, Yoon K, Chintharlapalli S, Papineni S, Kim K, Wang H, Safe S.** 2010. Inactivation of the orphan nuclear receptor TR3/Nur77 inhibits pancreatic cancer cell and tumor growth. Cancer Res **70:**6824–6836. http://dx.doi.org/10.1158/0008-5472.CAN-10-1992.
26. **Lee SO, Andey T, Jin UH, Kim K, Singh M, Safe S.** 2012. The nuclear receptor TR3 regulates mTORC1 signaling in lung cancer cells expressing wild-type p53. Oncogene **31:**3265–3276. http://dx.doi.org/10.1038/onc.2011.504.
27. **Lee SO, Jin UH, Kang JH, Kim SB, Guthrie AS, Sreevalsan S, Lee JS, Safe S.** 2014. The orphan nuclear receptor NR4A1 (Nur77) regulates oxidative and endoplasmic reticulum stress in pancreatic cancer cells. Mol Cancer Res **12:**527–538. http://dx.doi.org/10.1158/1541-7786.MCR-13-0567.
28. **Lee SO, Li X, Hedrick E, Jin UH, Tjalkens RB, Backos DS, Li L, Zhang Y, Wu Q, Safe S.** 2014. Diindolylmethane analogs bind NR4A1 and are NR4A1 antagonists in colon cancer cells. Mol Endocrinol **28:**1729–1739. http://dx.doi.org/10.1210/me.2014-1102.
29. **Hedrick E, Lee SO, Kim G, Abdelrahim M, Jin UH, Safe S, Abudayyeh A.** 2015. Nuclear receptor 4A1 (NR4A1) as a drug target for renal cell adenocarcinoma. PLoS One **10:**e0128308. http://dx.doi.org/10.1371/journal.pone.0128308.
30. **Hedrick E, Lee SO, Doddapaneni R, Singh M, Safe S.** 2015. Nuclear receptor 4A1 as a drug target for breast cancer chemotherapy. Endocr Relat Cancer **22:**831–840. http://dx.doi.org/10.1530/ERC-15-0063.
31. **Zhou F, Drabsch Y, Dekker TJ, de Vinuesa AG, Li Y, Hawinkels LJ, Sheppard KA, Goumans MJ, Luwor RB, de Vries CJ, Mesker WE, Tollenaar RA, Devilee P, Lu CX, Zhu H, Zhang L, Dijke PT.** 2014. Nuclear receptor NR4A1 promotes breast cancer invasion and metastasis by activating TGF-beta signalling. Nat Commun **5:**3388. http://dx.doi.org/10.1038/ncomms4388.
32. **Wilson TE, Padgett KA, Johnston M, Milbrandt J.** 1993. A genetic method for defining DNA-binding domains: application to the nuclear receptor NGFI-B. Proc Natl Acad Sci U S A **90:**9186–9190. http://dx.doi.org/10.1073/pnas.90.19.9186.
33. **Philips A, Lesage S, Gingras R, Maira MH, Gauthier Y, Hugo P, Drouin J.** 1997. Novel dimeric Nur77 signaling mechanism in endocrine and lymphoid cells. Mol Cell Biol **17:**5946–5951. http://dx.doi.org/10.1128/MCB.17.10.5946.
34. **Parvani JG, Galliher-Beckley AJ, Schiemann BJ, Schiemann WP.** 2013. Targeted inactivation of β1 integrin induces β3 integrin switching, which drives breast cancer metastasis by TGF-β. Mol Biol Cell **24:**3449–3459. http://dx.doi.org/10.1091/mbc.E12-10-0776.
35. **Truong HH, Xiong J, Ghotra VP, Nirmala E, Haazen L, Le Devedec SE, Balcioglu HE, He S, Snaar-Jagalska BE, Vreugdenhil E, Meerman JH, van de Water B, Danen EH.** 2014. β1 Integrin inhibition elicits a prometastatic switch through the TGFβ-miR-200-ZEB network in E-cadherin-positive triple-negative breast cancer. Sci Signal **7:**ra15. http://dx.doi.org/10.1126/scisignal.2004751.
36. **Madamanchi A, Zijlstra A, Zutter MM.** 2014. Flipping the switch: integrin switching provides metastatic competence. Sci Signal **7:**pe9. http://dx.doi.org/10.1126/scisignal.2005236.
37. **Villa-Garcia M, Li L, Riely G, Bray PF.** 1994. Isolation and characterization of a TATA-less promoter for the human β3 integrin gene. Blood **83:**668–676.
38. **Kurakula K, Koenis DS, van Tiel CM, de Vries CJ.** 2014. NR4A nuclear receptors are orphans but not lonesome. Biochim Biophys Acta **1843:**2543–2555. http://dx.doi.org/10.1016/j.bbamcr.2014.06.010.
39. **Pearen MA, Muscat GE.** 2010. Nuclear hormone receptor 4A signaling: implications for metabolic disease. Mol Endocrinol **24:**1891–1903. http://dx.doi.org/10.1210/me.2010-0015.
40. **Safe S, Jin UH, Morpurgo B, Abudayyeh A, Singh M, Tjalkens RB.** 23 April 2015. Nuclear receptor 4A (NR4A) family - orphans no more. J Steroid Biochem Mol Biol http://dx.doi.org/10.1016/j.jsbmb.2015.04.016.

41. **Liu JJ, Zeng HN, Zhang LR, Zhan YY, Chen Y, Wang Y, Wang J, Xiang SH, Liu WJ, Wang WJ, Chen HZ, Shen YM, Su WJ, Huang PQ, Zhang HK, Wu Q.** 2010. A unique pharmacophore for activation of the nuclear orphan receptor Nur77 in vivo and in vitro. Cancer Res **70:**3628–3637. http://dx.doi.org/10.1158/0008-5472.CAN-09-3160.
42. **Kolluri SK, Zhu X, Zhou X, Lin B, Chen Y, Sun K, Tian X, Town J, Cao X, Lin F, Zhai D, Kitada S, Luciano F, O'Donnell E, Cao Y, He F, Lin J, Reed JC, Satterthwait AC, Zhang XK.** 2008. A short Nur77-derived peptide converts Bcl-2 from a protector to a killer. Cancer Cell **14:**285–298. http://dx.doi.org/10.1016/j.ccr.2008.09.002.
43. **Zhan YY, Chen Y, Zhang Q, Zhuang JJ, Tian M, Chen HZ, Zhang LR, Zhang HK, He JP, Wang WJ, Wu R, Wang Y, Shi C, Yang K, Li AZ, Xin YZ, Li TY, Yang JY, Zheng ZH, Yu CD, Lin SC, Chang C, Huang PQ, Lin T, Wu Q.** 2012. The orphan nuclear receptor Nur77 regulates LKB1 localization and activates AMPK. Nat Chem Biol **8:**897–904. http://dx.doi.org/10.1038/nchembio.1069.
44. **Wu H, Lin Y, Li W, Sun Z, Gao W, Zhang H, Xie L, Jiang F, Qin B, Yan T, Chen L, Zhao Y, Cao X, Wu Y, Lin B, Zhou H, Wong AS, Zhang XK, Zeng JZ.** 2011. Regulation of Nur77 expression by beta-catenin and its mitogenic effect in colon cancer cells. FASEB J **25:**192–205. http://dx.doi.org/10.1096/fj.10-166462.
45. **Lin B, Kolluri SK, Lin F, Liu W, Han YH, Cao X, Dawson MI, Reed JC, Zhang XK.** 2004. Conversion of Bcl-2 from protector to killer by interaction with nuclear orphan receptor Nur77/TR3. Cell **116:**527–540. http://dx.doi.org/10.1016/S0092-8674(04)00162-X.
46. **Zhang XK.** 2007. Targeting Nur77 translocation. Expert Opin Ther Targets **11:**69–79. http://dx.doi.org/10.1517/14728222.11.1.69.
47. **Ferlini C, Cicchillitti L, Raspaglio G, Bartollino S, Cimitan S, Bertucci C, Mozzetti S, Gallo D, Persico M, Fattorusso C, Campiani G, Scambia G.** 2009. Paclitaxel directly binds to Bcl-2 and functionally mimics activity of Nur77. Cancer Res **69:**6906–6914. http://dx.doi.org/10.1158/0008-5472.CAN-09-0540.
48. **Pipaon C, Tsai SY, Tsai MJ.** 1999. COUP-TF upregulates NGFI-A gene expression through an Sp1 binding site. Mol Cell Biol **19:**2734–2745. http://dx.doi.org/10.1128/MCB.19.4.2734.
49. **Shimada J, Suzuki Y, Kim SJ, Wang PC, Matsumura M, Kojima S.** 2001. Transactivation via RAR/RXR-Sp1 interaction: characterization of binding between Sp1 and GC box motif. Mol Endocrinol **15:**1677–1692. http://dx.doi.org/10.1210/mend.15.10.0707.
50. **Sugawara A, Uruno A, Kudo M, Ikeda Y, Sato K, Taniyama Y, Ito S, Takeuchi K.** 2002. Transcription suppression of thromboxane receptor gene by peroxisome proliferator-activated receptor-gamma via an interaction with Sp1 in vascular smooth muscle cells. J Biol Chem **277:**9676–9683. http://dx.doi.org/10.1074/jbc.M104560200.

AMERICAN SOCIETY FOR MICROBIOLOGY | Molecular and Cellular Biology®

AUTHOR CORRECTION

Correction for Hedrick et al., "NR4A1 Antagonists Inhibit β1-Integrin-Dependent Breast Cancer Cell Migration"

Erik Hedrick,[a] Syng-Ook Lee,[b] Ravi Doddapaneni,[c] Mandip Singh,[c] Stephen Safe[a]

Department of Veterinary Physiology and Pharmacology, Texas A&M University, College Station, Texas, USA[a]; Department of Food Science and Technology, Keimyung University, Daegu, Republic of Korea[b]; Department of Pharmaceutics, College of Pharmacy and Pharmaceutical Sciences, Florida A&M University, Tallahassee, Florida, USA[c]

Volume 36, no. 9, p. 1383–1394, 2016, https://doi.org/10.1128/MCB.00912-15. Page 1385, Fig. 1: The β-actin controls for the MCF-7 cell lysate analysis for panels A and B were run on the same gel. We inadvertently used in panel A the last two β-actin lanes of panel B, left. The corrected MCF-7 β-actin bands for panel A should appear as shown below.

Page 1386, Fig. 2: The same lysates and β-actin bands from Fig. 1 were used in panels A and B, with the same problem. Therefore, the corrected MCF-7 β-actin bands for panel A should appear as shown above.

Citation Hedrick E, Lee S-O, Doddapaneni R, Singh M, Safe S. 2017. Correction for Hedrick et al., "NR4A1 antagonists inhibit β1-integrin-dependent breast cancer cell migration." Mol Cell Biol 37:e00197-17. https://doi.org/10.1128/MCB.00197-17.

European Journal of Pharmaceutics and Biopharmaceutics 108 (2016) 168–179

Contents lists available at ScienceDirect

European Journal of Pharmaceutics and Biopharmaceutics

journal homepage: www.elsevier.com/locate/ejpb

Research paper

Novel diindolylmethane derivatives based NLC formulations to improve the oral bioavailability and anticancer effects in triple negative breast cancer

Chandraiah Godugu [a,b,1], Ravi Doddapaneni [a,1], Stephen H. Safe [c], Mandip Singh [a,*]

[a] College of Pharmacy and Pharmaceutical Sciences, Florida A&M University, Tallahassee, FL, USA
[b] Department of Regulatory Toxicology, National Institute of Pharmaceutical Education and Research (NIPER), Hyderabad, Telangana 500037, India
[c] Department of Veterinary Physiology and Pharmacology, Texas A&M University, College Station, TX, USA

ARTICLE INFO

Article history:
Received 20 March 2016
Revised 29 July 2016
Accepted in revised form 15 August 2016
Available online 30 August 2016

Keywords:
Triple negative breast cancer (TNBC)
Diindolylmethane
Nano structured lipid carriers
Oral bioavailability

ABSTRACT

The present study demonstrates the promising anticancer effects of novel C-substituted diindolylmethane (DIM) derivatives DIM-10 and DIM-14 in aggressive TNBC models. In vitro studies demonstrated that these compounds possess strong anticancer effects. Caco-2 permeability studies resulted in poor permeability and poor oral bioavailability was demonstrated by pharmacokinetic studies. Nano structured lipid carrier (NLC) formulations were prepared to increase the clinical acceptance of these compounds. Significant increase in oral bioavailability was observed with NLC formulations. Compared to DIM-10, DIM-10 NLC formulation showed increase in C_{max} and AUC values by 4.73 and 11.19-folds, respectively. Similar pattern of increase was observed with DIM-14 NLC formulations. In dogs DIM-10 NLC formulations showed an increase of 2.65 and 2.94-fold in C_{max} and AUC, respectively. The anticancer studies in MDA-MB-231 orthotopic TNBC models demonstrated significant reduction in tumor volumes in DIM-10 and DIM-14 NLC treated animals. Our studies suggest that NLC formulation of both DIM-10 and 14 is effective in TNBC models.

1. Introduction

Triple negative breast cancer (TNBC) is defined by tumors that do not express estrogen, progesterone and human epidermal growth factor receptors, representing approximately 20% of breast cancers. These types of cancers are clinically more aggressive. Currently available chemotherapy based treatment options for TNBC exhibit poor therapeutic benefits and possess serious toxicity issues [19,13]. Considering the challenges involved in treating TNBC and its inherent poor prognosis, there is a need for novel and safer drugs to treat this type of cancer. Recent research is focused on the use of natural products to combat various types of cancer [10,30]. Natural products are available in various dietary supplements; therefore, consumption of these compounds at early stages of cancer may act as chemopreventive agents. On the other hand, the oral route, which is most desirable in anticancer therapy is not possible with many anticancer natural product drugs due to their inherent water insolubility and poor oral absorption. One of the classical examples is curcumin, which has demonstrated to have promising anticancer effects in various cancer types; however, its poor aqueous solubility and limited oral bioavailability limited its broad spectrum applications. Bis(3[1]-indolyl)methane (or 3, 3[1]-diindolylmethane (DIM) is an active metabolite of indole-3-carbinol derived from cruciferous vegetables and exhibits a broad spectrum of anticancer activities. DIM compounds have been reported to be useful in combating various cancer types [36,2]. However, DIM has poor oral bioavailability due to its low solubility/high lipophilicity and has limited oral absorption [14]. Pharmacokinetic studies with DIM indicated that dose-dependent absorption and nonlinear increase in plasma maximum concentrations (C_{max}), suggesting the saturation of systemic absorption [26,27]. In another study, microencapsulated extended release DIM formulations produced increased oral bioavailability, suggesting that solubility is the rate-limiting step in oral bioavailability [27]. Although few studies are available on un-substituted DIM based anticancer effects, their potency was found to be low and C-substituted DIM-analogues were reported to be superior in producing the anticancer effects in lung, breast, prostate cancer, etc. Recently we have also demonstrated that novel self emulsified based DIM-14 and DIM-P formulations produce better anticancer

* Corresponding author.
E-mail address: mandip.sachdeva@gmail.com (M. Singh).
[1] Both the authors contributed equally.

http://dx.doi.org/10.1016/j.ejpb.2016.08.006
0939-6411/

effects in lung cancer models (Ref). Therefore, development of novel orally active C-substituted DIM derivatives (C-DIM analogs) will have major clinical implications for the treatment of TNBC. Among different types of C-DIM analogs reported, DIM-10 and DIM-14 are expected to have significant impact in the treatment of TNBC.

Supplementary Fig. 1 shows the chemical structure of DIM-10 and DIM-14. Our vitro anticancer studies suggested that both DIM-10 and DIM-14 have promising anticancer effects on TNBC cells. However, these compounds found to possess poor aqueous solubility. The Caco-2 permeability studies also indicated the poor permeability. To overcome the limited solubility and associated poor oral bioavailability problems of these promising C-DIM analogs, novel nanotechnology based oral formulations were attempted. There is a growing interest in enhancing the bioavailability of poorly bioavailable drugs using novel nanoformulations mediated enhanced lymphatic absorption. In order to bring these compounds more closer to the human applications as orally administrable anticancer and chemopreventive agents, we have developed DIM-10 and DIM-14 loaded nano structured lipid carriers (NLCs) based novel nanoformulations [3]. The pharmacokinetic (PK) studies were performed in rats and selected formulations were further studied in dogs. Finally, these formulations were evaluated in MDA-MB-231 orthotopic TNBC mouse models. This is the first attempt to prepare DIM-10 and DIM-14 loaded NLC formulations and demonstrate their anticancer effects in orthotopic TNBC nude mode models.

2. Materials and methods

2.1. Materials

DIM-10 and DIM-14 were synthesized and provided by Dr. Stephen Safe (Texas A&M University). The primary antibodies Cleaved Caspase 3, Cyclin D1, PCNA and B-actin were procured from Santa Cruz Biotechnology Inc. Protein assay kit was purchased from Pierce™ BCA Protein Assay Kit. VEGF kit was purchased from Thermo Fisher scientific Inc. Human TNBC cell lines (MDA-MB-231, 453 and 468) and other breast cancer cell lines such as SKBR3 and BT474 cells and Caco-2 cell lines were procured from ATCC, USA.

2.2. DIM-10 and DIM-14 in vitro anticancer activities

In vitro cytotoxicity, cell migration and clonogenic studies were performed to demonstrate the anticancer activity of DIM-10 and DIM-14 on TNBC cell lines (MDA-MB-231, MDA-MB-468 and MDA-MB-435 cells). For cytotoxicity assay, TNBC cells were plated in 96 well plates at 10,000 cells/well density. After overnight incubation, cells were treated with various concentrations of DIM-10 and DIM-14, and 0.1% DMSO treated cells were considered as control cells. After 72 h treatment, cells were fixed and cell viability was measured by crystal violet staining (0.05%). Cell viability Percentage was calculated by considering DMSO treated control cells as 100% viable. Clonogenic assay was performed to demonstrate the inhibitory effects C-DIMs on cell reproduction. For this assay, MDA-MB-468 cells were placed in 24-well plate at a density of 100 cells/well, after 24 h cells were treated with DIM-10 and DIM-14. The cells were washed with media 48 h after the treatment and were allowed to grow for 2 weeks, and during this period medium was changed every alternative day. The individual cells grown as spheroids were fixed with glutaraldehyde and stained with crystal violet. The groups of cells more than 50 in number were considered as colonies. Colonies were counted under microscope, their sizes were recorded, and representative spheroid images were captured.

Effect of DIM-10 and DIM-14 on cell migration: Cell migration assay is performed to study the antimetastatic effect of compounds in in vitro conditions. In this assay 50,000/well of MDA-MB-231 cells were placed in 24 well plates, cells were allowed to grow near to full confluence, after reaching the confluence, after which in the middle portion of each well, cells were scratched by using pipette tip, which results in the gap (injury formation). Scratched cells were removed by washing with PBS. Then cells were treated with different concentrations of DIM-10 and DIM-14. After 48 h the width of the gaps was measured microscopically and images were captured. In control cells due to high migratory potential of MDA-MB-231 cells, they are moved into scratched gaps, which will result in narrowing down (closure) of gaps. The width of the gap was measured in all wells and effect of DIM-10 and DIM-14 on cell migration was calculated.

2.3. Experimental solubility and lipophilicity

Saturation solubility measurements were performed using shake-flask method followed by reverse-phase HPLC analysis. *The details of these studies were provided in supplementary information.*

2.4. Preparation of NLC formulations

NLC formulations were prepared with optimized proportions of the following ingredients: Drug DIM-10 or DIM-14, Compritol 888, Miglyol 812, Vitamin E TPGS and water were used as vehicle. All the above-mentioned formulation excipients are FDA approved and found to be safe in clinical applications. C-DIMs loaded NLC formulations were prepared by hot melt homogenization technique [23]. In brief, 20 mg of drug was dissolved in dichloromethane and mixed with lipid phase comprised of Compritol (7.0% w/w) and Miglyol (3.0% w/w). Later, organic phase was removed on a rotary evaporator for 2–3 h at 80 °C and to the heated lipid phase the aqueous solution (40 ml) containing vitamin E TPGS (1.5% w/w) surfactant was added at same temperature under high speed mixing using a polytron homogenizer at 20,000 rpm for 1–2 min. The resultant oil-in-water dispersion was passed through nano-DeBEE high-pressure homogenizer at 5000 psi for 5 cycles. Throughout the process temperature was maintained at 80 °C. Prepared formulation was cooled to room temperature while stirring. This process resulted in the hardening of NLCs with drug entrapped in it. Prepared nanoparticles were analyzed for size and surface charge using BI-90 particle sizer (Brookhaven Instruments, Boston, USA), which is based on the principle of dynamic light scattering and Zeta potential measurement was carried with Zeta plus (Brookhaven Instruments). The entrapment efficiency of drug in NLC was measured according to the standard protocols.

2.5. In vitro drug release studies

In vitro drug release profile of DIM-10 and DIM-14 NLCs was studied in PBS containing tween 80 at pH 5.8. The details were given in supplementary information.

2.6. Caco-2 permeability studies

For in vitro permeability study Caco-2 cells were maintained and permeability studies were performed as per our reported method [10]. *The detail of this study was provided in supplementary information.*

2.7. Animals

Male Sprague Dawley rats (320–350 g weights) were used for pharmacokinetic studies. Female nude mice (5–6 weeks age) were used for in vivo tumor studies. IACUC of FAMU approved all the animal protocols and during the experiments, animals were handled humanly. *The details of the study are provided in supplementary information.*

2.8. Pharmacokinetic studies

Initially, the oral bioavailability profile of both DIM-10 and DIM-14 free drugs was evaluated in Sprague Dawley rats. The oral PK results indicated that both these promising C-DIMs have limited oral absorption. To overcome this limitation, we prepared NLC formulations, the oral bioavailability and Pharmacokinetic profile of DIM-10-NLC and DIM-14-NLC formulations were studied. DIM-10 free drug at the dose of 30 and 100 mg/kg and DIM-10-NLC at the dose of 30 mg/kg were administered orally. In case of DIM-14, 30 mg/kg oral dose of free drug and NLC formulation was administered. Rats were fasted overnight before the start of the experiments and randomly divided into different experimental groups. After oral administration of these drugs as free drugs and NLC formulations, blood samples (250 μl) were withdrawn from tail veins at predetermined time points (0.25, 0.5, 1, 2, 4, 6, 8, 12, 18 and 24 h) and rest of the procedure for pharmacokinetic study is followed as per our previous methods.

2.9. PK study in dogs

Pharmacokinetic profile of DIM-10 and its NLC formulation were studied in dogs after intravenous and oral administration at a dose of 5 mg/kg. Animals were randomly distributed into three experimental groups (n = 3–4). A central venous catheter on long saphenous vein was placed on each dog on the day of study. Overnight fasted dogs were used for the PK study. Blood samples were collected from the venous catheters into heparinized tubes. Samples were collected at 0, 0.25, 0.5, 1, 2, 4, 6, 8, 12, 18 and 24 h after administration of a single dose of DIM-10 solution and NLC formulation.

2.10. Anticancer studies in orthotopic TNBC mouse models

MDA-MB-231 cells induced orthotopic breast cancer model was used for anticancer evaluations of DIM formulations. MDA-MB-231 cells (2 million in 100 μl PBS) were injected orthotopically into mammary fat pads. DIM-10 and DIM-14, free drugs and NLC formulations were administered at the dose of 30 mg/kg daily orally for 4 weeks and tumor sizes were monitored every week. Four weeks after drug treatment animals were sacrificed; final tumor volumes and weights were recorded. Tumor size and volume analysis was done as per standard methods (*Supplementary information*).

2.11. Western blot analysis

The protein extraction, sample preparation, SDS page and transfer of proteins to nitrocellulose membrane were performed according to our previous methods [8,9]. Membranes were probed with antibodies against cleaved caspase 3 (1:1000), Cyclin D1 (1:1000), PCNA (1:1000), and β-actin, and all these primary antibodies were purchased from Santa Cruz Biotechnology, Santa Cruz, CA. Horseradish peroxidase-conjugated secondary antibodies (Santa Cruz Biotechnology, Santa Cruz, CA) were used. Proteins were visualized using enhanced chemiluminescent solution (Pierce, Rockford, IL) and exposed to Kodak X-OMAT AR autoradiography film (Eastman Kodak, Rochester, NY). The intensity of the western blot bands was quantified by densitometric analysis using imageJ software.

2.12. Quantification of VEGF by ELISA

VEGF levels were estimated in tumor homogenates by ELISA method [8,9]. Tumors were homogenized in RIPA lysis buffer containing protease inhibitors. After centrifugation, the resultant supernatant was used in subsequent analysis. Total protein concentration was determined with a BCA protein assay method. VEGF concentrations were determined according to the manufacturer's protocols and VEGF levels were expressed as pg/mg protein. A minimum of 3 tumors in duplicate per group were analyzed.

2.13. Immunohistochemical analysis of tumor sections

MDA-MB-231 tumors were fixed in formalin saline and processed for normal histopathological procedures and 5–10 μm sections were made. After deparaffinization and rehydration, sections were processed for immunohistochemical (IHC) protocols as per our established methods [8–10]. Antigen retrieval for Cleaved caspase 3, ki67 and CD31 was carried out for 10 min in 0.01 M sodium citrate buffer (pH 6), and heated at 95 °C in a steam bath followed by cooling for 30 min. The samples were incubated overnight at 4 °C with Cleaved caspase 3, ki67 and CD31 antibodies or incubated with biotinylated secondary antibody followed by streptavidin. After exposing the peroxidase treated sections to chromagen substrate, brown color was developed at positive sites. After counter staining the sections with hematoxylin, the Cleaved caspase 3, ki67 and CD31 expressions were identified by presence of the brown cytoplasmic staining. Number of positive cells per filed was quantified by counting 10 different fields from each section. Based on the CD31 positive cells, microvessel density (MVD) was calculated.

3. Results

3.1. In vitro anticancer activity of DIM-10 and DIM-14

Both DIM-10 and DIM-14 exhibited concentration dependant increase in the anticancer effects; the cell viability was decreased with increased concentration. The IC_{50} values were in the range of 10–20 μM on different breast cancer cell types. 72 h after the treatment, the IC_{50} values of DIM-10 on MDA-MB-231, MDA-MB-435, MDA-MB-468, BT474 and SKBR3 cells were found to be 11.63 ± 0.89, 12.45 ± 1.84, 11.03 ± 1.04, 13.83 ± 1.21 and 8.10 ± 0.73 μM, respectively. In case of DIM-14, the IC_{50} values 72 h after the treatment on MDA-MB-231, MDA-MB-435, MDA-MB-468, BT474 and SKBR3 cells were found to be 18.86 ± 1.62, 13.30 ± 2.46, 14.11 ± 1.30, 17.05 ± 2.24 and 11.75 ± 1.62 μM, respectively (Fig. 1A–F). The clonogenic assay also demonstrated the significant anticancer effects of DIM-10 and DIM-14 (Fig. 2A). Fig. 2D shows representative images of colonies stained with crystal violet. At the highest concentration studied, both DIM-10 and DIM-14 produced 3.39 and 2.26-fold significant reduction in the spheroid number. Further, the spheroid sizes were found to be concentration dependently decreased, and at 10 μM concentration resulted in 7.66 and 6.17-fold, respectively significant decrease in the spheroid sizes (Fig. 3B). The 2D migration gap closure assay performed with C-DIMs also showed significant ($p < 0.001$) decrease in gap closing compared to control. DIM-10 and DIM-14 showed 2.95 and 2.49-fold, respectively significant decrease in the gap closure, whereas in control cells due to high metastatic migratory nature the gap was narrowed down. Fig. 2C shows the

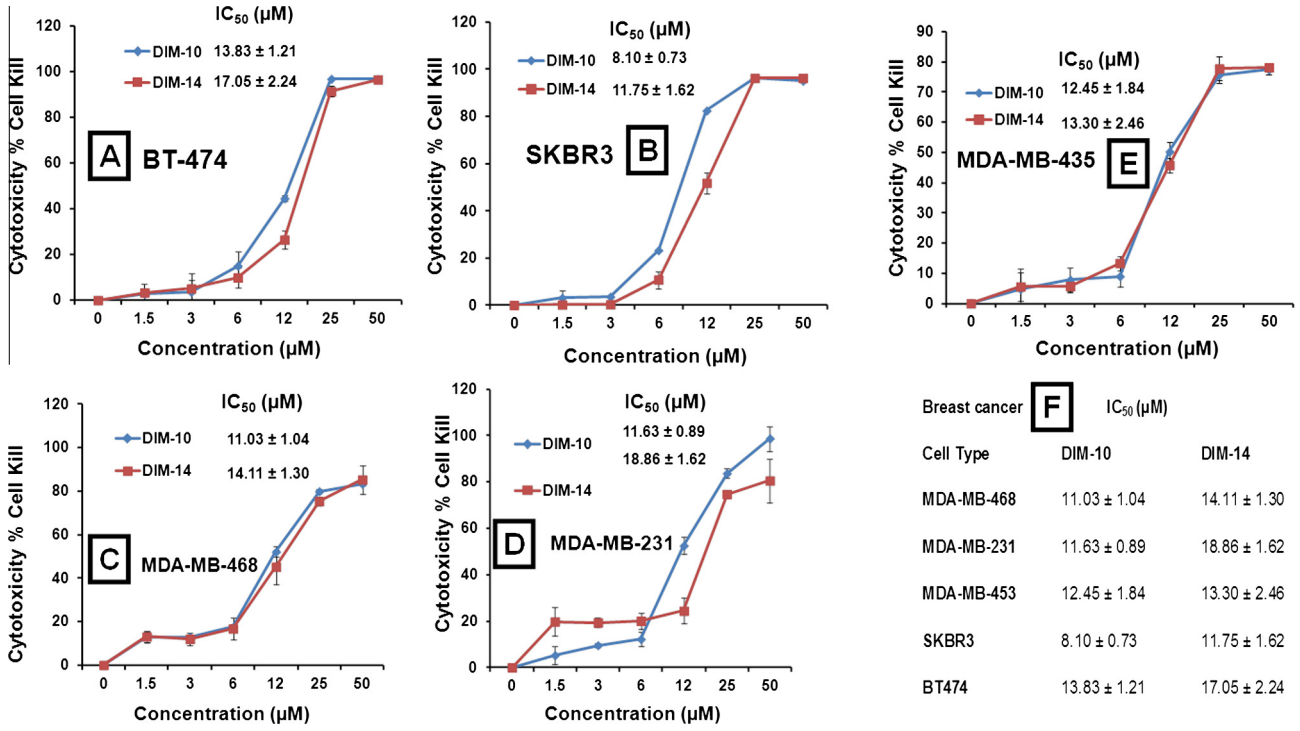

Fig. 1. Cytotoxicity assay. Effect of DIM-10 and DIM-14 on different breast cancer cell lines, (A) BT474, (B) SKRB3, (C) MDA-MB-468, (D) MDA-MB-231, (E) MDA-MB-453 and (F) the IC_{50} values of DIM-10 and DIM-14 on all these breast cancer cell lines. Each data is represented as mean ± sem (n = 6–8).

different gap widths calculated in different groups with MDA-MB-231 based cell migration assay. Fig. 2E shows the representative images of cell migration assays.

3.2. Solubility and lipophilicity of DIM-10 and DIM-14

The experimental solubility of DIM-10 was found to be 0.54 ± 0.06 μg/ml at pH 7.4, whereas the solubility of DIM-14 was found to be 0.31 ± 0.04 μg/ml. The solubility of both these drugs was also not altered at pH 2 and 8, suggesting that the solubility of DIM-10 and DIM-14 was relatively independent of pH in the range of pH 2–8 ($p > 0.05$).

3.3. Characterization of DIM-10 and DIM-10 NLC formulations

The average sizes of the C-DIM derivates loaded NLC particles were found to be in 210–222 nm range. The zeta potentials were −21.43 and −14.34 mV, respectively for DIM-10 and DIM-14 NLC formulations. The entrapment efficiency of DIM-10 and DIM-14 into the NLC particles was found to be 86.23 and 91.68%, respectively (Table 1).

3.4. Bidirectional permeability of DIM-10 and DIM-14

The TEER values and mean permeability values of paracellular control Lucifer Yellow were >450 Ω cm^2 and <0.15 × 10^{-6} cm/s, respectively. These TEER and permeability values are within normal limits, and thus confirms the paracellular integrity of Caco-2 monolayers. The average P_{eff}, A-B of DIM-10 across Caco-2 cell monolayers was 0.28 ± 0.05 × 10^{-6} cm/s, and B-A was 0.43 ± 0.06 × 10^{-6} cm/s (Fig. 3A). In case of DIM-14 the average P_{eff}, A-B of across Caco-2 cell monolayers was 0.26 ± 0.04 × 10^{-6} cm/s, and B-A was 0.38 ± 0.07 × 10^{-6} cm/s (Fig. 3B). With both DIM-10 and DIM-14, the Caco-2 permeability studies performed at different pH conditions (5, 5.8 and 6.8) did not differ in the permeability (Fig. 3A&B). The TEER values were not significantly changed throughout the Caco-2 permeability studies with DIM-10 and DIM-14, which is indicative of tight junction integrity upon treatment with these drugs. The P_{eff}, A-B of DIM-10 NLC formulation across Caco-2 cell monolayers was 0.85 ± 0.02 × 10^{-5} cm/s, and for DIM-14 NLC formulation the average P_{eff}, A-B of across Caco-2 cell monolayers was 0.72 ± 0.04 × 10^{-5} cm/s, respectively. Compared to free drugs, the P_{eff} A-B of DIM-10 and DIM-14 NLC formulations was found to be 2.59 and 2.56-fold significantly increased (Fig. 3C&D). The in vitro drug release studies indicated that both DIM-10 and DIM-14 NLC formulations showed sustained drug release profile (Fig. 3E&F). The percentage of drug release was significantly increased in NLC formulation groups compared to free drug groups. The maximum % of drug release found to have increased by 2.94 and 3.08-fold, respectively in DIM-10 and DIM-14 NLC formulations compared to respective free drugs. After 72 h, the cumulative amount of DIM-10 released in free drug and NCL formulation was found to be 30.2 and 88.7 μg/ml, respectively, whereas the cumulative amount of DIM-14 released in free drug and NLC formulations was found to be 29.8 and 91.9 μg/ml, respectively. These released amounts in NLC formulation groups seem to be above the normal solubility limits of these compounds, however, due to increased solubility of DIM-10 and DIM-14 in NLC form might have achieved increased solubility through super saturation. These in vitro drug release studies suggest the increased solubility and sustained release behavior of C-DIM derivates in NLC formulations.

3.5. Pharmacokinetic analysis of DIM-10, DIM-14 free drugs and NLC nanoformulations

Initial pharmacokinetic studies in rats with DIM-10 and DIM-14 showed limited oral absorption. For DIM-10 at 30 and 100 mg/kg doses, the C_{max} concentrations were found to be 2.68 ± 0.27 and 8.77 ± 0.87 μg/ml, respectively. At these doses, the AUC levels were

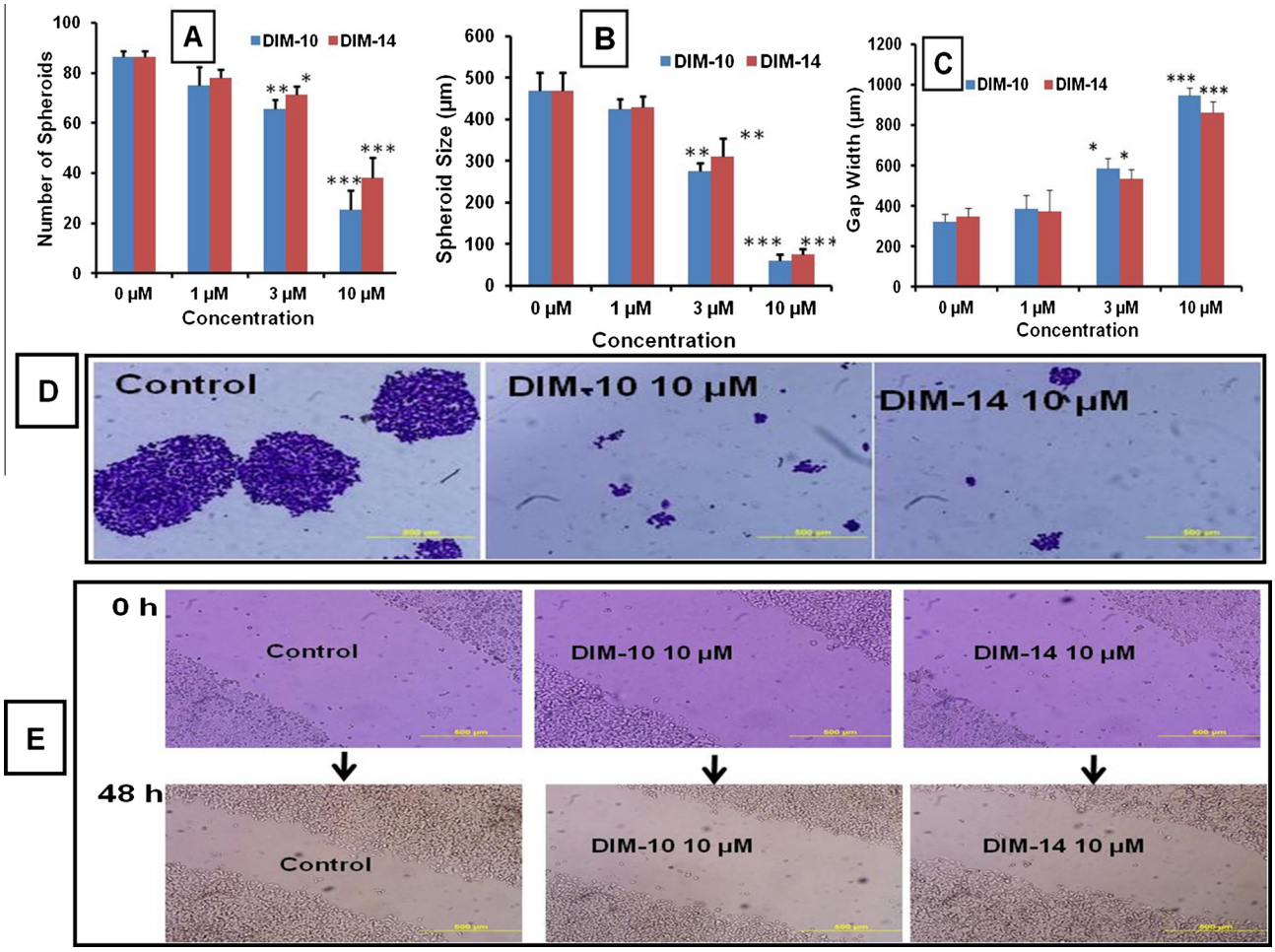

Fig. 2. Effect of DIM compounds on clonogenic and cell migration potential. (A) Effect of DIM-10 and DIM-14 on total number of spheroids in clonogenic assay studied with MDA-MB-468 cells, (B) effect on the spheroid/colony sizes. (C) Effect of DIM-10 and DIM-14 on cell migration potential of MDA-MB-231 cells studied by wound/gap closure assay, (D) representative spheroids from different groups and (E) representative images of cell migrations captured at 0 and 48 h time points. Each data is represented as mean ± sem (n = 6–8). $^{***}P < 0.001$, $^{**}P < 0.01$, $^{*}p < 0.05$ Vs control.

found to be 9.56 ± 0.97 and 34.42 ± 4.12 μg h/ml, respectively. In the DIM-10 NLC formulation treated group, significant increase in the oral absorption profile was observed. Compared to DIM-10 free drug, NLC formulation resulted in significant increase in the pharmacokinetic parameters such as C_{max}, AUC and MRT were observed. The C_{max} concentration in DIM-10 formulation was 4.73-fold increased. The AUC levels were 11.19-fold significantly increased in NLC formulations compared to DIM-10 free drug group (Fig. 3G and Table 2). Another drug DIM-14 NLC nanoformulation also exhibited superior oral bioavailability profile compared to free drug. The C_{max} and AUC levels were 2.12 and 8.31-fold significantly increased in DIM-14 NLC formulations ($p < 0.001$) compared to free drugs (Fig. 3H and Table 3).

3.6. Pharmacokinetic analysis of DIM-10 NLC in dogs

In dogs, DIM-10 free drug at 5 mg/kg, the C_{max} levels was found to be 2.5 ± 0.24 μg/ml, whereas in DIM-10 NLC formulations at the same 5 mg/kg dose, C_{max} concentrations were found to be 6.55 ± 0.64 μg/ml. There was a 2.62-fold increase in the C_{max} levels in DIM-10 NLC formulations compared to free drug ($p < 0.001$). AUC levels were found to be 42.69 ± 4.08 and 125.90 ± 35.78 μg h/ml, respectively in DIM 10 free drug and DIM-10 NLC formulations. The fold increase was found to be 2.94. The percentage oral bioavailability was 27.09 ± 3.57% in DIM-10 free drug and in NLC formulation it was 80.06 ± 8.36%. There is a 2.95-fold significant increase ($p < 0.001$) in the absolute oral bioavailability of DIM-10 in NLC formulation compared to free drug in dogs pharmacokinetic study. The mean residence time (MRT) and $t_{1/2}$ values were also significantly increased in NLC formulations (Fig. 3I and Table 4). In dogs PK study, treatment with DIM 10 NLC formulation at 5 mg/kg by oral route produced sustained drug concentrations and the plasma concentrations were found to be significantly higher in NLC group (3 μg/ml) at 24 post dosing. Several factors might have contributed for this effect such as (1) sustained release of drug from NLC particles which are uptaken intact into GIT epithelial cells, (2) altered metabolism of drug in NLC form and (3) decreased hepatic metabolism of drug in NLC form due to lymphatic uptake pathways.

3.7. Anticancer effects of DIM-10 and DIM-14 NLC formulations in TNBC xenograft models

In orthotopic TNBC models, anticancer effects of DIM-10 and DIM-14 free drugs and NLC formulations were evaluated at the dose of 30 mg/kg. Treatment was started 1 week after the tumor cell implantation and continued for 4 weeks. Compared to untreated control groups, DIM-10 free drug and NLC based formulations produced significant anticancer effects in xenograft models. Compared to free drug, DIM-10 NLC formulation produced significantly higher reduction in the tumor volume (Fig. 4A&B). The

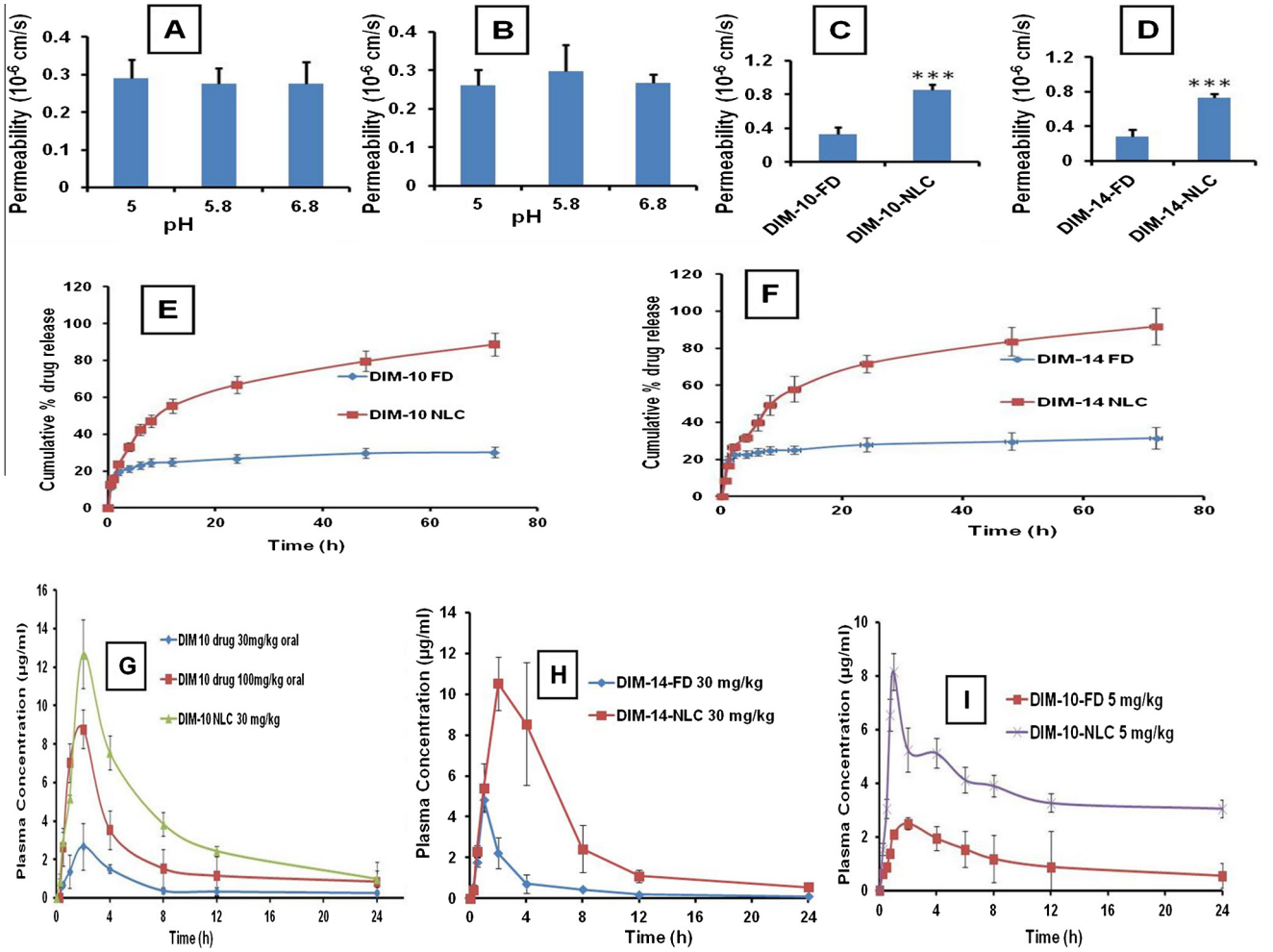

Fig. 3. Caco-2 permeability study. (A and B) Apical to Basolateral permeability of DIM-10 and DIM-14 at different pH conditions, (C and D) Caco-2 permeability of DIM-10 and DIM-14 NLC formulations at pH 5.8, (E and F) the in vitro drug release profile of DIM-10 and DIM-14 NLC formulations. Each data point was represented as mean ± sem (n = 3–4). $^{***}P < 0.001$ Vs control group. Oral Pharmacokinetic study of DIM-10 and 14 in Rats, (G) pharmacokinetic profile of DIM-10 free drug (at 30 and 100 mg/kg) and DIM-10 NLC (at 30 mg/kg), (H) pharmacokinetic profile of DIM-14 free drug and DIM-14 NLC (at 30 mg/kg) following oral administration to rats. Each data point was represented as mean ± sem (n = 5–6). (I) Oral Pharmacokinetics of DIM-10 NLC in Dogs. Oral Pharmacokinetic profile of DIM-10 free drug and DIM-10 NLC (at 5 mg/kg) in dogs. Each data point was represented as mean ± sem (n = 3–4).

Table 1
Different formulation characteristics of DIM-10 and DIM-14 NLC formulations.

Parameters	DIM-10 NLC	DIM-14 NLC
Size (nm)	214–222	210
Surface charge (mV)	−21.43	−14.34
PDI	0.19	0.25
Drug loading	10%	10%
Entrapment efficiency (%)	86.23%	91.68%

tumor weights were also significantly reduced in DIM-10 NLC formulations compared to free drug treated animals (Fig. 4C). Fig. 4D shows the representative tumor bearing animals and isolated tumors in different groups. The anticancer effects of DIM-14 also demonstrated similar kind of anticancer effects like DIM-10. DIM-14 NLC formulations produced significantly higher reduction in the tumor volumes (Fig. 5A). DIM-14 formulation produced 2.12 higher anticancer effect compared to free drug treated group (Fig. 5B). Similarly, DIM-14 oral formulation, 4 weeks after the treatment resulted in 2.56-fold significant reduction ($p < 0.001$) in the tumor weight compared to free drug treated animals (Fig. 5C). Fig. 5D shows the representative tumor bearing animals and isolated tumors in different groups. The anticancer studies indicate that both DIM-10 and DIM-14 formulations possess superior anticancer effects in vivo in TNBC models.

Table 2
The pharmacokinetic parameters of DIM-10 free drug (at 30 and 100 mg/kg) and DIM-10 NLC (at 30 mg/kg) after oral administration. The table also shows the PK profile of i.v. (5 mg/kg) treated groups. Each data point was represented as mean ± sem (n = 3–4).

Parameter	DIM-10 i.v. 5 mg/kg	DIM-10 free drug 30 mg/kg	DIM-10 free drug 100 mg/kg	DIM-10 NLC 30 mg/kg
T_{max} (h)	0.00	1 ± 0.12	1 ± 1.43	2 ± 0.24
C_{max} (µg/ml)	14.83 ± 1.48	2.68 ± 0.27	8.77 ± 0.87	12.68 ± 1.27
$t_{1/2}$ (h)	0.78 ± 0.81	4.41 ± 0.52	5.26 ± 0.61	13.47 ± 1.52
AUC (µg h/ml)	15.58 ± 1.67	9.56 ± 0.97	34.42 ± 4.12	107.0 ± 11.23
AUMC (µg h/ml)	14.98 ± 1.55	58.46 ± 5.93	247.55 ± 25.87	1469.56 ± 148.23
MRT (h)	0.96 ± 0.16	6.11 ± 0.67	7.19 ± 0.83	13.73 ± 1.46

3.8. Western blot analysis of DIM-10 and DIM-14 treated tumor samples

The western blot analysis also supported the superior anticancer effects of DIM-10 and DIM-14 in NLC formulations. Compared to control tumors, Cleaved caspase 3 expression was 1.90-fold increased in DIM-10 free drug (FD) treated tumors, whereas in DIM-10-NLC treated tumors its expression was 4.73-fold significantly increased (Fig. 6A and D). PNCA expression was 1.19-fold decreased in DIM-10 free drug treated tumors, whereas in DIM-10 NLC formulations, PCNA expression was 2.05-fold decreased (Fig. 6A and B). Further, the cyclin D1 expression was 1.12 and 2.05-fold, respectively decreased in DIM-10 free drug and NLC formulation treated tumors compared to untreated control tumors (Fig. 6A and C). All the studied markers, DIM-10 NLC formulation produced, 2.48, 1.72 and 1.82-fold respective change in cleaved

Table 3
The pharmacokinetic parameters of DIM-14 free drug (30 mg/kg) and DIM-14 NLC (at 30 mg/kg) after oral administration. The table also shows the PK profile of i.v. (5 mg/kg) treated groups.

Parameter	DIM-14 i.v. 5 mg/kg	DIM-14 free drug 30 mg/kg	DIM-14 NLC 30 mg/kg
T_{max} (h)	0.00	1 ± 0.34	2 ± 0.45
C_{max} (μg/ml)	21.48 ± 3.59	4.86 ± 0.67	10.34 ± 2.04
$t_{1/2}$ (h)	0.68 ± 0.31	3.83 ± 0.61	10.78 ± 1.22
AUC (μg h/ml)	17.83 ± 3.93	10.13 ± 1.62	84.20 ± 15.30
AUMC (μg h/ml)	18.34 ± 2.63	61.01 ± 7.63	1291.08 ± 383.66
MRT (h)	0.81 ± 0.27	5.67 ± 0.45	11.84 ± 2.16

Table 4
The pharmacokinetic parameters of DIM-10 free drug after oral and i.v. administration at 5 mg/kg dose and DIM-10 NLC formulation (5 mg/kg oral) in dogs model.

Parameter	DIM-10 i.v. 5 mg/kg	DIM-10 free drug 5 mg/kg	DIM-10 NLC 5 mg/kg
T_{max} (h)	0.00	2.00 ± 0.19	1.00 ± 0.13
C_{max} (μg/ml)	45.61 ± 4.38	2.50 ± 0.24	6.55 ± 0.64
$t_{1/2}$ (h)	1.11 ± 0.16	19.61 ± 1.87	64.90 ± 6.25
AUC (μg h/ml)	31.78 ± 3.02	42.69 ± 4.08	125.90 ± 35.78
MRT (h)	1.50 ± 0.16	24.99 ± 2.37	92.21 ± 8.92
% Bioavailability	–	27.09 ± 3.57	80.06 ± 8.36

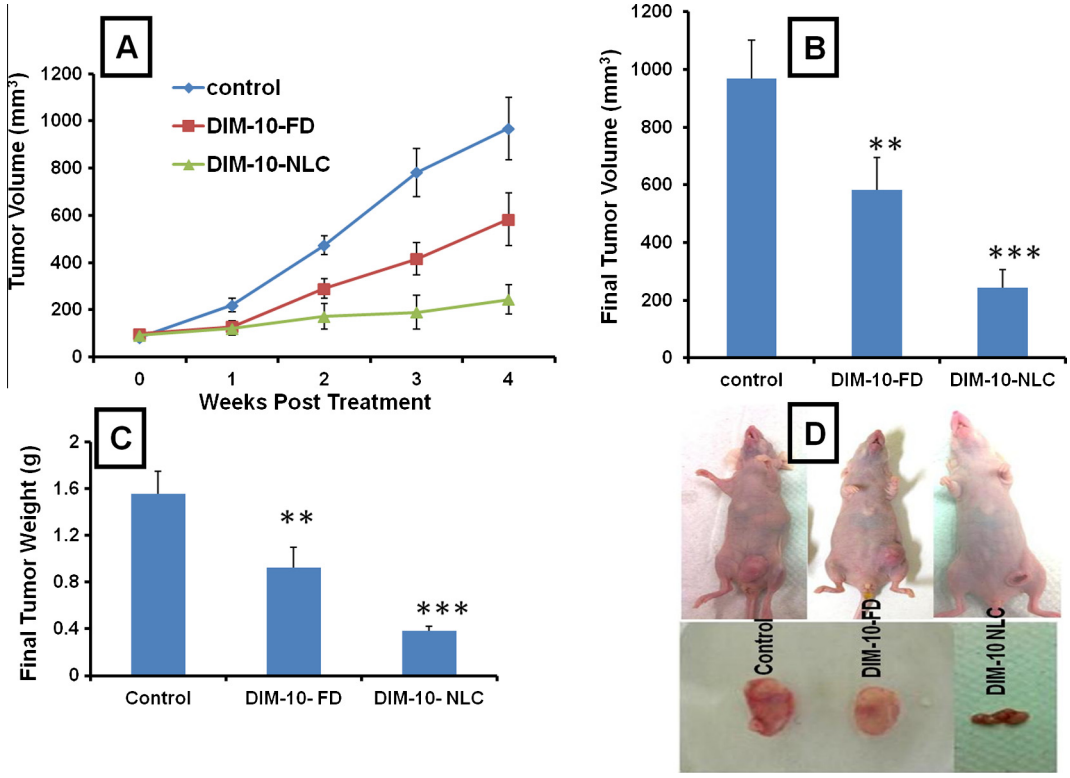

Fig. 4. Anticancer effects of DIM-10 NLC formulation in orthotopic TNBC model. (A) Tumor volumes during the 4 weeks of DIM-10 NLC oral administration in TNBC bearing mice, (B) final tumor volumes, (C) final tumor weights after completion of 4 weeks of DIM-10 free drug and NLC treatment at the dose of 30 mg/kg dose orally and (D) representative photomicrographs of tumor bearing mice and isolated tumors from different groups. Each data point was represented as mean ± sem (n = 6–8). $^{*}p < 0.05$ and $^{***}p < 0.001$ Vs untreated groups.

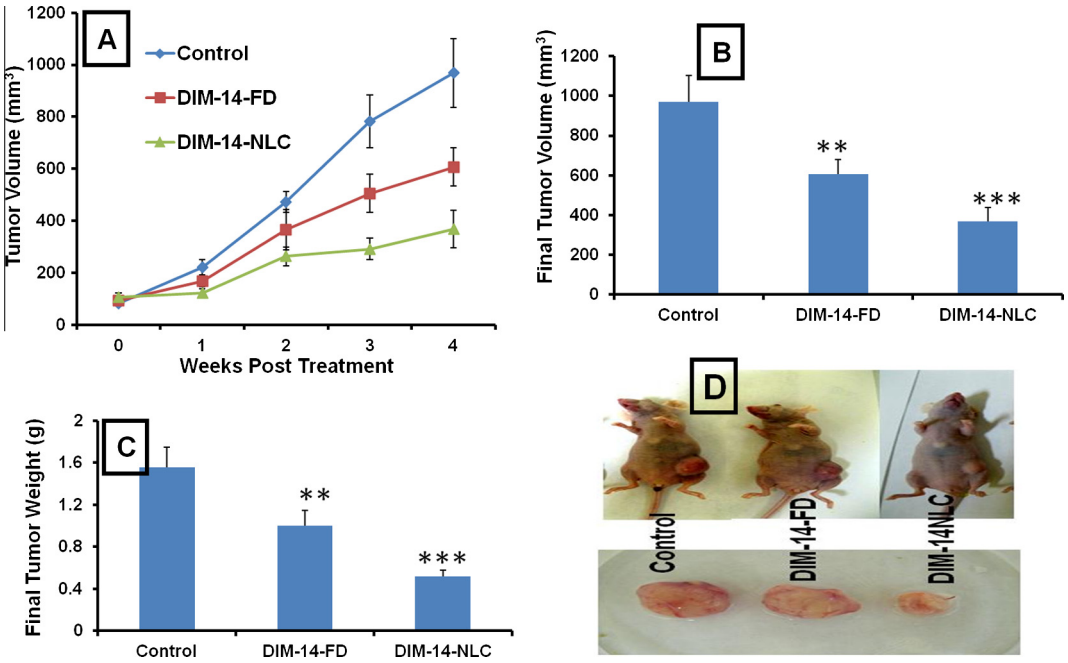

Fig. 5. Anticancer effects of DIM-14 NLC formulation in TNBC model. (A) Tumor volumes during the 4 weeks of DIM-14 NLC oral administration in TNBC bearing mice, (B) final tumor volumes, (C) final tumor weights after completion of 4 weeks of DIM-14 FD and NLC treatment at the dose of 30 mg/kg dose. (D) Representative photomicrographs of tumor bearing mice and isolated tumors from different groups. Each data point was represented as mean ± sem (n = 6–8). $^{**}p < 0.01$ and $^{***}p < 0.001$ Vs untreated groups.

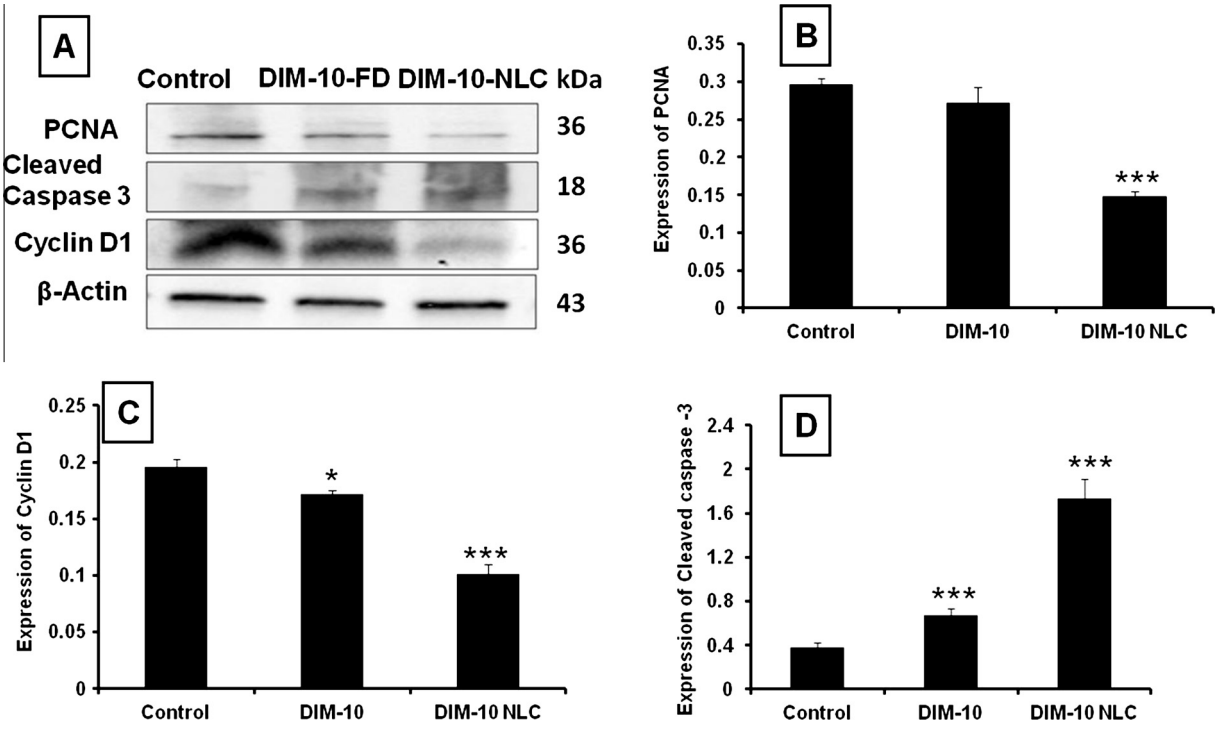

Fig. 6. Western Blot analysis. (A) Effect of DIM-10 NLC on PCNA, Cleaved caspase 3 and Cyclin D1 expression in tumor lysates (representative images). Densitometric quantitative analysis of (B) PCNA, (C) Cyclin D1 and (D) Cleaved caspase 3 expression. Each data point is represented as mean ± sem (n = 3–4). $^{***}P < 0.001$, $^{*}p < 0.05$ Vs control groups.

caspase 3, PCNA and cyclin D1 expression compared to DIM-10 free drug treated tumors. Treatment with DIM-14 also produced favorable anticancer effects. The cleaved caspase 3, which is an apoptotic marker was 1.56 and 2.68-fold, respectively increased in DIM-14 free drug and NLC formulation treated groups (Fig. 7A and C). The PNCA expression was 1.28 and 3.51-fold ($p < 0.05$ and $p < 0.001$), respectively significantly decreased in free drug and DIM-14 NLC formulation treated groups (Fig. 7A and B). Similarly, cyclin D1 expression was 2.28 and 6.63-fold down regulated ($p < 0.001$) in free drug and formulation treated groups (Fig. 7A and D). DIM-14 NLC formulation produced, 1.71, 2.74 and 2.90-fold respective change ($p < 0.001$) in cleaved caspase 3,

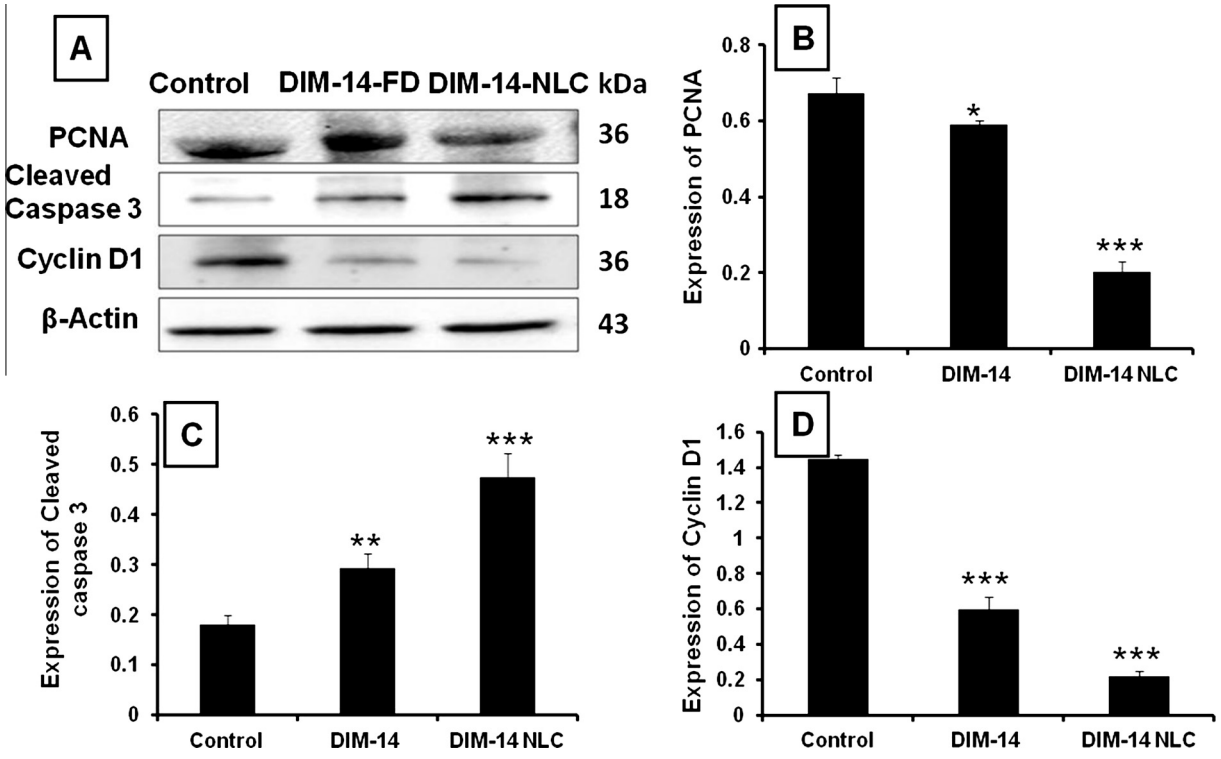

Fig. 7. Western Blot analysis. (A) Effect of DIM-14 NLC on expression of PCNA, Cleaved caspase 3 and Cyclin D1 in tumors lysates (representative images). Densitometric quantitative analysis of (B) PCNA, (C) Cleaved caspase 3 and (D) Cyclin D1 expression. Each data point is represented as mean ± sem (n = 3–4). $^{***}P < 0.001$, $^{**}P < 0.01$, $^{*}p < 0.05$ Vs control groups.

PCNA and cyclin D1 expression compared to DIM-14 free drug treated tumors (Fig. 7).

3.9. Immunohistochemical analysis of tumors

The IHC analysis of TNBC tumor sections also indicated the superior anticancer effects of DIM-10 and DIM-14 NLC formulations compared to free drug treated tumors (Fig. 8A). Cleaved caspase 3 was found to be 2.26 and 2.78-fold significantly increased in DIM-10 free drug and NLC formulation groups (Fig. 8B). The increased Cleaved caspase 3 suggests that these compounds produce anticancer effects through induction of apoptosis. Due to anticancer effects of DIM-10, a significant decrease in the cell proliferation marker Ki67 was observed. A 1.42 and 2.90-fold ($p < 0.01$ and $p < 0.001$) decrease in the Ki-67 expression was observed in DIM-10 free drug and DIM-10 NLC formulation treated tumors (Fig. 8A and C). The CD31 that is indicator of microvascular density (MVD) of tumors was found to be 1.60 and 2.47-fold significantly decreased in DIM-10 free drug and NLC formulation treated tumors compared to control tumors (Fig. 8A and D). In all the three markers studied (cleaved caspase 3, Ki-67 and CD31), NLC formulation produced 1.22, 2.04 and 1.54-fold significant change compared to free DIM treated groups (Fig. 8A–D). Similar pattern of increased anticancer effects in IHC analysis was observed with DIM-14 NLC formulations (data not shown). The body weight changes and histopathological examination of DIM-10 and DIM-14 as in free drug and NLC formulations did not induce any kind of adverse effects.

3.10. Effect of DIM-10 and DIM-14 on VEGF levels

VEGF levels in tumor lysates were significantly reduced in DIM-10 and DIM-14 free drug and NLC formulation treated groups. Compared to free drug treated groups, NLC formulations produced more reduction in the VEGF levels. Compared to control tumors, in DIM-10 free drug groups, 1.69-fold reduction and in DIM-10-NLC formulation groups, 2.88-fold reduction in the VEGF levels were observed (Fig. 8E). Similarly, in DIM-14 treated groups, 1.55 and 2.49-fold respective decrease in free drug and NLC groups was observed. Compared to free drug, 1.70 and 1.60-fold respective reduction in DIM-10 and DIM-14 NLC formulation groups was observed (Fig. 8E).

4. Discussion

Developing the anticancer drugs against TNBC is urgently needed, due to rapid increase in the breast cancer patients. There is no selective and efficient drug available to treat TNBC, and currently used drugs are associated with severe toxicity concerns [13,35]. We have chosen two of C-DIM analogs, DIM-10 and DIM-14 and evaluated them in TNBC models. Cytotoxicity assays revealed that both these C-DIM analogs produced concentration dependent cell kill on MDA-MB-231, MDA-MB-468, MDA-MB-453, BT474 and SKBR3 cell types. Our results are in agreement with the previous reports of promising anticancer effects of C-DIMs in different cancer types [34,33,4,11,22].

Approximately 30% of the NCEs suffer with poor oral bioavailability, due to which pharmaceutical companies discontinue further development of many potent NCEs. In our studies, it was observed that both DIM-10 and DIM-14 have poor aqueous solubility. The absolute oral bioavailability of both DIM-10 and DIM-14 was found to be approximately <20%. Because many studies demonstrated the promising role of different nanoformulations in overcoming poor aqueous solubility [25,31,5,28], we chose NLC formulation approach [17,32,6,24]. Initially, prepared NLC formulation were subjected to in vitro drug release profiles and found that both DIM-10 and DIM-14 release were significantly increased

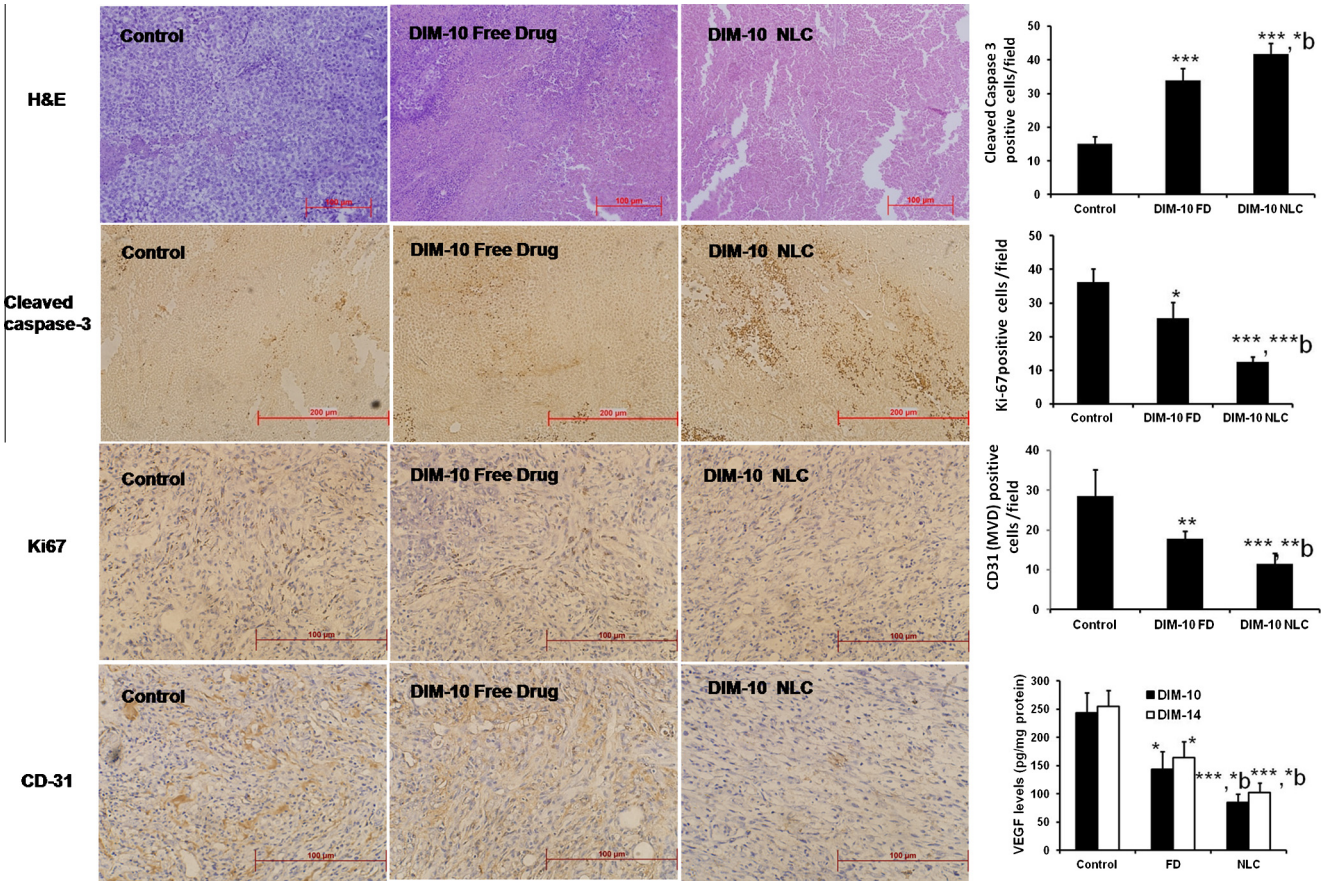

Fig. 8. Histopathology and Immunohistochemical analysis. (A) Representative images of Hemotoxylin and Eosin stained tumor sections (first row) and IHC analysis fields for Cleaved caspase 3 (second row), Ki-67 (third row) and CD-31 (fourth row) markers. The brown color stained fields indicate the positive expression of particular markers. Quantitative analysis of IHC study for (B) Cleaved caspase 3, (C) Ki-67, (D) CD-31 (tumor microvascular density and (E) VEGF levels in tumors. Each data point was represented as mean ± sem (n = 3). $^{*}p < 0.05$, $^{**}p < 0.01$ and $^{***}p < 0.001$ Vs control groups and b Vs DIM-10 free drug (FD) group.

in NLC formulations compared to free drugs; this increased drug release is due to increase solubility of DIMs in nanocarrier systems. Caco-2 permeability studies demonstrated the increased permeability of DIM-10 and DIM-14 NLC formulations. The increased permeability of C-DIMs through Caco-2 monolayers might mainly taken place through intact NLC uptake into cells. Therefore, the increased absorption of drug from NLC based formulations is due to increased drug solubility and NLC based increased permeation into monolayers. This increased oral absorption was further supported by pharmacokinetic studies in rats by increased bioavailability of DIM-10 and DIM-14. NLC formulation of DIM-10 exhibited superior oral bioavailability profile. The C_{max}, AUC levels of DIM-10 NLC formulation at 30 mg/kg dose were superior to 100 mg/kg free drug oral formulation. This suggests that NLC based formulations produced greater than 10-fold increase in the oral bioavailability. Therefore, by using NLC based formulation approaches we can reduce the dose to almost 1/3rd of the free drug. This observation clearly demonstrates the usefulness of NLC based oral formulation approach to increase bioavailability of poorly soluble drugs. Similarly, the oral pharmacokinetic profile of DIM-14 NLC formulation was also significantly increased. Curcumin is a classical example of a drug which needs high doses for therapeutic benefits because of poor aqueous solubility and poor permeability [12,1]. Several nanoformulation approaches exhibited significant improvement in oral bioavailability of curcumin [15,21,1]. In a similar fashion, using NLC formulation based approach, the doses of DIM-10 and DIM-14 can be significantly reduced. In an effort to increase the clinical relevancy, the pharmacokinetic profile of DIM-10 formulation was studied in dogs. The dog pharmacokinetic data also suggested promising effects of NLC formulations. Upon comparison of DIM-10 NLC formulations in rat and dog models, the C_{max} values were found to be 2.62-fold significantly increased in dog model compared to 4.73-fold increase observed in rat oral bioavailability studies. Similarly, the AUC values were found to be 2.94-fold increase in dogs compared to 10.96-fold significant increase in rat models. Though the level of increase was different between dog and rat models, both the animal models demonstrated significant improvement in oral bioavailability compared to free drug. Upon DIM-10 NLC treatment, compared to dogs, rats exhibited higher bioavailability profile. The probable reason for this varied response may be physiological differences between the models and also varied uptake and drug disposal mechanisms. Similar types of observations were also reported by us with self emulsified DIM formulations (Ref). Further, the absolute oral bioavailability of DIM-10 was increased from 27 to 80% in NLC formulations compared to free drug. The possible reasons for increased oral absorption of NLC formulations are increased solubility in nanoparticle form, increased absorption of intact nanoparticles via lymphatic and other GI uptake mechanisms [3,29]. Our studies are in line with published reports indicating the role of NLC formulations to increase oral bioavailability of several drugs. Further, the effect of GIT degradation to limit the oral bioavailability of DIM compounds was reported in previous studies [18]. In both rat and dog models, NLC formulations resulted in increase in the MRT. NLC formulations due to their sustained release behavior might have

contributed to the increased residence time of the drug [20]. In dogs, 5 mg/kg dose of DIM-10 in free drug and NLC form was well tolerated. No evidence of toxicity was noticed in dogs treated with DIM-10; therefore, our DIM-10 NLC formulation may be suitable for the clinical use after appropriate trials are done.

The in vitro cytotoxicity and clonogenic assays indicated that both DIM-10 and DIM-14 have very good anticancer effects. The cell migration assay suggested that both these compounds produced significant antimetastatic effects. However, the promising anticancer effects exhibited by DIM-10 and DIM-14 in cell culture based studies did not translate into similar anticancer effects when studied in orthotopic nude mice models. However, our NLC formulations that have shown significant increase in the oral pharmacokinetic profiles, produced superior anticancer effects compared to DIM-10 and DIM-14 free drug treated animals. The NLC based oral formulation produced 2–3-fold increase in the anticancer effects compared to respective free drug treated groups. Among several possible mechanisms of anticancer effects, both DIM-10 and DIM-14 induced anticancer effect through inhibition of VEGF levels. Significant reduction in the VEGF levels was observed in tumor lysates in C-DIM treated groups. The role of VEGF in angiogenesis is very well documented in several studies and antiangiogenic effects of C-DIM were also reported in previous studies, which are in agreement with our present findings [2,7]. Our NLC based oral formulation approach may provide superior anticancer drug delivery strategies for poorly water soluble drugs to improve the pharmacokinetics problems associated with several interesting anticancer agents.

Another mechanism of anticancer effects of DIM-10 and DIM-14 oral formulation is through induction of apoptosis. The western blot analysis demonstrated significant increase in cleaved caspase 3 levels in free drug and NLC formulation treated groups. The apoptosis inducing potential of C-DIMs in different cancer types has been reported earlier [16]. The decreased expression of cyclin D1 in C-DIMs in free drug and NLC formulations suggests that these compounds inhibit the cell proliferation by blocking the cell cycle dependent kinases. Further, the decreased expression of PCNA confirms the role of these drugs to prevent cell proliferation. Previous studies also demonstrated the effect of C-DIM derivatives on cyclin D1 and PNCA expression [36,2]. In all the in vivo anticancer effects (Tumor volume and tumor weight) and western blot parameters, the superior anticancer effects of DIM-10 and DIM-14 formulations were demonstrated compared to respective free drug groups. This is the first study to demonstrate the anticancer effects of DIM-10 and DIM-14 on TNBC models. Further, applying the NLC formulation approach and demonstrating the improved pharmacokinetic profile of these formulations in dog models are unique, scalable and translational. Similarly, the Immunohistochemical (IHC) analysis of tumor sections supported the superior anticancer effects of NLC formulations compared to free drug treated animals. The IHC markers such as Ki 67, cleaved caspase 3 and CD31 were significantly different compared to free drug treated groups. Further, the western blotting analysis also resulted in superior anticancer effects of DIM NLC formulations compared to free drugs. Upon chronic administration of C-DIM free drugs and NLC formulations did not induce any kind of toxic effects. The Histopathological evaluation of GIT section ileum did not result in any observable morphological toxic effects on GIT. This strongly suggests that NLC formulations are well tolerated upon chronic administration.

5. Conclusions

Our in vitro and in vivo studies demonstrate that novel C-DIM analogs (DIM-10 and DIM-14) have potential anticancer effects in TNBC models. Further, novel NLC based formulations of DIM-10 and DIM-14 resulted in significant increase in the oral bioavailability and anticancer activity in animal models. The pharmacokinetic studies in dogs also resulted in significant increase in the oral bioavailability of DIM-10 NLC formulation and suggest its translation potential for clinical application. The anticancer effects of DIM-10 and DIM-14 NLC were found to be superior to free drug treated groups. All the molecular parameters such as western blot and IHC assay confirmed the enhanced anticancer effects of NLC formulations compared to free drug treatment. Therefore, our studies clearly demonstrate the beneficial role of DIM-10 and DIM-14 NLC formulations to treat the TNBC. Further, it is also suggested to use NLC based formulation approach to increase oral bioavailability of poorly water soluble drugs from synthetic and photochemical origin.

Conflict of interest

The authors report no declarations of interest.

Acknowledgments

The authors acknowledge the financial assistance of this research from the Department of Defense (DOD) Breast Cancer Program [Grant # W81XWH-11-1-0211 to M.S]; the National Institute on Minority Health and Health Disparities (NIMHD) P20 program [Grant # 1P20MD006738-03; to M.S.] and the National Institutes of Health (NIH) SC-1 grant [Grant # 5SC1CA161676-03 to M.S].

Appendix A. Supplementary material

Supplementary data associated with this article can be found, in the online version, at http://dx.doi.org/10.1016/j.ejpb.2016.08.006.

References

[1] M.Z. Ahmad, S.A. Alkahtani, S. Akhter, F.J. Ahmad, J. Ahmad, M.S. Akhtar, N. Mohsin, B.A. Abdel-Wahab, Progress in nanotechnology-based drug carrier in designing of curcumin nanomedicines for cancer therapy: current state-of-the-art, J. Drug Target. (2015) 1–21.
[2] T. Andey, A. Patel, T. Jackson, S. Safe, M. Singh, 1,1-Bis (3′-indolyl)-1-(p-substitutedphenyl)methane compounds inhibit lung cancer cell and tumor growth in a metastasis model, Eur. J. Pharm. Sci. 50 (2) (2013) 227–241.
[3] A. Beloqui, M.A. Solinis, A.R. Gascon, A. del Pozo-Rodriguez, A. des Rieux, V. Preat, Mechanism of transport of saquinavir-loaded nanostructured lipid carriers across the intestinal barrier, J. Control. Release 166 (2) (2013) 115–123.
[4] C.H. Boakye, R. Doddapaneni, P.P. Shah, A.R. Patel, C. Godugu, S. Safe, S.K. Katiyar, M. Singh, Chemoprevention of skin cancer with 1,1-Bis (3′-indolyl)-1-(aromatic) methane analog through induction of the orphan nuclear receptor, NR4A2 (Nurr1), PLoS ONE 8 (8) (2013) e69519.
[5] L. Bregoli, D. Movia, J.D. Gavigan-Imedio, J. Lysaght, J. Reynolds, A. Prina-Mello, Nanomedicine applied to translational oncology: A future perspective on cancer treatment, Nanomedicine 12 (1) (2015) 81–103.
[6] M. Elmowafy, A. Samy, M.A. Raslan, A. Salama, R.A. Said, A.E. Abdelaziz, W. El-Eraky, S. El Awdan, T. Viitala, Enhancement of bioavailability and pharmacodynamic effects of Thymoquinone Via Nanostructured Lipid Carrier (NLC) formulation, AAPS PharmSciTech 17 (3) (2015) 663–672.
[7] C. Godugu, R. Doddapaneni, A.R. Patel, R. Singh, R. Mercer, M. Singh, Novel Gefitinib Formulation with Improved Oral Bioavailability in Treatment of A431 Skin Carcinoma, Pharm. Res. 33 (1) (2015) 137–154.
[8] C. Godugu, A.R. Patel, U. Desai, T. Andey, A. Sams, M. Singh, AlgiMatrix based 3D cell culture system as an in-vitro tumor model for anticancer studies, PLoS ONE 8 (1) (2013) e53708.
[9] C. Godugu, A.R. Patel, R. Doddapaneni, S. Marepally, T. Jackson, M. Singh, Inhalation delivery of Telmisartan enhances intratumoral distribution of nanoparticles in lung cancer models, J. Control. Release 172 (1) (2013) 86–95.
[10] C. Godugu, A.R. Patel, R. Doddapaneni, J. Somagoni, M. Singh, Approaches to improve the oral bioavailability and effects of novel anticancer drugs berberine and betulinic acid, PLoS ONE 9 (3) (2014) e89919.
[11] A.A. Goldberg, H. Draz, D. Montes-Grajales, J. Olivero-Verbel, S.H. Safe, J.T. Sanderson, 3,3′-Diindolylmethane (DIM) and its ring-substituted halogenated analogs (ring-DIMs) induce differential mechanisms of survival and death in androgen-dependent and -independent prostate cancer cells, Genes Cancer 6 (5–6) (2015) 265–280.

[12] S.C. Gupta, S. Patchva, B.B. Aggarwal, Therapeutic roles of curcumin: lessons learned from clinical trials, AAPS J. 15 (1) (2013) 195–218.
[13] V.S. Jamdade, N. Sethi, N.A. Mundhe, P. Kumar, M. Lahkar, N. Sinha, Therapeutic targets of triple-negative breast cancer: a review, Br. J. Pharmacol. 172 (17) (2015) 4228–4237.
[14] P.H. Jellinck, H.L. Makin, D.W. Sepkovic, H.L. Bradlow, Influence of indole carbinols and growth hormone on the metabolism of 4-androstenedione by rat liver microsomes, J. Steroid Biochem. Mol. Biol. 46 (6) (1993) 791–798.
[15] W.H. Lee, C.Y. Loo, P.M. Young, D. Traini, R.S. Mason, R. Rohanizadeh, Recent advances in curcumin nanoformulation for cancer therapy, Expert Opin. Drug Deliv. 11 (8) (2014) 1183–1201.
[16] P. Lei, M. Abdelrahim, S.D. Cho, X. Liu, S. Safe, Structure-dependent activation of endoplasmic reticulum stress-mediated apoptosis in pancreatic cancer by 1,1-bis(3′-indoly)-1-(p-substituted phenyl)methanes, Mol. Cancer Ther. 7 (10) (2008) 3363–3372.
[17] Y. Liu, L. Wang, Y. Zhao, M. He, X. Zhang, M. Niu, N. Feng, Nanostructured lipid carriers versus microemulsions for delivery of the poorly water-soluble drug luteolin, Int. J. Pharm. 476 (1–2) (2014) 169–177.
[18] D.J. McClements, F. Li, H. Xiao, The nutraceutical bioavailability classification scheme: classifying nutraceuticals according to factors limiting their oral bioavailability, Annu. Rev. Food Sci. Technol. 6 (2015) 299–327.
[19] S.A. O'Toole, J.M. Beith, E.K. Millar, R. West, A. McLean, A. Cazet, A. Swarbrick, S. R. Oakes, Therapeutic targets in triple negative breast cancer, J. Clin. Pathol. 66 (6) (2013) 530–542.
[20] S. Okonogi, P. Riangjanapatee, Physicochemical characterization of lycopene-loaded nanostructured lipid carrier formulations for topical administration, Int. J. Pharm. 478 (2) (2015) 726–735.
[21] A.L. Palange, D. Di Mascolo, C. Carallo, A. Gnasso, P. Decuzzi, Lipid-polymer nanoparticles encapsulating curcumin for modulating the vascular deposition of breast cancer cells, Nanomedicine 10 (5) (2014) 991–1002.
[22] A.R. Patel, C. Godugu, H. Wilson, S. Safe, M. Singh, Evaluation of spray BIO-Max DIM-P in dogs for oral bioavailability and in Nu/nu mice bearing orthotopic/metastatic lung tumor models for anticancer activity, Pharm. Res. 32 (7) (2015) 2292–2300.
[23] R.R. Patlolla, M. Chougule, A.R. Patel, T. Jackson, P.N. Tata, M. Singh, Formulation, characterization and pulmonary deposition of nebulized celecoxib encapsulated nanostructured lipid carriers, J. Control. Release 144 (2) (2010) 233–241.
[24] R. Qi, Y.Z. Li, C. Chen, Y.N. Cao, M.M. Yu, L. Xu, B. He, X. Jie, W.W. Shen, Y.N. Wang, M.A. van Dongen, G.Q. Liu, M.M. Banaszak Holl, Q. Zhang, X. Ke, G5-PEG PAMAM dendrimer incorporating nanostructured lipid carriers enhance oral bioavailability and plasma lipid-lowering effect of probucol, J. Control. Release 210 (2015) 160–168.
[25] D.V. Ratnam, G. Chandraiah, A.K. Meena, P. Ramarao, M.N. Kumar, The co-encapsulated antioxidant nanoparticles of ellagic acid and coenzyme Q10 ameliorates hyperlipidemia in high fat diet fed rats, J. Nanosci. Nanotechnol. 9 (11) (2009) 6741–6746.
[26] G.A. Reed, D.W. Arneson, W.C. Putnam, H.J. Smith, J.C. Gray, D.K. Sullivan, M.S. Mayo, J.A. Crowell, A. Hurwitz, Single-dose and multiple-dose administration of indole-3-carbinol to women: pharmacokinetics based on 3,3′-diindolylmethane, Cancer Epidemiol. Biomarkers Prev. 15 (12) (2006) 2477–2481.
[27] G.A. Reed, J.M. Sunega, D.K. Sullivan, J.C. Gray, M.S. Mayo, J.A. Crowell, A. Hurwitz, Single-dose pharmacokinetics and tolerability of absorption-enhanced 3,3′-diindolylmethane in healthy subjects, Cancer Epidemiol. Biomarkers Prev. 17 (10) (2008) 2619–2624.
[28] A. Shakeri, A. Sahebkar, Nanotechnology: a successful approach to improve oral bioavailability of phytochemicals, Recent Pat. Drug Deliv. Formul. 10 (1) (2016) 4–6.
[29] H.K. Shete, N. Selkar, G.R. Vanage, V.B. Patravale, Tamoxifen nanostructured lipid carriers: enhanced in vivo antitumor efficacy with reduced adverse drug effects, Int. J. Pharm. 468 (1–2) (2014) 1–14.
[30] J.A. Siddiqui, A. Singh, M. Chagtoo, N. Singh, M.M. Godbole, B. Chakravarti, Phytochemicals for breast cancer therapy: current status and future implications, Curr. Cancer Drug Targets 15 (2) (2015) 116–135.
[31] K. Thanki, R.P. Gangwal, A.T. Sangamwar, S. Jain, Oral delivery of anticancer drugs: challenges and opportunities, J. Control. Release 170 (1) (2013) 15–40.
[32] T.H. Tran, T. Ramasamy, D.H. Truong, H.G. Choi, C.S. Yong, J.O. Kim, Preparation and characterization of fenofibrate-loaded nanostructured lipid carriers for oral bioavailability enhancement, AAPS PharmSciTech 15 (6) (2014) 1509–1515.
[33] K. Vanderlaag, Y. Su, A.E. Frankel, R.C. Burghardt, R. Barhoumi, G. Chadalapaka, I. Jutooru, S. Safe, 1,1-Bis(3′-indolyl)-1-(p-substituted phenyl)methanes induce autophagic cell death in estrogen receptor negative breast cancer, BMC Cancer 10 (2010) 669.
[34] K. Vanderlaag, Y. Su, A.E. Frankel, H. Grage, R. Smith 3rd, S. Khan, S. Safe, 1,1-Bis(3′-indolyl)-1-(p-substituted phenyl)methanes inhibit proliferation of estrogen receptor-negative breast cancer cells by activation of multiple pathways, Breast Cancer Res. Treat. 109 (2) (2008) 273–283.
[35] H.A. Wahba, H.A. El-Hadaad, Current approaches in treatment of triple-negative breast cancer, Cancer Biol. Med. 12 (2) (2015) 106–116.
[36] M. York, M. Abdelrahim, S. Chintharlapalli, S.D. Lucero, S. Safe, 1,1-bis(3'-indolyl)-1-(p-substitutedphenyl)methanes induce apoptosis and inhibit renal cell carcinoma growth, Clin. Cancer Res. 13 (22 Pt 1) (2007) 6743–6752.

Pharm Res (2017) 34:2371–2384
DOI 10.1007/s11095-017-2244-x

RESEARCH PAPER

Liposomes co-Loaded with 6-Phosphofructo-2-Kinase/Fructose-2, 6-Biphosphatase 3 (PFKFB3) shRNA Plasmid and Docetaxel for the Treatment of non-small Cell Lung Cancer

Nusrat Chowdhury[1] • Imran Vhora[1] • Ketan Patel[1,2] • Ravi Doddapaneni[1,3] • Arindam Mondal[1] • Mandip Singh[1]

Received: 26 April 2017 / Accepted: 31 July 2017 / Published online: 5 September 2017

ABSTRACT

Purpose Non-small cell lung cancer is the leading cause of cancer related deaths globally.
Considering the side effects and diminishing chemosensitivity to chemotherapy, novel treatment approaches are sought. Hence, we aim to develop a liposomal co-delivery system of pDNA expressing shRNA against PFKFB3 (pshPFKFB3) and docetaxel (DTX).

Methods Cationic DTX liposomes complexed with pshPFKFB3 (PSH-DL) were developed. *In vitro* cell line studies were performed to evaluate transfection, PFKFB3 mRNA silencing, cytotoxicity, pGP inhibition, and protein markers expression. *In vivo* efficacy study was performed in A549 xenograft nude mice model.

Results Cytotoxicity studies showed significantly enhanced anticancer activity of PSH-DL against individual treatment alone confirming the chemoenhancing effect of pshPFKFB3 on DTX activity. Fluorescence microscopy and RT-PCR showed effective transfection and RNAi by pshPFKFB3. pGP inhibition assay and western blotting revealed that PFKFB3 downregulation caused diminution of pGP activity leading to changes in cell cycle (Cdk2), survival (survivin), apoptosis (Bcl2 and cleaved caspase 3) and stress (p-JNK and p-p38) markers so that induces apoptosis by PSH-DL in NSCLC cells. PSH-DL also showed ~3.8-fold reduction in tumor volume in A549 xenograft model which was significantly higher than individual treatments alone.

Conclusion Targeting PFKFB3 through shRNA based RNAi is a promising approach for potentiating activity of DTX in NSCLC.

KEY WORDS docetaxel liposome · gene delivery · lung cancer · PFKFB · shRNA

ABBREVIATIONS

3PO	3-(3-pyridinyl)-1-(4-pyridinyl)-2-propen-1-one
AO/EB staining	Acridine orange and ethidium bromide staining
DDAB	Dimethyldioctadecyl-ammonium bromide
DL	Docetaxel liposomes
DOTAB	N- (2, 3-Dioleoyloxy-1-propyl) trimethylammonium bromide
DPPC	1,2-dipalmitoyl-sn-glycero-3-phosphocholine
DSPE-PEG-2000	1,2-Distearoyl-sn-glycero-3-phosphoethanolamine-N- methoxy (polyethyleneglycol) 2000
DTX	Docetaxel
EPR	Enhanced permeation and retention
GFP	Green fluorescent protein
LF2K100	Lipofectamine-2000 complexed with pshPFKFB3 100 ng
MLV	Multi-lamellar vesicles
N/P	Nitrogen to phosphate ratio
NC	Negative control plasmid
NC-pDNA-DL	

Electronic supplementary material The online version of this article (doi:10.1007/s11095-017-2244-x) contains supplementary material, which is available to authorized users.

✉ Mandip Singh
mandip.sachdeva@famu.edu

[1] College of Pharmacy and Pharmaceutical Sciences, Florida A&M University, Tallahassee, Florida 32307, USA

[2] College of Pharmacy and Health Sciences, St. John's University, Jamaica, New York 11439, USA

[3] Department of Ophthalmology, Bascom Palmer Eye Institute, University of Miami Miller School of Medicine, Miami, Florida 33136, USA

	Docetaxel loaded iposomes complexed with negative control plasmid
NC-pDNA-L	Liposomes complexed with negative control plasmid
NSCLC	Non-small cell lung cancer
pDNA	Plasmid Deoxyribonucleic acid
PFK15	1-(4-pyridinyl)-3-(2-quinolinyl)-2-propen-1-one
PFKFB3	6-Phosphofructo-2-Kinase/Fructose-2, 6-Biphosphatase 3
pGP	P-glycoprotein
PSH-DL	Docetaxel loaded liposomes complexed with pshPFKFB3
PSH-L	Blank liposomes complexed with pshPFKFB3
pshPFKFB3	6-Phosphofructo-2-Kinase/Fructose-2, 6-Biphosphatase 3 shRNA plasmid
Rh123	Rhodamine 123
RNA	Ribonucleic acid
RNAi	RNA interference
shRNA	Short hairpin RNA

INTRODUCTION

Lung cancer and particularly non-small cell lung cancer (NSCLC) is the foremost cancer killer for both men and women in the United States (1). The survival rate with lung cancer is approximately 15% which is significantly less than other prevalent cancers, such as breast and prostate cancer. First line of treatment for lung cancer has been chemotherapy for decades and only little success has been achieved; the therapy usually is accompanied with serious dose-limiting side effects (2). Hence, delivery approaches for effective treatment with limited toxicity are sought.

Cancer cells maintain an unusually high glycolytic rate even in the presence of oxygen, a phenomenon first described by Otto Warburg over 75 years ago (3). The glycolytic flux is 2 to 17-folds higher in tumor cells compared to normal cells (4). This is because of the high expression of all the glycolytic enzymes such as phosphofructokinase (6-Phosphofructo-2-Kinase/Fructose-2, 6-Biphosphatase-3, PFKFB3), hexokinase, pyruvate kinase, etc. and transporters induced by several oncogenes and the hypoxia-inducible factor-1 (HIF-1) (5). This leads to the excretion of large amounts of lactate even under aerobic conditions, a phenomenon known as the "Warburg effect". This high glycolytic rate contributes to the ATP supply for cellular work and provides numerous intermediaries which are precursors for the synthesis of macromolecules, such as polysaccharides, nucleic acids, triglycerides and proteins required for cell proliferation (6). Thus, such high glycolytic flux extrapolates well to tumor progression, invasiveness, metastatic tendency and patient mortality and morbidity (7,8). Hence, glycolytic pathway is a suitable target in which over-expressed enzymes can be exploited for drug delivery for the treatment of cancer.

The type of isoenzyme expression is another important parameter besides the higher glycolytic rate exhibited by tumor cells (9). Among the enzymes playing role in glycolysis, four allosteric PFKFB enzymes 1–4 expressed by four independent PFKFB genes, catalyze the rate-limiting phosphorylation of fructose-6-phosphate to fructose-1, 6-bisphosphate, using ATP as the energy source in the glycolysis pathway. Among these four allosteric enzymes, PFKFB3 enzyme retains the highest Kinase/Biphosphatase activity ratio and is expressed by PFKFB3 gene which has been demonstrated to be highly expressed in leukemic cells and in solid tumors (10). Moreover, mitogenic, hypoxic and inflammatory conditions have an inductive effect on the expression of PFKFB3. Hence upregulation of PFKFB genes specific to cancer cells compared to their normal counterparts (from the same patients) with more robust over-expression in breast and lung cancer make it a more appropriate target (8).

There are few reports of potent and selective PFKFB3 inhibitors. Briefly, 3-(3-pyridinyl)-1-(4-pyridinyl)-2-propen-1-one (3PO) is a PFKFB3 inhibitor and has shown cytostatic activity in leukemic and other cancer cells (11). Recently, a novel derivative, PFK158, which is a potent and selective inhibitor of PFKFB3 is being investigated in phase I study in patients with advanced solid malignancies (12). According to Boyd *et al.*, 3PO and PFK158 are inactive in the PFKFB3 kinase assay due to absence of binding sites in these molecules. Other inhibitors, such as pyridazinone inhibitors are also being investigated which have been reported to have an IC_{50} greater that 1 mM (13). Thus, we propose to use a gene delivery system which will utilize plasmid for shRNA against PFKFB3. The approach is novel in its being a plasmid which will provide constant shRNA expression for RNAi (RNA interference) and provide better therapeutic action by removing the target mRNA and hence the protein, unlike the inhibitors which will only block the function of protein. This approach is also advantageous over siRNA based RNAi by having low off-target effects, low immunological reactivity and toxicity, high *in vivo* stability and therapeutic potential (14).

Docetaxel (DTX) has been used as a primary agent for the treatment of solid tumors such as in lung, breast and pancreatic cancers (15–17). Currently available marketed formulations of taxanes (DTX and paclitaxel) face issues of resistance development and toxicities which are dose limiting (18). Abraxane, which is a nanoparticle albumin-bound paclitaxel, has been approved for metastatic pancreatic, lung and breast cancer. It is used in combination with carboplatin for the initial treatment of patients with locally advanced or metastatic NSCLC who are not candidates for curative surgery or radiation therapy (19). Taxotere and taxol, which are micellar formulations of DTX and paclitaxel, respectively, are used for

intravenous therapy of breast, lung, prostate, gastric, head and neck, ovarian and pancreatic cancer. However, both the drugs have dose dependent side effects like neutropenia, alopecia and anemia. Hence, a formulation strategy is required that can overcome its toxicity while providing better alternative treatment approach in comparison to those available in the clinic. Liposomes are able to entrap hydrophobic drugs in the bilayer and provide protection from degradation, reduce toxicity, and possibly help in overcoming multidrug resistance (20). Furthermore, liposomes can be modified using appropriate selection of lipids to load large hydrophobic drugs such as DTX in the bilayer along with the use of cationic lipids to complex with therapeutic genes (21). Liposomal co-delivery of the drug with the shRNA plasmid against PFKFB3 would be of added advantage by providing a simultaneous delivery of drug and gene using the same nano-particulate carrier to the tumor site.

The objective of this study was to evaluate the therapeutic potential of plasmids to provide pool of shRNA in cells for silencing PFKFB3 and evaluate the efficacy of the co-delivery of a chemotherapeutic agent with such RNAi agent. The objective here was to develop a non-toxic liposomal system of DTX and plasmid which can express PFKFB3 shRNA for inhibiting a key enzyme in the glucose metabolism for parental delivery. The co-delivery liposomal system was evaluated in lung cancer cells *in vitro* for its therapeutic effects. Further, *in vivo* A549 xenograft model was used to evaluate the therapeutic potential of the system and proof-of-concept was established through mechanistic studies to characterize the involvement of specific pathways in the therapeutic effectiveness of the combination.

MATERIALS AND METHODS

Materials

Docetaxel (DTX) (LC Laboratories, Woburn, MA) was dissolved in dimethyl sulfoxide (DMSO) to prepare 1 mM stock solution and aliquots were stored at −20°C. Stock solutions were diluted to the desired final concentrations with medium just before use. 1,2-dipalmitoyl-sn-glycero-3-phosphocholine (DPPC), N- (2,3-Dioleoyloxy-1-propyl) trimethylammonium bromide (DOTAB) and 1,2-Distearoyl-sn-glycero-3-phosphoethanolamine-N- methoxy (polyethyleneglycol) (DSPE-PEG-2000) were obtained from Lipoid LLC, Germany. Dimethyldioctadecyl-ammonium bromide (DDAB) was purchased from Sigma–Aldrich (St. Louis, Missouri). All the chemicals were used without any further purification. The mouse antibodies against β- actin were purchased from Santa Cruz Biotechnology (Dallas, TX). The rabbit antibodies against Cdk2, Survivin, Bcl2, Cleaved Caspase 3, JNK, pJNK, p38 and p-p38 were purchased from Cell Signaling Technology (Danvers, MA). Secondary goat anti-rabbit or anti-mouse antibodies conjugated with horseradish peroxidase was bought from Santa Cruz Biotechnology (Dallas, TX). iScript™ Advanced cDNA Synthesis Kit and SsoAdvanced™ Universal SYBR® Green Supermixwere purchased from Bio rad (California, USA). Q-PCR primers for mouse PFKFB3 were purchased from Origene (Rockville, MD). PFKFB3 plasmid (pshPFKFB) was obtained from Origene Technologies (Rockville, MD).

Cell Lines

The cell lines, A549 (CCL- 185), H460 (HTB- 177) and HEK293 (CRL- 1573), were obtained from American Type Culture Collection (ATCC). All cell lines were maintained in Dulbecco's Modified Eagle's medium (DMEM; Sigma Aldrich, St Louis, MO) nutrient mixture supplemented with 10% fetal bovine serum (FBS) from Invitrogen (Grand Island, NY) and antibiotic-antimycotic mixture comprising penicillin (5000 U/mL), streptomycin (0.1 mg/mL) and neomycin (0.2 mg/mL) from Sigma Aldrich (St Louis, MO, USA). The cell lines were sub-cultured when they were approximately 80% confluent with 0.25% trypsin-EDTA (Invitrogen, Grand Island, NY).

Methods

Preparation and Characterization of co-Loaded Liposomes

Preparation of Different Liposomal Formulations. DTX liposomes (DL) were prepared by ether injection method. Briefly, DTX, DOPC, DOPE, DOTAP, DDAB and DSPE-$mPEG_{2000}$ were dissolved in 1.5 mL diethyl ether. The solution was then injected into 10 ml of distilled water at 55°C. The suspension formed was kept at the same temperature for 60 min under constant stirring to form multi-lamellar vesicles (MLV). The small unilamellar vesicles were obtained from the MLV suspension by ultra-sonication (Vibra Cell™, 130w, 20 kHz, 4 min). DL were optimized using DoE study using Box-Behnken design (Design Expert 7.0, Sate Ease, MA) using entrapment efficiency and particle size. Optimized liposomes were used for complexation with pshPFKFB3 to obtain co-loaded liposomes (PSH-DL). DTX liposomes complexed with negative control pDNA (NC-pDNA) (NC-pDNA-DL) were used for *in vitro* and *in vivo* studies. For this, DL were incubated with pshPFKFB3 or NC-pDNA at room temperature at increasing w/w ratio of pshPFKFB3 to cationic lipids and were analyzed for complexation efficiency. Similarly, liposomes without DTX complexed with pshPFKFB3 (PSH-L) were also prepared using the same lipid composition for *in vitro* studies.

Physicochemical Characterization of Liposome. Particle size and polydispersity of the liposomes were determined by photon

correlation spectroscopy (PCS) using Zeta sizer (PSS Systems, USA). Zeta potential of liposomes was determined by electrophoretic mobility determination using Zeta sizer (PSS systems, USA). The liposome samples were analyzed after appropriate dilution with deionized water.

For the entrapment efficiency, the amount of DTX encapsulated in the liposomes was determined by HPLC. A reverse-phase HPLC column (Agilent Eclipse XDB-C18, 4.6 × 250 mm, 5 μm) was used. Briefly, formulation was centrifuged at 5000 rpm for 10 min for pelleting the unentrapped DTX. Supernatant containing DTX liposomes was mixed with methanol (1:4 v/v) for liposomal disruption and then diluted appropriately with mobile phase consisting of acetonitrile and deionized water (60:40, v/v). The flow rate of mobile phase was set to 1.0 mL/min. The run time was set at 15 min and the column temperature was ambient. Prior to the injection of the drug solution, the column was equilibrated for at least 0.5 h with the mobile phase flowing through the system. The column effluent was detected with a PDA detector at 227 nm. The calibration curve was linear in the range of 50–50,000 ng/ml with a regression coefficient $R^2 = 0.999$. The drug encapsulation efficiency was defined as the percentage of the amount of DTX encapsulated in the liposomes to total amount of drug.

$$\%\,\text{Entrapment efficiency} = \text{Amount of drug entrapped} \times 100/\text{Total amount of drug}$$

Complexation efficiency of pshPFKFB3 with the liposomes was evaluated by centrifugation and UV analysis was done using NanoDrop 1000 (ThermoScientific, USA). Briefly, PSH-L and PSH-DL were centrifuged at 18000 rpm for 2 h at 4°C (Beckman J2-HC Centrifuge, Beckman, US) to settle down the liposomes. Supernatant was analyzed spectrophotometrically and content of pDNA was calculated using the standard expression OD1 = 50 μg/mL of double stranded pDNA. Readings from formulations were compared to readings from standard dilution of naked pshPFKFB3. Complexation efficiency was calculated using following equation;

$$\%\,\text{Complexation efficiency} = \left(A_{\text{pshPFKFB3standard}} - A_{\text{supernatant}}\right) \times 100/A_{\text{pshPFKFB3standard}}$$

Where, $A_{\text{pshPFKFB3standard}}$ is absorbance of the standard naked pshPFKFB3, $A_{\text{supernatant}}$ is absorbance of supernatant after centrifugation:

In Vitro Cell Cytotoxicity

Briefly, A549, H460 and HEK293 cells were plated at 10,000 cells/well in a 96-well plate. Cells were treated either with DTX solution or NC-pDNA-DL at different concentrations for 48 h to check the effect of the liposomes. Cells were transfected with either control plasmid or plasmid directed against PFKFB3 (pshPFKFB3) at 40 ng/well along with DTX liposomes with various concentrations for 48 h. Cells were washed with PBS and 100 μl of 0.5% (v/v) glutaraldehyde was added for fixing the plate and incubated for 30 min. Next 0.5% (w/v) crystal violet dye was added and the plate was incubated for another 20 min. The plate was washed with tap water and dried before adding 1% (w/*v*) sodium lauryl sulfate (SLS) and read at 570 nm.

Cellular Uptake and Transfection Efficiency

Briefly, A549 cells were grown to 60–70% confluency and incubated in serum-free medium with PSH-L for 4 h at 37°C and 5% CO_2 in quantities required to deliver 20–100 ng of DNA per 10,000 cells. 100 ng of pshPFKFB3 was complexed with Lipofectamine 2000 using manufacturer's protocol to use as positive reference control. The cells were incubated for 48 h with regular media. After incubation, the medium was removed and cells were washed twice with sterile PBS and GFP expression was visualized by fluorescence microscopy using an Olympus BX40 fluorescence microscope (22).

Quantitative RT-PCR

Total RNA from cells was extracted using Tiazol reagent and treated with RNase-free DNase to remove any residual genomic DNA. Single-stranded cDNAs were synthesized by incubating total RNA (5 μg) with 5X reaction mix, reverse transcriptase and Nuclease free water at 46°C for 20 min and 95°C for 1 min in a final volume of 20 μl. Quantitative real-time PCR (RT-PCR) was performed to compare expression levels of each of the total RNA sample. RT-PCR was performed on CFX96 Real-Time System (Bio rad, California, USA) in the presence of 10 μl SYBR Green Supermix, 1 μl cDNA, and H_2O was added to a final volume of 20 μl. RT-PCR was performed with an initial denaturation step of 30 s at 95°C, followed by 40 cycles of 30 s at 95°C, 5 s at 65°C and annealing temperature at 60°C. PCR products were monitored in real time by measuring the increase in fluorescence caused by the binding of SYBR Green I Dye.

pGP Inhibition Assay

Briefly, A549 cells were plated in 20,000 cells/well in a 24-well plate and allowed to attach overnight. The cells were treated with different concentrations of pshPFKFB3, and incubated for 24 h at 37°C. Wells were treated with Rh123 alone or with PSH-L /verapamil and incubated for 60 min and then washed twice with PBS. Fluorescence microscopic images were taken to observe

the uptake of Rh123 in the presence of pshPFKFB3 and verapamil.

Apoptosis Analysis AO/EB Double-Staining and Fluorescent Microscopy

Briefly, A549 and H460 cells were seeded at a density of 10,000 cells/well plate in a 96-well plate and allowed to attach for 24 h. The cells were treated with or without pshPFKFB3, DL and PSH-DL complexes and incubated for 24 h at 37°C. A control was maintained as untreated cells. The cells were washed twice with PBS and incubated with 3 mg/ml acridine orange (AO) and 3 mg/mL ethidium bromide (EB) for 30 min. The cells were washed twice with PBS before observing them with fluorescence microscopy using an Olympus BX40 fluorescence microscope.

Western Blot

Western blotting was carried out on cells treated with different formulations for analyses of various protein markers Cdk2, Survivin, Bcl2, Cleaved Caspase 3, JNK, pJNK, p38 and p-p38 and PFKFB3. Protein lysates were prepared from A549 and H460 cells. Briefly, after 48 h post incubation with PSH-L, DL and PSH-DL; the cells were incubated in RIPA buffer (50 nM Tris-HCl, pH 8.0, with 150 nM Sodium Chloride, 1.0% Igepal CA-630 (NP-40), 0.5% Sodium Deoxychlorate, and 0.1% sodium dodecyl sulfate) with protease inhibitor (500 mM phenylmethylsulfonyl fluoride). Protein concentrations were determined according to BCA protein assay using manufacturer's protocol (Rockford, IL) and the standard plot was generated by using bovine serum albumin (BSA). Briefly, 50 µg of protein from the control sample and all the different treatment samples were denatured by boiling at 100°C for 5 min in SDS sample buffer and subsequently electrophoresed in 10% SDS-PAGE gel and then transferred into nitrocellulose membranes followed by blocking with 5% BSA in tris-buffered saline with Tween 20 (10 mM tris-HCl (pH 7.6), 150 mM NaCl, and 0.5% Tween), and probed with antibodies against Cdk2, Survivin, Bcl2, Cleaved Caspase 3, JNK, pJNK, p38 and p-p38 at 1:500 and PFKFB3 at 1:200 for the lung cancer cells. Proteins were detected with HRP conjugated secondary antibodies using SuperSignal West pico chemiluminescent solution (PIERCE, Rockford, IL). Densitometric analysis of bands was performed as per our previous methods using Chemi-Doc XRS+ Imaging system (Bio-Rad). Results were expressed as percentage ratios of protein expression to beta-actin (set to 100%) and plotted against the relative intensity compared to the control.

In Vivo Anti-Tumor Activity

The antitumor efficacy of different formulations of PSH-L, DL and PSH-DL were, investigated using A549 tumor xenograft model in nude mice already established in our laboratory. BALB/c athymic nudes were purchased from Charles River Laboratories (Wilmington, Maryland) and were kept in specific pathogen-free conditions in a facility approved by the American Association for Accreditation of Laboratory Animal Care (AAALAC). All experiments were done in accordance with the guidelines of the Institutional Animal Care and Use Committee (IACUC) at Florida A&M University. For this, $4x10^6$ A549 human lung cancer cells were subcutaneously injected into the right flank of the mice. When tumor volume approximately reached 150 mm^3, respective formulations were given intravenously at a dose of 5 mg/kg of DTX, once every 3 days for 2 weeks. Subsequently, tumor volume was measured at specified time using Vernier caliper in two dimensions. Tumor volume (V) was measured by the formula: $V = (LxW^2)/2$, where length (L) is the longest diameter and width (W) is the shortest diameter perpendicular to length.

RESULTS

Preparation and Characterization of Dual Functioning Liposomes

Preparation of DTX Liposomes

DTX liposome formulation was prepared by solvent evaporation method by using different ratios of phospholipid mixtures. Several batches of DTX liposomes were prepared according to the DoE studies using the Box Behnken design with the quadratic model. The results are shown in the Supplementary information S1. The particle size of DTX liposomes ranged from 84.0 nm to 133.7 nm and the entrapment efficiency of DTX ranged from 43.6% to 98.9%. Optimized DTX liposome (using Desirability index based selection method) was made based on lowest particle size and highest entrapment efficiency and the composition of optimum batch was 10 mg DTX, 150 mg DOPC, 40 mg cationic lipids (DOTAP and DDAB), 40 mg DOPE and 30 mg DSPE-$mPEG_{2000}$. This formulation had particle size of 91.2 ± 9.4 nm, zeta potential of +22.3 ± 1.8 mV, entrapment of 87.3 ± 2.6% as shown in supplementary information S1. Docetaxel loading in total lipids used is 3.36 ± 0.09% w/w. The optimized lipid composition was further used for complexation with pshPFKFB3 or with NC-pDNA. Particle size distribution, zeta potential and entrapment efficiency data of different liposomal formulations are shown in Table I.

Table I Characteristics of Docetaxel Liposome Formulation and the Corresponding Placebo

Formulation	Particle size (nm)	Polydispersity	Zeta potential (mV)	Entrapment efficiency (%)
Blank liposomes (without DTX and pshPFKFB3)	87.3 ± 2.3	0.204 ± 0.009	+21.6 ± 1.9	–
DTX liposomes (From DoE)	91.2 ± 9.4	0.269 ± 0.012	+22.3 ± 1.8	87.3 ± 2.6
DL	105.6 ± 7.4	0.265 ± 0.021	+17.8 ± 2.2	89.7 ± 4.1
PSH-DL	110.3 ± 8.3	0.285 ± 0.019	+18.5 ± 0.9	88.9 ± 3.4

Preparation of PSH-DP

Briefly, pshPFKFB3 complexed liposomes were prepared using the lipid composition utilized for DTX liposomes. The results are shown in Fig. 1. The complexation efficiency of liposomes was evaluated by centrifugation/UV spectrophotometric analyses at different w/w ratios of cationic lipids to pDNA. The weight ratio that allowed complete complexation of the pDNA was found to be 2:1 and it corresponded to the N/P ratio of 2.2 indicating 2.2 M excess of cationic lipids over phosphates of pDNA. The weight ratio higher than 2.2 did not significantly increase the pDNA complexation. Similarly, DTX lipoplexes complexed with NC-pDNA were prepared at the same weight ratio. The particle size and zeta potential of the complexed liposomes were found to be 110.3 ± 8.3 nm and 18.5 ± 0.9 mV. Complexation of the pDNA did not cause any significant increase in the size of the liposomes indicating that the liposomal bilayer retained its integrity upon complexation with pDNA and maintained the small unilamellar vesicular structure. The marginal increase in the mean particle size can be accounted to the pDNA complexation to the liposomes. Moreover, as expected, reduction in the zeta potential of the liposomes was in line with the pDNA complexation to the cationic liposomes.

Cytotoxicity of DTX and pshPFKFB3

Optimized liposomes of DTX and pshPFKFB3 were first evaluated for their cytotoxicity against NSCLC cells *in vitro*. Initially, individual cytotoxicity of the DTX liposomes complexed with NC-pDNA (negative control pDNA) and PSH-L without DTX loading were formulated to determine their individual effects.

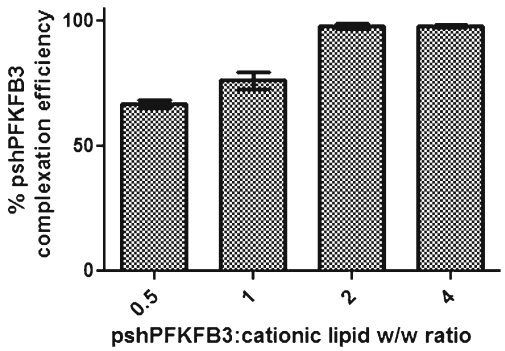

Fig. 1 Complexation efficiency of pshPFKFB3 with DL at different w/w ratios of plasmid to cationic lipids. The results show mean ± SEM of three independently performed experiments.

Cytotoxicity of DTX Liposome

The cytotoxicity of DL was evaluated against DTX solution against A549 and H460 cells by incubating cells with various concentrations of DTX for 24 and 48 h. In-vitro cytotoxicity results showed that after 48 h of exposure to DTX solution, the IC_{50} values of A549 and H460 cells were 0.43 μM and 0.37 μM and were decreased to 0.32 μM and 0.20 μM, respectively when treated with DTX liposomes. *The time dependent cytotoxicity by DTX* observed with the DTX-liposomal formulation was possibly due to cell internalization of nanoparticles over a period of time (Table II).

Cytotoxicity of Cationic Lipids on Normal Cells

The cytotoxicity of the blank liposomes was evaluated against HEK293 cells to determine the safety of the formulated delivery systems (23) (Fig. 2). The cells were treated with different concentrations of cationic lipids and incubated for 48 h. The cells showed a viability of approximately 60% even in the highest concentration of 6 mg/mL of cationic lipid and up to 3 mg/mL concentration, cells retained ≥80% viability.

Cytotoxicity of DTX-pshPFKFB3 in Combination

The effect of PSH-L was evaluated with A549 and H460 cells and it was observed that cytotoxicity of pshPFKFB3 was 3.3% and 3.8% for A549 and H460, respectively; but when combined with DL at concentrations of 0.25 μM, 0.50 μM and 1.0 μM, the cytotoxicity increased to 66.6%, 72.5% and

Table II IC50 of Different Lung Cancer Cells for Docetaxel Solution and Docetaxel Liposome over a Period of 24 and 48 h

Treatment	Cell line	24 H	48 H
DTX Solution (μM)	A549	0.95	0.43
	H460	>2	0.37
DTX Liposome (μM)	A549	0.23	0.32
	H460	>2	0.20

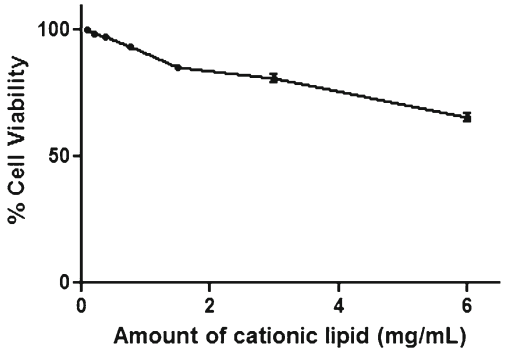

Fig. 2 *In vitro* cell viability of blank liposome for HEK293 cells.

85.4% for A549 NSCLC cells; 30.8%, 52.4% and 70.4% for H460 NSCLS cells respectively (Fig. 3). Both A549 and H460 showed dose dependent increase in cellular toxicity.

Effect of pshPFKFB3 on the Anticancer Activity of DTX Liposome

Inhibition of PFKFB3 mRNA Levels by pshPFKFB3

For quantitative estimation of effect of formulations on PFKFB3 mRNA expression, total RNAs from A549 cells were analyzed by RT- PCR after reverse transcription of the RNA into cDNA. The results are shown in Fig. 4. Glyceraldehyde-3-phosphate dehydrogenase (GAPDH) mRNA was kept as a housekeeping gene. Liposomes prepared with negative control plasmid (NC-pDNA-L) did not show any silencing of the PFKFB3 mRNA. It was observed that the PFKFB3 mRNA levels decreased by approximately 11% at 20 ng and 35% at 40 ng plasmid level as compared to the control which was significantly lower than control. Interestingly, there was no significant decrease ($p > 0.05$) in the PFKFB3 mRNA level when concentration of plasmid was increased from 40 ng to up to 100 ng per 10,000 cells. Therefore, inhibition of PFKFB3 mRNA expression by developed PSH-L was found to be effective between 40 ng - 100 ng of the pshPFKFB3 complexed with liposomes.

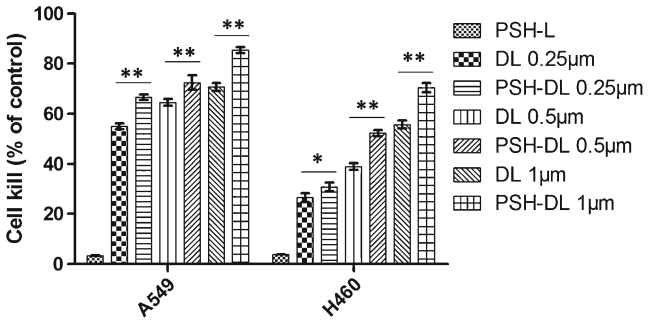

Fig. 3 Cytotoxicity of PSH-DL complexes against A549 and H460. The results show mean ± SEM of three independently performed experiments. ns, statistically non-significant, compared with DL. *, $P < 0.05$, compared with DL. **, $P < 0.01$, compared with DL.

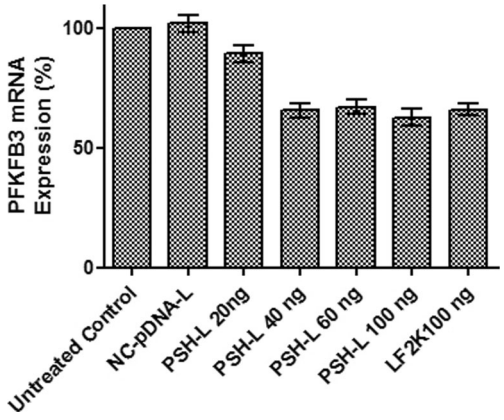

Fig. 4 Impact of PSH-L at different doses of pshPFKFB3 on PFKFB3 mRNA expression in A549 cells. Bar graph depicts real-time RT-PCR expression of PFKFB3 as compared to untreated control cells. The results show mean of three independent experiments with SEM. NC-pDNA-L liposomes with 100 ng of NC-pDNA, LF2K100 = Lipofectamine-2000 complexed with pshPFKFB3 100 ng, PSH-L20, 40, 60 and 100 = PSH-L with 20 ng, 40 ng, 60 ng and 100 ng of pshPFKFB3.

Fluorescence Microscopy for Expression of pshPFKFB3

Cell internalization and expression of GFP by PSH-L was visualized by fluorescence microscopy. The results of A549 lung cancer cells with different test formulations and control cells are presented in Fig. 5. Fluorescence from the control cells eliminated the possibility of background fluorescence from the cells. Naked pshPFKFB3 was not able to transfect the cells and hence did not show any GFP expression which goes in line with the RT-PCR studies. This fluorescence may result from some cell transfection via nonspecifically captured plasmid-bearing liposomes. Fluorescence microscopy images also revealed that the treatment of A549 cells with PSH-L resulted in an increase in cellular fluorescence. Hence, the liposomes were being internalized in the cells and could express GFP. Expression of GFP from the vector also suggests the expression of the shPFKFB3 as well. The cells treated with the complexes demonstrated a substantially higher fluorescence, i.e., a higher transfection outcome at a concentration of 40 ng per 10,000 cells. At similar conditions, 100 ng pshPFKFB3 complexes prepared with Lipofectamine-2000 (LF2K100), a commercial transfection reagent, provided higher extent of fluorescence level compared with the PSH-L40.

Effect of pshPFKFB3 on pGP Activity

Rhodamine123 exclusion assay was performed for demonstration of pGP activity after PSH-L treatment of A549 cells. The microscopic images are shown in Fig. 6. Verapamil with rhodamine was used as a positive control, Rh123 as a negative control and lipofectamine-2000 as reference control. The accumulation of Rh123 was noted to differ for different

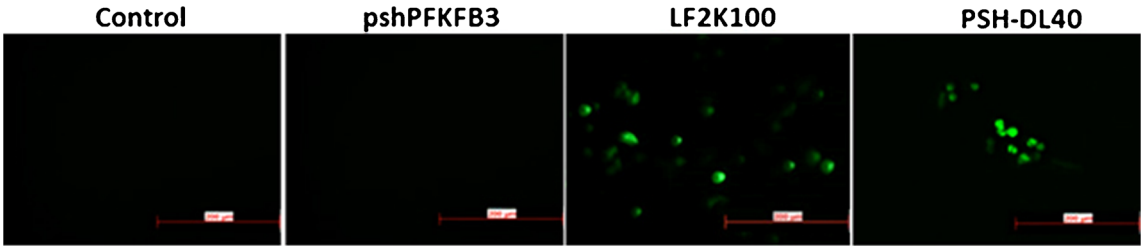

Fig. 5 *In vitro* expression of GFP after pshPFKFB3 plasmid transfection. pPFKFB3 plasmid contains GFP expressing sequence that can express GFP after transfection. Control indicates cells without any treatments. pshPFKFB3 indicates cells treated with naked pshPFKFB3. LF2K100 = Lipofectamine-2000 complexed with 100 ng pshPFKFB3, PSH-L 40 = PSH-L with 40 ng of pshPFKFB3. Scale bar is of 200 μm size.

formulations or controls indicating differential pGP activity in the cells after different treatments. Verapamil being a pGP inhibitor led to highest accumulation of Rh123 in the cells as seen by the highest green fluorescence in the cells. Also, pshPFKFB3 liposomes led to reduced exclusion of Rh123. It was visually discernible that there was reduction in Rh123 efflux after treatment with pshPFKFB3 liposomes from 20 ng/well to 40 ng/well. However, increasing levels of pshPFKFB3 i.e. 60 ng and 100 ng did not cause any visually apparent increase in the fluorescence compared to 40 ng level and the Rh123 accumulations were almost similar to 40 ng treatment.

Apoptosis Analysis by AO/EB Double-Staining and Fluorescent Microscopy

After treatment with PSH-L, DL and PSH-DL complexes for 48 h, apoptosis induction was demonstrated using acridine orange and ethidium bromide on A549 and H460 cells. As shown (Fig. 7) in the control group (no treatment), a scarce number of apoptotic cells were visible. Same observation was there with the PSH-L as well; while in DL group and PSH-DL group, the number of apoptotic cells increased. PSH-DL showed highest number of apoptotic cells to the magnitude of 2–3 folds higher when co-loaded liposomes were used. A similar trend was observed in the H460 cells as well which had the highest number of apoptotic cells in the PSH-DL group.

Western Blot Analyses

Western blotting was performed to see the effects of different formulations on expression of various cell apoptosis, survival and stress markers. Densitometric analysis of bands showed that PFKFB3 was significantly downregulated as compared to control in the PSH-L and similar results were observed with PSH-DL treated cells (Fig. 8). Further, the densitometric analysis of western blot bands revealed that PFKFB3 relative band density was reduced to 0.41 for the PSH-DL in comparison to untreated control cells for both, A549 and H460 cells. A significant down regulation of Cdk2 was observed in both the NSCLC. The combination caused a decrease in the relative intensity to 0.43 and 0.66 in A549 and H460 cells respectively, as compared to the control. Cell survival marker, survivin, expression also decreased significantly ($p < 0.05$) to 0.31 and

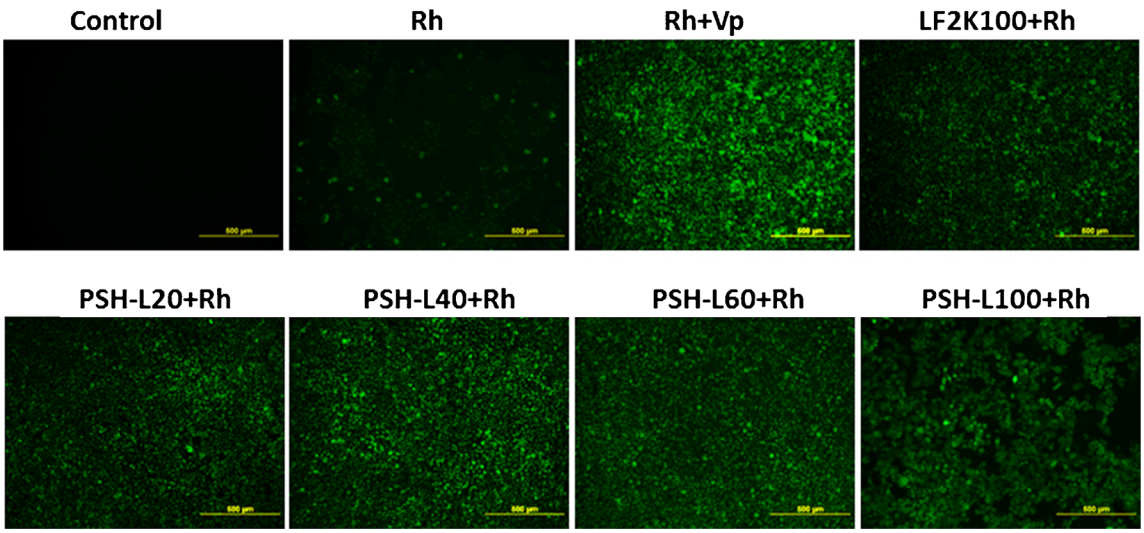

Fig. 6 pGP inhibition assay using Rh123. Fluorescence microscopy images of A549 lung cancer cells incubated with Rh123 after treatment with different formulations. Rh = Rh123, Vp = verapamil, LF2K100 = Lipofectamine-2000 complexed with pshPFKFB3 100 ng, PSH-L20, 40, 60 and 100 = PSH-L with 20 ng, 40 ng, 60 ng and 100 ng of pshPFKFB3.

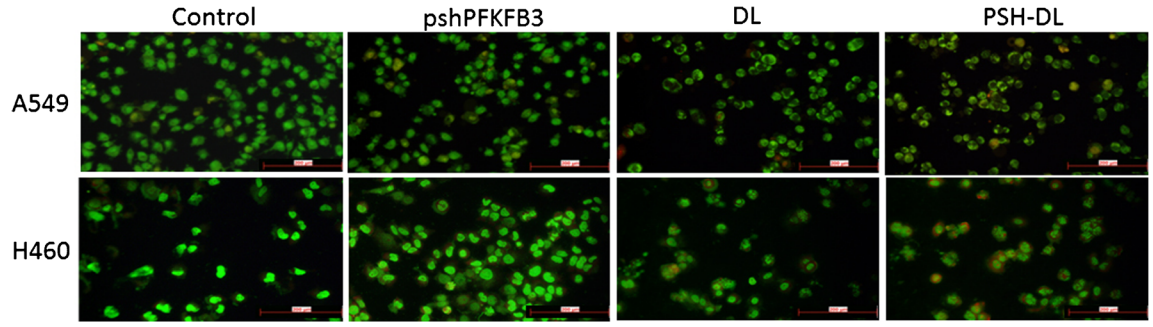

Fig. 7 Apoptosis by AO/EB dual staining. Fluorescent microscopic images of A549 and H460 NSCLC cells after different treatments.

0.24 in A549 and H460 respectively in the PSH-DL complexes as compared to the control. The expression of Bcl2, an apoptotic marker, was significantly down regulated ($p < 0.05$) to 0.04 and 0.06 in the PSH-DL complexes for

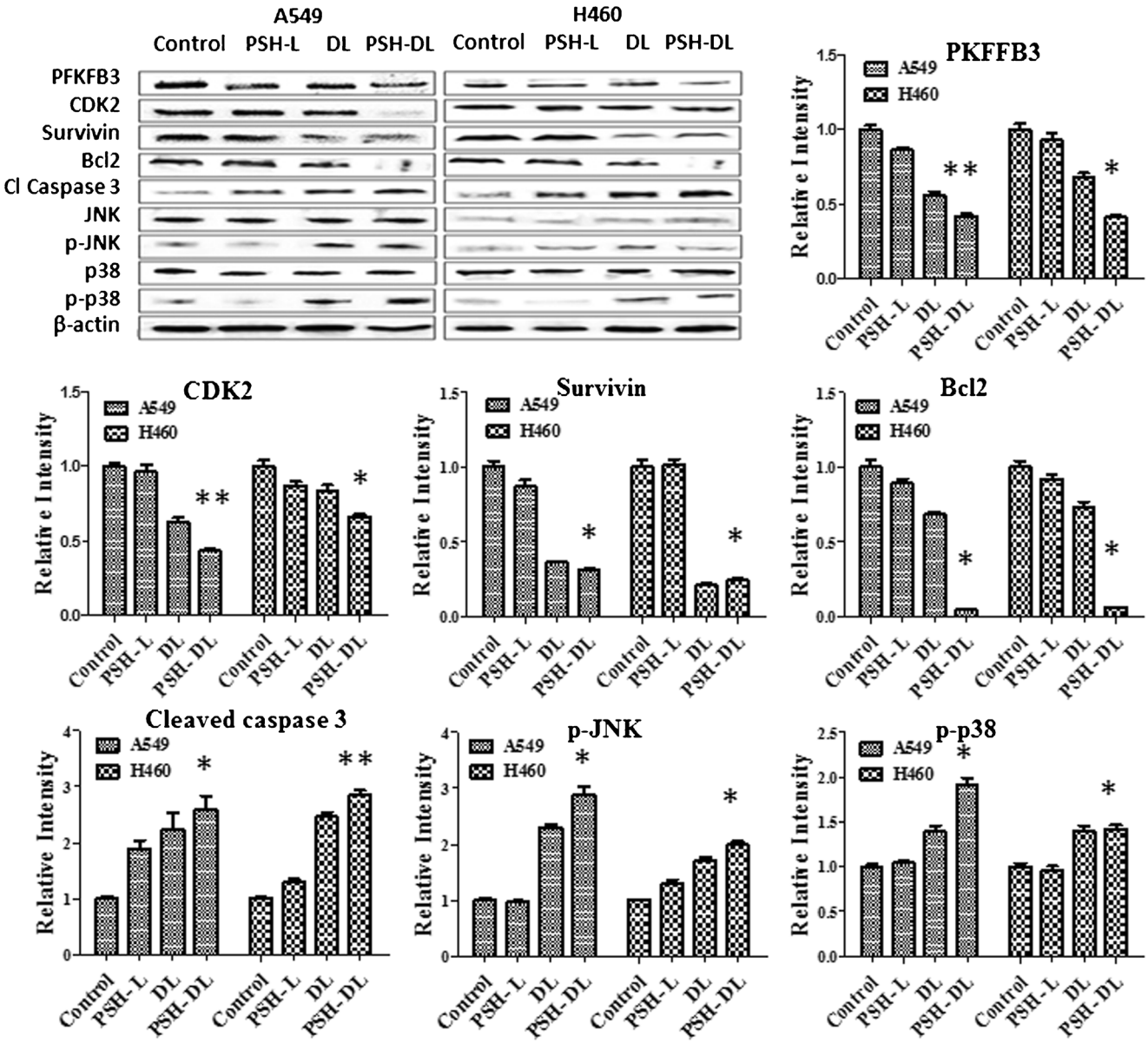

Fig. 8 A. Western blot densitometric analysis of PFKFB3, various cell survival markers, apoptotic markers and stress related markers. The results show mean of three independent experiments. * indicates $p < 0.05$ compared with untreated controls; ** indicates $p < 0.01$ compared to untreated controls.

A459 and H460 cells respectively compared to control cells (Fig. 8). A significant up-regulation of cleaved caspase-3 was also found in the PSH-DL complexes. The relative intensity increased to 2.39 **(**$p < 0.05$**)** and 2.54 **(**$p < 0.01$**)** for A549 and H460, respectively. Up-regulation of p-JNK and p-p38 was also observed indicating that activation of stress-related pathways may have triggered apoptosis.

In Vivo Anti-Tumor Activity

Tumor volume significantly decreased after treatment with DL or PSH-DL complexes compared to control (Fig. 9). PSH-L did not show a significant decrease ($p > 0.05$) in tumor volume. Tumor volume for the combination treatment averaged 848 mm^3compared with 1597 mm^3 for DL treatment or 3207 $mm^3$for PSH-L treatment on day 21 post tumor cell implantation. It is evident that combination treatment was most effective in inhibiting tumor growth compared to DTX or pshPFKFB3 treatments.

DISCUSSION

The present study of development of co-delivery system for plasmid for expression of shRNA against PFKFB3 mRNA along with docetaxel was hypothesized based on cancer tumor's two basic characteristics that are flaunted by their different physical attributes a) outer highly proliferating mass of cells and b) deep-lying comparatively slow proliferating hypoxic mass of cells. This makes the use of single agent therapeutics to be less effective in eradicating the cancer cells due to their higher effectiveness against these highly proliferating cells as compared to the hypoxic low proliferating cancer cells. Hence, targeting the pathways that are specific to hypoxia along with use of chemotherapeutic agents is a better way to treat cancer. Glycolysis being the predominant energy production mechanism in cancer cells, it can be targeted using several of glycolytic inhibitors which target specific enzymes of glycolytic pathways (24). PFKFB3 being a rate limiting enzyme in glycolytic pathway, it has been recently explored as a therapeutic target for cancer treatment using small molecule inhibitors of PFKFB3 such as 3-(3-pyridinyl)-1-(4-pyridinyl)-2-propen-1-one (3PO) and 1-(4-pyridinyl)-3-(2-quinolinyl)-2-propen-1-one (PFK15) (25,26).

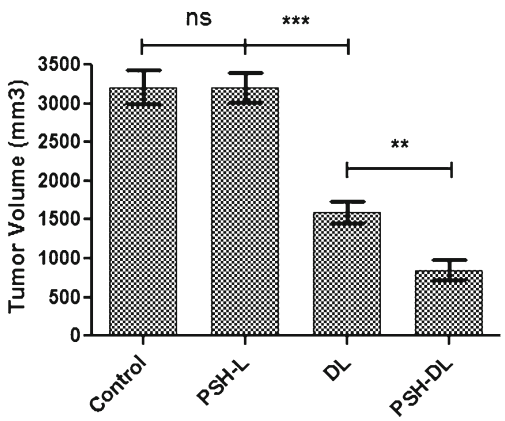

Fig. 9 Effects of different liposomes on human A459 lung tumor xenograft model tumor volume. Measurements were made on day 21 after tumor cell implantation. Tumor volumes are captured in mm^3. The results show mean of three independent experiments with the SEM. ns, statistically nonsignificant, compared with untreated control; ** indicates $p < 0.01$, compared to DL; and *** indicates $p < 0.001$, compared with untreated controls.

In the present study, we have developed a novel liposomal delivery system for the co-delivery of pshPFKFB3 (plasmid for shRNA against PFKFB3) and DTX. Selection of plasmid for shRNA over siRNA itself was based on the stability of the plasmid *in vivo* milieu and more importantly, the expression of plasmid would provide constant supply of shRNA over time which would exert its silencing activity on the PFKFB3 mRNA. Such shRNA based targeting offers additional advantages over RNAi by siRNA due to low likelihood of off-target effects and low immunological reactivity and toxicity (14,27). Moreover, the co-delivery of pshPFKFB3 with DTX could act in synergy through i) energy deprivation of cells leading to either cytostasis/ cytotoxicity, ii) inhibition of energy dependent pathways and processes iii) sensitization to/synergism with chemotherapeutic agents through reduction of hypoxia-linked resistance or ATP dependent MDR (24). Hence, our formulation strategy would make it possible to act on both hypoxic and non-hypoxic tumor cells.

We have used unsaturated lipids such as DOPC, DOPE, and DOTAP all of which have unsaturated oleoyl chains and provide bilayer deformities to accommodate the drug in the lipid bilayer. Moreover, DOPE was used for its endosomal escape capabilities through transition of bilayer phase to inverted hexagonal phase under acidic condition of endosomes leading to cytosolic release of nucleic acid cargo (28,29). Furthermore, development of a co-delivery system through co-loading of gene and drug in same liposomal carrier gives advantage over other polymeric system in their more biocompatibility and possibility for co-loading hydrophilic/ hydrophobic drugs in liposomal core/bilayer without extensive modifications of the system.

Liposomes were initially optimized for the drug loading and particle size using DoE approach using a Box-Benken design (See supplementary information-1). Using the same lipid composition, pshPFKFB3 complexed liposomes – PSH-L and PSH-DL were prepared. We separately evaluated the effect of PSH-L and DL. For co-delivery, optimized liposomal formulation of DTX was further used for complexation with pshPFKFB3. Developed DTX-pshPFKFB3 liposomes were 110.3 nm with a positive surface charge of 18.5 mV and had an entrapment efficiency of ~89% which is equivalent to drug to lipid ratio of ~3.7 mol%. PEGylation which would impart long circulation character to liposomes and

nano range particle size infers that the developed liposomes would be able to provide tumor tissue penetration through enhanced permeation and retention (EPR) effect in the lung tumors (30). Reduced zeta potential of PSH-DL compared to DTX liposomes is due to the complexation of cationic liposomes with pshPFKFB3 which makes ionic complex through its phosphates with cationic head groups of DOTAP and DDAB (31). Moreover, the reduction in the zeta potential is also in part due to the surface masking as a result of PEGylation. The complexation N/P ratio of 2.2:1 suggests that there is two times molar excess of cationic nitrogens of DOTAP and DDAB over phosphates of the pDNA which goes in concordance with the literature data. This supports the external model of complexation of pDNA with liposomes (i.e. complexation of pDNA on the external liposomal surface) with cationic lipids on the inner side of the bilayer not used for complexation (32).

We assessed the extent of cancer cell killing by the DTX solution, blank cationic liposomes and DTX liposomes complexed with NC-pDNA and pshPFKFB3 liposomes on A549 and H460 NSCLC cell lines. Blank liposomes showed negligible toxicity on all the cancer cell lines used in the cytotoxicity studies (<5%). DTX liposomes complexed with NC-pDNA were used for cytotoxicity studies as DTX liposomes alone would be taken up more efficiently than the pDNA complexed liposomes. Hence, DTX liposomes complexed with NC-pDNA (DL) were used for cytotoxicity studies and other studies to represent the actual liposomal formulation which considers the effect of complexation of pDNA on cell uptake and toxicity. Moreover, the NC-pDNA-L did not show any cytotoxicity to cells indicating there is no carrier dependent cytotoxicity nor there is any cytotoxicity due to off-target effects by the plasmid vector. Hence, the toxicity rendered by the liposomes is due to DTX only. For both DTX formulations i.e. DTX solution and DL, we observed a decrease in IC_{50} with time i.e. 24 h *vs.* 48 h showing the time dependent cytotoxicity by DTX which goes in line with the increasing cellular mitotic spindle formation defects induced by DTX on longer duration of exposure (33). However, there was a statistically significant improvement in the cytotoxicity of the DL against the DTX solution which is due to the improved uptake of liposomes in the cells compared to free drug. Moreover, this study established that the developed liposomal delivery is able to deliver DTX to lung cancer cells more effectively over solution.

Our developed liposomes are cationic systems with membrane destabilizing lipids, hence we evaluated toxicity of the liposomes on normal epithelial cell line (HEK cell line) which would give an idea about the toxicity of liposomes to other normal cells of the body (34). HEK cells were treated with blank liposomes and cytotoxicity estimations were made. Results revealed that even up to a concentration of 3 mg/mL of cationic lipids, liposomes showed more than 80% cell viability suggesting that at therapeutically effective concentration of DTX and pshPFKFB, there would be negligible toxicity posed by cationic lipids.

Next, we evaluated the effect of pshPFKFB3 on the cellular PFKFB3 expression in A549 cells. The level of expression of shRNA was confirmed through RT-PCR studies in which the down-regulation of pshPFKFB3 was monitored through RT-PCR for PFKFB3 mRNA. No PFKFB3 mRNA silencing by NC-pDNA liposomes suggested there is no nonspecific silencing by the NC plasmid and by the vector used in the study. This concludes that the silencing of the PFKFB3 mRNA is due to the pshPFKFB3 only. With the PSH-L, the levels of PFKFB3 mRNA gradually decreased with increasing concentration of pshPFKFB3 up to 40 ng level. However, further increase up to 100 ng in the pshPFKFB3 level did not cause any apparent down-regulation in PFKFB mRNA. This suggests that the level of expressed PFKFB3 mRNA reaches a plateau after certain levels of expression of shRNA. It can be deduced from these results that increased expression of shRNA will not be effective to further down-regulate the PFKFB3 mRNA due to saturation of the RNAi machinery required for effectiveness of shRNA which will ultimately lead to saturation of the efficacy of pshPFKFB3 (26,35). Further, we evaluated the expression of plasmid through fluorescence microscopy studies using GFP expression and we also evaluated if the naked plasmid itself is able to do any transfection. Results confirmed that naked plasmid has been reported in literature, is not able to transfect the cells due to the high molecular weight and negative charge. However, both the liposomal carriers i.e. lipofectamine-2000 and developed PSH-L could transfect cells effectively as it can be seen from the fluorescence inside the cells due to GFP expression. Results also showed that LF2K complexed with pshPFKFB3 at 100 ng of plasmid showed higher expression of GFP compared to GFP expression by PSH-DL at 40 ng plasmid level. This indicates that the expression of mRNA for GFP and hence, mRNA for shRNA from plasmid might be higher at higher pshPFKFB3 levels (60 and 100 ng). However, as speculated in the mRNA expression studies, saturation of the shRNA silencing machinery would be the reason for the plateaued silencing after 40 ng plasmid level. However, the cellular GFP expression studies undoubtedly conclude that developed liposomal vector is effective in expressing the mRNA either for GFP expression or for further metabolism to convert to shRNA for silencing PFKFB3. Based on this study, the treatment level of pshPFKFB3 was kept constant at 40 ng/well for 96 well plate and appropriate scaling of pshPFKFB3 level was done to keep this level constant for further experimentation in the 24 well plates, 12 well plates and 25 cm^2 T-flasks for use with different levels of DTX.

Confirming the amount of pshPFKFB, we next evaluated the cytotoxicity of PSH-L as well as PSH-DL compared to DL in both A549 and H460 NSCLC cell lines to validate the

results that were observed in aforementioned studies. For this, cytotoxicity studies were carried out on A549 cells with PSH-L, DL and PSH-DL keeping 40 ng/well (for 96 well plate or for 10,000 cells) of pshPFKFB3 constant. It was observed that PSH-L had negligible effect on the cytotoxicity of A549 and H460 cells suggesting that glycolytic seizure rendered at the selected dose of pshPFKFB3 is not causing cell killing. This might be due to the cytostatic and not cytotoxic effect of pshPFKFB3 on the cancer cells. Similar results have been observed for certain glycolysis inhibitors where cell proliferation was arrested instead of cell killing (11,26). However, our results show that in A549 and H460 cells, statistically insignificant improvement of mean cancer cell death was there ($p > 0.05$). Moreover, cytotoxicity of PSH-DL was significantly ($p < 0.05$) higher compared to PSH-L and DL. This deduces that even at the concentration of pshPFKFB3 which did not show effective cell killing, it enhanced the cytotoxicity of DTX liposomes.

It is known that the epidermal cells enter division only in the presence of glucose (36). This contention can be extended to proliferation of all epithelial cells including epidermal cells i.e. lung epithelial cells. Moreover, NSCLC cells bearing a cancerous genotype exhibit higher glucose requirements for proliferation and growth. Bullough analyzed and established that one of the rate limiting step that controls energy production as well as mitosis is PFKFB mediated (36,37). Hence, the pshPFKFB3 is effective in blocking the energy supply in the cells that provides ATP supplies to the energy dependent processes of the cell. As pshPFKFB3 transfection alone is not cytotoxic to cancer cells, improvement in the cytotoxicity of DTX liposomes in presence of pshPFKFB3 might be due to a mechanism other than the energy deprivation of cells due to glycolysis inhibition. This can be justified by the effective blocking of glycolysis that provides for the energy requirement for mechanisms other than just inhibition of proliferation due to energy deprivation of cancer cells (38). We hypothesized this mechanism to be energy dependent pGP efflux of drug which is active in the NSCLC cells and gets ceased with the pshPFKFB3 transfection. Moreover, other biochemical processes involved in cellular response to damage caused by anticancer drugs are energy dependent inhibition of processes which due to diminution of PFKFB3 mRNA by pshPFKFB3 has enhanced the cytotoxicity of the DTX on cancer cells.

To confirm the aforementioned hypothesis and for the direct measurement of activity of PFKFB3 shRNA expressed from pshPFKFB3 on pGP, we carried out the pGP inhibition assay with Rhodamine123 (Rh123) which is a pGP substrate (39). Our studies confirmed that the inhibition of glycolysis by pshPFKFB3 liposomes reduced the activity of the pGP which ultimately leads to higher accumulation of Rh123 in cells. Due to the active pGP efflux in A549 cells, accumulation of Rh123 and hence fluorescence was of low intensity when cells were treated only with Rh123. Verapamil which is used as the positive control, showed highest accumulation of the Rh123 due to its blocking activity on pGP efflux. All the pshPFKFB3 liposomal formulations showed increasing fluorescence as compared to control indicating inhibition of glycolysis by pshPFKFB3 was able to reduce the pGP based efflux of Rh123. Hence, it confirms that increased cytotoxicity seen with the lipoplexes is due to the reduced DTX efflux by pGP due to simultaneously inhibited PFKFB3 mRNA by the pshPFKFB3.

In order to identify and confirm various markers involved in the cytotoxicity by the co-delivery, we carried out the western blotting for apoptotic markers in A549 and H460 cells (40). Protein markers of cell survival and apoptosis were evaluated. Activation of the caspase-3 pathway is a hallmark of apoptosis (41). Our liposome formulation was successful in up-regulating the cleaved caspase 3 in the lung cancer cells. Moreover, other apoptotic markers such as p38 and JNK were also up-regulated including their activated (phosphorylated) forms. JNK-p38 pathway is also a well-established indicator of apoptosis in cancer cells (42). Many chemotherapeutic agents including DTX require p38 activity for the induction of apoptosis (43). Once activated, p38 proteins translocate from the cytosol to the nucleus causing cellular responses through the phosphorylation of its downstream transcription factors. Our liposomal formulation have shown to reduce the expression of Cdk2 which is critical during the G1 to S phase transition (44). Moreover, reduction in expression of Bcl-2 and survivin are also involved in apoptosis induction in lung cancer cells. Ultimately, the formulation was evaluated in the *in vivo* model of NSCLC. The *in vivo* therapeutic activity was evaluated in the A549 tumor xenograft model. The results further confirmed that the plasmid alone was not able to reduce the tumor size in the animal model. However, the co-loaded liposomes PSH-DL were showing significantly higher tumor volume reduction. The results of *in vivo* study are in line with and validate the results of *in vitro* studies. PSH-L alone is ineffective in the tumor volume reduction while PSH-DL demonstrated statistically significant reduction in the tumor volume with co-delivery compared to DL. This suggest that the liposomal formulation is effective in penetrating the tumor and delivering the pshPFKFB3 and DTX to the cancer cells that works in a synergistic fashion with the DTX.

CONCLUSION

Overall, we demonstrated for the first time that the combination of pshPFKFB3 with docetaxel can be effectively used for lung cancer treatment. The liposomes carrying the pshPFKFB3 and DTX demonstrated anticancer activity by increasing apoptosis and cellular stress. In summary, the present findings establish that the co-delivery of docetaxel and pshPFKFB3 can prove to be of great therapeutic value for

lung cancer treatment due to the ability of RNAi based glycolytic inhibitor to enhance the therapeutic efficacy of docetaxel. Moreover, our study provides a proof-of-concept for simultaneous delivery of synergistic combination of gene and drug to cancer cells through co-loading of gene and drug in the same liposomal system. Furthermore, such treatment needs to be evaluated in more bio-relevant *in vivo* models such as PDX models and also utility of this formulation can be evaluated for the treatment of NSCLC not responding to or resistant to traditional therapies. In summary, chemosensitization of NSCLC cells through glycolysis inhibition could possibly a better mechanism of an effective lung cancer treatment.

ACKNOWLEDGEMENTS

This research was supported with funding from: the National Institutes of Health's Minority Biomedical Research Support (MBRS)-SC1 program (Grant #SC1 GM092779–01); and the Department of Defense (DOD) Breast Cancer Program(Grant #W81XWH-11–1–0211).

REFERENCES

1. Siegel RL, Miller KD, Jemal A. Cancer statistics, 2016. CA Cancer J Clin. 2016;66(1):7–30.
2. Laskin JJ, Sandler AB. First-line treatment for advanced non-small-cell lung cancer. Oncology (Williston Park, NY). 2005;19(13):1671–6. discussion 1678-1680
3. Warburg O. On the origin of cancer cells. Science (New York, NY). 1956;123(3191):309-14.
4. Marín-Hernández A, López-Ramírez SY, Del Mazo-Monsalvo I, Gallardo-Pérez JC, Rodríguez-Enríquez S, Moreno-Sánchez R, et al. Modeling cancer glycolysis under hypoglycemia, and the role played by the differential expression of glycolytic isoforms. FEBS J. 2014;281(15):3325-45.
5. Semenza GL. Involvement of hypoxia-inducible factor 1 in human cancer. Intern Med. 2002;41(2):79–83.
6. Zheng JIE. Energy metabolism of cancer: glycolysis versus oxidative phosphorylation (review). Oncol Lett. 2012;4(6):1151–7.
7. Bares R, Klever P, Hauptmann S, Hellwig D, Fass J, Cremerius U, et al. F-18 fluorodeoxyglucose PET in vivo evaluation of pancreatic glucose metabolism for detection of pancreatic cancer. Radiology. 1994;192(1):79–86.
8. Atsumi T, Chesney J, Metz C, Leng L, Donnelly S, Makita Z, et al. High expression of inducible 6-Phosphofructo-2-kinase/fructose-2, 6-Bisphosphatase (iPFK-2; PFKFB3) in human cancers. Cancer Res. 2002;62(20):5881–7.
9. Pelicano H, Martin DS, Xu RH, Huang P. Glycolysis inhibition for anticancer treatment. Oncogene. 2006;25(34):4633-46.
10. Chesney J. 6-phosphofructo-2-kinase/fructose-2,6-bisphosphatase and tumor cell glycolysis. Curr Opin Clin Nutr Metab Care. 2006;9(5):535–9.
11. Vuyyuri SB, Rinkinen J, Worden E, Shim H, Lee S, Davis KR. Ascorbic acid and a cytostatic inhibitor of glycolysis synergistically induce apoptosis in non-small cell lung cancer cells. PLoS One. 2013;8(6):e67081.
12. O'Neal J, Tapolsky G, Clem B, Telang S, Chesney J. Identification of a PFKFB3 inhibitor suitable for phase I trial testing that synergizes with the B-Raf inhibitor vemurafenib. Cancer Res. 2014;74(19):962.
13. Boyd S, Brookfield JL, Critchlow SE, Cumming IA, Curtis NJ, Debreczeni J, et al. Structure-based design of potent and selective inhibitors of the metabolic kinase PFKFB3. J Med Chem. 2015;58(8):3611–25.
14. Rao DD, Vorhies JS, Senzer N, Nemunaitis J. siRNA vs. shRNA: similarities and differences. Adv Drug Deliv Rev. 2009;61(9):746–59.
15. Patel K, Chowdhury N, Doddapaneni R, Boakye CH, Godugu C, Singh M. Piperlongumine for enhancing oral bioavailability and cytotoxicity of docetaxel in triple-negative breast cancer. J Pharm Sci. 2015;104(12):4417–26.
16. Patel K, Doddapaneni R, Chowdhury N, Boakye CH, Behl G, Singh M. Tumor stromal disrupting agent enhances the anticancer efficacy of docetaxel loaded PEGylated liposomes in lung cancer. Nanomedicine. 2016;11(11):1377–92.
17. Patel K, Doddapaneni R, Sekar V, Chowdhury N, Singh M. Combination approach of YSA peptide anchored docetaxel stealth liposomes with oral antifibrotic agent for the treatment of lung cancer. Mol Pharm. 2016;13(6):2049–58.
18. Kampan NC, Madondo MT, McNally OM, Quinn M, Plebanski M. Paclitaxel and its evolving role in the management of ovarian cancer. Biomed Res Int. 2015;2015:413076.
19. Miele E, Spinelli GP, Miele E, Tomao F, Tomao S. Albumin-bound formulation of paclitaxel (Abraxane (R) ABI-007) in the treatment of breast cancer. Int J Nanomedicine. 2009;4(1):99–105.
20. Immordino ML, Dosio F, Cattel L. Stealth liposomes: review of the basic science, rationale, and clinical applications, existing and potential. Int J Nanomedicine. 2006;1(3):297–315.
21. Balazs DA, Godbey W. Liposomes for use in gene delivery. J Drug Deliv. 2011;2011:326497.
22. Boakye CH, Patel K, Doddapaneni R, Bagde A, Marepally S, Singh M. Novel amphiphilic lipid augments the co-delivery of erlotinib and IL36 siRNA into the skin for psoriasis treatment. J Control Release. 2017;246:120-32.
23. Boakye CH, Patel K, Doddapaneni R, Bagde A, Behl G, Chowdhury N, et al. Ultra-flexible nanocarriers for enhanced topical delivery of a highly lipophilic antioxidative molecule for skin cancer chemoprevention. Colloids Surf B: Biointerfaces. 2016;143:156–67.
24. Scatena R, Bottoni P, Pontoglio A, Mastrototaro L, Giardina B. Glycolytic enzyme inhibitors in cancer treatment. Expert Opin Investig Drugs. 2008;17(10):1533–45.
25. Clem BF, O'Neal J, Tapolsky G, Clem AL, Imbert-Fernandez Y, Kerr DA, et al. Targeting 6-Phosphofructo-2-kinase (PFKFB3) as a therapeutic strategy against cancer. Mol Cancer Ther. 2013;12(8):1461–70.
26. Clem B, Telang S, Clem A, Yalcin A, Meier J, Simmons A, et al. Small-molecule inhibition of 6-phosphofructo-2-kinase activity suppresses glycolytic flux and tumor growth. Mol Cancer Ther. 2008;7(1):110–20.
27. DiGiusto DL, Krishnan A, Li L, Li H, Li S, Rao A, et al. RNA-based gene therapy for HIV with lentiviral vector-modified CD34(+) cells in patients undergoing transplantation for AIDS-related lymphoma. Science Translational Medicine. 2010;2(36):36ra43.
28. Hoekstra D, Martin OC. Transbilayer redistribution of phosphatidylethanolamine during fusion of phospholipid vesicles. Dependence on fusion rate, lipid phase separation, and formation of nonbilayer structures. Biochemistry. 1982;21(24):6097–103.
29. Zuhorn IS, Bakowsky U, Polushkin E, Visser WH, Stuart MC, Engberts JB, et al. Nonbilayer phase of lipoplex-membrane mixture

determines endosomal escape of genetic cargo and transfection efficiency. Mol Ther. 2005;11(5):801–10.
30. Kolate A, Baradia D, Patil S, Vhora I, Kore G, Misra A. PEG—a versatile conjugating ligand for drugs and drug delivery systems. J Control Release. 2014;192:67–81.
31. Son KK, Patel DH, Tkach D, Park A. Cationic liposome and plasmid DNA complexes formed in serum-free medium under optimum transfection condition are negatively charged. Biochim Biophys Acta. 2000;1466(1–2):11–5.
32. Ferrari ME, Rusalov D, Enas J, Wheeler CJ. Trends in lipoplex physical properties dependent on cationic lipid structure, vehicle and complexation procedure do not correlate with biological activity. Nucleic Acids Res. 2001;29(7):1539–48.
33. Orth JD, Loewer A, Lahav G, Mitchison TJ. Prolonged mitotic arrest triggers partial activation of apoptosis, resulting in DNA damage and p53 induction. Mol Biol Cell. 2012;23(4):567–76.
34. Yingyongnarongkul BE, Radchatawedchakoon W, Krajarng A, Watanapokasin R, Suksamrarn A. High transfection efficiency and low toxicity cationic lipids with aminoglycerol-diamine conjugate. Bioorg Med Chem. 2009;17(1):176–88.
35. Kurreck J. RNA interference: from basic research to therapeutic applications. Angew Chem Int Ed Engl. 2009;48(8):1378–98.
36. Gelfant S. The energy requirements for mitosis. Ann N Y Acad Sci. 1960;90:536–49.
37. Boscá L, Corredor C. Is phosphofructokinase the rate-limiting step of glycolysis? Trends Biochem Sci. 1984;9(9):372–3.
38. Ganapathy-Kanniappan S, Geschwind JF. Tumor glycolysis as a target for cancer therapy: progress and prospects. Mol Cancer. 2013;12:152.
39. Twentyman PR, Rhodes T, Rayner S. A comparison of rhodamine 123 accumulation and efflux in cells with P-glycoprotein-mediated and MRP-associated multidrug resistance phenotypes. Eur J Cancer. 1994;30A(9):1360–9.
40. Doddapaneni R, Patel K, Chowdhury N, Singh M. Noscapine chemosensitization enhances docetaxel anticancer activity and nanocarrier uptake in triple negative breast cancer. Exp Cell Res. 2016;346(1):65–73.
41. McIlwain DR, Berger T, Mak TW. Caspase functions in cell death and disease. Cold Spring Harb Perspect Biol. 2013 Apr 1;5(4): a008656.
42. Sui X, Kong N, Ye L, Han W, Zhou J, Zhang Q, et al. p38 and JNK MAPK pathways control the balance of apoptosis and autophagy in response to chemotherapeutic agents. Cancer Lett. 2014;344(2):174–9.
43. Cuadrado A, Nebreda AR. Mechanisms and functions of p38 MAPK signalling. Biochem J. 2010;429:403–17.
44. Yalcin A, Clem BF, Imbert-Fernandez Y, Ozcan SC, Peker S, O'Neal J, et al. 6-Phosphofructo-2-kinase (PFKFB3) promotes cell cycle progression and suppresses apoptosis via Cdk1-mediated phosphorylation of p27. Cell Death Dis. 2014;5:e1337.